THE

LONDON, EDINBURGH, AND DUBLIN

PHILOSOPHICAL MAGAZINE

AND

JOURNAL OF SCIENCE.

[SEVENTH SERIES.]

APRIL 1931.

LXXI. *The Absorption and Scattering of Light in Opal Glasses.* *By* Dr. G. M. Dreosti *.

ABSTRACT.

THE present work is concerned with the determination of the coefficients of scattering and absorption in milk glass.

As no complete theory of the scattering and absorption of light in thick layers of big particles exists, the theory of Schuster was expanded to include this case. This theory was developed for a parallel incident beam as well as for a diffuse one.

Measurements of the light transmitted by thick layers of coloured mastic emulsion were made with a visual spectrophotometer ; curves are given for all combinations of scattering and absorption. The directly transmitted light follows the law of Beer exactly, but for thick layers the repeatedly scattered light is added to the direct light.

The optical properties of technical milk glasses are not determined by the ordinary coefficients of absorption (κ) and scattering (σ), but by the absorption coefficient for diffuse incident light ($c\kappa$), and by the fraction scattered

* Communicated by Prof. L. S. Ornstein. This paper includes the chief results of a thesis for the doctorate of the University of Utrecht, 1930 ("Absorpsie ne Verstrooiing van Lig in Melkglas "), written in the South African language.

backwards for such illumination ($cn\beta\sigma$). From the transmitted light we determine $\sqrt{\kappa(\kappa+2n\beta\sigma)}$; from the rejected light a second relation is obtained. By this simple method the values of $c\kappa$ and $cn\beta\sigma$ are compared for Philips Argenta bulbs and those manufactured at Leerdam.

ONE of the fundamental problems in light technology is that of determining the coefficients of scattering (σ) and of absorption (κ) for a given specimen of opal glass. The present work is concerned with the development of a method for such determinations.

Experimental Method.

The elementary laws of scattering and absorption have been sought by measuring the transmission and rejection * for coloured emulsions; not only is it difficult, but it is

TABLE I.

Grams of mastic per litre of emulsion	5	5
,, ,, ,, ,, alcohol	45	225
$\sigma \times$ thickness of the layer	43	110

also theoretically incorrect, to grind a sheet of opal glass to a certain thickness for such measurements, for the concentration of the scattering material is not uniform over the thickness of any sheet. It is also out of the question to vary the ratio $\frac{\kappa}{\sigma}$ in a known manner in such glasses.

In emulsions, however, all this is possible.

1. Concentrated emulsions of big particles were made by pouring concentrated alcoholic solutions of mastic into distilled water, then boiling off the alcohol from the emulsion, and finally filtering the latter through old rags which have been washed many times.

The more concentrated the alcoholic solution of mastic is, the greater is the chance of obtaining an emulsion of big particles (see Table I.). Various concentrations of

* The light here measured is the narrow pencil which enters the field of the photometer.

an emulsion were obtained by diluting the stock emulsion with distilled water.

As colouring material aqueous solution of acid fuchsine was eventually chosen; all basic colouring matters coagulate the mastic particles. It was found that the solutions (or emulsions coloured with them) only follow the law of Beer after CO_2 has been bubbled through them for about five minutes.

Fig. 1.

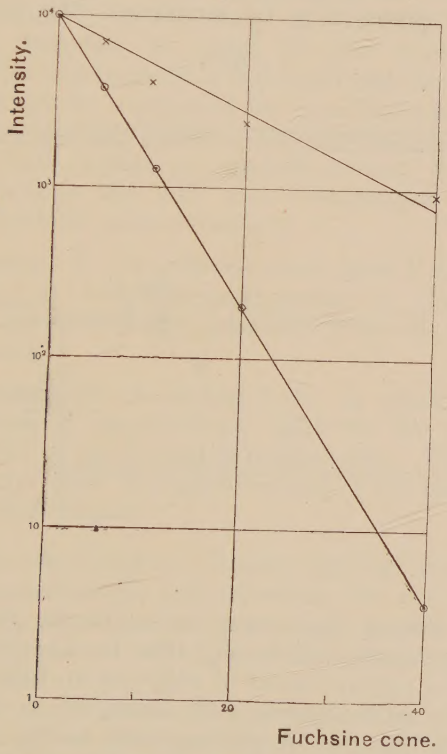

For example, points × in fig. 1 were obtained before and points ⊙ after CO_2 was bubbled through the solutions.

Acid fuchsine has a maximum absorption at $\lambda = \pm 530\,\mu\mu$, *i. e.*, at the wave-length at which the eye is most sensitive to light. The variation of absorption with the wave-length λ is not so large there as to cause inaccuracy due to small errors in the adjustment of the photometer for a given wave-length.

2. Intensity measurements throughout the work were made with a Glan spectrophotometer *, of which the Nicol's prism was replaced in function by a photographic wedge—that is, a contact print of a smoked glass wedge. The photographic wedge was calibrated by means of the Nicol's prism of the photometer.

A visual method of intensity measurements was adopted, owing to the great range of intensity in which it can be worked visually.

Among the many advantages of an optical wedge over the Nicol's prism may be mentioned the considerable

Fig. 2.

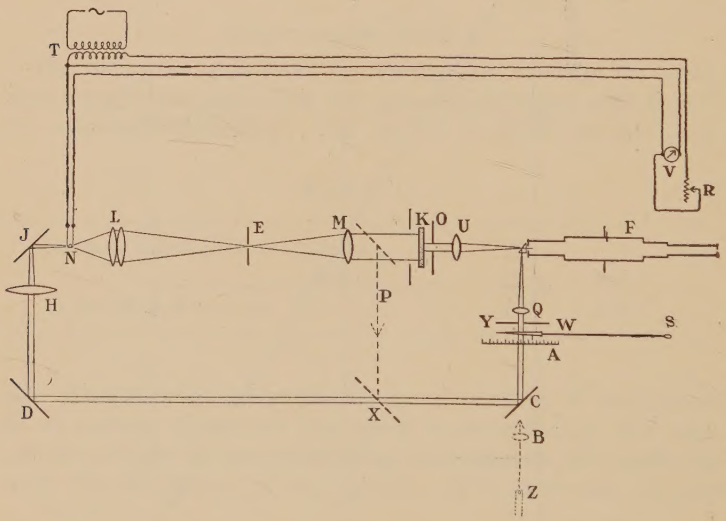

economy of time and labour, owing to the greater range of intensity ratios which may thus be measured without the aid of a calibrated set of reducers (in this case it was about 10^4, as compared with about 10 in the case of the Nicol's prism). A photographic wedge is especially recommended, owing among other things to its greyness if made properly—*i. e.*, by developing the plate for a long time with weak developer.

(*a*) The preceding figure (2) represents three arrangements for measuring the transmitted light *in the case of a parallel incident beam* on the emulsion in cell K.

* P. Glan, "Ueber ein neues Photometer," Wied. *Ann.* i. p. 351 (1887).

Arrangement A.—N is a 10-volt Philips motor headlight bulb. Lenses L project the light on to the small aperture E, where stray light of the glass bulb is screened off.

Achromatic lens M renders the beam parallel, and the directly transmitted light is focussed on the slit of the photometer by lens U.

Bulb N also supplies the light for the comparison field. (Path of light : mirror J, lens H, mirrors D and C, wedge W, lens Q, prism of photometer, etc.).

Transformer T is fed from the 220-volt mains, the secondary supplies 18 volts to the circuit. During readings the resistance R is regulated with the right hand, and the wedge W is adjusted for equal fields in the photometer with the left hand. The advantage of a single headlight bulb is that no constant current is necessary ; during readings the bulb was overcharged to 18 volts for short periods when necessary.

Arrangement B.—A polished plate glass P and a mirror X replace J, H, and D of arrangement A. This arrangement is convenient for measurements of very small transmissions.

Arrangement C.—A second bulb, Z, which is at the focus of lens B, supplies the light for the comparison field, instead of the former arrangements. This arrangement is convenient for measurements of the transmissions under various angles.

(*b*) *In the case of diffused incident light* the measurements of small transmissions and rejections are not only made with greater rapidity, but also with greater accuracy, owing to the greater intensity of light source which may be obtained.

The following figure (3) represents the arrangement for measuring both the transmitted and the rejected light.

The " diffuser " consists of a cubical wooden box of 40 cm. side, of which the inner walls are coated with mirrors. The light of the five 220-volt Philips shop window lamps N, which are fed with 270 volts during readings, is rendered diffused by the opal glass M, and the mirrors R virtually extend the sheet M to infinity.

For measurements of the light transmitted by the emulsion or glass at K mirrors P and X are used to

reflect the light into the photometer F, and for measuring the rejected light mirrors D and X are used.

In the latter case, a velvet rag E is introduced to remove ordinary reflected light. (Screen Z covers the hole *a* during measurements of the transmitted light.)

Further details of the intensity measurements may be summarized as follows:—

Five or six readings of the intensity were taken, and the average constituted one measurement. During the work the observer's eye becomes more and more sensitive to small intensity differences. Before measurements the eye is rested in the dark for a quarter of an hour, and again when the deviations between successive readings become appreciable.

Fig. 3.

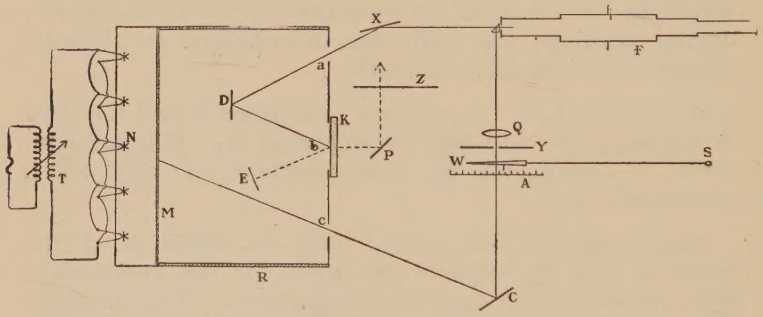

Owing to the fact that the sides of the cell were not quite plane and parallel, although the best cells obtainable were used, it was necessary to place the cell always in exactly the same position in the incident beam.

Volumes were measured with pipettes and measuring jars, except when the accuracy of intensity measurements was so small that this would be superfluous.

Development of a Theory of Scattering and Absorption in the Case of Big Particles.

In the case of *a parallel incident beam* the simplest results followed from measurements of the light transmitted by thin layers.

1. *Pure Scattering.*—It has been experimentally found that the directly transmitted light may be expressed as an exponential function of the product of the concentration

and the thickness of the layer. In disagreement with previous workers, this holds over a very large range of this product (see fig. 4 ; the deviation at the end is explained on p. 809).

Fig. 4.

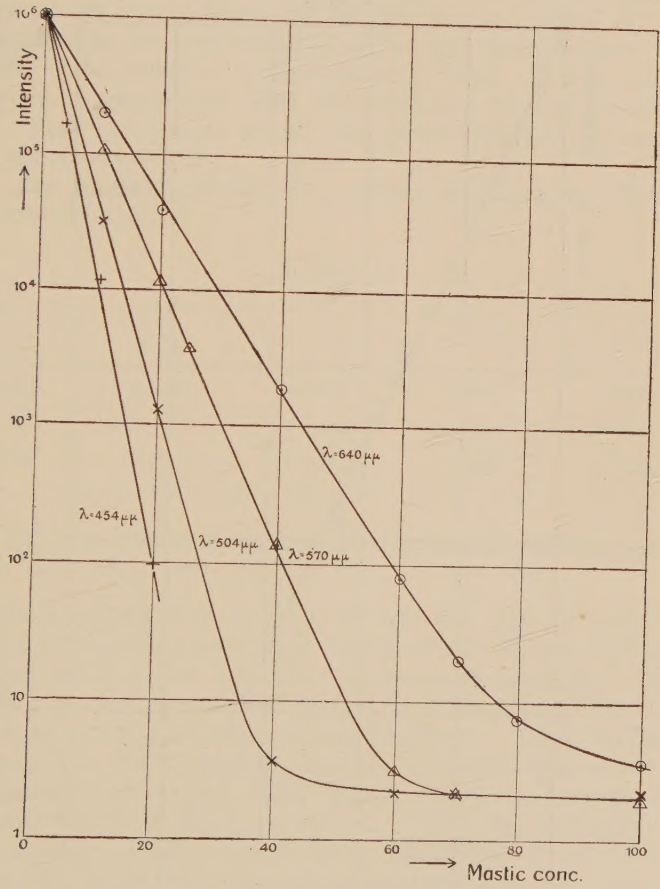

Thickness of cell 3 cm. The alcoholic solution contained 41·5 gm. mastic per litre ; the emulsion of concentration " 100 " contained 4·15 gm. per litre.

From the figure it is clear that for dilute emulsions we may write $I = I_0 e^{-\sigma x}$, where x is the concentration of the layer on an arbitrary scale (the thickness is included

in σ; in the following work this is always done). I is the directly transmitted light, and I_0 the incident light.

2. It has been found that in optically thin layers the scattering and absorption affect the directly transmitted

Fig. 5.

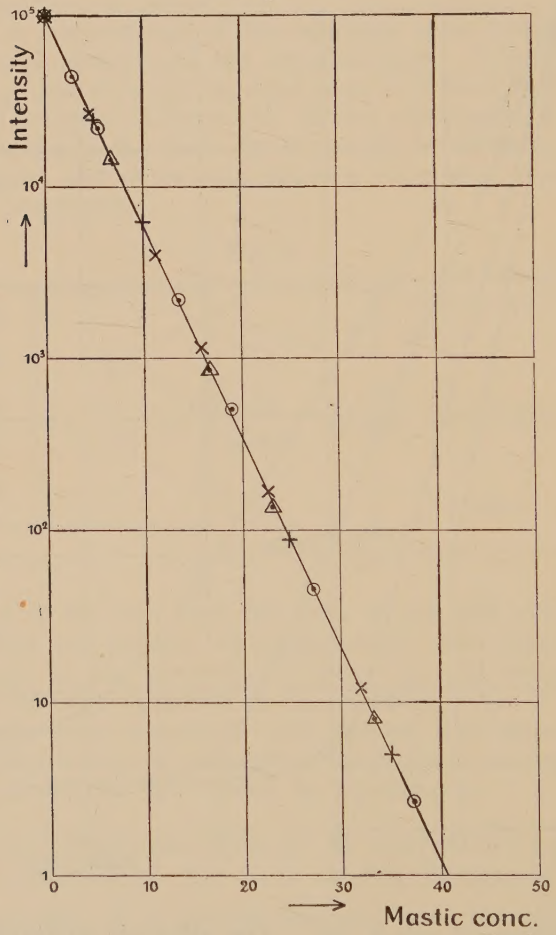

light independently of each other's presence. The preceding figure (5) shows the effect at $\lambda = 535\ \mu\mu$.

Points + followed from measurements of the transmission by uncoloured emulsions of various concentrations. To 200 c.c. of each emulsion was added 75 c.c. of

aqua dest. and 25 c.c. of acid fuchsine ($\kappa x = 18$). On again measuring the directly transmitted light the points △ were obtained. Points ⊙ follow after 25 c.c. of fuchsine and 25 c.c. of aqua dest. were added to 250 c.c. of each of these emulsions; and by a further addition of 50 c.c. to 250 c.c. of each of these emulsions again the points × were obtained. Thus, for all the points marked by the same sign, *the concentration of the dye was the same*, and only the mastic concentration varied. The various series of points have been displaced in a vertical direction, so that the points of all the series coincide at mastic concentration zero.

The following Table (II.) shows the effect at different wave-lengths:—

Table II.

in.	κ exp.	σ exp.	$(\kappa+\sigma)$ theor.	$(\kappa+\sigma)$ exp.
498	0·0040	0·0721	0·0761	0·0760
537	0·0061	0·0640	0·0701	0·0710
578	0·0012	0·0545	0·0557	0·0557

For the combined effect of absorption and scattering we may thus write $I = I_0 e^{-(\kappa+\sigma)x}$.

3. From fig. 4 it is clear that in the case of optically *thick* layers much more light is transmitted by the emulsion than that given by the exponential function. This effect has also been found by Lax, Schönborn, and Pirani *, but at a much smaller optical thickness. Their explanation of the effect, namely, that the excess of light is due to repeatedly scattered light which comes back into the direct pencil of light, is correct. That this deviation in their case already occurs at a reduction of 0·1 of the incident beam may be due to the fact that they did not select accurately the light transmitted in one single direction only. Their method of finding the contribution of repeatedly scattered light to the total transmission, by extrapolating from that scattered by optically *very* thick

* E. Lax, M. Pirani, and H. Schönborn, "Experimentelle Studien über die optischen Eigenschaften stark getrübter Medien, *Licht und Lampe*, nos. 5 & 6 (1928).

layers, is incorrect ; before this can be done a knowledge of the variation of the repeatedly scattered light with the optical thickness of the layer is necessary.

Fig. 6.

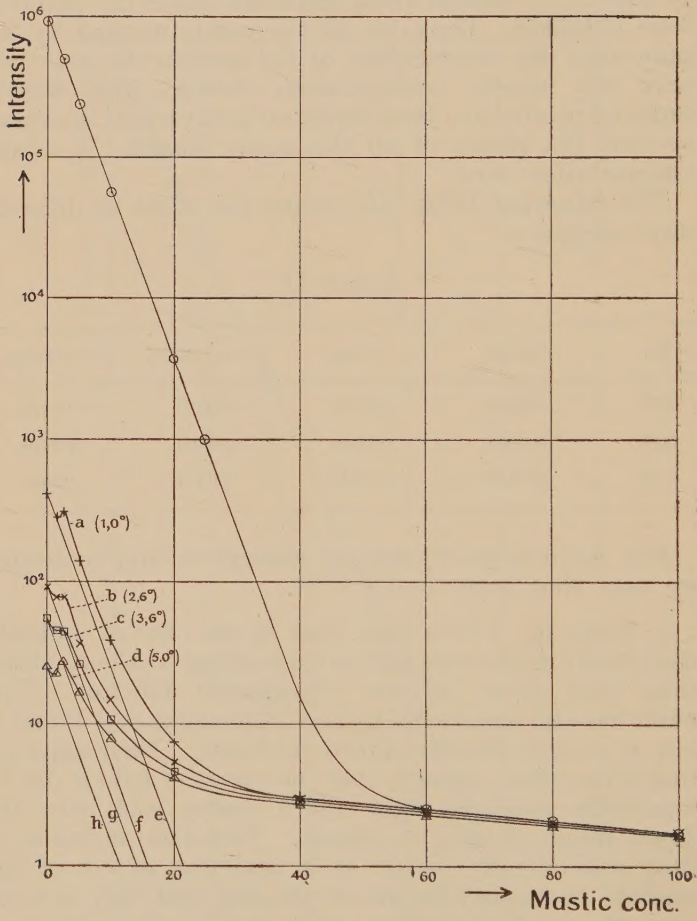

It is experimentally a simple matter to investigate how much directly transmitted light and how much scattered light enters the photometer.

This has been done by first measuring the total transmitted light under 0° with the normal to the face of the cell, and then the scattered light under small angles with

the normal by displacing lens U slightly to one side. The preceding figure (6) shows the results: points ⊙ represent the total transmission under 0°, and curves *a*, *b*, *c*, and *d* respectively the scattered light under the given small angles.

At concentration zero the scattered light is also zero; clearly the intensities shown in fig. 6 are thus due to

Fig. 7.

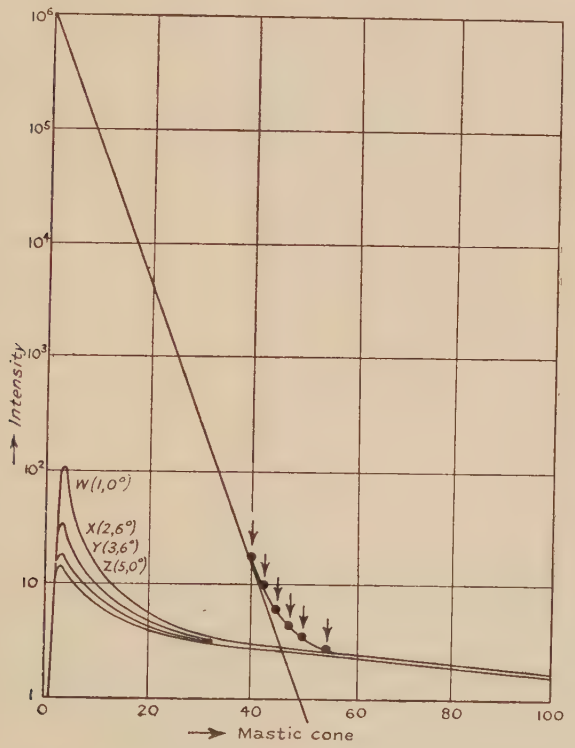

stray light (aberrations of lenses, etc.), and may be represented by an exponential function of the thickness of the layer given by the lines *o*, *f*, *g*, and *h* respectively, which are all parallel to the straight line through the points ⊙.

After subtraction of this stray light the curves *w*, *x*, *y*, and *z* in fig. 7 are obtained from the curves *a*, *b*, *c*, and *d*.

Finally, we plot for every concentration the scattered light as a function of the angle of deviation (fig. 8) ; the interpolation between the angles $+1°$ and $-1°$ may now

Fig. 8.

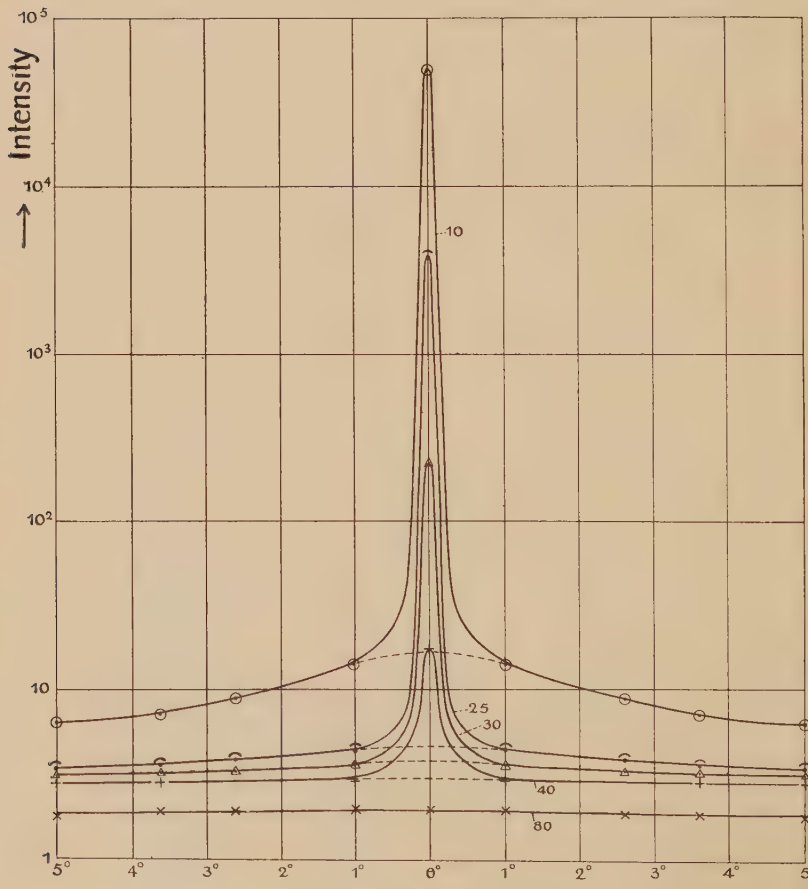

safely be done, so that we obtain the intensity of the repeatedly scattered light in the direction of the normal.

Points ↓ have been theoretically obtained by the addition of this scattered light and of the directly transmitted light at the various concentrations ; the form of the experimental curve is now entirely explained.

Further experiments * have confirmed this view on the subject. Let the direction of the parallel rays falling on the emulsion become more and more definite, and select for the measurement more and more carefully the same direction among the rays transmitted; then the proportion of repeatedly scattered light will correspondingly diminish compared with the directly transmitted light. In the limit the transmission will be represented by an exponential function even for the thickest layers.

4. We may attempt to describe the experimental facts by a theory similar to that of Schuster †. However, in this theory the assumption is made that every particle scatters isotropically in all directions.

For milk glass the case is quite different, because the particles have dimensions of the same order as the wave-

Fig. 9.

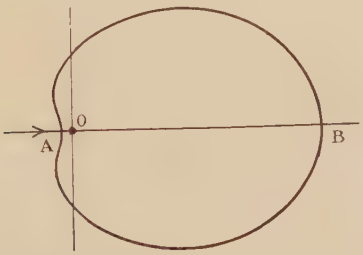

length. Following the methods of Mie, Blumer has calculated the radiation diagrams for such particles; such a diagram is drawn here (fig. 9) for a case corresponding to ours. We see that by far the greatest amount of the radiation is now scattered in the direction of the incident beam. No complete theory has been given for the diffusion of light in this case of extreme anisotropy of the scattering coefficient.

We will attempt to generalize the theory of Schuster by the introduction of a few quantities whereby the equations are still to be solved.

Firstly we introduce a quantity c, which represents the ratio of the scattering (or absorption) coefficient for

* See Dissertation (Utrecht, 1930).

† Sir A. Schuster, "Radiation through a Foggy Atmosphere," Astrophys. Journ. xxi. p. 1 (1905).

diffused light to that for a parallel beam. In the case of pure absorption and a very thin layer this quantity depends only upon the angular distribution of the incident light; for thicker layers we will neglect the variation of c with the depth in the layer, and consider its mean value for the layer as a whole. It then depends also upon the product of the concentration and the thickness of the layer.

When, however, the light is partly scattered the size and shape of the particles, the ratio $\frac{\kappa}{\sigma}$, etc., will have an influence.

For completely diffused incident light on a layer which only absorbs it we have

$$i_u = 2\pi i_0 \int_0^{\frac{\pi}{2}} \sin\vartheta \cos\vartheta e^{-\kappa \sec\vartheta . X} . d\vartheta$$

$$= 2\pi i_0 \int_0^{\frac{\pi}{2}} \sin\vartheta \cos\vartheta e^{-c\kappa X} . d\vartheta,$$

where i_u = transmitted light,

i_0 = incident light,

ϑ = angle between a beam of light and the normal.

With the aid of tables for integral log the equations may be solved, and we obtain the following table:—

TABLE III.

κX.	c.
0·0	2·0
0·5	1·63
1·0	1·52
2·0	1·40
3·0	1·34
∞	1·00

In the case of combined scattering and absorption the value of c is of course the same for scattering and for absorption at any point in the layer; the variation of c

with the optical thickness of the layer will, however, be different from that given in Table III.

Although the value of c is different for the transmitted and rejected light, it has in this work been regarded as constant for the sake of simplicity.

Secondly, a quantity β has been introduced to represent the fraction (of the total light scattered by a particle or elementary layer) which is scattered backwards in the case of a parallel incident beam.

The quantity $n\beta$ represents the same fraction for diffused incident light upon the particle or elementary layer.

The value of β depends among other things upon the size of the particles; for very small particles it is $\frac{1}{2}$ (Rayleigh); for big particles as we find them in milk glass the fraction scattered backwards is very small, and so is the value of β (see Blumer *).

Fig. 10.

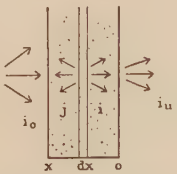

The quantity n further depends upon the angular distribution of the incident light, the ratio $\frac{\kappa}{\sigma}$, etc. It is clear that $\frac{1}{2} \geq n\beta > \beta$.

For the sake of simplicity the value of n has also incorrectly been regarded as constant throughout the layer and equal for the transmitted and rejected beams at any point in the layer. By such a theory, however, the experimental facts may be fairly well described.

5. Let i = the transmitted light at any point in the layer, and j = the rejected light at any point in the layer. We then write, in the case of diffused incident light,

$$\left.\begin{aligned} di &= cn\beta\sigma i\,dx - cn\beta\sigma j\,dx + c\kappa i\,dx, \\ dj &= cn\beta\sigma i\,dx - cn\beta\sigma j\,dx - c\kappa j\,dx. \end{aligned}\right\} \quad . \quad . \quad . \quad (1)$$

* H. Blumer, "Strahlungsdiagramme kleiner dielektrischer Kugeln," (I.) *Zeits. für Phys.* xxxii. p. 119 (1925), no. 2; (II.) *Zeits. für Phys.* xxxviii. p. 304 (1926), nos. 4 & 5.

The boundary conditions of the problem are

$$\left.\begin{aligned} &\text{at } x=X, \quad i=i_0, \\ &\text{at } x=0, \quad i=i_u. \end{aligned}\right\}$$

Solving with the ordinary methods for linear equations, and using the boundary conditions, we obtain for the transmitted light

$$i_{x=0}=i_u=\frac{2fi_0}{(f+a)e^{fx}+(f-a)e^{-fx}}.$$

In the same way the rejected light is found :

$$j_{x=X}=j=\frac{i_0(a^2-f^2)\{e^{fX}-e^{-fX}\}}{cn\beta\sigma\{(f+a)e^{fX}+e^{-fX}(f-a)\}},$$

where

$$f=c\sqrt{\kappa(\kappa+2n\beta\sigma)} \quad \text{and} \quad a=c(\kappa+n\beta\sigma).$$

(2)

Fig. 11.

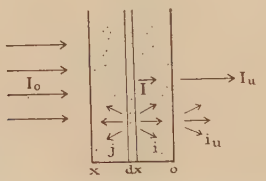

For such large values of X that $e^{fX}>>e^{-fX}$, we have

$$i_u=\frac{2fi_0e^{-fX}}{(f+a)} \quad \text{and} \quad j_u=\frac{i_0(a-f)}{cn\beta\sigma}. \qquad (3)$$

Thus, after a certain optical thickness has been reached, $\log i_u$ decreases linearly and j_u remains constant with increasing X.

For the case of pure scattering we put $\kappa=0$ in equations (1) ; the equations are then easily solved, and we find

$$i_u=\frac{i_0}{cn\beta\sigma X+1} \quad \text{and} \quad j_u=\frac{cn\beta\sigma X\,.\,i_0}{cn\beta\sigma X+1}. \qquad (4)$$

With increasing X, i_u tends to zero and j_u tends to i_0, as we of course expect.

6. In the case of a parallel incident beam the expressions for i_u and j_u become more complicated than in the case of diffused incident light.

A parallel beam (I_0) incident on the layer is reduced according to the law of Beer. The combined effects of absorption and scattering on this direct beam are included in the equation $I = I_0 e^{-(\kappa+\sigma)(x-X)}$, where $(X-x)$ is the optical thickness of the layer which the beam has traversed. For the diffuse radiation, which increases at the cost of the direct one, the differential equations are

$$\left.\begin{aligned} di &= (\beta n\sigma + \kappa)c\,i\,dx - \beta nc\sigma\, j\,dx - (1-\beta)\sigma I_0 e^{(\kappa+\sigma)(x-X)}, \\ dj &= \beta nc\sigma\, i\,dx - (\kappa + \beta n\sigma)c\,j\,dx + \beta\sigma I_0 e^{(\kappa+\sigma)(x-X)}, \end{aligned}\right\} \quad (5)$$

where i and j are the scattered beams travelling forwards and backwards at the point x respectively.

The solution is of the form

$$\left.\begin{aligned} i &= Ae^{m_1 x} + Be^{m_2 x} + Ce^{\delta x}, \\ j &= De^{m_1 x} + Ee^{m_2 x} + Fe^{\delta x}. \end{aligned}\right\} \quad . \quad . \quad . \quad . \quad (6)$$

After determining the coeficients we find the transmitted light

$$\begin{aligned} i_{x=0} = i_u = {} & \frac{\sigma I_0 e^{-(\kappa+\sigma)X}}{\kappa+\sigma-c\theta}\left[\beta^2 nc\sigma\phi + \beta - 1\right] \\ & \times \left[1 - e^{X(\kappa+\sigma-f)} - \frac{(f-c\theta)(1-e^{-2fX})e^{(\kappa+\sigma)X}}{(f-c\theta)e^{-fX} + (f+c\theta)e^{fX}}\right] \\ & + \frac{\beta^2 nc\sigma^2 I_0 e^{-X(\kappa+\sigma-f)}\cdot\phi\cdot(1-e^{-2fX})}{(f-c\theta)e^{-fX} + (f+c\theta)e^{fX}}, \quad . \quad . \quad (7) \end{aligned}$$

where

$$\phi = \frac{\sigma(nc-1) + \kappa(c-1)}{\kappa^2(1-c^2) + 2\kappa\sigma(1-\beta nc^2) + \sigma^2},$$

$$f = c\sqrt{\kappa(\kappa + 2n\beta\sigma)}, \quad \text{and} \quad \theta = n\beta\sigma + \kappa;$$

and the rejected light

$$\begin{aligned} j_{x=X} = j_u = {} & \frac{I_0(f^2 - c^2\theta^2)}{(\kappa+\sigma-c\theta)n\beta c}\left[\beta^2 nc\sigma\phi + \beta - 1\right] \\ & \times \left[\frac{e^{fX} - e^{-fX}}{(f-c\theta)e^{-fX} + (f+c\theta)e^{fX}}\right] \\ & + \beta\sigma I_0\cdot\phi - \frac{2fe^{-X(\kappa+\sigma)}\cdot\beta\sigma I_0\cdot\phi}{(f-a)e^{-fX} + (f+a)e^{fX}}. \quad . \quad . \quad (8) \end{aligned}$$

In practice, however, the expressions may be simplified by working with thick layers ; then

$$e^{(\kappa+\sigma)X} >> e^{-(\kappa+\sigma)X}, \quad e^{fX} >> e^{-fX}.$$

Further, in commercial opal glasses the absorption is generally small compared with the scattering, and thus $e^{(\kappa+\sigma-f)X}$ is also large.

Under these circumstances

$$i_u = \left[1-\beta-\frac{\beta^2 nc\sigma\{\sigma(nc-1)+\kappa(c-1)\}}{\kappa^2(1-c^2)+2\kappa\sigma(1-\beta nc^2)+\sigma^2}\right]\left[1+\frac{f-c\theta}{f+c\theta}\right]\times\frac{\sigma I_0 e^{-fX}}{\kappa+\sigma-c\sigma}, \quad . \quad . \quad . \quad . \quad (9)$$

and thus of the form $i_u = Ae^{fX}$, where A is constant for a given sort of glass.

Under the same conditions

$$j_u = \frac{I_0(f-c\theta)}{(\kappa+\sigma-c\theta)n\beta c}[\beta^2 nc\sigma\phi+\beta-1]+\beta\sigma I_0\phi. \quad (10)$$

Comparing equations (9) and (3) we find that, whether the incident light be a diffused or parallel beam, i_u may be expressed by the same exponential function of X after a certain optical thickness has been reached. Both i_u and j_u thus only differ by a constant coefficient in one case from those in the other case respectively.

For a parallel beam and a purely scattering emulsion the transmitted light reduces to

$$i_u = I_0\frac{1-\beta+cn\beta}{1+cn\beta X}, \quad . \quad . \quad . \quad . \quad (10')$$

which is again the same expression as for a diffuse incident beam, only the constant factor being modified.

7. By the aid of this theoretical work we can combine the observed quantities in *several* ways to give explicit expressions of $c\kappa$, $cn\beta\sigma$, and $\frac{\kappa}{n\beta\sigma}$.

The following explicit expressions have proved experimentally and theoretically to give the most accurate results :—

Write R = the limit of $\frac{j_u}{i_0}$ for an infinitely thick layer,

$$c\kappa = x \quad \text{and} \quad 2cn\beta\sigma = y.$$

Then we have

$$f = \sqrt{x(x+y)} \quad \text{and} \quad a = \left(x+\frac{y}{2}\right).$$

Further,

$$R = \frac{4(a-f)}{y},$$

and may be written

$$R = \frac{\sqrt{x+y}-\sqrt{x}}{\sqrt{x+y}+\sqrt{x}}.$$

Combining these expressions of f and R,

$$x = \frac{f(1-R)}{(1+R)}, \quad y = \frac{4fR}{1-R^2}, \quad \text{and} \quad \frac{x}{y} = \frac{(1-R)^2}{4R}, \quad (11)$$

which are the data wanted on the absorption and scattering of the milk glass.

8. *Preliminary application of the theory to the case of electric lamp bulbs.*—For this application we make several assumptions for the sake of simplicity, which may be summed up as follows :—

(1) The filament is exactly in the centre of the bulb, and it is very small, so that the light absorbed by it is negligible.

(2) The bulb is completely spherical; it has no neck.

(3) The heating effect on the filament, caused by the radiation rejected from the glass, is neglected.

(4) No account is taken of the effect of total reflexion at glass/air surfaces.

(5) The thickness of the glass is small compared with the radius of the bulb ; at any point the curvature may be neglected, and we can apply the equations for plane layers.

From the light emitted by the filament a quantity i_1 is directly transmitted by the glass and j_1 is rejected, the rest being absorbed by the glass. From the symmetry of the problem it is clear that the rejected light again falls on the glass with the *same* angular distribution as it was rejected by the glass.

Then, again, i_2 is transmitted and j_2 is rejected, and so on. Let

$$\frac{i_2}{j_1} = v \quad \text{and} \quad \frac{j_2}{j_1} = w.$$

The transmitted light is then

$$i_1 + vj_1(1 + w + \ldots) = i_1 + \frac{vj_1}{1-w} \quad . \quad . \quad . \quad . \quad (12)$$

As we may expect, the radius of the bulb has no influence on the transmitted light.

Substituting quantities of the order of those which are generally found in opal glasses, namely, $c=3{\cdot}0$, $\kappa=0{\cdot}05$, $n\beta\sigma=0{\cdot}5$, $n\beta=0{\cdot}015$, and $\beta=0{\cdot}0075$, we may approximately write

$$j_1 = \mathrm{I}_0\left(1-\sqrt{\frac{2\kappa}{n\beta\sigma}}\right)$$

for thick layers. Further

$$w = \frac{a-f}{cn\beta\sigma} \quad \text{and} \quad v = \frac{2fe^{-fX}}{(f+a)}$$

according to the theory for a diffused incident beam; we will use these expressions, although the incident beam is not quite diffuse, but has a definite distribution of the intensity according to the direction.

Substituting in (12), where i_1 is of the form $\mathrm{H}e^{-fX}$,

Light transmitted by bulb

Light emitted by filament

$$= \mathrm{H}e^{-fX} + \frac{(cn\beta\sigma - c\sqrt{2\kappa n\beta\sigma})2f \,.\, e^{-fX}}{(f+a)(cn\beta\sigma - a + f)}$$

$$= \mathrm{N}e^{-fX}.$$

The transmitted light in the case of bulbs may thus be expressed by the same exponential function of X as in the case of a plane sheet of opal glass.

Of course this is only a preliminary application of the theory. For further developments Milne's paper on the radiation of a planetary nebula will be found very useful *.

9. The terms "detour factor" and "effective path" of light in an emulsion may be discussed in terms of the above theory, and are capable of a precise definition.

By these terms, which are used by writers during recent years, is naturally meant that light waves traverse a longer path in a scattering medium than in a non-scattering medium of the same thickness.

* *Zeits. für Astrophys.* i. p. 98 (1930).

When a diffused incident beam i_0, or parallel incident beam I_0, falls on a layer, and the emitted light consists of a transmitted beam i_u and a rejected beam j_u, a quantity $i_0-(i_u+j_u)$ or $I_0-(i_u+j_u)$ respectively is converted into heat. The same quantity is absorbed in the layer, from which we imagine the scattering removed, when its thickness is ωX instead of X. We thus have the relations

$$i_0-(i_u+j_u)=i_0(1-e^{-c'\kappa\omega X})$$

and

$$I_0-(i_u+j_u)=I_0(1-e^{-\kappa\omega X})$$

respectively, where c' depends upon $\omega\kappa X$; thus the detour factor

$$\omega=\frac{1}{c'\kappa X}\log\frac{i_0}{i_u+j_u} \quad \text{or} \quad \omega=\frac{1}{\kappa X}\log\frac{I_0}{i_u+j_u}$$

respectively.

It is of importance to remember *that ω is not a constant;* it depends, *e. g.*, upon the concentration etc.

An example of the confusion which may arise if these terms are not carefully defined may be found in the work of Gehlhoff and Thomas*. This may be expressed as follows:—for a strongly absorbing opal glass (i_u+j_u) is found, and for the continuous phase of it κX, so that ω may be determined. The determination is now repeated on ordinary opal glass, and the authors apparently accepting that the "detour factor" should be constant, but finding that it increases, explain the effect by the absorption of light by the disperse phase. Their experiment, however, does *not* prove this.

It is not easy to express the "absorption" measured by them in the symbols used by us. Without attempting an exact description of the facts, we will suppose that the lamp bulb absorbs and scatters the incident light just as a milk-glass plate illuminated by a *perfectly diffuse* beam. Then from the above formulæ it follows directly that the "mean path" increases with decreasing κ.

Let us, for example, take $X=1$, $cn\beta\sigma=1$, and $c=3$. In general $i_u \ll j_u$, and thus

$$\omega=\frac{1}{c'\kappa X}\log\frac{cn\beta\sigma}{c(n\beta\sigma+\kappa)-f}$$

(see formulæ (2)).

* G. Gehlhoff and M. Thomas, "Zur Frage der Lichtabsorption von Opalglas," *Zeits. für Techn. Phys.* p. 172 no. 5 (1928).

With the aid of Table III. we find, by successive approximation,

$\omega = 5{\cdot}45$ for $c\kappa = 0{\cdot}2$ and $\omega = 99{\cdot}00$ for $c\kappa = 0{\cdot}02$.

The detour factor has thus increased by a factor 18!

Another example of confusion may be found in the work of Lax, Pirani, and Schönborn *. They measure $I_0 - (i_u + j_u)$ in order to express "the mean path" ωX as a function of i_u, j_u, and X. They find that ωX increases more and more rapidly with increasing thickness of the layer. According to the theory, however, ωX should become constant with increasing thickness of the layer, for $i_u \to 0$, $j_u \to$ constant, and thus $\frac{I_0}{i_u + j_u} \to$ constant.

That they find a different result is probably to be attributed to lack of accuracy in their determination of $I_0 - (i_u + j_u)$, a lack which the authors themselves admit.

10. *Polarization of the Scattered Light.*—In the foregoing theoretical work we have paid no attention to the fact that the light scattered by a particle is polarized. By successive scattering in optically thick layers the polarization will for the most part be averaged out over the various directions, therefore it is also common in the theory of the sun to neglect the effect of the polarization; this is done with the more confidence that the light from the disk of the sun is nowhere appreciably polarized.

Any small effect of polarization would in our case, together with that of the anisotropy of scattering, be sufficiently included in the quantities n, c, β, and σ.

Theory Applied to the Measurements on Thick Layers.

We have found that scattering and absorption act independently of each other so long as their effect on the directly transmitted light is investigated. However, they are intimately connected in their influence upon the repeatedly scattered light. A systematic series of measurements has been made to determine how the transmission of an emulsion varies as a function of the scattering and of the absorption coefficients, and to test the formulæ previously derived.

* *Loc. cit.*

The alcoholic solution of mastic contained 160 gr. per litre, the standard emulsion of "concentration 100" contained 8 gr. mastic per litre; it was coloured with acid fuchsine, and the measurements were made at λ 520 $\mu\mu$ with a parallel incident beam (lamp overcharged to 18 volt). We may assume that the particles were big. The results are plotted in fig. 12; each curve corresponds to definite

Fig. 12.

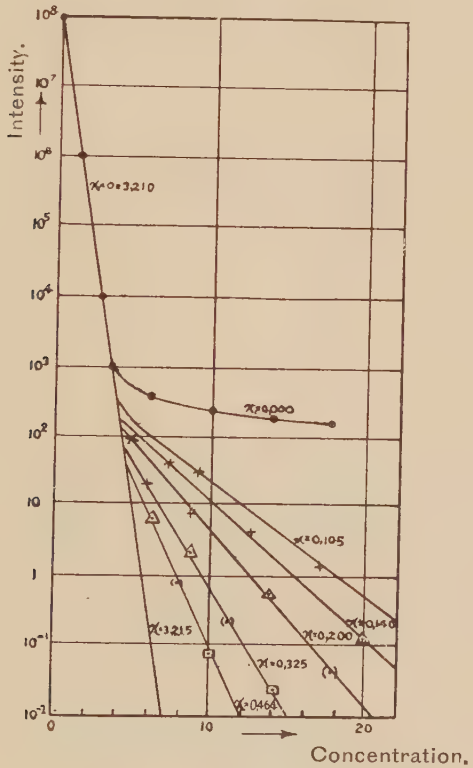

values of κ and σ, these being chosen so that their sum is the same ($=3{\cdot}215$) for all the curves. It is clear that in their first part all the curves coincide with the straight line for the directly transmitted light, corresponding to $e^{-(\kappa+\sigma)X}$. Further on the curves differ more and more, according to the proportion between the absorption and the scattering.

1. We can first test the theoretical expression for i_u (formula 10′) in the case of pure scattering :

$$i_u(1+\beta nc\sigma X) = 1-\beta+\beta nc = \text{constant}.$$

Let us assume that for thick layers i_u, the total radiation transmitted given by the formula is proportional to $i_u(0°)$, the radiation which emerges normally from the boundary ; then $i_u = Ki_u(0°)$, where K is a constant. With the aid of $\sigma = 2{\cdot}88$, and taking $n\beta c = 0{\cdot}085$ (see p. 827), we find that $(1+\beta nc\sigma X)i_u(0°)$ is indeed experimentally constant (see Table IV.).

Table IV.

X.	$i_u(0°)10^6$.	$(1+\beta nc\sigma X)$.	$(1+\beta nc\sigma X)i_u(0°)10^6$.
8.....	3·05	2·96	9·02
10.....	2·60	3·45	8·98
12.....	2·30	3·94	9·06
15.....	1·93	4·67	9·02
17.....	1·75	5·16	9·04
20.....	1·52	5·91	9·00

Theoretical considerations make it plausible that i_u is really proportional to $i_u(0°)$. This result was already reached by Schwarzschild for *small particles* and *pure scattering*, for he showed that in this case the distribution of the radiation over the different directions becomes constant as soon as a certain thickness of layer is reached. For *small particles* and a mixture of *scattering and absorption*, $\frac{\kappa}{\sigma}$ being $<\frac{1}{3}$, the author derived the same conclusion from Spykerboer's calculations *. For *large particles* we must take the anisotropy of the scattering into consideration by putting

$$\left.\begin{aligned} \sigma(\vartheta) &= A\cos^m\vartheta \quad \text{for } 0<\vartheta<\frac{\pi}{2}, \\ \sigma(\vartheta) &= 0 \qquad\quad \text{for } \frac{\pi}{2}<\vartheta<\pi. \end{aligned}\right\}$$

* See Dissertation, p. 85 (Utrecht, 1930).

If we take $m=6$ this law of scattering agrees roughly with the diagrams of Blumer * for particles of the size of those generally present in opal glasses.

The value of A is easily determined by the condition

$$\sigma = 2\pi \int_0^{\frac{\pi}{2}} A\cos^6\vartheta . \sin\vartheta . d\vartheta = \frac{2\pi}{7} A ;$$

so the law of scattering is here

$$\left.\begin{aligned} \sigma(\vartheta) &= \frac{7\sigma}{2\pi}\cos^6\vartheta, \\ \sigma(\vartheta) &= 0, \end{aligned}\right\}$$

In the physics of the sun it is common to calculate the light scattered normally to the layer from the consideration that for isotropic scattering a fraction $\frac{\sigma . d\omega}{4\pi}$ of the incident light is scattered in this direction by every volume element. The emergent radiation is then given by

$$i_u(0^\circ) = \int_0^x \frac{i+j}{4\pi} . e^{-\sigma x} . d\omega . \sigma . dx. \quad . \quad . \quad (13)$$

In our case, where the scattering is strongly anisotropic, we do not know the exact values of i and j in every point of the layer. Let us describe the angular distribution of the radiation in the layer by the first term of a development in spherical harmonics,

$$i(\theta) = a + b\cos\theta,$$

and from the definitions of i and j we have

$$a = \frac{i+j}{4\pi} \quad \text{and} \quad b = \frac{i-j}{2\pi}.$$

Each element of volume scatters along the normal, per unit solid angle, the radiation

$$2\pi \int_0^{\frac{\pi}{2}} A\cos^6\theta(a + b\cos\theta)\sin\theta . d\theta.$$

* *Loc. cit.*

Integrating, and substituting the above values for A, a, and b, we find

$$\frac{\sigma}{2\pi}[(\tfrac{1}{2}(i+j)+\tfrac{7}{8}(i-j)].$$

Each elementary volume may be regarded as a secondary source, and the total transmitted light is thus

$$i_u(0^\circ) = \frac{\sigma}{2\pi}\int_0^X [\tfrac{1}{2}(i+j)+\tfrac{7}{8}(i-j)]e^{-\sigma x}\,.\,dx,$$

where i and j are simple functions of x.

For pure scattering a parallel beam, thick layers, and small values of β follows

$$i_u(0^\circ) = \frac{11\,I_0\left(1+\frac{19}{11}n\beta c+\frac{8}{11}n^2\beta^2c^2\right)}{16\pi(1+n\beta c\sigma X)}.$$

In general, for a law of scattering $\sigma(\theta) = A\cos^m\theta$, we should find

$$i_u(0^\circ) = \left(\frac{1}{2}+\frac{m+1}{m+2}\right)\frac{I_0\left(1+\frac{19}{11}n\beta c+\frac{8}{11}n^2\beta^2c^2\right)}{2\pi(1+\beta nc\sigma X)}.$$

We thus have $i_u = Ki_u(0^\circ)$, which justifies our hypothesis.

2. We will assume now that similarly a limiting intensity distribution is reached in the case of simultaneous *scattering and absorption by large particles*. Let us test then formula (9), giving the intensity of the transmitted light.

Fig. 12 shows that the effect of absorption is much more pronounced in the case of thick layers than in the case of thin layers. (The lowest point ⊡ in the figure shows the greatest reduction of intensity, namely 10^{-10}, measured by the above-described arrangement for a parallel incident beam.)

From formula (9) we have concluded that for thick layers i_u is nearly an exponential function, so the transmission curves *must approximate to straight lines*. This important result is indeed confirmed by our experimental data.

Let us see how closely these straight lines are described by theory. We cannot expect that the formulæ will give the exact position of the straight line for every

emulsion, for we have not considered the repartition of the radiation over the different directions, and so, for thick layers, the right absolute value for $i_u(0°)$ cannot come out. But *the slope* of the curves must be correct, because from a certain thickness of layer the distribution of the intensity remains invariable.

These slopes give us the values for $f = c\sqrt{\kappa^2 + 2n\beta\sigma}$, which are written down in column 4 of Table V.

To test if these values conform to theory we multiply every line of the two last columns by numbers which render the coefficients of c^2 all equal; then, plotting f^2 against $n\beta c^2$, we find that the points lie satisfactorily on a straight line. This is again a confirmation of the theory.

TABLE V.

Series.	x.	σ.	f(exp.).	$c^2(x^2+2Xn\beta\sigma)$.
1.....	0·13	2·88	0·43	$c^2[0·0169+n\beta(0·75)]$
2.....	0·155	2·88	0·475	$c^2[0·024 +n\beta(0·895)]$
3.....	0·195	2·88	0·57	$c^2[0·038 +n\beta(1·125)]$
4.....	0·30	2·88	0·78	$c^2[0·09 +n\beta(1·73)]$

From the slope of the line we obtain $n\beta c^2 = 0·164$; from the intersection with the axis of ordinates $c = 1·93$. (In the case of very small values of $\frac{\kappa}{\sigma}$ the coefficient of $n\beta c^2$ is generally much bigger than that of c^2, and the latter may be neglected, thus simplifying the work.) The straight lines of fig. 12 have been drawn from the values of f, putting for all the lines $n\beta c^2 = 0·164$ and $c = 1·93$. They are seen to give an excellent representation of the experiments. To check the values of the constants along other lines would be difficult, but we may be satisfied with their plausibility; this is amply confirmed by our subsequent work, now to be described.

3. For thick layers the variation of the transmission with the optical thickness of the layer has been found experimentally *to be the same for a parallel as for a diffused incident beam.*

The following figure (13) shows this similarity. Curves *a* and *b* have been obtained from measurements of the transmitted light in the case of a parallel incident beam, whereas A and B have been obtained by measuring the transmission of the *same* emulsion respectively in the case of a diffused incident beam. We note that A is parallel to *a* and B to *b* (except in the very first parts). This is exactly what we had deduced from our theory (p. 818). The advantage of a diffused incident beam is, however, the greater intensity of the incident beam obtainable, thus making it possible to follow the curves over much

Fig. 13.

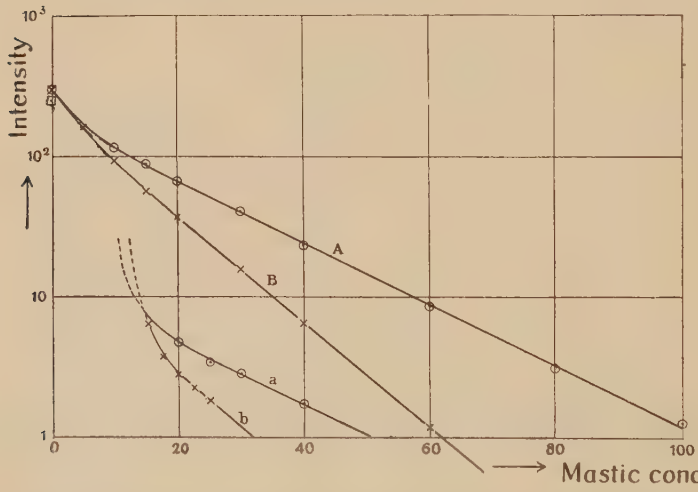

greater ranges. For emulsion A the value of $\kappa = 0{\cdot}00885$ and $\sigma = 0{\cdot}829$; for emulsion B $\kappa = 0{\cdot}02215$ and $\sigma = 0{\cdot}793$.

Subsequent determinations of f were therefore always made with a diffuse incident beam; one plate of the specimens to be measured is used to obtain the distribution of radiation among the different directions which corresponds to that particular kind of diffusing medium. Before this diffuser we put a second and then a third plate of the same specimen, in good optical contact with each other. The distribution of the intensity has reached its limiting value after the first plate; we may determine now the fractions transmitted by the second and third plates, and from these we calculate f.

4. *Criticism of the Method of Channon, Renwick, and Storr* *.—In this work the authors study the behaviour of fully diffused light in scattering media, and from their work follows a method of determining the Schuster constants κ and $\bar{\sigma}$. Their starting-point coincides with that in this work, namely, that "part of the light is rejected, part extinguished, and part transmitted by a scattering material." Their theoretical work, however, involves a number of mathematical transformations which are difficult to interpret physically. We shall here only summarize the necessary theoretical formulæ for the most important remarks. After calculating the light transmitted by two plates in optical contact by a method similar to that already adopted by Stokes † their formula $p^2-O_1^2-O_2$ follows for three *similar* plates in optical contact, where p=fraction of the incident light rejected by one plate, while O_1 and O_2 are the ratios: transmission by one plate divided by transmission by two and three plates respectively. Having in this way determined p for a sheet of glass it is then used as photometer diffuser.

A second relation

$$R_1^2(O_1^2-p^2)+R_1(O_2-1)-(O_1^2-O_2)=0$$

is then used, where R_1=fraction of the light rejected by *one sample* of glass. Further, the value of R is used for an infinitely thick layer, *i.e.*,

$$\frac{O_1R_1}{O_1-(1-pR_1)e^{-\gamma}}.$$

In these equations O_1 and O_2 are the ratios: transmission by photometer diffuser divided by the transmission by the diffuser plus one and two plates respectively. Comparison with the Schuster constants κ and σ shows that

$$R=\frac{\sqrt{\kappa+\sigma}-\sqrt{\kappa}}{\sqrt{\kappa+\sigma}+\sqrt{\kappa}} \quad \text{and} \quad \gamma^2=\bar{\kappa}(\bar{\kappa}+\bar{\sigma}).$$

* H. J. Channon, F. F. Renwick, and B. V. Storr, Proc. Roy. Soc. A, xciv. p. 222 (1912).

† G. Stokes, Proc. Roy. Soc. ii. p. 545 (1860–62)

It is very easy to see that their γ and R are the same as our f and $\left(\frac{j_u}{i_0}\right)_{X\to\infty}$ respectively, expressed in the Schuster constants.

Further, their method of determining γ experimentally corresponds to our determination of f from measurements of the transmission by one and two thick layers respectively. Their method of determining ρ is, however, useless. Choose, *e. g.*, to determine ρ for concentration 20 of fig. 13 (A). The experimental points give $\rho=1{\cdot}05$ and the *curve* gives $\rho=0$, both impossible values. The slightest deviation of the points measured from the theoretical curve makes the determination quite wrong. Further experiments have shown that the method may only be used with some profit in the case of thin layers of glass with a small coefficient of absorption *.

Fig. 14.

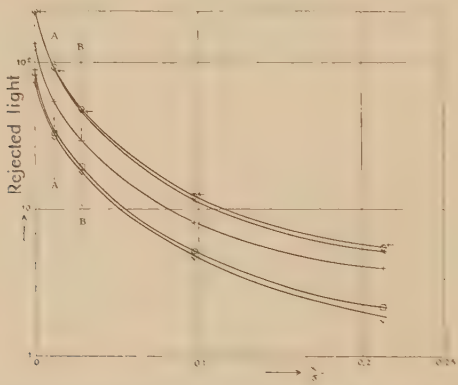

5. *Experimental Determination of the Light rejected by very Thick Layers as a Second Relation between the Unknown Quantities.*—We have now reached a point where we feel that it will be possible to determine $c\kappa$ and $cn\beta\sigma$ individually when a second relation between these quantities is determined with the same order of accuracy as that of $f=\sqrt{c\kappa(c\kappa+2cn\beta\sigma)}$. This second relation has been sought and found in *directly* determining the rejection by very thick layers.

Preliminary measurements of the rejection were made with a parallel incident beam. In fig. 14 the points ·←,

* Dissertation (Utrecht, 1930).

⊙, ×, and − respectively follow from measurements of the rejection by the same set of emulsions under angles of 65°, 60°, 32°, and 5° respectively at the given values of $\frac{\kappa}{\sigma}$ (taking $\frac{\kappa}{\sigma}=0$ for the uncoloured mastic).

The points A and B correspond to emulsions A and B respectively (see p. 828).

The curves through the points □ and ▽ represent the rejection by the above emulsions under 0° and 40° respectively in the case of diffused incident light. It is clear that all these curves are nearly the same; by a translation in a vertical direction they could be brought into coincidence. We may write R = rejection (emulsion or glass), ÷ rejection (perfect white reflecting surface). From the work of Henning and Heuze* we can take the total rejection by a fresh layer of magnesium oxide as 95·3 per cent., and we then find R (uncoloured mastic) = 0·77 (see Table VI.).

The average of *all* the rejections measured for emulsions A and B give $R_A=0{\cdot}312$ and $R_B=0{\cdot}17$. By the further aid of $f_A=0{\cdot}0515$ and $f_B=0{\cdot}087$ (see fig. 13) we obtain, by substitution in the formula,

$$(a)\quad c\kappa=0{\cdot}027 \quad\text{and}\quad cn\beta\sigma=0{\cdot}0354,$$

$$(b)\quad c\kappa=0{\cdot}0615 \quad\text{and}\quad cn\beta\sigma=0{\cdot}0305.$$

Using the known values of κ and σ (see p. 828) we obtain

$$(a)\ c=3{\cdot}05,\quad n\beta=0{\cdot}014,$$

and

$$(b)\ c=2{\cdot}78,\quad n\beta=0{\cdot}0138.$$

The values of c and $n\beta$ may be corrected, remembering that the mastic itself has also a slight absorption: taking $n\beta=0{\cdot}014$ for the "uncoloured" mastic emulsion for which R = 0·77, we find $\frac{\kappa}{n\beta\sigma}=0{\cdot}0346$. The corrected values are

$$(a)\ c=2{\cdot}92 \quad\text{and}\quad n\beta=0{\cdot}01465,$$

$$(b)\ c=2{\cdot}735 \quad\text{and}\quad n\beta=0{\cdot}0141.$$

We see that with increasing absorption the value of c decreases more rapidly than that of $n\beta$; this is generally

* F. Henning and W. Heuse, *Zeit. für Phys.* x. p. 111 (1922).

case (see §§ 5, 6, and 7). After the examination of the two emulsions with different concentrations of the dye we will compare a complete series with increasing values of $\frac{\kappa}{\sigma}$ both for large and small particles. Firstly, two emulsions G and K were made. Emulsion G (big particles) was made by pouring an alcoholic solution of 225 gm. of mastic per litre into aqua dest., the emulsion (of concentration "100") contained 5 gm. of mastic per litre; the value of σ, determined with a parallel incident beam, was 1·100. Emulsion K (small particles) was made by pouring a solution of 45 gm. of mastic per litre into aqua dest., the emulsion (of concentration "100") contained 17 gm. of mastic per litre; the value of σ was 1·465. The above mastic densities are already corrected for the mastic which does not go into emulsion, but coagulates, on pouring the solution into water.

The mean radii of the particles have been estimated with a Zeiss microscope, and were G 0·335 μ and K 0·245 μ. These radii are quite comparable with those of the particles in milk glass, which were found to be of the order 0·2 to 0·5 μ. The emulsions were then coloured with known quantities of acid fuchsine for which $\kappa X = 34{\cdot}3$ had been previously determined; the different values of κ and σ for the various coloured emulsions G(α), G(β)..... K(α), K(β)..... are given in Table VI. (For uncoloured mastic we have for simplicity put $\kappa = 0$.)

In the same table are also given the values of $j_u \cdot d\omega$ under 25° with the normal to the cell, for optically very thick layers of emulsion, of concentrated fuchsine, and a fresh thick layer of magnesium oxide, in the case of diffused incident light. (The value of $j_u \cdot d\omega$ for concentrated fuchsine gives a measure of the stray light which is to be subtracted from all other values of $j_u \cdot d\omega$.) The values of R have been calculated from these corrected values, taking R(MgO) = 0·953 *, and are also given in the table.

In Table VII. are set out the transmission in an arbitrary scale for diffused incident light, and also the corresponding values of f, for the various emulsions.

Substituting in our formulæ the above values of R and f, we find the values of $c\kappa$ and $cn\beta\sigma$ which are given in Table VIII.

* See F. Henning and W. Heuze, *Zeits. für Phys.* x. p. 111 (1922).

Dividing these quantities by κ and σ respectively (see Table VI.) we find the values of c and $n\beta$ also given in

TABLE VI.

Optically very thick layers.	κ.	σ.	$\frac{\kappa}{\sigma}$.	$j_u d\omega$.	R.
Magnesium oxide	..	..		125·7	0·953
Uncoloured mastic (G).	0·0	1·1	0·0	102·0	0·770
Acid fuchsine	34·3	0·0	∞	1·7	0·0
G(α)	0·00377	1·09	0·00346	52·7	0·392
G(β)	0·01105	1·065	0·0104	35·0	0·255
G(γ)	0·0346	0·99	0·0350	14·3	0·0970
G(δ)	0·0773	0·852	0·0905	6·2	0·0346
G(ε)	0·137	0·66	0·208	3·4	0·0131
Uncoloured mastic (K).	0·0	1·465	0·0	102·0	0·770
K(α)	0·00377	1·45	0·00260	70·7	0·530
K(β)	0·0163	1·395	0·0117	46·0	0·340
K(γ)	0·0522	1·24	0·0420	24·5	0·175
K(δ)	0·0980	1·045	0·0937	11·5	0·0885
K(ϵ)	0·1535	0·81	0·1895	5·83	0·0317
K(η)	0·1975	0·62	0·318	3·21	0·0116

TABLE VII.

ulsion.	G(α).	G(γ).	G(ε).	K(β).	K(γ).	K(ε).
	X. $i_u d\omega$.	X. $i_u d\omega$.	X. $i_u d\omega$.	X. $i_u d\omega$.	X. $i_u d\omega$.	X. $i_u d\omega$.
	37·5 46·0	12·5 53·0	6·25 64·0	12·5 45·00	8·3 34·000	8·125 20·00
	50·0 30·0	25·0 14·2	12·50 15·0	25·0 10·00	16·6 6·100	12·50 5·20
	75·0 13·2	37·5 3·6	18·75 3·5	37·5 2·75	25·0 1·420	18·75 0·65
	100·0 5·4	50·0 1·15	25·00 0·9	50·0 0·90	33·3 0·365	25·00 0·12(?
$f=$	0·0336	0·111	0·218	0·085	0·164	0·321

Table VIII. These values of c and $n\beta$ must still be corrected for the fact that $\kappa=0$ for an uncoloured mastic emulsion.

From R (mastic alone)=0·77 we find $\frac{\kappa}{n\beta\sigma}=0{\cdot}0346$. Using the values of $n\beta = 7{\cdot}3 \cdot 10^{-3}$ and $18{\cdot}3 \cdot 10^{-3}$ respectively (taken from the emulsion with the least quantity of dye, because $n\beta$ for the uncoloured mastic is not known), the above values of c and $n\beta$ have been been corrected and again corrected with the new values

Table VIII.

Emulsion.	$c\kappa$.	$cn\beta\sigma$.	$\frac{\kappa}{n\beta\sigma}$.	c.	$n\beta\times10^3$.
G(α)	0·0147	0·0312	0·472	3·90	7·3
G(γ)	0·0915	0·0218	4·20	2·65	8·3
G(ϵ)	0·212	0·0057	37·20	1·55	5·6
K(β)	0·0419	0·0656	0·64	2·57	18·3
K(γ)	0·115	0·0595	1·95	2·21	21·5
K(ϵ)	0·300	0·0203	14·8	1·95	12·8

Table IX.

Emulsion.	$c\kappa$.	$cn\beta$.	c.	$n\beta\times10^3$.
G(α).....	0·0147	0·0312	3·60	8·0
G(γ).....	0·0915	0·0218	2·62	8·4
G(ε).....	0·212	0·0057	1·54	5·6
K(β)	0·0419	0·0656	2·42	19·5
K(γ).....	0·115	0·0595	2·17	22·0
K(ε).....	0·300	0·0203	1·95	13·0

of c and $n\beta$, and so on *. In Table IX. we find the definitive values of c and $n\beta$ for the various emulsions.

From these numbers, we find for the uncoloured emulsion G that $\kappa/\sigma = 0{\cdot}000275$; and for the uncoloured emulsion K, 0·00066.

Clearly the slight effect of ignoring the absorption of the mastic itself is greater in the case of the less coloured emulsions.

* See also Dissertation, xi. (Utrecht, 1930).

These values of c and $n\beta$ appear quite plausible; they cannot, however, be checked quantitatively.

It is therefore of importance to discuss the values of c and $n\beta$ shortly.

6. *Short Discussion of the Values of c.*

For the transmitted beam the value of $c=c_1$ must be smaller than 2; this holds as well in the case of a parallel as in the case of a diffused incident beam. The value of c_1 is not constant throughout the layer, but it probably tends to a constant as the optical thickness of the layer is increased. It is further clear from considerations of the angular distribution of the light* that c_1 decreases with increasing κ/σ.

TABLE X.

τX.	$\frac{j(\tau X, 0{\cdot}5\pi)}{j(\tau X, 0)} = \nu_1$.	$\frac{j(\tau X, 0{\cdot}3\pi)}{j(\tau X, 0)} = \nu_2$.	c_2.	$\frac{j(0{\cdot}5\tau X, 0{\cdot}5\pi)}{j(0{\cdot}5\tau X, 0)} = \nu_3$.	$\frac{j(0{\cdot}5\tau X, 0{\cdot}3\pi)}{j(0{\cdot}5\tau X, 0)} = \nu_4$.	c_2.
0·0	∞	2·0		∞	2·0	
0·01	102·0	2·0	6·8	201·0	2·0	10·0
0·10	11·4	1·91	3·4	21·5	1·05	4·35
1·0	2·2			3·3		
3·0	1·39	1·19	2·05	1·8	1·0	2·20
9·0	1·10			1·2		
∞	1·0	1·0	2·0	1·0	1·0	2·0

In the case of the rejected beam, however, $c=c_2$ is generally greater than two. We can obtain an idea of its value *inside the layer* for the case of small particles by the approximation of Schwarzschild for pure scattering, namely,

$$j(\sigma x, \theta) = \frac{\sigma x + 0{\cdot}5 - \cos\theta}{\sigma x + 1} + \frac{\cos\theta - 0{\cdot}5}{\sigma x + 1} \cdot e^{-\sigma x \sec\theta}.$$

Using this formula the values of ν_1, ν_2, ν_3, and ν_4 in Table X. are easily calculated. The corresponding values of c_2 have been calculated from a set of these ν values.

The fact that $\frac{\nu_3}{\nu_1} > 1$ shows that on its way through

* J. Spykerboer, Dissertation (Utrecht, 1917).

the layer the rejected beam is weakened more rapidly in directions making small angles with the normal than under bigger angles; it is spreading more and more. What fraction of all the light at a point in the layer consists of transmitted, and what part of rejected light? From the differential equations it is easy to prove that at each point in the layer $i>j$, and that the ratio i/j increases at each point in the layer with increasing κ/σ till $i/j=\infty$ for $\kappa/\sigma=\infty$. We shall now assume that the experimental value of our mean c will lie nearer to c_1 or c_2 according as the transmitted beam is much or a little bigger than the rejected beam, *i. e.*, according as κ/σ is big or small. For $\sigma=0$ we have $c=c_1$, which confirms these assumptions for the limiting case. We can now understand why c decreases with increasing κ/σ. Two factors play a role: firstly, $c_1\to 1$ with increasing κ/σ, and, secondly, the ratio i/j increases at all points in the layer with increasing κ/σ. Here, of course, we make the further assumption that the change of the angular distribution of the weaker rejected beam with κ/σ has not sufficient influence on the value of c to balance the decrease due to the above-mentioned causes.

From our experimental results it is also clear that c is bigger for big than for small particles in the case of equal values of κ/σ. It seems plausible that this is due to the increase of c_2, while c_1 is less dependent upon the size of the particles. This is confirmed by an examination of the radiation diagrams.

7. *Discussion of the Experimental Values of $n\beta$.*

According to Mie * and others the radiation diagrams for spherical particles of the above order take very irregular forms and show a very much smaller scattering backwards than forwards, *i. e.*, β is very small. Graphical integration of the results of Blumer † show that $\beta<n\beta$ for any angular distribution of the incident light. The two limits of $n\beta$ are thus given by $\beta< n\beta< 0{\cdot}5$. We can take these limits to hold in the case of uneven particles as well. It is further clear that $n\beta$ is not only dependent upon β, but is also intimately connected with the *form* of the radiation diagram. Let the value of $n\beta$ for the transmitted light

* G. Mie, *Ann. d. Phys.* [4] xxv. p. 377 (1908).

† H. Blumer, *Zeits. für Phys.* xxxii. p. 119 (1925), no. 2; xxxviii. p. 304 (1926), nos. 4 & 5.

be $n_1\beta$, and for the rejected light $n_2\beta$. From the above work it is clear that $n_1\beta$ is smaller than $n_2\beta$. Similarly to the case of c we have in our theory taken $n_1\beta = n_2\beta$, although $n_1\beta$ and $n_2\beta$ as c_1 and c_2 are different and vary from point to point in the layer. Let us in the same way assume that the experimental value of $n\beta$ lies between the final values in the layer of $n_1\beta$ and $n_2\beta$, and that it lies nearer to $n_1\beta$ or $n_2\beta$ according as the transmitted beam is much or a little stronger than the rejected beam. Just as $c \to c_1$ with increasing κ/σ, the value of $n\beta \to n_1\beta$ with increasing κ/σ, because the rejected beam becomes weaker and weaker relatively to the transmitted beam with increasing κ/σ. Further, from considerations of angular distribution $n_1\beta$ decreases with an increase in κ/σ until, for $\kappa/\sigma = \infty$, we have the final value of $n_1\beta = \beta$*.

This expected decrease of $n\beta$ with an increase in κ/σ is, generally speaking, confirmed by the experiments (see Table IX.). That the experimental values of $n\beta$ increase slightly as κ/σ is increased from a *small* value to greater values (and then decrease) suggests that the proportion of the rejected light which is propagated under great angles with the normal increases as κ/σ is increased, and that at first this increase of $n_2\beta$ counterbalances the influence of the decreasing $n_1\beta$.

Let us examine now the influence of the size of the particles upon the value of $n\beta$.

The bigger the particles the smaller is β, and thus the smaller must be $n\beta$ for the same value of κ/σ (this strong effect is compensated only to a small extent by the change in the angular distribution of the weaker rejected beam with the size of the particles). This is indeed confirmed by the experimental values found for $n\beta$ (see Table IX.).

8. *Comparison of the Results obtained by a Balance, a Microscope, and a Spectrophotometer.*

We have already mentioned† the use of the values of $n\beta$ in Table IX. for approximately calculating

$$\left(\frac{\kappa_1}{\sigma}\right)_g = 0{\cdot}000275 \quad \text{and} \quad \left(\frac{\kappa_1}{\sigma}\right) = 0{\cdot}00066,$$

* One might therefore obtain a rough estimation of β by measuring $n\beta$ for thick layers for which κ/σ is large.

† See p. 834.

where κ_1 is the absorption coefficient of the uncoloured mastic, g and k referring to the big and small particles respectively. Using further the values of $(\sigma)_g$ and $(\sigma)_k$ as given in Table VI. we find $\frac{(\kappa_1)_g}{(\kappa_1)} = 0{\cdot}31$. The absorption by the mastic particles is independent of the size of the particles, and the coefficient of absorption is simply proportional to the mastic density. Now the ratio of the densities of g and k (for equal arbitrary concentrations) is indeed 0·295 (see p. 832). The coefficient of scattering is, however, dependent upon the size of the particles. Assuming that for particles of this size, just as for very small particles (Rayleigh), $\sigma = As r^3$, where A is a constant, s the concentration of the mastic, and r the radius of the particles, we obtain $\frac{s}{s'} = \frac{\sigma r'^3}{\sigma' r^3}$, where s, σ, and r refer to the big, and s', σ', and r' to the small particles. Substitution of the experimental data gives $\frac{s}{s'} = 0{\cdot}293$. The agreement between the results obtained along the three different rough methods is thus remarkably close.

9. *Application of the Work to various kinds of Opal Glasses.*

We propose now to determine κ and σ for a set of technical milk glass plates by the same method which has proved to work for emulsions. By the description of this process the whole succession of the operations to be performed will become clear. The specimens examined had an area of about 50 cm.^{2} and the measurements were made with the apparatus for diffused incident light, optical contact between different sheets of a specimen being obtained with cedar-wood oil. Table XI. gives an idea of the general appearance of the different specimens.

We first measure with diffuse incident light:

(*a*). *The light transmitted* by one sheet and two and three sheets in optical contact respectively; the results are set out in Table XII., the units of intensity at the various wave-lengths being arbitrary.

(*b*). These intensities have been plotted against the number of sheets on single logarithmic paper in the usual

TABLE XI.

Sort of glass.	Average thickness in mm.	Rejected light.	Transmitted light.
1.....	1·95	White.	White.
2.....	2·73	White, but pale greenish when seen beside sort 1.	Beside sort 1 pale greenish-yellow.
3.....	3·63	White, but pale light blue when seen beside sorts 2 and 3.	Bluish.
4.....	2·26	Pronounced greenish-yellow.	Deeper greenish-yellow than the rejected light.

TABLE XII.

Sort of glass.	λ in $\mu\mu$.	Transmitted light. No. of sheets. 1.	2.	3.	f per mm. thickness.	Rejected light. $j_u d_\omega$.	R.	Results. $c\kappa$ per mm. thickness.	$cn\beta\sigma$ per. mm. thickness.	$\frac{\kappa}{n\beta\sigma}$.
1.....	617	53·0	19·2	6·2	0·532	162	0·716	0·088	1·56	0·0565
	537	52·0	19·2	6·2	0·531	174	0·750	0·076	1·83	0·0415
	498	47·0	14·0	4·8	0·583	174	0·760	0·0795	2·10	0·0380
2.....	617	35·0	11·0	3·7	0·402	155	0·683	0·076	1·03	0·0740
	537	40·0	14·4	6·0	0·354	179	0·771	0·046	1·36	0·0340
	498	31·5	12·0	4·7	0·345	172	0·750	0·049	1·19	0·0415
3.....	617	18·8	2·5	0·7(?)	0·534	152·5	0·673	0·104	1·32	0·0790
	537	26·0	6·2	1·55	0·386	176	0·760	0·0525	1·40	0·0375
	498	21·5	7·2	2·0	0·300	176	0·766	0·040	1·12	0·0355
4.....	617	26·0	3·8	0·8(?)	0·838	89	0·394	0·365	0·785	0·465
	570	52·0	13·0	3·65	0·608	126	0·538	0·185	0·93	0·200
	537	64·0	19·0	6·4	0·488	130	0·560	0·140	0·80	0·175
	498	39·0	8·8	2·4	0·590	116	0·505	0·195	0·80	0·245
Magnesium oxide.	617					216	(0·953)			
	570					223	(0·953)			
	537					221	(0·953)			
	498					219	(0·953)			

way, and the slopes of the lines through the points have given the corresponding values of f per mm. thickness, also set out in the table.

(*c*). Measurements of *the light rejected* under 25° with the normal to the sheet, by a fresh thick layer of magnesium oxide and by very thick layers of the four glasses respectively are also given in an arbitrary scale for the same wave-lengths. The corresponding values of R in the table follow directly on taking $R(MgO)=0{\cdot}953$.

(*d*). Substituting in our formulæ (11) the above values of f and R we obtain the values of $c\kappa$ and $cn\beta\sigma$ per mm. thickness which are given in the "results" column of Table XII. Finally, the technically important quantities $\frac{\kappa}{n\beta\sigma}$ follow directly from the known values of R, thus experimentally a simple matter.

Comparing these results with those for the emulsions we note: whereas σ and c generally decrease with increasing wave-length relative to the particles. $n\beta$ generally increases, and so $cn\beta\sigma$ increases or decreases according as the former or latter influence plays the chief part.

For the white glasses the coefficient of absorption is greater for red light than for the other colours; the greenish-yellow glass absorbs more light of all colours than the white ones, absorbing the least at $\lambda=537\mu\mu$.

The quantities $\frac{\kappa}{n\beta\sigma}$ agree with the colours which the eye observes as rejected by the glasses.

The colour of the transmitted light depends upon the individual values of $c\kappa$ and $cn\beta\sigma$; these colours, as calculated from the values of $c\kappa$ and $cn\beta\sigma$ in the table, are those actually observed.

10. *The comparatively small Coefficients of Absorption, $c\kappa$, for the Glass of Philips' Argenta Bulbs and the Opal Glass Bulbs manufactured at Leerdam.*

Although our theory applies to *plane* sheets of glass of infinite area, we may use it to determine the coefficients for segments of bulbs provided the curvature is not too big. The coefficients have been determined with the apparatus for diffused incident light for bulbs of the above types of 8 cm. diameter (the Leerdam bulbs were new, but the Philips' bulbs had been used). The average thickness of the glass of the segments used was 0·810 mm.

in the case of the Philips' bulbs and 0·485 mm. in the case of the Leerdam bulbs. In the case of the Philips' bulbs, however, the opal glass bulbs had been blown over thin bulbs of transparent glass, estimated at about 1/12 of the total thickness; so the thickness of the *opal* glass was 0·74 mm.

The effective area of a sheet (or bulb segment) determined by the opening of the photometer and the dimensions of the arrangement was about 2·5 cm.^{2} for the rejected light and about 1·75 cm.^{2} for the transmitted light. As the segments of such bulbs do not fit in each other very well optical contact between them was obtained by placing them, pressed together, in a cell of xylol. Table XIII. contains the results of the measurements of the transmitted light at various wave-lengths and also the values of f obtained therefrom graphically as usual.

In the next row of the table we find the rejection under 25° by MgO. This was obtained by depositing a fresh thick layer of MgO on a Philips' bulb segment (holding the latter in the flame of a burning magnesium strip), and then placing the coated bulb before the opening b of the diffuser in the usual way. Then the rejection by seven bulb segments in air, as usual, between which optical contact had been obtained with Canada balsam, was also measured.

Taking R (MgO)=0·953, it is a simple matter to calculate the values of R for the Philips' bulbs given in the table.

In order to compare the rejections of the two types of bulbs as fairly as possible a new set of measurements was made in which optical contact between the segments was obtained by placing them in xylol, as above. The reasons for not using Canada balsam are, *e.g.* :—

(1) It is undesirable to have a thick layer of Canada balsam, which is not colourless, between the segments (they do not fit in each other well).

(2) The temperature of the diffuser ($\pm 30°$ C.) is sufficient to soften the Canada balsam, thus introducing difficulties and inaccuracies.

(3) The difficulties are even greater in the thin fragile Leerdam bulbs.

Table XIII.

	No. of bulb segments.	Wave-length in $\mu\mu$. 617	570	537	498	No. of bulb segments.	Wave-length in $\mu\mu$. 617	570	537	498
Transmitted light	2	57·0	52·0	52·0	52·0	2	61	58	58	55
	4	40·0	38·0	38·0	30·0	4	54	48	48	46
	7	26·5	26·0	26·0	22·2	7	30	28	28	26
f per mm. thickness		0·182	0·169	0·169	0·160		0·297	0·287	0·287	0·301
Rejected light in air	(MgO)	142	156	156	156					
Rejected light in air	7	116	132	132	132					
Rejected light in xylol	7	42	46	46	45	7	41·5+	46	46	42—
R		0·779	0·807	0·807	0·807		0·771	0·807	0·807	0·751
$c\kappa$ per mm. thickness		0·0225	0·018	0·018	0·017		0·0385	0·0305	0·0305	0·043
$cn\beta\sigma$ per mm. thickness		0·72	0·78	0·78	0·74		1·14	1·325	1·325	1·05
$\frac{\kappa}{n\beta\sigma}$		0·0315	0·023	0·023	0·023		0·034	0·023	0·023	0·0405
		Philips' Argenta bulbs.					Leerdam bulbs.			

Table XIV.

	Wave-length in $\mu\mu$.				Wave-length in $\mu\mu$.			
	617	570	537	498	617	570	537	498
Intensity in image (colourless glass)	22500·00	60000·00	35000·00	40000·00	22500·00	60000·00	35000·00	40000·00
Intensity in image (opal glass segment)	5·19	3·46	1·70	1·92	12·20	8·60	2·62	1·60
Intensity beside image (opal glass segment).	0·488	1·14	1·01	1·64	0·30	0·80	0·60	1·02
Directly transmitted light	4·65	2·20	0·59	0·12	11·87	7·72	1·96	0·48
σ per mm. thickness	24·5	29·0	31·5	36·5	23·5	28·0	30·5	35·5
cm^3	0·0295	0·0270	0·0250	0·0205	0·0485	0·0475	0·0435	0·0295
(c)	3	3	3	3	3	3	3	3
$\frac{\kappa}{\sigma} \times 10^4$	3·10	2·05	1·90	1·55	5·50	3·65	3·35	4·00
	Philips' Argenta bulbs.				Leerdam bulbs.			

The comparison between the light rejected by the Philips' and by the Leerdam bulbs in xylol gives the proportion between their values of R.

The values of $c\kappa$ and $cn\beta\sigma$ per mm. thickness come out greater for the Leerdam than for the Philips' bulbs. For the total thickness of the glass of the bulbs there is, however, little difference between the values of $cn\beta\sigma$ for the two sorts of glass, whereas the values of $c\kappa$, especially at $\lambda=498\,\mu\mu$, are slightly greater in the case of the Leerdam bulbs. The quantities $\frac{\kappa}{n\beta\sigma}$ only differ appreciably at $\lambda=498\,\mu\mu$.

11. *Separation of the Coefficients c, n, β, σ in the case of the Opal Glass Bulbs.*

The Leerdam bulbs were *just* transparent *, and a distant white body appears red when viewed through a segment of such a bulb (thus showing a stronger scattering for shorter wave-lengths). The Philips' bulbs were, however, generally intransparent, but after cutting up many bulbs a small area, which was only just transparent, was found just below the neck of a bulb.

With such abnormally thin segments it has been possible to measure σ (or, rather, $\kappa+\sigma$, but κ is very small compared to σ) for the glasses by means of the apparatus for a parallel incident beam. Firstly, the total light transmitted by the chosen transparent bulb segments was measured, then that by a microscope coverslip (to correct for reflexion effects, at the surfaces of the opal glass segments), and, finally, the lens U was displaced to the side to project the image of the source N to the side of the slit of the photometer and the *scattered* light was measured under 2·5° with the direction of the incident light.

All these measurements are given in Table XIV.

Instead of extrapolating the light scattered under 0° from measurements of that scattered under several small angles with the normal this extrapolation was roughly performed, for the sake of economy, with the aid of the results for the mastic emulsions (see p. 812).

* It may be noted here that a second batch of bulbs, which were manufactured at Leerdam at a later date than the above ones, were quite intransparent.

This was done as follows :—The light scattered under 2·5° was subtracted from the total transmitted light, and substitution in the formula $I=I_0e^{-\sigma X}$ gave a value of $\sigma X \gtrsim 10$. (Of course the light transmitted by the cover-slip was substituted for I_0 to correct for reflexions.) For $\sigma X \gtrsim 10$ the ratio of the light scattered under 0° to that under 2·5° is 1·1 for the mastic emulsion ; so, taking this to be the case more or less in the case of the segments, the results in the third row of Table XIV. were multiplied by 1·1 and subtracted from those in the second row to give I for the above formula. The thickness of the Philips' bulb segment at the spot where the transmission was measured was 0·35 mm., and that of the Leerdam bulb segment was 0·32 mm. Substitution in the formula $I=I_0 e^{-\sigma X}$ of I, I_0 and the thickness of the glass have given the values of σ per mm. thickness in the table.

The order of the values of σ has been found to be the same for various specimens cut from different bulbs of the same sort *.

The values of σ per mm. thickness have been found to be the same for both types of glass ; from the variation of σ with the wave-length $n=2·2$ (in the formula $\sigma=a\lambda^{-n}$, where a is a constant) for both cases, if we duly attach more importance to the more accurate values of σ obtained from the measurements at the longer wave-lengths.

By dividing the values of $cn\beta\sigma$ (see Table XIII.) by those of σ the values of $cn\beta$ in Table XIV. were obtained ; the decrease of $cn\beta$ with the wave-length is just what we should expect from the work on emulsions (see Table IX.). The values of $cn\beta$ are bigger for the Leerdam bulbs than for the Philips' bulbs, from which we conclude that, if the particles and the continuous phases are of the same material in both cases, the particles in the Philips' bulbs are probably bigger than those in the other bulbs. The sizes of the particles have been estimated by observing fine powder of the glasses with a Zeiss microscope ; the mean radius of the particles of the Philips' bulbs have been estimated at $0·3\,\mu$ and the others at $0·2\,\mu$, so the possibility of similar substances is not excluded.

By substitution of the coefficients here determined in our formulæ (2) and (9) for the transmitted light we find that for equal thicknesses, not too small, of the glasses

* See Dissertation, cxxxiv. (Utrecht, 1930).

(*i. e.*, for the case of equal values of σ) more scattered light is transmitted by the Philips' bulbs than by the Leerdam bulbs. For the bulbs as they are produced, however, little can be said, as, *cet. par.*, the smaller transmission per mm. thickness in the case of the Leerdam bulbs is compensated by the thinner glass in this case.

Finally, taking $c=3$ in both cases, a rough estimation of the values of κ/σ has been obtained. The table shows how small the values of κ/σ are for such good white opal glasses as the bulbs are made of.

With a deep feeling of gratitude I wish to thank Professor L. S. Ornstein for the many facilities offered me at the Physical Institute, Utrecht, during my two years' stay here; also for his constant interest and assistance in the problem which he set me.

If I were to add also my thanks to Dr. M. Minnaert for the very pleasant and able way in which he assisted me throughout my research on opal glasses I should be in danger of ending this publication with sentimentalism.

LXXII. *The Molecular Theory of Surface Energy: the Surface Energy of the Liquefied Inert Gases.* *By* R. S. Bradley *.

THE surface tensions σ of liquids fall strikingly into a number of groups. At the lower end of the scale lie the inert elements and the gases liquefiable with difficulty, with σ about 10 dynes per cm. Next come the organic liquids, for which σ is about 30, the dipolar liquids, such as water (σ about 70), and the fused salts, with σ roughly from 100 to 200 dynes per cm. Finally, the metals have the highest surface tensions, in some cases as much as 1000 dynes per cm. Although for comparative purposes the total surface energy is better than the surface tension, the arrangement above brings out well enough the effect on the surface tension of the predominance of a new type of intermolecular force. In the case of the inert elements the van der Waals force accounts for the cohesion. In polar liquids, such as water, the cohesive force is predominantly

* Communicated by the Author.

interdipolar, in fused salts it is interionic, and, finally, in the metals the cohesion is that between the positive ions and the surrounding electron gas (*i.e.*, the metal resembles a colloid). In this paper only the first type of intermolecular force will be considered.

For the calculation of the surface energy of a pure liquid the concept of surface pressure applicable to the study of dilute surface films does not help, and it is still better to work in terms of cohesive forces. These are now known with some precision.

Let the attractive force between two masses of liquid m, m' be $mm'\phi(r)$, where r is the distance between them. The surface energy may be calculated as follows [1]:—The attraction of a mass m of the fluid on a rod of fluid whose ends are distant r and ∞ from m, and whose mass per unit length is m', is in the direction of the rod

$$mm' \int_r^\infty \phi(r) \, . \, dr = mm' \Pi(r).$$

The attraction of a mass m on an infinite mass of liquid whose plane surface is distant r from m, and whose density is ρ, is therefore

$$2\pi m\rho \int_r \Pi(r) \, . \, r \, . \, dr = 2\pi m\rho \, \psi(r).$$

Hence the mutual attraction of two masses of fluid whose plane surfaces are distant r from one another is per unit area

$$2\pi\rho^2 \int_r^\infty \psi(r) \, dr = 2\pi\rho^2 \, \theta(r).$$

The work required to separate a liquid into two halves and thus form two surfaces is therefore per unit surface area

$$2\pi\rho^2 \int_d^\infty \theta(r) \, dr,$$

where d is the distance between two adjacent molecular centres in the fluid.

Hence

$$U_s = \pi\rho^2 \int_d^\infty \theta(r) \, dr,$$

where U_s is the surface energy in ergs per sq. cm., and is therefore $\frac{dU}{dS}$, where S is the surface.

The force fields for the inert gases may be expressed in the form [2]

$$mm'\phi(r) = \frac{\lambda_n}{r^n} - \frac{\lambda_m}{r^m}.$$

This gives

$$U_s = \left(\frac{N}{M}\right)^2 \frac{\pi\rho^2\lambda_m}{(m-1)(m-3)(m-4)(m-5)d^{m-5}} - \left(\frac{N}{M}\right)^2 \frac{\pi\rho^2\lambda_n}{(n-1)(n-3)(n-4)(n-5)d^{n-5}},$$

where N is Avogadro's number and M is the atomic weight. This method cannot be used if either n or m is equal or less than 5. The requirement that

$$\mathrm{Lt}_{r\to\infty} r^3\left(e^{\frac{\Pi(r)}{KT}} - 1\right) = 0$$

restricts n and m to values greater than 4 [2]. Lennard-Jones has worked out most of his models for $m = 5$. However for argon and helium he gives alternatives for $m = 6$. These fit the observed second virial coefficients for the gases, but the first does not give the interatomic distance and the heat of vaporization of the solid as well as the model for $m=5$. It corresponds, however, to a repulsive index $n = 9$, which is that obeyed by argon-like ions, rather than $n = 15$, the value corresponding to $m = 5$ for the gas. The values used in this paper are

He [3] $m = 6$, $n = 11$, $\lambda_m = 1{\cdot}97\ 10^{-52}$, $\lambda_n = 7{\cdot}47\ 10^{-90}$.

A [4] $m = 6$, $n = 9$, $\lambda_m = 1{\cdot}7\ 10^{-59}$, $\lambda_n = 1{\cdot}518\ 10^{-72}$.

As no alternative is given for Ne, U_s will not be calculated for this gas.

The calculated values of U_s may be compared with the observed surface tensions σ by means of the equation [5]

$$U_s = \sigma - p\left(\frac{\delta\sigma}{\delta p}\right)_{T,s} - T\left(\frac{\delta\sigma}{\delta T}\right)_{p,s}.$$

The term $p\left(\frac{\delta\sigma}{\delta p}\right)_{T,s}$ will be neglected. K. Onnes gives the "molecular surface energy" $\sigma\left(\frac{M}{\rho}\right)^{\frac{2}{3}}$ of helium at 4° as 1·19 [6]. Since ρ at this temperature is ·1284 [7]. σ is 1·2 dynes per cm. The value for argon is given by Baly

and Donnan[8]. Calculated and observed values are in satisfactory agreement.

Liquid.	T.	Obs.	U obs.	U calc.
Argon	84	11·46	24·5	21·6
Helium ...	4	·12	·6	·2

It is hoped in subsequent papers to study the surface energies of polar liquids and of metals.

References.

(1) Raleigh, Phil. Mag. xxx. p. 285 (1890).
(2) Lennard-Jones, Proc. Roy. Soc. cvi. p. 440 (1924).
(3) Lennard-Jones, Proc. Roy. Soc. A, cvii. p. 157 (1925).
(4) Lennard-Jones, Proc. Roy. Soc. A, cix. p. 476 (1925).
(5) Schottky, *Thermodynamik*, p. 114 (1929).
(6) Comm. Phys. Lab. Leiden, No. 179.
(7) Comm. Phys. Lab. Leiden, No. 170.
(8) Journ. Chem. Soc. lxxxi. p. 907 (1902).

The University, Leeds.
January 1931.

LXXIII. *Vortex Formation behind Obstacles of various Sections.* *By* E. Tyler, *D.Sc., F.Inst.P., Lecturer, Physics Department, College of Technology, Leicester**.

Introduction.

IN a previous paper †, entitled "Vortices behind Aerofoil Sections and Rotating Cylinders," a few preliminary results were included on the measurement of the frequency of vortex formation behind aerofoil sections in air at low angles of incidence. In that paper, the effect of increasing the angle of inclination has been investigated, and the results show that the rate of production of the vortices increases as the angle of inclination decreases for a given fluid speed, in analogous behaviour to the effect observed by Fage and Johansen ‡ for an inclined plate in air. The object of this work is to extend the range of investigation beyond the former, and is classified thus :—

1. Determination of the frequency of formation of vortices behind inclined aerofoils and plates over a wider

* Communicated by the Author.
† Phil. Mag. (March 1928).
‡ Proc. Roy. Soc. A, cxvi. (1927).

range of inclination than in the previous paper, by different methods, and also for cylinders at low values of Reynolds number.

2. Hot-wire methods for determining the longitudinal and lateral spacings of vortices behind obstacles, with their application to cylinders, aerofoils, and plates.

Frequency Determination of Vortices behind Inclined Aerofoils and Cylinders in Water.

Results with Vibrating Aerofoil Pendulums.

It is known that the periodic detachment of vortices behind a body placed in a fluid stream, produces a periodic alternating cross force on the body, tending to make it vibrate across the stream. If the body is free to vibrate, and its natural period of vibration is equal to the time interval between the disengagement of two successive vortices from the same side of the body, a condition of resonance will exist between the natural vibration of the body and those forces, and the vibrations of the body will be maintained across the stream. Experiments based on this fact have been carried out by many experimenters using cylindrical pendulums and thin wires. In particular, Richardson* has obtained a few results for brass aerofoils immersed in water for varying angles of incidence from $\theta = 0°$ to $30°$, with an unsuccessful attempt to connect the non-dimensional quantity $\frac{V}{ND}$ with $0°$, for different values of Reynolds' number $\frac{VD}{\nu}$, D being the maximum thickness of the aerofoil.

The method used by me is a modification of his, but my results cover a much wider range of investigation. Instead of using the rotating-tank method, I resorted to a straight rectangular water channel $170 \times 12 \times 14$ cm., provided with a V notch at one end, with two sets of baffle plates at the other. Water from the mains was fed in at this end *via* a valve regulator, and the models were placed about two-thirds the length of the channel from the same end.

The aerofoils, from 5 to 10 cm. in length, were immersed with about 1 or 2 cm. below the water surface, and were

* Proc. Phys. Soc. xxxvii. (April 1925).

each attached to a small clamp fixed at the lower end of a long, vertical, thin steel blade, which was so arranged as to be able to vibrate in a plane perpendicular to the stream.

The clamp could itself rotate about a vertical axis, for it was screwed into a piece of metal soldered on to the end of the blade, and could be fixed in any position by means of a small set-screw.

TABLE I.

Water Results. (Vibrating Aerofoils.)

Type of aerofoil.	θ.	N.	V. cm./sec.	$\frac{N.b}{V}$.	$\frac{Nb.\sin\theta}{V}$.
No. 1. Maximum width: b=5·00 cm. Maximum thickness: D=·755 cm.	0	1·350	7·40	·915	0
	5	·967	6·81	·710	·062
	12	·500	4·70	·532	·111
	15	·556	5·27	·529	·136
	20	·498	6·00	·415	·142
	25	·480	6·09	·395	·167
	30	·480	7·30	·329	·164
	40	·425	7·70	·275	·177
No. 2. Width: b=2·45 cm. Thickness: D=·325 cm.	15	·625	2·85	·538	·138
	20	·715	3·75	·468	·160
	40	·625	6·81	·225	·144
	50	·560	7·15	·192	·147
	55	·560	8·04	·171	·140
	60	·515	7·50	·168	·145
	75	·538	8·04	·164	·158
	90	·540	8·58	·154	·154
No. 3. Width: b=1·20 cm. Thickness: D=·188 cm.	25	1·18	3·96	·358	·151
	30	1·17	4·68	·299	·149
	35	1·23	5·17	·287	·164
	40	·589	2·83	·250	·163
	60	·589	3·53	·200	·173
	80	1·54	12·00	·154	·151
	85	1·51	11·55	·156	·155
	90	·62	5·00	·149	·149

Attached to this metal and also to the clamp were two horizontal metal pointers, each about 20 cm. long, and they were arranged to be just above each other, and at right angles to each other when the angle of inclination of the aerofoil to the stream was 90°. Thus θ° for any other setting of the aerofoil was a measure of the angle between the pointers, as measured by a protractor. The lower edge of the blade also carried a small mirror, and, by using

a lamp and scale, the vibrations of the aerofoil were followed very closely, especially at small angles of incidence, when the strength of the vortices was small.

Thus, for a given frequency N (made variable by altering the length of the blade, and measured by timing a given number of vibrations with a stop-watch) the speed of flow was adjusted until resonance occurred between the pendulum and the vortex formation, a maximum maintained deflexion being observed on the scale.

Fig. 1.

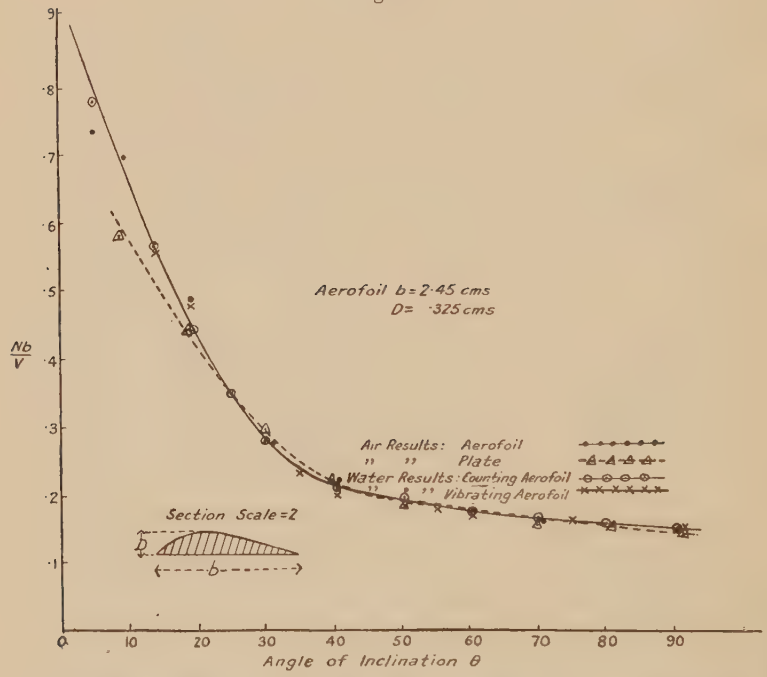

V was found within 1 per cent. by timing the movement of small dust particles over the water surface 20 to 30 cm. in advance of the aerofoil.

Results for different models are shown in Table I., which are also incorporated in figs. 1, 2, and 3.

Results by Visual Observation.

The water channel was again used, and lycopodium powder or aluminium dust was scattered over the liquid surface, and the vortex formation followed by the eye.

The value of the frequency N behind both inclined aerofoils and cylinders was found by observing the time required for the detachment of ten vortices near the body, and also the time for ten vortices to pass a point about 10 or 15 cm. to the rear of it. For a given speed, no change in N could be observed within the experimental error for both positions.

The method of varying $\theta°$ for the aerofoils was the same as used previously, with the exception that the lower end

Fig. 2.

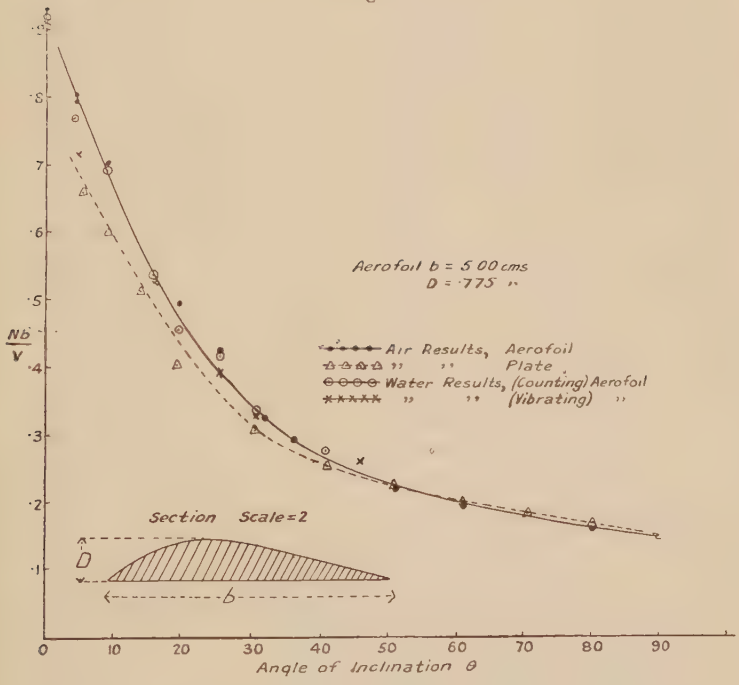

of the blade was now clamped. Both in this and the previous methods it was not possible to extend the observations beyond $\theta = 35°$ when using the larger models, owing to boundary effects coming into play.

Results are also included in Table II. and figs. 1, 2, and 3 which show good agreement with those for the vibrating aerofoil pendulums. Included in Table III. are results for cylinders at low values of $\frac{V \cdot D}{\nu}$.

Results by Hot-wire Method.

In order to extend the range of investigation beyond that for the water channel it was found necessary to adopt some other method whereby higher speeds of flow could be obtained. A circular tank, 3 ft. diameter and 6 in. depth, was therefore used. It was nearly filled with water, and a disk slightly smaller in diameter than that of the tank was made to revolve in a horizontal plane about a vertical

Fig. 3.

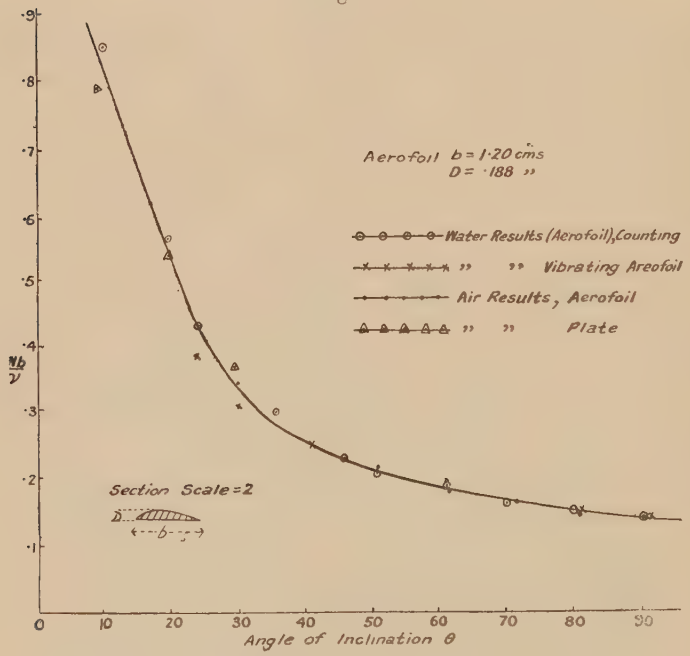

axis concentric with the tank, and as near as possible to the bottom.

The aerofoils were immersed in the same way as for visual method in water, but care was taken to place them in a position in the tank where the velocity (tangential) was most uniform over a radial distance equal to the width of the aerofoil. This was found by preliminary experiments, by timing the movement of dust particles over the water surface for different distances from the edge for a constant speed of rotation of the disk.

The measurement of the frequency of the vortices was similar to that described in the next section for results in air, in which the periodic heating and cooling of a hot nickel wire caused by the vortex formation was determined

TABLE II.

Water Results for Aerofoils. (Counting.)

Type of aerofoil.	θ°.	N.	V. cm./sec.	$\frac{N.b}{V}$.	$\frac{Nb.\sin\theta}{V}$.
No. 1. b=5·0 cm. D=·775 cm.	0	1·03	4·51	·921	0
	5	·696	4·71	·768	·067
	10	·582	4·30	·680	·117
	15	·489	4·55	·539	·139
	20	·445	5·00	·445	·152
	25	·404	4·82	·419	·177
	30	·472	7·00	·337	·168
	35	·386	7·00	·286	·164
No. 2. b=2·45 cm. D=·325 cm.	5	1·250	3·95	·775	·068
	15	·905	4·00	·553	·153
	20	·660	3·73	·434	·148
	25	·520	3·75	·339	·143
	35	·441	3·93	·275	·157
	45	·328	3·77	·213	·150
	50	·616	7·50	·201	·154
	60	·552	7·50	·180	·156
	70	·528	7·50	·173	·163
	80	·455	7·15	·156	·153
	90	·435	6·99	·152	·152
No. 3. b=1·20 cm. D=·188 cm.	20	1·50	3·20	·560	(·192)
	25	1·11	3·20	·415	·175
	30	·778	3·10	·300	·150
	40	1·05	5·00	·255	·164
	45	·625	3·22	·233	·164
	50	1·10	6·16	·214	·163
	60	·519	3·20	·194	·167
	70	·409	3·00	·163	·153
	80	·458	3·40	·162	·159
	90	·370	3·00	·148	·148

by a vibration galvanometer-transformer coupled to the wire.

The wire, carrying a current of 1 amp., was mounted vertically behind the model in a most suitable position, and the speed of flow adjusted until resonance occurred. The speed of flow was then determined by timing the movement of dust particles over a known distance.

TABLE III.

Water Results for Cylinders. (Counting.)

Diameter. D cm.	N.	V. cm./sec.	$\frac{V}{N.D}$.	$\frac{V.D}{\nu}$.
3·15	·300	4·69	4·97	985
2·90	·389	5·45	4·85	675
2·90	·241	3·49	4·99	1040
2·20	·374	3·95	4·79	572
2·60	·600	7·50	4·80	1300
2·60	·566	7·15	4·86	1240
1·60	·323	2·86	5·55	301
1·60	·512	4·12	5·02	433
1·30	1·08	7·50	5·33	650
·705	·695	3·00	6·12	141
·705	2·08	8·10	5·51	377
·590	·90	3·33	6·30	131
·590	1·21	3·98	5·58	156
·420	1·49	4·02	6·40	112

TABLE IV.

Water Results for Aerofoils. (Hot-wire V.G. Method.)

Type of aerofoil.		N.	V. cm./sec.	$\frac{N.b}{V}$.	$\frac{Nb.\sin\theta}{V}$.
	0	16·5	17·5	1·13	0
	10	16·5	24·0	·825	·143
	15	16·5	29·0	·683	·176
	15	16·5	28·5	·695	·180
	25	10·0	28·4	·423	·179
b=1·20 cm.	30	10·0	35·8	·335	·167
D=·188 cm.	45	10·0	49·0	·245	·173
	45	6·0	31·0	·232	·164
	60	6·0	38·1	·189	·164
	60	6·0	39·2	·184	·159
	90	6·0	49·0	·147	·147
	90	6·0	47·5	·152	·152
	5	15·0	10·4	·920	·080
	10	15·0	13·1	·731	·127
	20	10·0	11·6	·551	·189
b=·64 cm.	30	10·0	17·9	·357	·178
D=·82 mm.	45	6·0	19·0	·202	·143
	60	6·0	22·7	·169	·146
	90	6·0	27·0	·142	·142

Included in Tables IV. and V. and figs. 1, 2, and 3 are the results obtained by this method. It will be seen that

there is good agreement between these and the results obtained by other methods.

Frequency Determination of Vortices behind Inclined Aerofoils, Plates, and Cylinders in Air.

Method 1. (*Hot-wire Method at Low Frequencies.*)

It is difficult to observe with any precision over any appreciable distance the vortices formed in air behind obstacles, even though the air be rendered visible by mixing with smoke. The periodic heating and cooling of a hot wire of small diameter, however, serves to indicate the

Table V.

Water Results for Cylinders. (Hot-wire V.G. Method.)

Diameter D. cm.	N.	V. cm./sec.	$\frac{V}{N.D}$.	$\frac{V.D}{\nu}$.
·640	10	32·50	5·07	1860
·352	10	19·10	5·41	600
·327	10	17·20	5·25	502
·315	15	25·00	5·29	702
·238	15	18·70	5·22	397
·207	15	17·15	5·50	315
·162	15	14·10	5·78	204

frequency of formation of the vortices, as was first shown by Relf and Simmons *, who succeeded in measuring the value of $\frac{V}{ND}$ for a cylindrical rod past which air was streaming for high values of $\frac{V.D}{\nu}$. In the present research, I have employed a modification of this method, previously described by me elsewhere †.

An electrically heated platinum wire (1 in. long and ·001 in. diameter) was mounted vertically behind the obstacle, and at a suitable position, either at the end of a whirling arm (radius 3 ft.) driven by a one-eighth horse-power motor when using low speeds, or in a wind channel ($1\frac{1}{2} \times 1\frac{1}{2} \times 14$ ft.) for higher speeds. The wire was connected in series with the primary of a step-up transformer

* Phil. Mag. xlix. p. 519 (1925).
† Phil. Mag. v. (March 1928).

(ratio 1 : 2), and was supplied with a constant heating current, sufficient to keep it just below a dull glow. The secondary of the transformer formed part of a vibration galvanometer circuit (see fig. 4).

When using the whirling arm, the model was clamped vertically at a known angle of inclination, and rotated until its speed relative to the air was such that resonance occurred between the periodic heating and cooling of the wire due to the vortices formed, and the galvanometer set at known frequency, the latter being previously calibrated with the intermittent current from the make-and-break of

Fig. 4.

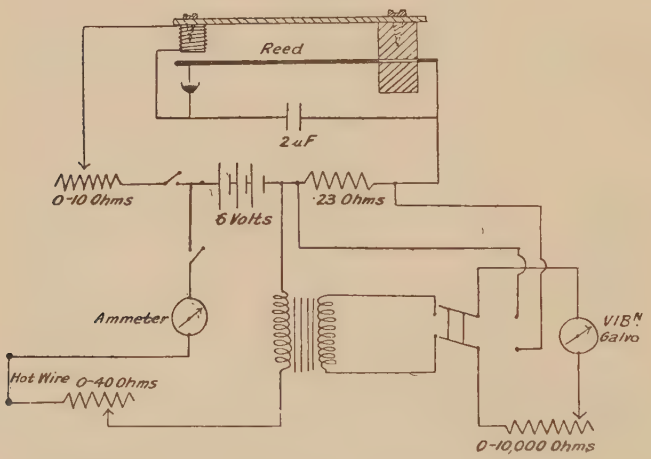

a vibrating reed. The length of the reed was varied and its frequency found stroboscopically. The galvanometer frequency was also checked by stroboscoping a reflected spot of light from the mirror attached to the string of the instrument.

Using the wind-channel method, the air speeds for resonance were measured by means of a hot wire and potentiometer device as follows :—

A platinum wire (length 1 in. and diameter ·001 in.), heated electrically, formed one arm of a Wheatstone's bridge, as shown in fig. 5, and was placed in the position previously occupied by the model in the channel. Its resistance, and therefore temperature, was maintained

constant at all speeds by means of a variable resistance in the battery circuit of the bridge. The P.D. between the ends of the wire, which is a function of the wind speed at that position in the channel, was measured on a potentiometer. To convert the potentiometer readings into wind speed values the same wire was mounted vertically at the end of a whirling arm, and for given wind speeds (measured by timing a given number of revolutions of the whirler) the

Fig. 5.

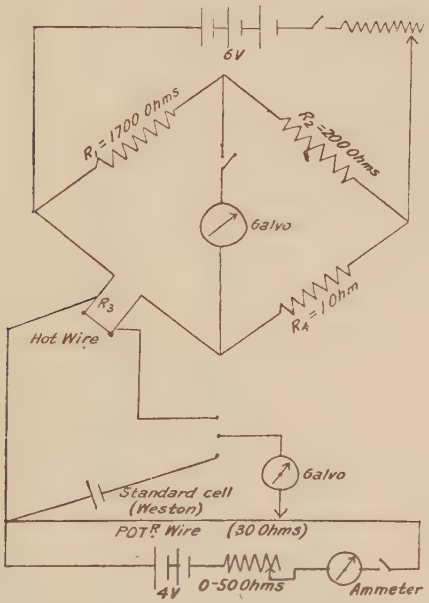

corresponding P.D.s across the wire (still kept at the same constant temperature) were measured, and from these results a calibration graph was obtained.

These speeds were subsequently checked by means of a tilting manometer calibrated from a Pitot tube placed in the centre of the stream, where the wire was previously.

As hitherto mentioned, using a hot wire as a detector of fluctuating air speeds, greatest sensitivity is obtained at low speeds and at low frequencies of fluctuation. These conditions were met with partly in the design of the models, used in conjunction with a vibration galvanometer capable

TABLE VI.

Air Results for Aerofoils. (Whirler and Wind Channel.)

Type of aerofoil.	θ°.	N.	V. cm./sec.	$\frac{N \cdot b}{V}$.	$\frac{Nb \cdot \sin\theta}{V}$.
No. 1. b=5·00 cm. D=·775 cm.	0	8·0	44·1	·908	0
	0	10·0	53·0	·952	0
	5	6·6	41·6	·792	·069
	5	10·0	62·0	·815	·071
	10	9·0	65·0	·693	·120
	15	8·0	66·7	·600	·155
	15	9·0	79·0	·570	·147
	20	6·6	67·0	·493	·168
	25	6·6	77·0	·425	·179
	30	10·2	162·0	·315	·157
	30	6·6	101·5	·325	·162
	35	6·6	112·5	·293	·168
	40	5·9	123·5	·240	·154
	40	5·0	96·0	·260	·167
	50	5·0	118·0	·313	·163
	60	5·0	133·0	·188	·162
	60	5·9	156·2	·189	·162
	70	5·0	134·0	·187	·175
	80	5·0	150·5	·166	·163
	90	5·9	198·0	·149	·149
No. 2. b=2·45 cm. D=·325 cm.	5	11·3	37·9	·731	·064
	10	11·3	40·3	·690	·120
	15	6·67	29·2	·554	·143
	20	6·67	34·2	·474	·162
	30	8·0	67·0	·292	·146
	30	6·6	56·0	·290	·145
	40	8·0	89·0	·220	·142
	50	6·6	75·0	·216	·165
	50	8·0	99·0	·198	·152
	60	6·6	83·4	·194	·168
	60	11·3	147·0	·189	·162
	70	8·0	113·0	·173	·162
	70	6·6	92·0	·176	·165
	80	8·0	126·0	·156	·154
	90	8·0	133·0	·148	·148
	90	6·6	111·2	·145	·145
No. 3. b=1·20 cm. D=·188 cm.	30	10·0	37·3	·322	·161
	30	6·67	23·9	·335	·167
	40	6·60	30·7	·260	·167
	40	10·0	46·2	·260	·167
	50	12·0	63·3	·227	·174
	60	6·6	42·0	·188	·162
	70	12·0	90·0	·160	·150
	70	10·0	71·3	·168	·158
	80	6·67	53·1	·151	·148
	90	10·0	83·5	·144	·144

of being tuned down to low frequencies (about 5), employed with the whirling arm apparatus, the latter never being run at a speed greater than 1 rev. per second; in most cases at much lower speeds than this. At the lower angles of incidence, for the higher speeds the fluctuating P.D.s across the wire were amplified by means of a five-valve amplifier with the vibration galvanometer included in the plate circuit of the fifth valve.

Results using both the whirling-arm and the wind-channel methods are included in Table VI. and figs. 1, 2, and 3 for the aerofoils, and a few results for cylinders and plates at low values of $\frac{V \cdot D}{\nu}$ are shown in Tables VII. and VIII.

TABLE VII.

Air Results for Cylinders. (Whirler and Wind Channel.)

Diameter. D, cm.	N.	V. cm./sec.	$\frac{V}{N \cdot D}$.	$\frac{V \cdot D}{\nu}$.
3·15	7·05	110·0	4·95	2340
3·15	6·30	98·0	4·95	2060
1·90	7·05	66·5	4·95	855
·895	7·85	41·3	5·87	250
·895	6·60	33·1	6·35	200
·895	10·90	54·9	5·60	327
·655	7·45	31·0	6·35	137
·655	10·10	40·0	6·03	175
2·00	30·50	296·0	4·85	4000
2·00	27·50	264·0	4·80	3550
1·25	10·10	66·5	5·27	558
1·25	6·07	42·3	5·56	356

Method 2.—Hot-wire Amplifier Method at Audible Frequencies.

As an alternative method, especially at the higher speeds, where the sensitivity is much reduced, and where the frequency of vortex formation was above the lower limit of audibility, advantage was taken by employment of the five-valve amplifier already mentioned in the previous section. The small oscillating E.M.F.s induced in the secondary of the transformer were amplified, and by replacing the vibration galvanometer by either a telephone or a loud-speaker in the plate circuit of the fifth valve, an audible note of the same frequency N as the vortex formation was produced (see fig. 10).

The value of N was determined by comparing the note heard with a similar note produced on a monochord

Table VIII.

Air Results for Plates. (Whirler and Wind Channel.)

Plate.	θ°.	N.	V. cm./sec.	$\frac{N \cdot b}{V}$.	$\frac{Nb \cdot \sin\theta}{V}$.
	5	10·0	29·25	·651	·057
	10	10·0	32·0	·594	·103
	20	10·0	47·1	·403	·138
b=1·90 cm.	30	10·0	66·5	·286	·143
Length=23·0 cm.	40	10·0	73·0	·260	·167
Thickness=·96 mm.	50	10·0	83·7	·227	·174
	60	10·0	100·0	·190	·164
	80	10·0	113·6	·167	·164
	90	10·0	123·6	·154	·154
	10	10·0	52·4	·552	·092
	20	10·0	67·2	·430	·147
	30	10·0	96·0	·302	·151
b=2·90 cm.	40	10·0	130·5	·222	·143
Length=30·0 cm.	50	7·0	104·5	·195	·149
Thickness=1·09 mm.	60	7·0	115·5	·173	·150
	70	7·0	122·0	·167	·157
	80	7·0	134·0	·151	·149
	90	7·0	142·2	·143	·143

Table IX.

Air Results for Cylinders. (Using Amplifier.)

D. cm.	N.	V. cm./sec.	$\frac{V}{N \cdot D}$.	$\frac{V \cdot D}{\nu}$.
·420	140	288	4·92	818
·310	70·5	117	5·37	245
·163	234	198	5·20	218
·163	483	432	5·50	476
·120	422	270	5·33	219
·120	215	150	5·80	122
·060	468	197	7·05	79·8
·060	661	253	6·40	102·8
·046	525	190	7·89	59·0
·046	776	260	7·30	80·7
·046	373	155	9·02	48·2
·046	453	167	8·00	52·0

standardized with a 256 fork. Tables IX., X., and XI., incorporate results for cylinders, aerofoils, and plates. It will be observed that the results are in good agreement

TABLE X.

Air Results for Aerofoils. (Using Amplifier.)

Type of aerofoil.	θ°.	N.	V cm./sec.	$\frac{N.b}{V}$.	$\frac{Nb.\sin\theta}{V}$.
	0	256	286	1·07	0
	0	235	265	1·06	0
	0	187	215	1·04	0
	0	331	350	1·14	0
b=1·20 cm.	10	320	390	·985	·170
D=·188 cm.	15	270	425	·765	·196
	20	131	302	·520	·178
	25	156	390	·479	·202
	30	92	302	·363	·181
	30	120	425	·339	·169
	0	712	450	1·01	0
	5	458	302	·971	·085
	5	467	313	·957	·084
b=·64 cm.	15	352	402	·560	·145
D=·82 mm.	20	347	402	·552	·189
	30	250	450	·355	·177
	45	145	450	·205	·145

TABLE XI.

Air Results for Plates. (Using Amplifier.)

Type of plate.	θ°.	N.	V. cm./sec.	$\frac{N.b}{V}$.	$\frac{Nb.\sin\theta}{V}$.
	0	765	467·5	·970	0
	0	898	485	1·09	0
	5	730	465	·928	·081
b=·59 cm.	10	398	415	·568	·096
D=·50 mm.	10	478	480	·588	·102
	30	226	465	·288	·144
	45	157	465	·199	·141
	70	124	465	·158	·148
	90	116	465	·147	·147
	10	632	371	·722	·125
	20	422	402	·447	·153
b=·425 cm.	30	203	287	·300	·150
D=·50 mm.	45	169	333	·215	·152
	60	129	347	·158	·137
	90	141	417	·144	·144

with those obtained by the other methods, and it is of interest to compare them with those of Piercy and Richardson * for cylinders obtained by a similar method.

* Phil. Mag. ii. (Nov. 1928).

Longitudinal Spacing of Vortices behind Cylinders, Plates, and Aerofoils.

The method of measurement employed was a modification of that first used successfully by Fage and Johansen*, who measured the longitudinal spacing of vortices behind an inclined plate in an air stream. It is based upon the fact that the velocity fluctuations at two points without and on the same side of a vortex street are in phase when the longitudinal distance between the points is equal to the distance between successive vortices in the same row, or a multiple of this distance.

By using two hot wires, one fixed vertically outside one vortex row, and the other moved up and down the stream along a line usually outside the opposite vortex row, they obtained simultaneous photographic records of the velocity disturbances behind the plate, for different positions of the hot wires by means of an Einthoven galvanometer fitted with a lantern and camera. By referring to a standard time base, also photographically recorded, the phase difference between any two points was thus obtained. Plotting the phase difference against distance downstream of the movable hot wire, a straight-line graph was obtained, the slope of which was a measure of the longitudinal spacing of successive vortices in the same row.

Instead of using the Einthoven galvanometer and photographic camera, I resorted to a differential maximum and minimum deflexion method which has been described elsewhere †.

Two arrangements were used :—

(1) A hot-wire vibration galvanometer method at low frequencies.

(2) A hot-wire amplifier method at higher frequencies.

Method 1.—*Hot-wire Vibration Galvanometer Method.*

The arrangement used in this method is as in fig. 6.

Two platinum wires, each of length 1 in. and diameter ·001 in., formed part of two similar electrical circuits. Each wire, supplied with a constant heating current of

* Proc. Roy. Soc. cxvi. (1927).

† 'Journal of Scientific Instruments,' Oct. 1929.

·30 amps., was coupled to a vibration galvanometer by means of separate primaries of a transformer, the secondary of which included the vibration galvanometer and a variable resistance R which controlled its sensitiveness. The obstacles were arranged vertically in the middle of the wind channel, through which a steady stream of air flowed at constant speed, and behind the obstacles were placed the wires, each mounted vertically at the ends of prongs of separate forks.

One wire was kept stationary in a suitable position in one vortex row which gave a suitable deflexion of the galvanometer (generally the maximum) previously tuned

Fig. 6.

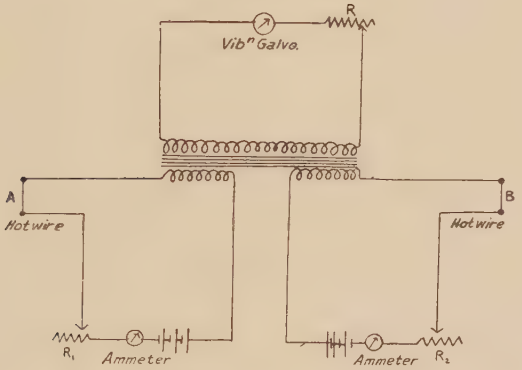

to resonance with the frequency of formation of the vortices passing downstream, while the other wire was moved up and down the stream along a line in the opposite vortex row, which also gave a suitable deflexion of the galvanometer of the same magnitude as that produced by the other wire.

For all positions of the wires the heating currents were kept constant, and the maximum deflexion of the galvanometer due to both wires acting simultaneously was observed.

When the wires were in such positions that the velocity fluctuations at these points were in the same phase the fluctuating P.D.s across the wires, being also in the same phase, produced a reinforcement of the galvanometer deflexion, giving a maximum value.

Fig. 7.

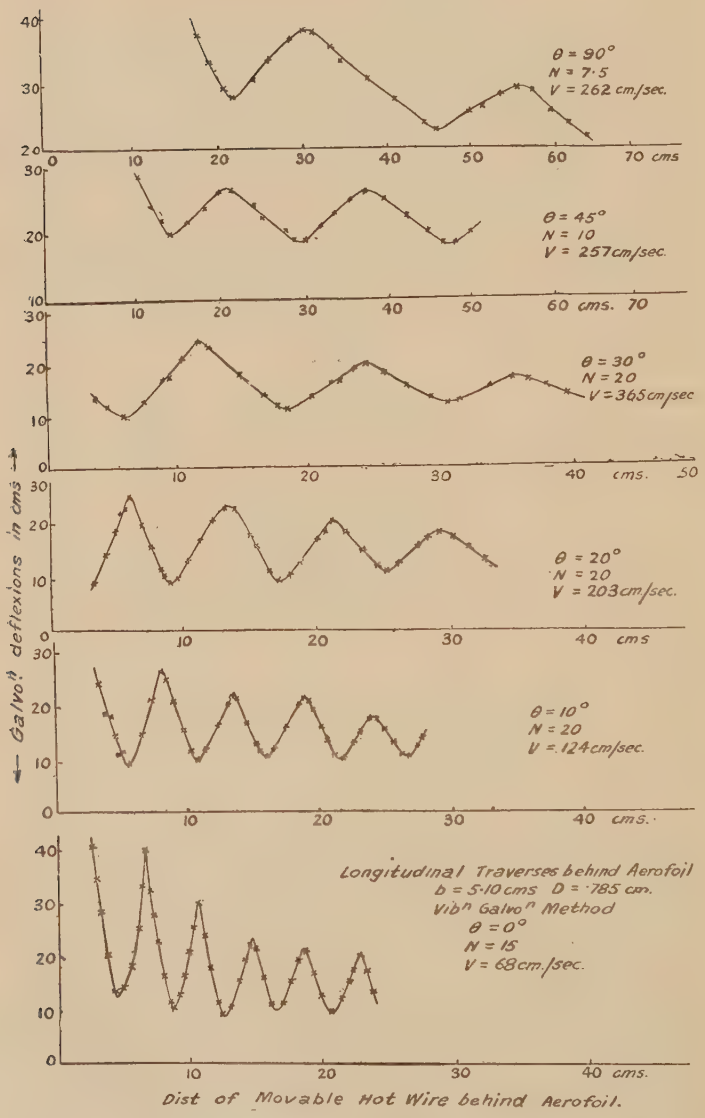

When the wires were in positions corresponding to a phase difference of 180°, the fluctuating P.D.s across them opposed each other, and a minimum deflexion of the

Fig. 8.

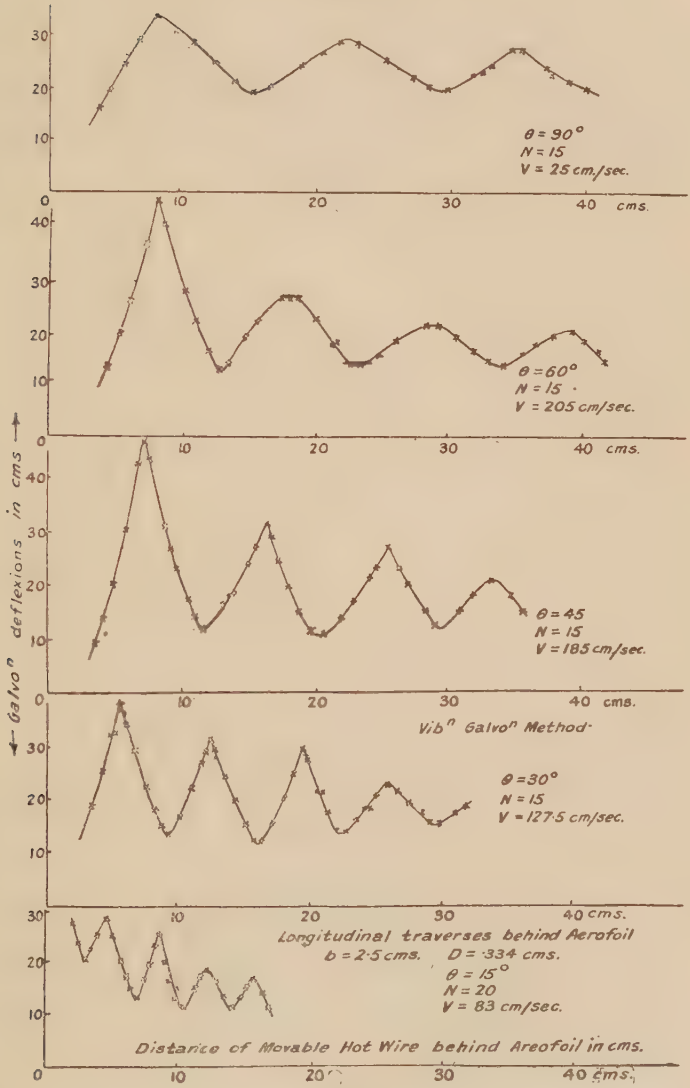

galvanometer was produced. Hence, to obtain the longitudinal spacing of the vortices the maximum galvanometer deflexions were observed for the corresponding positions of the movable hot wire downstream, and a graph exhibiting maximum and minimum values of deflexions was obtained.

The distance between two successive maxima or minima was taken as a measure of the longitudinal spacing between successive vortices in the same row.

Typical results for cylinders and inclined aerofoils are shown in figs. 7, 8, and 9, and a summary of the results, together with the corresponding lateral spacings, are given in Tables XII., XIII., XIV., and XV.

Fig. 9.

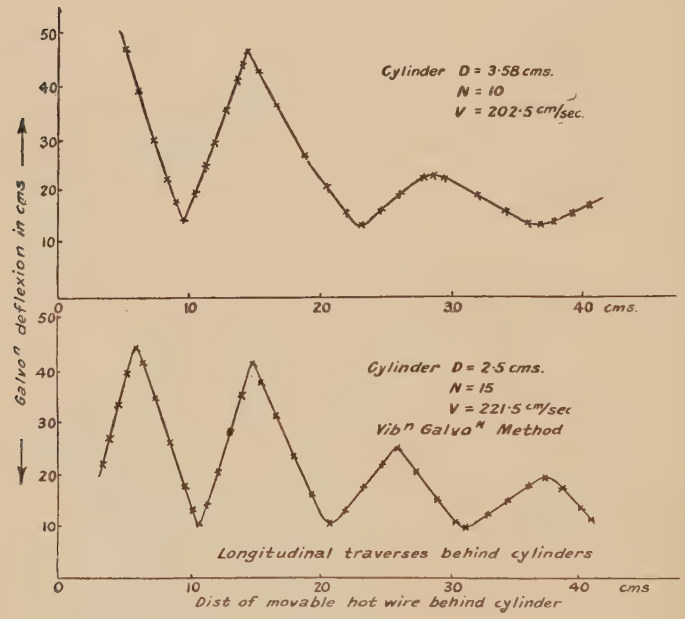

Table XII.

Vibration Galvanometer Method.

Cylinder D=3·58 cm.

N=10. V=202·7 cm./sec. $\frac{V}{N.D}=5{\cdot}66$. $\frac{V.D}{\nu}=4900$.

Dist. behind cylinder $=x$ (cm.).	h. cm.	l. cm.	$\frac{h}{l}$.	$b=\frac{l}{D}$.	$a=\frac{u}{V}$.	$\frac{b}{1-a}=\frac{V}{N.D}$.	$\frac{x}{D}$.
11·50	3·80	13·00	·293	3·64	·358	5·67	3·22
16·50	4·25	13·50	·314	3·77	·334	5·66	4·62
25·00	4·80	14·00	·342	3·90	·308	5·64	6·98
31·50	5·00	14·75	·339	4·12	·272	5·66	8·80

Table XII. (*cont.*).

Vibration Galvanometer Method.

Cylinder D = 2·50 cm.

N = 15. V = 222 cm./sec. $\frac{V}{N.D} = 5{\cdot}91$. $\frac{V.D}{\nu} = 3820$.

Dist. behind cylinder $= x$ (cm.).	h. cm.	l. cm.	$\frac{h}{l}$.	$b = \frac{l}{D}$.	$a = \frac{u}{V}$.	$\frac{b}{1-a} = \frac{V}{N.D}$.	$\frac{x}{D}$.
10·0	3·00	9·80	·306	3·92	·339	5·93	4·00
14·0	3·45	10·30	·335	4·12	·302	5·90	5·60
21·0	3·50	10·80	·325	4·32	·270	5·91	9·40
26·0	3·50	10·80	·325	4·32	·270	5·91	10·40
31·0	3·60	11·20	·321	4·48	·244	5·92	12·40

Cylinder D = 1·40 cm.

N = 15. V = 114·3 cm./sec. $\frac{V}{N.D} = 5{\cdot}45$. $\frac{V.D}{\nu} = 1080$.

Dist. behind cylinder $= x$ (cm.).	h. cm.	l. cm.	$\frac{h}{l}$.	$b = \frac{l}{D}$.	$a = \frac{u}{V}$.	$\frac{b}{1-a} = \frac{V}{N.D}$.	$\frac{x}{D}$.
10·0	1·70	5·55	·305	3·96	·271	5·45	7·10
12·0	1·79	5·60	·320	4·00	·265	5·44	8·59
17·0	1·80	5·60	·321	4·00	·265	5·44	12·12

Table XIII.

Values of "l."

Aerofoil $b = 2{\cdot}50$ cm. D = ·334 cm.

$\theta°$.	V. cm./sec.	N.	$\frac{x}{b}$.	l. cm.
90	251	15	6·60	13·50
			9·00	13·50
			12·00	13·50
60	205	15	5·20	10·40
			7·20	10·50
			9·20	10·50
			11·40	10·50
			13·60	10·65

TABLE XIII. (*cont.*).

Values of "*l*."

Aerofoil $b = 2{\cdot}50$ cm. $D = {\cdot}334$ cm.

θ°.	V. cm./sec.	N.	$\frac{x}{b}$.	*l*. cm.
45	185	15	4·60	9·20
			6·60	9·00
			8·40	9·00
			10·40	9·00
30	127·5	15	3·80	6·70
			5·00	6·70
			6·60	6·80
			7·80	6·60
			9·00	6·80
			10·40	6·80
15	83	20	2·80	3·80
			3·48	3·70
			4·27	3·75
			4·88	3·85
			5·80	3·70

TABLE XIV.

Values of "*l*."

Aerofoil $b = 5{\cdot}10$ cm. $D = {\cdot}785$ cm.

θ°.	V. cm./sec.	N.	$\frac{x}{b}$.	*l*. cm.
90	262	7·5	6·08	25·5
			9·20	25·6
60	238	7·5	4·90	20·0
			6·87	20·0
45	257	10	4·30	16·50
			5·88	16·75
			7·45	17·75
30	365	20	1·96	12·25
			3·43	12·00
			4·60	12·00
			5·88	12·00
20	203	20	1·76	7·75
			2·55	8·25
			3·34	8·20
			4·21	8·25
			4·90	8·35

TABLE XIV (*cont.*).

Values of "l."

Aerofoil b=5·10 cm. D=·785 cm.

θ°.	V. cm./sec.	N.	$\frac{x}{b}$.	l. cm.
10	124	20	1·56	5·25
			2·15	5·25
			2·55	5·25
			3·14	5·25
			3·73	5·25
			4·60	5·40
0	68	15	1·18	4·00
			1·67	4·00
			2·00	4·00
			2·35	4·10
			2·75	4·00
			3·14	4·00
			3·73	4·10
			4·02	4·20

TABLE XV.

Vibration Galvanometer Method.

Type of aerofoil.	θ°.	N.	V. cm./sec.	$\frac{Nb \cdot \sin\theta}{V}$	l (mean). cm.	h (mean). cm.	$\frac{h}{l}$.	$\frac{l}{b \cdot \sin\theta}$.
b=2·50 cm. D=·334 cm.	90	15	251	·149	13·50	3·50	·260	5·40
	60	15	205	·159	10·51	3·12	·295	4·85
	45	15	185	·144	9·05	2·88	·318	5·12
	30	15	127	·148	6·73	2·06	·304	5·40
	15	20	83	·156	3·76	1·07	·284	5·59
b=5·10 cm. D=·785 cm.	90	7·5	262	·146	25·50	6·52	·256	5·02
	45	10	257	·140	17·00	4·88	·287	4·72
	30	20	365	·140	12·06	3·40	·281	4·74
	20	20	203	·172	8·26	2·48	·300	4·74
	10	20	124	·143	5·25	1·60	·205	5·94
	0	15	68	0	4·05	—	—	∞

Method 2.—Hot-wire Amplifier Method.

The desirability of using a differential hot-wire arrangement for measuring the longitudinal and lateral spacings of vortices behind obstacles of smaller section than previously used, necessitates greater sensitivity being obtained, as indicated in an earlier paper *, and the following

* Phil. Mag., June 1930.

method was successfully employed at frequencies ranging from 100/second upwards—fig. 10 shows the arrangement. The same platinum wires were again used, each forming part of two similar electrical circuits, the five-valve amplifier used in the earlier investigations replacing the vibration galvanometer of method 1.

Both wires were coupled separately to the grid input circuit of the amplifier by means of separate primaries of a transformer, and the plate circuit of the last valve transformer-coupled to a circuit consisting of a crystal rectifier and a shunted reflecting galvanometer.

The mounting of the wires behind the obstacle in the wind channel, and procedure of traversing, was precisely similar to that used in method 1, each wire being similarly

Fig. 10.

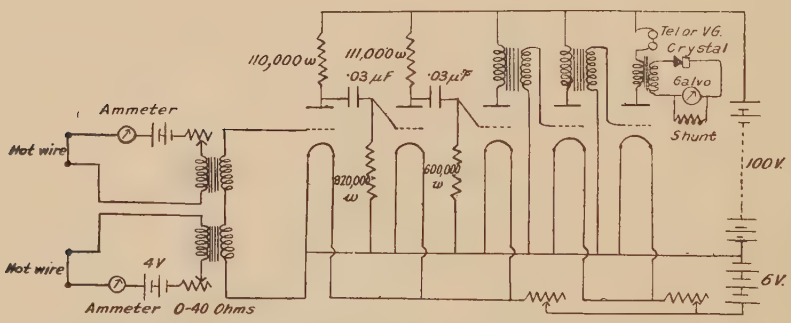

placed, one in each vortex row, where the greatest velocity fluctuations occurred. Under such conditions a periodic change in the resistance of each wire will occur with the same frequency as the frequency of formation of the vortices, with a consequent periodic variation of P.D. across them.

These varying P.D.s. after amplification, will therefore produce periodic changes in the anode current of the fifth valve which simultaneously produce induced currents in the crystal circuit of the same periodicity; hence, after rectification by the crystal, a steady deflexion of the galvanometer will be obtained. It is this deflexion which is observed for all relative positions of the hot wires, when the periodic heating and cooling of both wires are acting simultaneously. When the two wires are in such positions that the velocity fluctuations at these points are in phase,

the fluctuating P.D.s across them being also in phase, after amplification will produce a reinforcement of the fluctuations of anode current, with a resulting increase in the rectified current, thereby producing a maximum steady

Fig. 11.

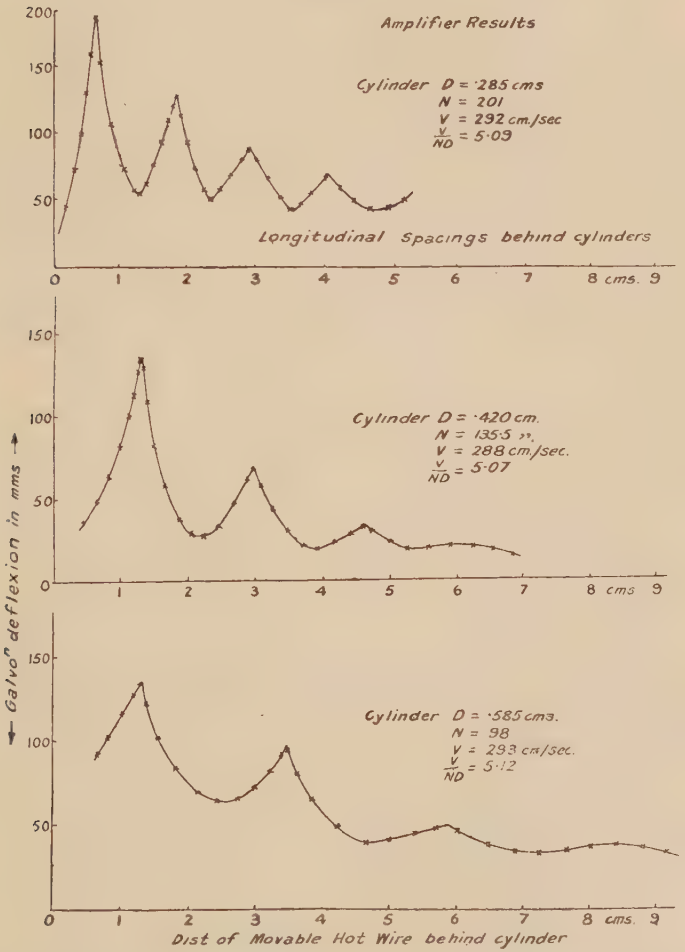

deflexion of the galvanometer. When in positions corresponding to a phase difference of 180°, the fluctuating P.D.s across the wires, being in direct opposition, will produce a minimum rectification after amplification, and hence a minimum steady deflexion of the galvanometer.

Thus, to obtain the longitudinal spacing of the vortices the galvanometer deflexions due to the rectified currents

Fig. 12.

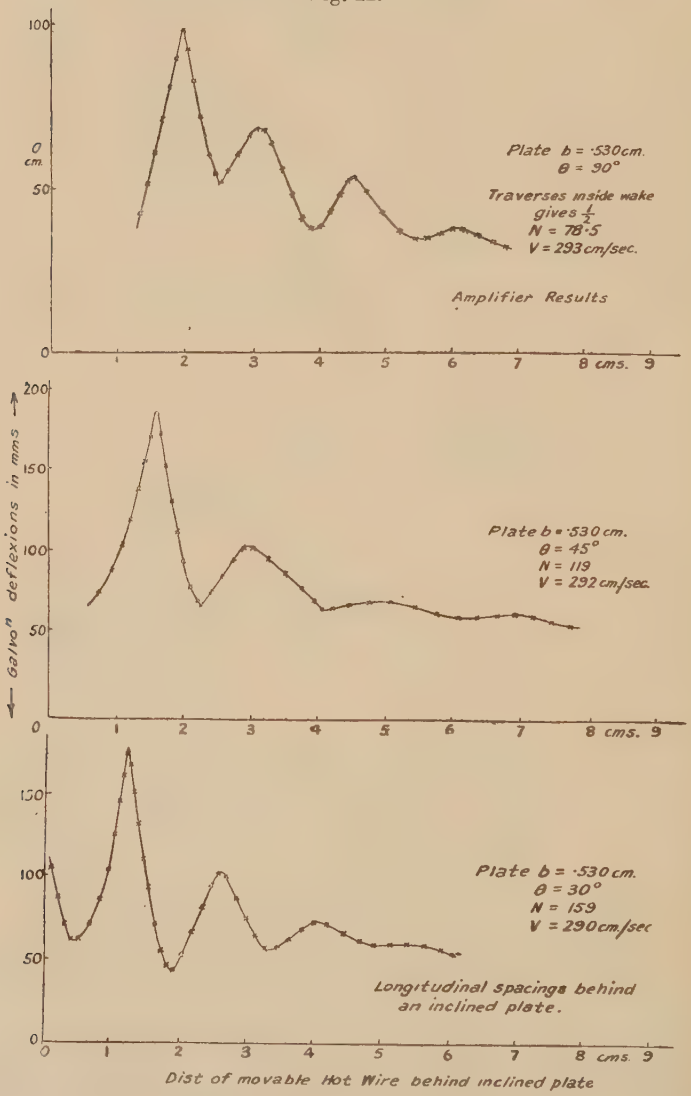

were observed for the corresponding hot-wire positions downstream, and by plotting these deflexions against the

distance of the movable hot wire behind the obstacle downstream similar results were obtained to those using the vibration galvanometer method, the graphs exhibiting maximum and minimum values of deflexion. The distance between two successive maxima or minima was assumed a measure of the longtitudinal spacings between successive vortices in the same row.

Results for cylinders and an inclined plate are included in Tables XVI. and XVII. and figs. 11 and 12, and it will be observed that each traverse is characteristic of a decrease in the maximum peak values as the distance downstream is increased, due to a decrease of vortex strength, or loss in entirety, results which are consistent with those published in an earlier paper.

Figs. 13 and 14 show the effect of using one wire only, transformer-coupled to the amplifier as in fig. 12 and traversed laterally in a vertical plane at right angles to the

TABLE XVI.

Amplifier Method.

Cylinder D = ·320 cm.

N = 182. V = 295 cm./sec. $\frac{V}{N \cdot D} = 5{\cdot}07$. $\frac{V \cdot D}{\nu} = 639$.

Dist. behind cylinder = x. cm.	h. cm.	l. cm.	$\frac{h}{l}$.	$b = \frac{l}{D}$.	$a = \frac{u}{V}$.	$\frac{V}{N \cdot D} = \frac{b}{1-a}$.	$\frac{x}{D}$.
1·0	·345	1·100	·319	3·44	·321	5·07	3·12
2·0	·410	1·260	·326	3·94	·222	5·06	6·24
3·0	·430	1·350	·319	4·210	·167	5·04	9·36
4·0	·450	1·420	·318	4·44	·124	5·08	12·48

Cylinder D = ·285 cm.

N = 201. V = 292 cm./sec. $\frac{V}{N \cdot D} = 5{\cdot}09$. $\frac{V \cdot D}{\nu} = 562$.

Dist. behind cylinder = x. cm.	h. cm.	l. cm.	$\frac{h}{l}$.	$b = \frac{l}{D}$.	$a = \frac{u}{V}$.	$\frac{V}{N \cdot D} = \frac{b}{1-a}$.	$\frac{x}{D}$.
1·30	·355	1·125	·315	3·95	·225	5·10	4·57
1·80	·370	1·125	·329	3·95	·225	5·10	6·31
2·30	·380	1·125	·337	3·95	·225	5·10	8·07
2·90	·385	1·150	·335	4·04	·209	5·10	10·20
3·50	·400	1·150	·348	4·04	·209	5·10	12·30
4·10	·400	1·150	·348	4·04	·209	5·10	14·40

TABLE XVI. (*cont.*).

Amplifier Method,

Cylinder D = ·420 cm.

N = 135·5.	V = 288 cm./sec.			$\frac{V}{N.D}$ = 5·07.		$\frac{V.D}{\nu}$ = 818.	
Dist. behind cylinder = x. cm.	h. cm.	l. cm.	$\frac{h}{l}$.	$b=\frac{l}{D}$.	$a=\frac{u}{V}$.	$\frac{V}{N.D}=\frac{b}{1-a}$.	$\frac{x}{D}$.
2·0	·415	1·650	·252	3·92	·227	5·07	4·76
3·0	·450	1·750	·257	4·17	·180	5·10	7·15
4·0	·480	1·675	·287	4·00	·215	5·10	9·52
4·5	·490	1·750	·297	4·17	·180	5·09	10·72

Cylinder D = ·585 cm.

N = 98.	V = 293 cm./sec.			$\frac{V}{N.D}$ = 5·12.		$\frac{V.D}{\nu}$ = 1160.	
Dist. behind cylinder = x. cm.	h. cm.	l. cm.	$\frac{h}{l}$.	$b=\frac{l}{D}$.	$a=\frac{u}{V}$.	$\frac{V}{N.D}=\frac{b}{1-a}$.	$\frac{x}{D}$.
2·50	·560	2·15	·265	3·67	·279	5·10	4·28
3·50	·620	2·40	·258	4·10	·196	5·10	6·00
5·00	·620	2·40	·258	4·10	·196	5·10	8·55
6·00	·640	2·40	·267	4·10	·196	5·10	10·25
8·50	·645	2·40	·269	4·10	·196	5·10	12·80

air stream, at different distances behind the obstacle, (cylinders D = ·285 and ·320 cm.), the steady galvanometer deflexion being observed for each position of the wire, maintained always at constant heating current. Each traverse exhibits two maxima similar in characteristic to those obtained by the vibration galvanometer method described elsewhere.* The maximum peaks evidently correspond to positions where the amplitude of the velocity fluctuations are a maximum, thereby producing periodic heating and cooling of the hot wire; and since these positions are supposed to occur along the paths of the centres of the vortices †, the distance between such

* Phil. Mag., March 1928.

† Cowley and Levy, 'Theory of Aeronautics.' Streamline contours behind a cylinder.

maxima was taken as a measure of the lateral spacing between the centres of the two rows of vortices.

Notice that beyond $\frac{x}{D} = 10$ for the cylinders, overlapping of the two rows of vortices is sufficient to produce a region

TABLE XVII.

Plate $b = \cdot 53$ cm. Thickness $= \cdot 50$ mm.

θ.	V. cm./sec.	N.	$\frac{Nb \cdot \sin\theta}{V}$	$\frac{x}{b}$	$\frac{l}{2}$ cm.	$\frac{l}{b \cdot \sin\theta}$
				4·72	1·150	4·35
				5·66	1·400	5·30
90	293	78·5	·142	7·36	1·400	5·30
				8·69	1·525	5·75
				10·00	1·550	5·85
						mean = 5·31
					l.	
				4·15	1·575	4·20
				5·66	1·875	5·00
45	292	119	·152	7·55	1·895	5·05
				9·45	2·050	5·47
				11·32	2·100	5·60
						mean = 5·06
					l.	
				2·27	1·400	5·28
				3·40	1·450	5·47
30	290	159	·146	4·72	1·450	5·47
				6·03	1·450	5·47
				7·55	1·550	5·85
						mean = 5·50

of uniform velocity fluctuation ; no peaks are exhibited, but merely a traverse having a flat top.

These lateral traverses are consistent with a few preliminary measurements made by Dryden and Kuethe* on the velocity fluctuations behind a cylinder of diameter 7·50 cm., using a hot-wire anemometer arrangement.

* Report No. 320, p. 25, fig. 20 (Jan. 8, 1929), National Advisory Committee of Aeronautics, Bureau of Standards, Washington.

Theory and Discussion of Results.

Frequency of Formation of Vortices behind Cylinders, Inclined Aerofoils, and Plates.

Relation between $\frac{N.D.}{V}$ *and* $\frac{V.D.}{\nu}$ *for Cylinders.*

The frequency of formation (N) of vortices formed be-

Fig. 13.

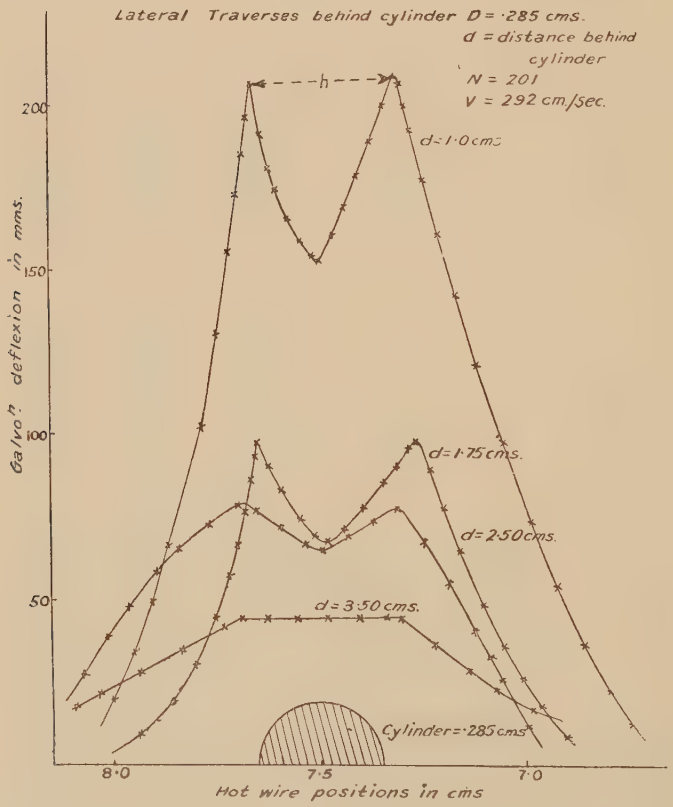

hind a stationary cylinder of diameter D placed in a steady fluid stream of velocity V can be expressed as

$$\frac{N.D}{V} = K.f\left(\frac{\nu}{V.D}\right),$$

where ν = kinematic viscosity of the fluid and $f\left(\frac{\nu}{V.D}\right)$

is unknown and is to be determined from the experimental results.

Assuming that $\frac{N \cdot D}{V}$ would be affected by a change in viscosity ν and expanding $f\left(\frac{\nu}{V \cdot D}\right)$ as a Maclaurin's

Fig. 14.

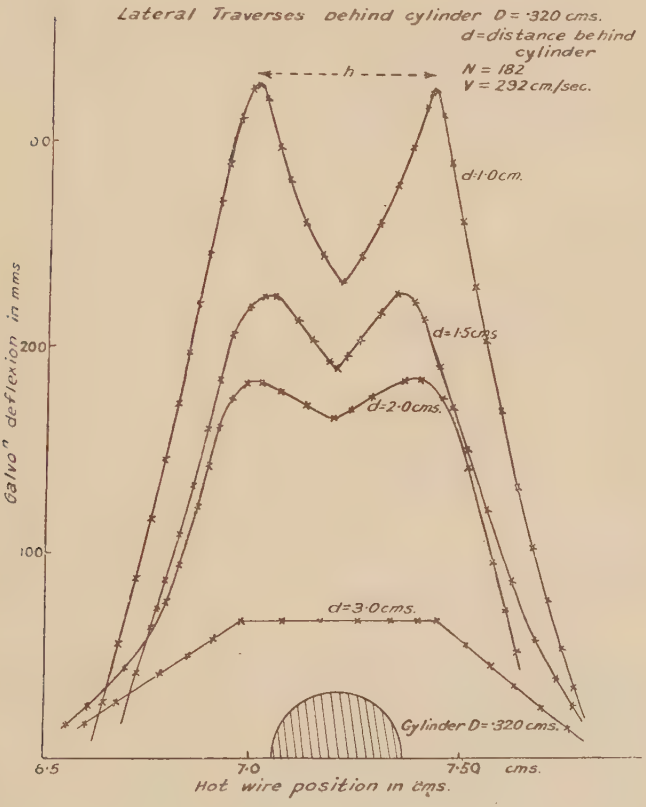

series, we get

$$\frac{N \cdot D}{V} = a + b\left(\frac{\nu}{V \cdot D}\right) + c\left(\frac{\nu}{V \cdot D}\right)^2 + \ldots,$$

where a, b, c, ... are constants.

Since $\frac{\nu}{V \cdot D}$ is small with respect to $\frac{N \cdot D}{V}$ neglecting

the higher power terms of $\left(\frac{\nu}{V.D}\right)$ above the first order, we obtain

$$\frac{N.D}{V} = a + b\left(\frac{\nu}{V.D}\right)$$

$$= A\left(1 + B\frac{\nu}{V.D}\right). \quad . \quad . \quad . \quad . \quad (1)$$

where A and B are constants.

Since the equation is linear, by plotting the experimental values of $\frac{N.D}{V}$ and $\frac{\nu}{V.D}$ we should expect to get a

Fig. 15.

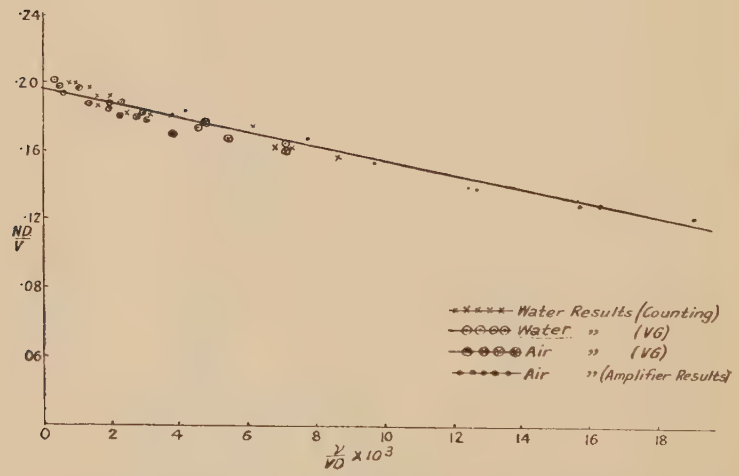

straight line graph. Fig. 15 shows such results plotted, from which A = ·198 and B = −19·7 are obtained. Hence, retaining the viscosity term we get

$$\frac{N.D}{V} = \cdot 198\left(1 - 19\cdot 7\frac{\nu}{V.D}\right), \quad . \quad . \quad . \quad (2)$$

which well represents the experimental results over the range considered, and compares favourably with some earlier results *. The constants are nearly identical with those deduced by Rayleigh † from Strouhal's ‡ results

* Phil. Mag., June 1930.
† Rayleigh, 'Sound,' ii. pp. 413–414.
‡ *Ann. d. Phys.* v. p. 12 (1878).

obtained by a different method, A and B having values of ·195 and 20·1 respectively.

It must be understood, however, that such an equation is only representative at values of $\frac{V.D}{\nu}$ less than 500, for at higher values $\frac{N.D}{V}$ is constant, (5·05), as revealed by the results on fig. 16, and is consistent with the results of other experimenters *.

The upper limit of $\frac{V.D}{\nu}$ ($=5\times10^5$), where the sudden shifting back of the point where the vortex layer leaves the

Fig. 16.

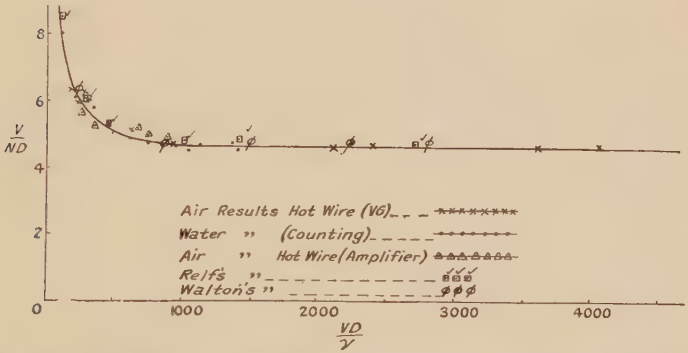

surface of the cylinder, thus producing a change in $\frac{N.D}{V}$, was not reached in these experiments.

Relation between $\frac{N.b}{V}$ *and* θ *for Inclined Plates and Aerofoils in Air.*

A summary of the results for aerofoils and plates by the different methods is included in Tables XVIII. and XIX., the figures in the brackets denoting the number of independent observations made. The average of the results for the inclined plates suggest that at angles of inclination θ between 20° and 90° $\frac{Nb.\sin\theta}{V}$ =·158, and is constant for

* Benard, *Comptes Rendus*, cxlvii. p. 839 (1908). Tyler, Phil. Mag., June 1930. Relf, Phil. Mag. xlii. p. 173 (1921). Richardson, Proc. Phys. Soc. xxxvi. (1924). Kruger, *Ann. d. Phys.* lx. p. 279 (1919).

the different plates, whereas the aerofoils show a constancy of $\frac{Nb \,.\, \sin\theta}{V} = \cdot 150$ at angles of 20° upwards.

Between 0° and 30° there is, however, a difference between the plate and the aerofoil results, which is to be expected, since at such low angles of incidence the maximum thickness D of the aerofoil plays a more important part in controlling the rate of formation of the vortices, and D must replace $b \,.\, \sin\theta$.

Summary of Results for Inclined Aerofoils and Plates $\left(\frac{Nb \,.\, \sin\theta}{V}\right.$ *between* 20° *and* 90°$\left.\right)$.

TABLE XVIII.

(Aerofoil Results.)

Type of aerofoil.	Water results. Vibrating aerofoil.	Water results. Counting.	Air results. Hot wire method with V.G.	Air results. Wind channel & whirler. Hot wire with V.G.	Air results. Wind channel & whirler. Hot wire amplifier.
No. 1.					
b=5·00 cm.	·162 (4)	·165 (4)	—	—	—
D=·755 cm.	—	—	·163 (13)	—	—
No. 1*a*.					
b=5·10 cm.	—	—	·149 (4)	—	—
D=·785 cm.					
No. 2.					
b=2·45 cm.	·149 (7)	·153 (9)	—	·155 (13)	—
D=·325 cm.					
No. 2*a*.					
b=2·50 cm.	—	—	—	·150 (4)	—
D=·334 cm.					
No. 3.					
b=1·20 cm.	·157 (8)	·160 (9)	·163 (8)	·159 (10)	·176 (3)
D=·188 cm.					
No. 4.					
b=·64 cm.	—	—	·159 (5)	—	·170 (3)
D=·82 cm.					

Average=·158.

Figues in brackets represent number of observations.

Fage and Johansen *, using a much wider plate than in my experiments, obtained constancy of $\frac{Nb \,.\, \sin\theta}{V} = \cdot 148$ between 30°–90°.

It is therefore highly probable that the vortex frequency of formation behind an inclined plate or aerofoil at θ° to

* Proc. Roy. Soc. A, p. 116 (1927).

the fluid stream, and of width b cm., is similar to that behind a plate or aerofoil normal to the stream, and having effective width $b \cdot \sin\theta$. In such a case both the longitudinal and lateral spacings will be modified proportionally as the inclination is varied. Confirmation of this is revealed in the results for the longitudinal and lateral spacings behind such obstacles, for $\frac{l}{b \cdot \sin\theta} = 5{\cdot}25$, and is constant for angles between 30° and 90°.

TABLE XIX.

(Plate Results.)

Length. cm.	Thickness. mm.	Width. b, cm.	$\frac{Nb \cdot \sin\theta}{V}$. V.G. method.	$\frac{Nb \cdot \sin\theta}{V}$. Amplifier method.
23·0	·95	1·90	·157 (7)	—
30·0	·95	2·90	·151 (8)	—
20·0	·50	·59	—	·145 (4)
20·0	·50	·425	—	·147 (5)
20·0	·50	·53	—	·146 (3)

Average = ·150.

Longitudinal and Lateral Spacings.

1. *Spacings behind Cylinders.*

Referring to Tables XII. and XVI., the mean value of $\frac{h}{l} = {\cdot}308$ the upper and lower limits being ·348 and ·252, whereas Karman's theoretical stability condition for two parallel rows of vortices in an infinite fluid is given as $\frac{h}{l} = {\cdot}281$.

There is a general tendency of a widening out of the paths of the vortices as they recede from the body, together with a proportional increase in the longitudinal spacings, and both of these effects produce a retardation on the relative speed u of the vortices with respect to the fluid stream, for there is a marked decrease in $\frac{u}{V}$ in most cases as the distance downstream is increased.

This increase in the longitudinal and lateral spacings has been observed by Fage and Johansen* for a large plate in an air stream. They found that $\frac{h}{l}$ increased by 100 per cent. for $\frac{x}{b}=5{\cdot}0$ when $\frac{h}{l}={\cdot}245$ to $\frac{x}{b}=20$ when $\frac{h}{l}={\cdot}525$, and the results given in the above-mentioned tables show a gradual increase, not, however, at so great a rate as found by Fage and Johansen. Rosenhead† has shown that the stability of a double row of vortices, taking into consideration the image effects of the walls of the channel, is given as $\frac{h}{l}={\cdot}281-{\cdot}090\left(\frac{l^2}{\mathrm{H}}\right)$, where 2H is the breadth of the channel, and in the presence of the walls $\frac{h}{l}$ is always less than ·281.

Professor Levy and Hooker‡ regard any such formation of vortices in the wake of a body as a system not completely stable, and attribute the instability not to the influence of the image system replacing the walls, but to the fact that the vortices themselves may be considerably affected by the spreading of the boundary layer, such that it intermingles with the vortices. As a result thereof the vortices will be in a field in which a velocity gradient, called the basic velocity gradient, exists. In Fage and Johansen's results such a velocity gradient has been shown to exist, thereby affecting the stability of the system. In my results much lower speeds were used, and it is probable that this cause of interference is not so marked, especially with the smaller models.

By plotting $\frac{l}{\mathrm{D}}$ against $\frac{\mathrm{D}}{x}$ for the different cylinders, as in fig. 17, the results are well represented by the linear relation

$$\frac{l}{\mathrm{D}}=4{\cdot}50\left(1-{\cdot}62\frac{\mathrm{D}}{x}\right),$$

which compares favourably with Karman and Rubach's§ value of $\frac{l}{\mathrm{D}}=4{\cdot}30$ for a cylinder in water, and Fage's‖

* Proc. Roy. Soc. A, p. 116 (1927).
† Phil. Trans. A, ccxxviii. pp. 275–329.
‡ Phil. Mag., March 1930.
§ *Phys. Zeits.* xiii. p. 49 (1912).
‖ Roy. Aero. Soc. Journ., Jan. 1928.

value of $\frac{l}{D}=4{\cdot}27$ for a cylinder in air. Beyond $\frac{x}{D}=12$ the variations of $\frac{l}{D}$ are of the same order as the experimental errors. With such small models, it is only at this value of $\frac{x}{D}$ that one might assume the speed of the vortices relative to the surrounding fluid to be constant.

Fig. 17

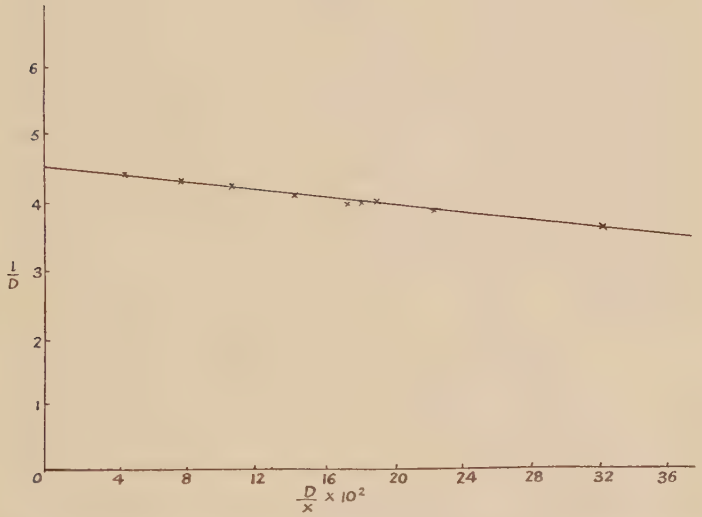

2. *Longitudinal Spacings behind Inclined Aerofoils and Plates.*

Tables XV. and XVII. include results for aerofoils $b=2{\cdot}50$ cm. and $5{\cdot}10$ cm., and plate $b={\cdot}52$ cm. There is again the same tendency for a gradual increase in $\frac{h}{l}$ as the vortices move downstream. It will be observed that between 20°–90° there is a constancy of $\frac{l}{b\,.\sin\theta}=5{\cdot}25$ (average value) for the aerofoil, and $\frac{l}{b\,.\sin\theta}=5{\cdot}29$ for the plate, both being in excellent agreement with Fage and Johansen's value $5{\cdot}32$ for a much larger plate, and this firmly supports the idea that the flow behind an inclined obstacle such as a plate or aerofoil would be similar to that of a

plate or aerofoil placed normal to the stream and having the same effective width as the inclined body.

Relation between $\frac{N.D}{V}$ *and Longitudinal Spacings.*

Experimenting with cylinders and plates in water, Karman and Rubach, photographing the vortices formed behind such models, found that at some distance behind the obstacles, $\frac{h}{l} = \cdot 281$, a constant independent of D and V, but l was proportional to b and greater than D, *i. e.*, $l = b\mathrm{D}$ for a given obstacle. The velocity of the vortices (u) relative to the stream was less than but proportional to V, *i. e.*, $u = a\mathrm{V}$. Now these conditions can only be true when there is no basic velocity gradient; the results outlined above would not apply in the case of the first few pairs of vortices formed, especially with those dealt with in the foregoing experiments, and a modification of Karman's formula is necessary.

If N = the number of vortices passing any fixed point per second in either vortex row,

and T = time interval between the passages of two successive vortices past the fixed point in the same row,

and l = longitudinal spacings between any two successive vortices in the same row,

then

$$\mathrm{N} = \frac{1}{\mathrm{T}} = \frac{\mathrm{V} - u}{l},$$

whence

$$\frac{u}{\mathrm{V}} = 1 - \frac{\mathrm{N}.l}{\mathrm{V}} = a, \quad . \quad . \quad . \quad . \quad . \quad (1)$$

and

$$\frac{\mathrm{N}.\mathrm{D}}{\mathrm{V}} = \frac{\mathrm{D}}{l}\left(\frac{\mathrm{V} - u}{\mathrm{V}}\right) = \frac{1 - a}{b}, \quad . \quad . \quad . \quad (2)$$

which is constant if a and b are constant. This is the theoretical formula deduced by Kruger *. and also referred to by Benard †, Richardson, and others.

* *Ann. d. Phys.* lx. p. 279 (1919).
† *Comptes Rendus*, clxxxii. no. 25 (June 21, 1926).

Equation (1) enables one to obtain values of $\frac{u}{V}$, and these are included in the tables. Benard concluded from measurements made in viscous liquids that such an equality as given by equation (2) is far from being true, and for the range covered in his experiments, in which $\frac{V.D}{\nu}$ varied from 73 to 1202, $\frac{N.D}{V}$ varied from ·092 to ·250, and is somewhat at variance with Relf's results. Furthermore, from a series of photographs taken, he established evidence that there was considerable variation in the value of b and a, far from being in agreement with the laws of Karman.

If, now, we substitute for a and b in equation (2), we get

$$\frac{N.D}{V} = \frac{1-\frac{u}{V}}{\frac{l}{D}},$$

and since $\frac{l}{D}$ is not constant, as revealed by the previous experiments, but is given as

$$\frac{l}{D} = 4{\cdot}50\left(1-{\cdot}62\frac{D}{x}\right),$$

therefore

$$\frac{N.D}{V} = \left(1-\frac{u}{V}\right) \div 4{\cdot}50\left(1-{\cdot}62\frac{D}{x}\right),$$

giving

$$\frac{u}{V} = 1-4{\cdot}50\frac{N.D}{V}\left(1-{\cdot}62\frac{D}{x}\right), \quad . \quad . \quad . \quad (3)$$

and this equation satisfies fairly well the results obtained by the methods used. Such a result might be expected to be only a true representation of the experimental results when the effect of viscosity in the guise of $\frac{V.D}{\nu}$ has a constant influence on the value of $\frac{N.D}{V}$, *i. e.*, when $\frac{V.D}{\nu}$ is greater than 500, and $\frac{N.D}{V}$ is approximately constant (see fig. 16). At lower values of $\frac{V.D}{\nu}$, where $\frac{N.D}{V}$ undergoes a marked change, the above equation is no longer true,

and a correcting term involving $\frac{V.D}{\nu}$ must be introduced. Hence, substituting the value of

$$\frac{N.D}{V} = \cdot 198\left(1 - 19\cdot 7\frac{\nu}{V.D}\right)$$

in equation (3), we get

$$\frac{u}{V} = 1 - \cdot 890\left(1 - \cdot 62\frac{D}{x}\right)\left(1 - 19\cdot 7\frac{\nu}{V.D}\right), \quad . \quad (4)$$

which takes into effect viscosity, and the retardation of the vortices moving downstream, and is an empirical relation which should satisfy the experimental results when $\frac{\nu}{V.D}$ is appreciable.

At some distance behind the cylinders, where conditions are steady, *i.e.*, where $\frac{D}{x}$ is small, we have the relation

$$\frac{u}{V} = A + B\frac{\nu}{V.D}, \quad . \quad . \quad . \quad . \quad . \quad (5)$$

where A and B are constants.

This is a linear relation in $\frac{u}{V}$ and $\frac{\nu}{V.D}$, which is what might be expected from dimensional reasoning, putting $\frac{u}{V} = f\left(\frac{\nu}{V.D}\right)$, and expanding as a Maclaurin's series. In my results, however, $\frac{N.D}{V}$ is approximately constant, and the effect of $\frac{V.D}{\nu}$ is practically negligible.

An attempt to investigate the relation between $\frac{u}{V}$ and $\frac{V.D}{\nu}$ for cylinders in water has been made by Walton*, and his results show considerable variations, the average values, however, lying on a well-defined curve, indicating that $\frac{u}{V}$ decreased rapidly at first from a value of ·40 at $\frac{V.D}{\nu} = 250$, and then approaches asymptotically a value of ·15 at $\frac{V.D}{\nu} = 3000$ (approx.). At values of $\frac{V.D}{\nu}$ greater than 3000 the average value of $\frac{u}{V} = \cdot 146$, in agree-

* Scientific Proc. Roy. Dublin Soc. xviii. no. 47 (Jan. 1928).

ment with the value for a perfect fluid. The variations in $\frac{u}{V}$ in his experiments are no doubt due to not considering the term $\left(1-\cdot 62\frac{D}{x}\right)$, which in his experiments would be appreciable.

If we assume $\frac{D}{x}$ is small, the average of his results does confirm the relation given by equation (5).

Summary and Conclusions.

Different methods of estimating the frequency of formation of the vortices behind cylinders, areofoils, and plates in air and water are described, and dimensional theory included which satisfies the results.

For cylinders

$$\frac{N\,.\,D}{V}=\cdot 198\left(1-19\cdot 7\frac{\nu}{V\,.\,D}\right),$$

and for inclined plates and aerofoils, $\frac{Nb\,.\,\sin\theta}{V}$ is constant between 20° and 90°, having values of ·158 and ·150 for the plates and aerofoils respectively.

Differential methods are described in which two electrically heated platinum wires are used in conjunction with either a vibration galvanometer at low frequencies, or a valve amplifier at audible frequencies, for measuring the longitudinal spacings af vortices formed behind cylinders, inclined plates, and aerofoils. Measurements of the lateral spacings h of the vortex rows are also included, and the average values of $\frac{h}{l}=\cdot 308$ compares favourably with Karman's theoretical value ·281. The upper and lower limits, however, are at too great a variance to be regarded as experimental errors, and the possibility of the existence of a basic velocity gradient may account for these variations.

The longitudinal spacings behind the inclined plates and aerofoils show constancy of $\frac{l}{b\,.\,\sin\theta}=5\cdot 29$ and $5\cdot 25$ respectively between $\theta=30°$ and 90°.

Behind the cylinders the tendency of l to increase downstream is governed by the relation

$$\frac{l}{\mathrm{D}} = 4{\cdot}50\left(1 - {\cdot}62\frac{\mathrm{D}}{x}\right).$$

Empirical formulæ connecting $\frac{u}{\mathrm{V}} \cdot \frac{\mathrm{N}.\mathrm{D}}{\mathrm{V}}$ and $\frac{\mathrm{V}.\mathrm{D}}{\nu}$ are given, in which

$$\frac{u}{\mathrm{V}} = 1 - 4{\cdot}5\frac{\mathrm{N}.\mathrm{D}}{\mathrm{V}}\left(1 - {\cdot}62\frac{\mathrm{D}}{x}\right),$$

when the effect of viscosity is constant so as not to influence $\frac{\mathrm{N}.\mathrm{D}}{\mathrm{V}}$, and

$$\frac{u}{\mathrm{V}} = 1 - {\cdot}890\left(1 - {\cdot}62\frac{\mathrm{D}}{x}\right)\left(1 - 19{\cdot}7\frac{\nu}{\mathrm{V}.\mathrm{D}}\right),$$

when the effect of viscosity is appreciable and has an effect on $\frac{\mathrm{N}.\mathrm{D}}{\mathrm{V}}$.

LXXIV. *On the Anomalous Flow of a Strong Solution of Lithium Chloride through Narrow Glass Tubes.* *By* G. W. Scott Blair, *M.A.*, *and* R. K. Schofield, *M.A.*, *Ph.D.* (*Soil Physics Department, Rothamsted Experimental Station, Harpenden, England*) *.

Introduction.

IT has long been known that many colloidal systems do not obey the Poiseuille law, but solutions of simple inorganic salts are generally believed to do so. One of the purposes of this paper is to show that this assumption is incorrect in the case of strong solutions of lithium chloride.

According to Bingham [1] and other subsequent workers the discrepancies for many suspensions may be expressed by introducing a term into the Poiseuille equation in the form of a pressure to be subtracted from the applied pressure difference. This involves a modification of the Maxwell assumption in the sense that for such systems the velocity gradient at any point is found to be proportional to the stress applied at that point over and above a certain critical

* Communicated by the Authors.

stress. This critical stress has produced a strain which is maintained during the shearing, and does not relax very rapidly as postulated by Maxwell[2] for the case of fluids.

It has already been shown by Hatschek and Jane[3] that Maxwell's hypothesis does not hold for solutions of ammonium oleate where large ions, probably micelles, are present (see also Bingham and Robertson[4]).

It has been pointed out by Grinnell Jones and Dole[6] that in their equation relating viscosity of solutions to concentration there is a constant, A, which "probably represents the stiffening effect on the solution of the electric forces between the ions which tend to maintain a space lattice structure. The value of A is zero for non-electrolytes." Some additional viscosity due to such causes was suggested many years ago by Sutherland[7], who, expressing himself in terms of Maxwell's rigidity, anticipated a rigidity of the system breaking down so quickly that it would constitute merely an additional viscosity. Although the Debye-Hückel theory of solution cannot be expected to hold for very strong salt solutions in any direct sense, yet the tendency for the ionic distribution to be somewhat ordered, as postulated in this theory, suggests the possibility that there should be a definite rigidity in strong solutions even of salts having small ions. There is no *à priori* reason for supposing that this rigidity should dissipate itself instantly, since the persistent tendency of the ions to maintain a non-random distribution may well lead to the presence of a Bingham term.

Very little work has been done on the viscosity of really concentrated salt solutions. The classical papers of Grüneisen[8], Applebey[9], and Merton[10] are confined to dilute solutions, and although Hoskins[11] has shown that the viscosity and conductivity-temperature curves are of the same form for lithium chloride and other salt solutions almost up to saturation, his experiments were restricted to the measurement of supposedly simple viscosity, Poiseuille's law being assumed to hold exactly for his solutions. Cohen[12] has shown that the viscosity of strong salt solutions increases at very high pressures, but not only were the stresses used of a very high order of magnitude, but also the presence of a Bingham term would have the effect of showing an apparent decrease in viscosity as pressure increases, and this decrease would be extremely small at any but the lowest pressures.

It was therefore considered of interest to obtain curves relating stress to flow for strong solutions of lithium

chloride, this being a convenient salt. The saturated solution was first used, but owing to the possible objection that minute crystals of salt might affect the results, a slightly more dilute solution ($N = 10{\cdot}9$) was investigated, and it is this solution to which the following data refer.

Experimental part.

An apparatus for obtaining flow-curves relating V (volume of flow per second) to P (pressure-difference) has already been described [5] and no repetition of this description will be given here for the reason that each set of data quoted is accompanied by a parallel set for a glycerine-water mixture, which, by its behaviour throughout as a true fluid, precludes the possibility of the anomalies shown by the LiCl solution being due to deficiencies in the apparatus or experimental technique. Further, the straightness of the glycerine-water flow-curve makes it clear that the critical velocity for turbulence was not reached. The measurements were carried out in a thermostat at 25° C. in all cases, the same capillary tubes being employed as were used in the earlier work [5*b*].

The glycerine-water mixture used in experiment (1) was adjusted to have a viscosity almost exactly the same as that of the LiCl solution. In the case of experiment (2), the glycerine-water mixture curve was obtained at an earlier date, and is reproduced from the paper already referred to. The viscosity is slightly different, but is sufficiently similar to show the marked difference in properties.

Experiment 1.—The flow-curve for the LiCl solution is given in fig. 1, and that for the glycerine-water mixture in fig. 2. Within the limits of experimental error, the curve for LiCl is certainly a straight line, but shows a significant Bingham intercept on the stress axis.

Experiment 2.—When it was observed from experiment 1 that LiCl solution does not obey the Poiseuille law it was decided to investigate it further by using a variety of tubes of different radius and length. It was shown in a previous paper [5*b*] that certain suspensions display a phenomenon which we have called the σ-phenomenon, in that their flow properties cannot be explained by any of the usual modifications of the Poiseuille law, nor in fact by any relation obtained by assuming the velocity gradient to be a single-valued function of the stress. Although no explanation of the cause of this phenomenon has been given, it was shown that it indicates the existence of a region of constant thickness

showing modified and easier flow in the neighbourhood of the wall of the tube. That such a phenomenon should

Fig. 1.

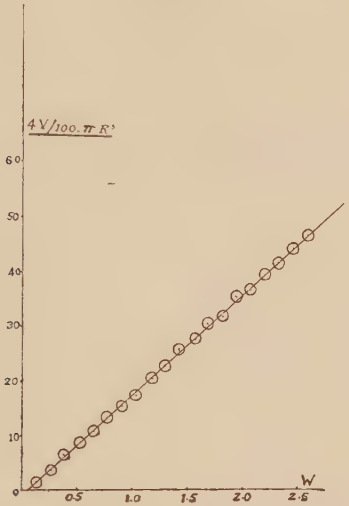

Flow-curve for lithium chloride solution.

Fig. 2.

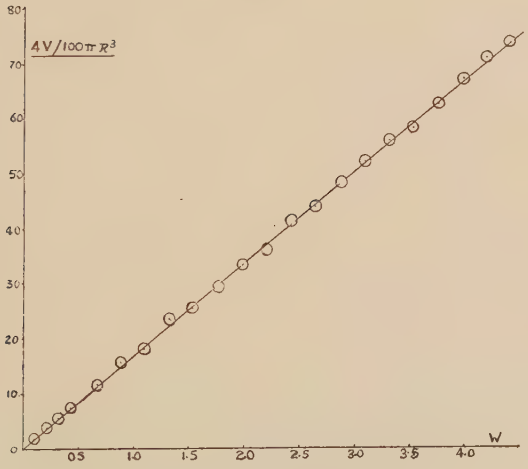

Flow-curve for glycerine-water mixture.

manifest itself in the case of a LiCl solution seemed extremely improbable, but the matter was investigated, and it is quite clear that *the σ-phenomenon is definitely present.*

If the mean velocity ($v = V/\pi R^2$, where R is radius of tube) is plotted against the stress at the wall (W), the slope of the straight-line curve obtained, dv/dW, which is termed σ, should, for a system obeying the R^4 law, be proportional to the radius of the tube—in other words, the σ/R curve should be a straight line passing through the origin and

Data for flow of LiCl solution through four different tubes.

v is mean velocity in metre/secs. $\left(= \frac{V}{100\pi R^2}\right)$, where V is flow in c.c./secs. and R is radius.

W is stress per unit area at wall in dynes/mm.^{2} $\left(= \frac{PRg}{100 \times 2L}\right)$, where P is pressure and L is length of tube.

Tube no. III.—R = 0·073 cm.; L = 12·10 cm.

v ...	0·002	0·04	0·07	0·09	0·11	0·13	0·15	0·18	0·21	0·24
W...	0·08	0·16	0·24	0·32	0·40	0·48	0·56	0·64	0·72	0·80

Tube no. VII.—R = 0·059 cm.; L = 10·60 cm.

v ...	0·01	0·05	0·08	0·10	0·14	0·18	0·24	0·28	0·32	0·37
W...	0·07	0·18	0·30	0·37	0·56	0·74	0·93	1·11	1·29	1·48

Tube no. IV.—R = 0·48 cm.; L = 12·25 cm.

v ...	0·02	0·04	0·08	0·10	0·13	0·15	0·18	0·20	0·25	0·27
W...	0·13	0·26	0·39	0·52	0·65	0·78	0·91	1·04	1·17	1·30
v ...	0·30	0·32	0·36	0·38	0·42	0·44	0·47	0·49	0·53	0·56
W...	1·42	1·56	1·68	1·82	1·94	2·07	2·20	2·34	2·46	2·60

Tube no. V.—R = 0·40 cm.; L = 12·30 cm.

v ...	0·01	0·03	0·06	0·07	0·11	0·15	0·20	0·24	0·27	0·32	0·36
W...	0·11	0·22	0·33	0·44	0·66	0·88	1·10	1·32	1·54	1·76	1·98
v ...	0·41	0·43	0·48	0·53	0·56	0·62	0·65	0·69	0·74	0·78	0·82
W...	2·20	2·42	2·64	2·86	3·08	3·30	3·52	3·75	3·96	4·18	4·40

have a slope $= \frac{1}{4\eta}$. Where the σ-phenomenon is present this line does not on extrapolation pass through the origin, but makes an intercept (σ_0) on the σ axis. The real shape of the σ/R curves has been discussed in a later paper[5 d] now in the press.

In the table are given the figures for v and W for the LiCl solution, and in fig. 3 are shown the σ/R curve for LiCl and

also, for comparison, that for a glycerine-water mixture. It is quite clear that whereas the glycerine-water behaves normally, the LiCl solution shows a small but definitely significant intercept on the σ axis.

Discussion.

The result of experiment 1 is interesting, but not very surprising in view of what was said in the introduction. The smallness of the Bingham intercept makes it unlikely

Fig. 3.

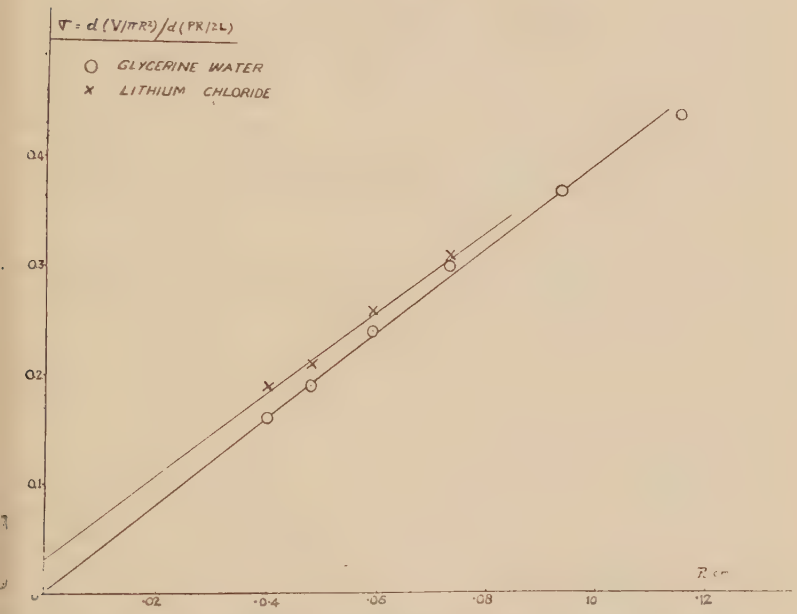

σ/R curves for lithium chloride solution and glycerine-water mixture.

that any serious errors have been introduced into previous measurements of viscosity of salt solutions from this cause, but this does not detract from its theoretical interest. Experiment 2, on the other hand, shows an anomaly hitherto believed to exist only in suspension containing solid matter in a more or less coarse state, and is most unexpected. The uncertainties brought about by the presence of a σ phenomenon are more serious. It will be observed, for example, from fig. 3 that a computation of the viscosity from the data for any single tube would yield a viscosity for

lithium chloride lower than that for the glycerine mixture. If, on the other hand, the viscosity is determined from the slope of the best straight line drawn through all the points on the σ/R curve, it appears that the lithium chloride is the more viscous.

Summary.

Two distinct anomalies are apparent in the flow properties of a strong solution of lithium chloride :

1. The flow-pressure curve, although linear, gives on extrapolation a small intercept on the pressure axis. This indicates that small strains are not dissipated immediately during the flow, which may well be due to the persistent tendency of the ions to maintain a non-random distribution.

2. The simple R^4 law is not exactly obeyed, indicating anomalous flow close to the wall of the tube. This phenomenon was previously thought to be confined to suspensions, and no explanation of it is offered.

Parallel experiments with glycerine-water mixtures which behave normally prove that these anomalies are not due to defects in the experimental technique.

References.

(1) Bingham, E. C., ' Fluidity and Plasticity ' (1922).
(2) Maxwell, J. C., Phil. Mag. xxxv. p. 133 (1868).
(3) Hatschek, E., and Jane, R. S., *Koll. Zeits.* xxxix. p. 300 (1926).
(4) Bingham, E. C., and Robertson, J. W., *Koll. Zeits.* xlvii. p. 1 (1929).
(5 *a*) Scott Blair, G. W., and Crowther, E. M., J. Phys. Chem. xxxiii. p. 321 (1929).
(5 *b*) Schofield, R. K., and Scott Blair, G. W., J. Phys. Chem. xxxiv. p. 248 (1930).
(5 *c*) Scott Blair, G. W., J. Rheology, i. p. 128 (1930).
(5 *d*) Schofield, R. K., and Scott Blair, G. W. In process of publication (J. Phys. Chem.).
(5 *e*) Scott Blair, G. W., *Koll. Zeits.* xlvii. p. 76 &c. (1929).
(5 *f*) Keen, B. A., and Scott Blair, G. W., J. Agric. Sci. xix. p. 684 (1929).
(6) Grinnell Jones and Dole, M., J. Amer. Chem. Soc. li. p. 2950 (1929).
(7) Sutherland, W., Phil. Mag. xiv. p. 1 (1907).
(8 *a*) Grüneisen, E., *Wiss. Abl. Phys. Tech. Reichs.* iv. p. 151 (1905).
(8 *b*) Grüneisen, E., *Wiss. Abl. Phys. Tech. Reichs.* iv. p. 237 (1905).
(9) Applebey, M. P., J. Chem. Soc. xcvii. p. 2000 (1910).
(10) Merton, T. R., J. Chem. Soc. xcvii. p. 2454 (1910).
(11) Hoskins, R., Phil. Mag. vii. p. 469 (1904).
(12) Cohen, R., *Ann. der Phys.* xlv. p. 666 (1892).

LXXV. *Electromagnetic Reactions between Conducting and Magnetic Material, and an Alternating Current.* By S. Whitehead, *M.A., A.M.I.E.E.**

Summary.

The present paper is mainly mathematical in nature. It deals with the eddy currents and secondary magnetic fields due to the presence of a cylinder or plate of conducting and magnetic material in the neighbourhood of a current. Solutions are deduced for certain particular cases, such as the magnetic effect alone, eddy currents alone, and the effect of material of infinite thickness. A number of solutions of particular cases by different authors are shown to form part of a general scheme and to be deducible from a general solution.

The present report furnishes a basis for deducing solutions for further particular cases which may arise, since the analysis is of wide application. Among these applications may be mentioned the following :—

Sheath losses in cables, the effect of metal work in the neighbourhood of cables upon the impedance and loading, proximity effects between conductors, the heating of flanges in transformer bushings, the forces on an arc drawn near metallic bodies and earth currents, including fault impedance and telephone interference.

Contents.

	Page
I. Introduction	898
II. Current in a Cylinder	898
(*a*) General Equations	898
(*b*) Current along Axis	902
(*c*) Infinitely Thick Cylinder	902
(*d*) Thin Cylinder	903
(*e*) Current outside Cylinder	903
(*f*) Return Current through the Cylinder	904
(*g*) Several Disturbing Currents	905
(*h*) Eddy Currents and Magnetic Distortion separately	906
III. Current Parallel to a Plate	906
(*a*) General Equations	906
(*b*) Thin Plates	908
(*c*) Semi-infinite Solid	908

* Being Report Ref. XZ/T4 of the British Electrical and Allied Industries Research Association. Communicated by E. B. Wedmore, M.I.E.E., F.Inst.P.

Page
(*d*) Eddy Currents and Magnetic Distortion separately .. 910
(*e*) Several Disturbing Currents 910
(*f*) Return Current through the Plate 910
IV. General Considerations 911
(*a*) Completeness of Solution 911
(*b*) The Increase of Resistance 912
(*c*) Effect on Inductance 912
(*d*) The Force on the Current 943

I. Introduction.

WHEN conducting and magnetic material is brought near an alternating current two actions take place :—

(i.) Eddy currents are induced in the material which give rise to an energy loss and give also a magnetic field which reacts upon the current, giving rise to an additional in-phase voltage drop with a reduced self-inductance and a force on the current repelling it from the disturbing material.

(ii.) The field is distorted by the permeability of the material giving rise to a force on the current attracting it to the disturbing material and an additional reactive voltage drop, *i. e.*, increased self-inductance.

It may be noted that the action under (i.) occurs whether the material is magnetic or not, but does not occur with D.C., while the action under (ii.) occurs both with A.C. and D.C., but only with magnetic material.

Simple cases have been treated from time to time, but usually by separating the two effects. In the present note it is proposed to develop general solutions for a current in a cylinder parallel to the axis and a straight current parallel to a magnetic plate. It is assumed that the cylinder is infinitely long and the plate of infinite area, so that end effects may be neglected.

II. Current in a Cylinder.

(a) *General Equations.*

Consider a section of the cylinder ; let the centre be the origin of coordinates, and let the radius through the point of intersection of the current, which is parallel to the axis at a distance c, be the initial line. If the internal radius of the cylinder is a, then when $r < a$ the magnetic field may be considered as made up of two portions, one derived from the

normal magnetic field H′, and the other, H_1, derived from a magnetic potential ϕ_1 due to the cylinder. ϕ_1 satisfies Laplace's equation, since there is no magnetic material present; thus

$$\nabla^2\phi_1 = 0, \quad . \quad . \quad . \quad . \quad . \quad . \quad . \quad (1)$$

and it may be assumed as of the form

$$\phi_1 = \sum_{n=1}^{\infty} C_n \left(\frac{r}{a}\right)^n \sin n\theta; \quad . \quad . \quad . \quad . \quad . \quad (2)$$

$$\therefore \qquad H_{1r} = -\frac{1}{r}\sum_{n=1}^{\infty} nC_n\left(\frac{r}{a}\right)^n \sin n\theta, \quad . \quad . \quad . \quad (3.1)$$

$$H_{1\theta} = -\frac{1}{r}\sum_{n=1}^{\infty} nC_n\left(\frac{r}{a}\right)^n \cos n\theta, \quad . \quad . \quad . \quad (3.2)$$

where r and θ as subscripts give the radial and tangential components. If the external radius of the cylinder is b, then, when $a<r<b$, the magnetic field H is derived from an electric field E by the equation

$$\mu\omega j\mathrm{H} = \mathrm{curl\ E}, \quad . \quad . \quad . \quad . \quad . \quad . \quad . \quad (4)$$

where μ = permeability, $\omega = 2\pi$ frequency, j refers to displacement in time. E satisfies the equation

$$\nabla^2\mathrm{E} - k^2\mathrm{E} = 0, \quad . \quad . \quad . \quad . \quad . \quad . \quad . \quad (5)$$

where $k^2 = 4\pi\mu\omega j\sigma$, σ = conductivity of cylinder.

Indeed H must also satisfy this equation, but the relation between H_θ and H_r is more easily shown by this approach. When the end effects are neglected it is clear that E is parallel to the axis, so that (4) is two-dimensional and refers to the sectional plane, while (5) reduces to a scalar equation. For cylindrical coordinates (5) becomes

$$\frac{d^2\mathrm{E}}{dr^2} + \frac{1}{r}\frac{d\mathrm{E}}{dr} + \frac{1}{r^2}\frac{d^2\mathrm{E}}{d\theta^2} - k^2\mathrm{E} = 0, \quad . \quad . \quad (5.1)$$

and we may assume the solution

$$\mathrm{E} = +\mu\omega j \sum_{n=0}^{\infty} \{A_n I_n(kr) + B_n K_n(kr)\} \cos n\theta, \quad . \quad (6)$$

where A_n and B_n are arbitrary constants, while I_n and K_n are Bessel's functions of first and second kind and imaginary argument. It is easily deduced from (4) and (6) that

$$H_r = -\frac{1}{r}\sum_{0}^{\infty} (A_n I_n + B_n K_n) n \sin n\theta, \quad . \quad . \quad . \quad . \quad . \quad (7.1)$$

$$H_\theta = +\frac{1}{r}\sum_{0}^{\infty} \{A_n(krI_{n+1} + nI_n) - B_n(krK_{n+1} - nK_n)\} \cos n\theta.$$

$$. \quad . \quad . \quad (7.2)$$

When $r>b$ we again have two fields, H′ and H_0, and the latter is derived from a potential, ϕ_0, satisfying (1), and may be assumed as

$$\phi_0 = \Sigma\, D_n \left(\frac{b}{r}\right)^n \sin n\theta. \quad . \quad . \quad . \quad . \quad . \quad (8)$$

The normal field H′ may be expressed as

$$H_r' = -\frac{2I}{r} \sum_0^\infty \left(\frac{c}{r}\right)^n \sin n\theta, \quad . \quad . \quad . \quad (9.1)$$

$$H_\theta' = \frac{2I}{r} \sum_0^\infty \left(\frac{c}{r}\right)^n \cos n\theta, \quad . \quad . \quad . \quad . \quad (9.2)$$

where I is the current.

At $r=a$

$$H_{1\theta} + H_\theta' = H_\theta, \quad . \quad . \quad . \quad . \quad . \quad (10.1)$$

$$H_{1r} + H_r' = \mu H_r. \quad . \quad . \quad . \quad . \quad (10.2)$$

At $r=b$

$$H_{0\theta} + H_\theta' = H_\theta, \quad . \quad . \quad . \quad . \quad . \quad (10.3)$$

$$H_{0r} + H_r' = \mu H_r. \quad . \quad . \quad . \quad . \quad (10.4)$$

But

$$H_{1\theta} = -\frac{1}{r}\frac{d\phi_1}{d\theta}, \quad . \quad . \quad . \quad . \quad . \quad (11.1)$$

$$H_{1r} = -\frac{d\phi_1}{dr}, \quad . \quad . \quad . \quad . \quad . \quad . \quad (11.2)$$

$$H_{0\theta} = -\frac{1}{r}\frac{d\phi_0}{d\theta}, \quad . \quad . \quad . \quad . \quad . \quad (11.3)$$

$$H_{0r} = -\frac{d\phi_0}{dr}. \quad . \quad . \quad . \quad . \quad . \quad . \quad (11.4)$$

Thus each term in equations (10) may be expressed as a series in $\cos n\theta$ or $\sin n\theta$, so that the coefficients of $\cos n\theta$ and $\sin n\theta$ may be equated, giving

$$nC_n = -A_n\{ka I_{n+1}(ka) + n I_n(ka)\} + B_n\{ka K_{n+1}(ka) - n K_n(ka)\} + 2I\frac{c^n}{a^n}, \quad (12.1)$$

$$nC_n = \mu n\{A_n I_n(ka) + B_n K_n(ka)\} - 2I\frac{c^n}{a^n}, \quad . \quad . \quad (12.2)$$

$$nD_n = -\{A_n(Kb I_{n+1}(kb) + n K_n(kb)) - B_n(kb K_{n+1}(kb) - n K_n(kb))\} + 2I\frac{c^n}{b^n}, \quad . \quad (12.3)$$

$$nD_n = -\mu n\{A_n I_n(kb) + B_n K_n(kb)\} + 2I\frac{c^n}{b^n}. \quad . \quad (12.4)$$

These equations do not hold when $n=0$, since $C_0=D_0=0$, so that A_0 and B_0 are found from

$$A_0I_1(ka)-B_0K_1(ka)=\frac{2I}{ka}, \quad . \quad . \quad (12.5)$$

$$A_0I_1(kb)-B_0K_1(kb)=\frac{2I}{kb}. \quad . \quad . \quad . \quad (12.6)$$

From these equations may be deduced the following values :—

$$\begin{aligned} A_n = 4I\frac{c^n}{a^n}\{&n(\mu-1)K_n(kb)+kbK_{n+1}(kb)\}/[\{n(\mu+1)I_n(ka)\\ &+kaI_{n+1}(ka)\}\{n(\mu-1)K_n(kb)+kbK_{n+1}(kb)\}\\ &-\{n(\mu-1)I_n(kb)-kbI_{n+1}(kb)\}\{n(\mu+1)\\ &\times K_n(ka)-kaK_{n+1}(ka)\}], \quad . \quad . \quad . \quad . \quad . \quad (13.1)\end{aligned}$$

$$\begin{aligned} B_n = -4I\frac{c^n}{a^n}\{&n(\mu-1)I_n(kb)-kbI_{n+1}(kb)\}/[\{n(\mu+1)I_n(ka)\\ &+kaI_{n+1}(ka)\}\{n(\mu-1)K_n(kb)+kbK_{n+1}(kb)\}\\ &-\{n(\mu-1)I_n(kb)-kbI_{n+1}(kb)\}\{n(\mu+1)\\ &\times K_n(ka)-kaK_{n+1}(ka)\}], \quad . \quad . \quad . \quad . \quad . \quad (13.2)\end{aligned}$$

$$A_0=\frac{2I}{abk^2}\frac{[kbK_1(kb)-kaK_1(ka)]}{I_1(ka)K_1(kb)-I_1(kb)K_1(ka)}, \quad . \quad . \quad . \quad . \quad (13.3)$$

$$B_0=\frac{2I}{abk^2}\frac{[kbI_1(kb)-kaI_1(ka)]}{I_1(ka)K_1(kb)-I_1(kb)K_1(ka)}. \quad . \quad . \quad . \quad . \quad (13.4)$$

By substituting equations (13) in equations (7) the field H in the material of the cylinder is given.

Again,

$$C_n=\mu\{A_nI_n(ka)+B_nK_n(ka)\}-2I\frac{c^n}{na^n}, \quad . \quad (14)$$

and

$$D_n=\mu\{A_nI_n(kb)+B_nK_n(kb)\}+2I\frac{c^n}{na^n}, \quad . \quad (15)$$

$$C_0=D_0=0,$$

so that the distortion of the magnetic field inside and outside the cylinder is known.

The current density in the cylinder i is given by

$$i=\sigma E=\frac{k^2}{4\pi}\sum_0^\infty\{A_nI_n(kr)+B_nK_n(kr)\}\cos n\theta, \quad . \quad (16)$$

and the energy loss per unit length is given by

$$W = \int_a^b \int_0^{2\pi} \sigma i^2 r d\theta \, dr. \quad . \quad . \quad . \quad . \quad (17)$$

(b) *Current along Axis.*

If the current is central, that is, if $c=0$, then A_n, B_n, C_n, and D_n are all zero except A_0 and B_0. As is otherwise obvious, there is no magnetic distortion due to the cylinder, the magnetic field in which is everywhere tangential and given by

$$H = k\{A_0 I_1(kr) - B_0 K_1(kr)\}, \quad . \quad . \quad . \quad (18)$$

the magnetic flux being μH.

The current density i is given by

$$i = \frac{k^2}{4\pi}\{A_0 I_0(kr) + B_0 K_0(kr)\}. \quad . \quad . \quad . \quad (19)$$

The cases when the cylinder is infinitely thick or very thin have already been solved by Rudenberg * and Carter †.

(c) *Infinitely Thick Cylinder.*

Rudenberg, however, has only treated the case of a central current, and uses Hankel functions, which correspond to the K functions. If in equations (13) $b \to \infty$, $K_n \to 0$ we find

$$A_n = 0\,; \quad B_n = 4I \frac{c^n}{a^n} \Big/ \{(\mu+1)nK_n(ka) - ka K_{n+1}(ka)\}, \quad . \quad . \quad . \quad (20.1)$$

$$A_0 = 0\,; \quad B_0 = -2I/ka\, K_1(ka), \quad . \quad . \quad . \quad . \quad . \quad . \quad (20.2)$$

$$i = -\frac{Ik^2}{\pi} \sum_0^\infty \frac{c^n}{a^n} \frac{K_n(kr)\cos n\theta}{\{(\mu+1)nK_n(ka) - ka K_{n+1}(ka)\}}; \quad (21)$$

and if $C=0$ and $\mu=1$,

$$i = \frac{Ik K_0(kr)}{2\pi a K_1(ka)}, \quad \text{where } k^2 = 4\pi\omega j\sigma, \quad . \quad (21.1)$$

which is Rudenberg's result. It is important to note, however, that increasing b to infinity illustrates a difficulty as to the return current. So far it has been assumed that this is sufficiently removed so as not to affect the magnetic field.

* Rudenberg, *Zs. für ang. Math.* v. p. 361 (1925).

† Carter, Proc. Camb. Phil. Soc. xxiii. p. 901 (1927); xxiv. p. 85 (1928); xxvi. p. 115 (1930).

If $b=\infty$ this is obviously impossible, and, accordingly, it is now found that the solution contains the return current, *i. e.*, the current I returns through the cylinder. The solution (19) does not contain the return current, the sum of i being zero. The eddy current changes sign as r increases, being zero at a certain value r_1, $a<r_1<b$. But when $b\to\infty$, r_1 also becomes infinite in the limit, and equations (21) give only currents of one sign (neglecting terms in $\cos n\theta$), the balancing currents are absent, and the sum of i is I in the opposite direction compared with the main current. This section of the analysis has been applied to earth currents.

(d) *Thin Cylinder.*

If the cylinder is very thin one must consider not the current density per unit area but the current density per generating filament of unit width. Provided μ is not unduly large (16) reduces to

$$\bar{i}=\frac{tk^2\mathrm{I}}{2\pi}\sum_1^\infty\left(\frac{c}{a}\right)^n\frac{\cos n\theta}{n\mu+k^2ta}, \quad . \quad . \quad . \quad . \quad (22)$$

where $\bar{i}$ is the current density per filament of unit breadth, *i. e.*,

$$\bar{i}=\text{Limit}\left[\frac{1}{r}\int_a^b ri\,dr\right], \quad \text{when } b\to a,$$

and $t=b-a=$ thickness of cylinder. This is identical with Carter's equation

$$\bar{i}=-\frac{m\mathrm{I}}{\pi a}\sum_1^\infty\left(\frac{c}{a}\right)^n\frac{n\cos pt+m\sin pt}{m^2+n^2}\cos n\theta, \quad . \quad (22.1)$$

where $m=2\pi at\sigma\omega$. This approximation involves the assumption that the cylinder is so thin that i does not depend upon r, so that the permeability has a negligible effect. Obviously this approximation is more likely to be valid for a given thickness when the permeability is small or when c, the displacement of the current from the axis, is small. The case of the thin cylinder has been of value in connexion with sheath losses in cables and the heating of metal conduits.

(e) *Current outside Cylinder.*

Another group of solutions is obtained if the current is outside the cylinder, but still parallel to the axis of the cylinder. The preceding analysis applies except that the

expression for H′ must be slightly modified, since $c>b$. H_r' and H_θ' are now given by

$$H_r' = -\frac{2I}{r}\sum_1^\infty \left(\frac{r}{c}\right)^n \sin n\theta, \quad . \quad . \quad . \quad (23.1)$$

$$H_\theta' = -\frac{2I}{r}\sum_1^\infty \left(\frac{r}{c}\right)^n \cos n\theta, \quad . \quad . \quad . \quad (23.2)$$

and the new values of A_n and B_n are found by replacing equations (9) by equations (23). It is to be noted that A_0 and B_0 are zero, since the cylinder contains no current, and the line integral of magnetic force round the cylinder must be zero. A_n and B_n are given by

$$\begin{aligned} A_n = \frac{4Ib^n}{c^n}\{n(\mu+1)K_n(ka) - kaK_{n+1}(ka)\}/[\{n(\mu-1)I_n(kb) \\ - kbI_{n+1}(kb)\}\{n(\mu+1)K_n(ka) - kaK_{n+1}(ka)\} \\ - \{n(\mu+1)I_n(ka) + kaI_{n+1}(ka)\}\{n(\mu-1) \\ \times K_n(kb) + kbK_{n+1}(kb)\}], \quad . \quad . \quad . \quad . \quad . \quad (24.1) \end{aligned}$$

$$\begin{aligned} B_n = -\frac{4Ib^n}{c^n}\{n(\mu+1)I_n(ka) + kaI_{n+1}(ka)\}/[\{n(\mu-1)I_n(kb) \\ - kbI_{n+1}(kb)\}\{n(\mu+1)K_n(ka) - kaK_{n+1}(ka)\} \\ - \{n(\mu+1)I_n(ka) + kaI_{n+1}(ka)\}\{n(\mu-1) \\ \times K_n(kb) + kbK_{n+1}(kb)\}]. \quad . \quad . \quad . \quad . \quad . \quad (24.2) \end{aligned}$$

(f) *Return Current through the Cylinder.*

It has already been shown that the return current is assumed so distant that its magnetic field is negligible. With an infinitely thick cylinder this is impossible, so the solution for this case already given includes the return current, which is assumed to flow in the cylinder. If the cylinder is of finite thickness and the main current is within it then the solution for the case when the current returns through the cylinder is easily obtained by assuming that H_θ' and H_r' have the values given by equations (9), when $r<a$, but are zero when $r>b$, that is, outside the cylinder. It is thus clear that the values of A_n and B_n will be given by (13.1) and (13.2) as before, but A_0 and B_0 will have different values, given by

$$A_0 = \frac{2I}{ka}\frac{K_1(kb)}{\{I_1(ka)K_1(kb) - I_1(kb)K_1(ka)\}}, \quad . \quad (25.1)$$

$$B_0 = \frac{2I}{ka}\frac{I_1(kb)}{\{I_1(ka)K_1(kb) - I_1(kb)K_1(ka)\}}. \quad . \quad (25.2)$$

The integral of i over the section of the cylinder is now $-I$ instead of zero. If the main current is outside the cylinder equations (24) will hold for A_n and B_n, as in previous paragraph, but A_0 and B_0 are obtained by adding a term

$$\frac{2I}{b}$$

to the expression for H_θ' at $r=b$, taking the magnetic effect of the return current into account, giving

$$A_0 I_1(ka) - B_0 K_1(ka) = -\frac{2I}{ka}, \quad . \quad . \quad (26.1)$$

$$A_0 I_1(kb) - B_0 K_1(kb) = -\frac{4I}{kb}. \quad . \quad . \quad (26.2)$$

Whence

$$A_0 = -\frac{2I}{k^2 ab} \frac{\{kbK_1(kb) - 2kaK_1(ka)\}}{\{I_1(ka)K_1(kb) - I_1(kb)K_1(ka)\}}, \quad (27.1)$$

$$B_0 = -\frac{2I}{k^2 ab} \frac{\{kbI_1(kb) - 2kaI_1(kb)\}}{\{I_1(ka)K_1(kb) - I_1(kb)K_1(ka)\}}. \quad (27.2)$$

This case gives the solution for proximity effect between a thin wire and a cylinder carrying equal and opposite currents. If $a=0$, then the proximity effect between a thin and a thick wire is obtained. Solutions for the latter case and for the former case when the cylinder is thin have been obtained by Dwight * by a method of successive approximation.

(g) *Several Disturbing Currents.*

If more than one current flows parallel to the axis the analysis may be extended to cover the case by using the appropriate expression for H′. In the general case

$$H_r' = -\frac{2}{r} \sum_{n=0}^{n=\infty} \left\{ \sum_{m=1}^{m=k} I_m \frac{c_m{}^n}{r^n} + \sum_{m'=1}^{m'=k'} I_{m'} \frac{r^n}{c_{m'}{}^n} \right\} \sin n\theta, \quad (28.1)$$

$$H_\theta' = \frac{2}{r} \sum_{n=0}^{n=\infty} \left\{ \sum_{m=1}^{m=k} I_m \frac{c_m{}^n}{r^n} - \sum_{m'=1}^{m'=k'} I_{m'} \frac{r^n}{c_{m'}{}^n} \right\} \cos n\theta. \quad . \quad (28.2)$$

The accents refer to the currents outside the cylinder, while both I and c must be regarded as vectors for the purpose of addition, the former in time, the latter in space.

* Dwight. J.A.I.E.E. xlii. p. 827 (1923); Trans. A.I.E.E. xlii. p. 830 (1923), xxxviii. p. 1379 (1918); Elec. Journal, xxi. p. 62 (1924); G.E.R. xxx. p. 531 (1927).

The case for three disturbing currents and a thin cylinder has been evaluated by Morgan and Whitehead *.

(h) *Eddy Currents and Magnetic Distortion separately.*

If the effects of eddy currents alone are required, these may be immediately deduced by writing $\mu=1$ and $k=4\pi\omega\sigma j$. If the effect of magnetic distortion is alone required, then the conductivity is assumed zero, that is, $\sigma=0$ and $k=0$. In such a case ϕ_1 has the following value :—

$$\phi_1 = 2(\mu-1)\mathrm{I}\sum_1^\infty \frac{1}{n}\left(\frac{cr}{a^2}\right)^n \frac{(1-\alpha^n)(1+\mu+\alpha^n)\sin n\theta}{\mu^2(1-\alpha^n)+\mu(2+\alpha^n+\alpha^{2n})+(1-\alpha^{2n})}, \quad . \quad . \quad . \quad (2.1)$$

where $\alpha=\frac{a}{b}$. A further approximation is

$$\phi_1 = 2\left(\frac{\mu-1}{\mu+1}\right)\mathrm{I}\sum_1^\infty \frac{1}{n}\left(\frac{cr}{a^2}\right)^n. \quad . \quad . \quad . \quad (2.2)$$

III. Current Parallel to a Plate.

(a) *General Equations.*

Let the axis of z be parallel to the current. Let the origin of coordinates be at centre of the plate perpendicularly beneath the current, the y axis passing through the current and the x axis transverse to it, so that the current is located at $y=h$, $x=0$, the surfaces of the plate being the planes $y=\pm t$. In air Laplace's equation holds, while in the plate equation (5) holds. As in the previous section, let H_1 be the magnetic field distortion due to the plate when $y>t$, H_0 be the same field when $y<-t$, H be the total field in the plate, and H′ the normal field of the current. Then the following forms may be adopted for H_1, H, H_0, and H′ :—

$$\mathrm{H}_{1x} = \int_0^\infty \phi_3 e^{-(y-t)\lambda}\cos x\lambda\, d\lambda, \quad . \quad . \quad . \quad . \quad . \quad . \quad . \quad (29.1)$$

$$\mathrm{H}_{1y} = -\int_0^\infty \phi_3 e^{-(y-t)\lambda}\sin x\lambda\, d\lambda, \quad . \quad . \quad . \quad . \quad . \quad . \quad (29.2)$$

$$\mathrm{H}_x = \int_0^\infty \left\{\phi_1 e^{(y-t)\sqrt{(\lambda^2+k^2)}} + \phi_2 e^{-(y+t)\sqrt{(\lambda^2+k^2)}}\right\} \times \cos x\lambda\, d\lambda, \quad (30.1)$$

* Wedmore, Morgan, and Whitehead, J.A.I.E.E. lxvii. p. 359 (1929).

$$H_y = \int_0^\infty \frac{\lambda}{\sqrt{(\lambda^2+k^2)}} \{\phi_1 e^{(y-t)\sqrt{(\lambda^2+k^2)}} - \phi_2 \times e^{-(y+t)\sqrt{(\lambda^2+k^2)}}\} \sin x\lambda \, d\lambda, \quad (30.2)$$

$$H_{0x} = \int \phi_4 e^{(y+t)\lambda} \cos x\lambda \, d\lambda, \quad . \quad . \quad . \quad . \quad . \quad . \quad . \quad . \quad (31.1)$$

$$H_{0y} = \int \phi_4 e^{(y+t)\lambda} \sin x\lambda \, d\lambda, \quad . \quad . \quad . \quad . \quad . \quad . \quad . \quad . \quad (31.2)$$

$$H_x' = 2I \int_0^\infty e^{-(h-y)\lambda} \cos x\lambda \, d\lambda, \quad . \quad . \quad . \quad . \quad . \quad . \quad . \quad (32.1)$$

$$H_y' = 2I \int_0^\infty e^{-(h-y)\lambda} \sin x\lambda \, d\lambda. \quad . \quad . \quad . \quad . \quad . \quad . \quad . \quad (32.2)$$

ϕ_1, ϕ_2, ϕ_3, and ϕ_4 are arbitrary functions of λ and

$$k^2 = 4\pi\mu\sigma\omega j,$$

as in Section II.

The boundary conditions are

$$y = t, \qquad H_{1x} + H_x' = H_x, \quad . \quad . \quad . \quad (33.1)$$

$$H_{1y} + H_y' = \mu H_y ; \quad . \quad . \quad . \quad (33.2)$$

$$y = -t, \qquad H_{0x} + H_x' = H_x, \quad . \quad . \quad . \quad (34.1)$$

$$H_{0y} + H_y' = \mu H_y. \quad . \quad . \quad . \quad (34.2)$$

Whence it may be shown

$$\phi_1 = \frac{4I\lambda_1(\lambda_1+\mu\lambda)e^{-(h-t)\lambda}e^{2t\lambda_1}}{\{(\lambda_1+\mu\lambda)^2 e^{2t\lambda_1} - (\lambda_1-\mu\lambda)^2 e^{-2t\lambda_1}\}}, \quad . \quad (35.1)$$

$$\phi_2 = -\frac{4I\lambda_1(\lambda_1-\mu\lambda)e^{-(h-t)\lambda}}{\{(\lambda_1+\mu\lambda)^2 e^{2t\lambda_1} - (\lambda_1-\mu\lambda)^2 e^{-2t\lambda_1}\}}, \quad . \quad (35.2)$$

while

$$\phi_3 = 2Ie^{-(h-t)\lambda}\left[-1 + \frac{2\lambda_1\{(\lambda_1+\mu\lambda)e^{2t\lambda_1} - (\lambda_1-\mu\lambda)e^{-2t\lambda_1}\}}{\{(\lambda_1+\mu\lambda)^2 e^{2t\lambda_1} - (\lambda_1-\mu\lambda)^2 e^{-2t\lambda_1}\}}\right], \quad . \quad . \quad . \quad (35.3)$$

where $$\lambda_1^2 = \lambda^2 + k^2.$$

The field is now everywhere given by equations (29), (30), (31), and (32) in an integral form when the above values are substituted, but lead to complicated series when it is attempted to give a general expression for them.

The electric force E in the plate is parallel to the current and given by

$$\mathrm{E} = -\mu\omega j \int_0^\infty \frac{1}{\lambda_1}\{\phi_1 e^{(y-t)\lambda_1} + \phi_2 e^{-(y+t)\lambda_1}\}\cos x\lambda\, d\lambda, \quad (36)$$

and the current density i is given by

$$i = \sigma\mathrm{E} = -\frac{k}{4\pi}\int_0^\infty \frac{1}{\lambda_1}\{\phi_1 e^{(y-t)\lambda_1} + \phi_2 e^{-(y+t)\lambda_1}\}\cos x\lambda\, d\lambda. \quad (37)$$

(b) *Thin Plates.*

When t is small the fundamental equations may be simplified. Thus

$$\mathrm{H}_{1y} = \mathrm{H}_{0y} \text{ at } y = 0, \quad (38.1)$$

$$4\pi i = \mathrm{H}_{0x} - \mathrm{H}_{1x} \text{ at } y = 0, \quad (38.2)$$

$$\frac{di}{dx} = -2\sigma t\omega j \mathrm{H}_{1y} + \mathrm{H}_y'. \quad (38.3)$$

$$\therefore \quad \frac{d}{dx}(\mathrm{H}_{1x} - \mathrm{H}_{0x}) = k_1(\mathrm{H}_{1y} + \mathrm{H}_y'), \quad (38.4)$$

where $k_1 = 8\pi\sigma t\omega j$, $2t =$ thickness.

From (38.1)
$$\phi_4 = -\phi_3.$$

From (38.4)
$$-2\lambda\phi_3 = k_1(2\mathrm{I}e^{-h\lambda} - \phi_3).$$

$$\therefore \quad \phi_3 = 2k_1\mathrm{I}e^{-h\lambda}/(k_1 - 2\lambda). \quad (39)$$

This is analogous to the method followed by Carter in dealing with thin cylinders. The permeability has no effect if the material is thin.

(c) *Semi-infinite Solid.*

This is the case which occurs when the thickness is indefinitely increased. The quantity $h-t$ remains finite and is replaced by h, the height of the current above the boundary surface, while if the x axis is transferred to the surface $y-t$ becomes y. Thus

$$\phi_1 = \frac{4\mathrm{I}\lambda_1}{\lambda_1 + \mu\lambda} e^{-h\lambda} \quad \phi_2 = 0, \quad (40.1)$$

$$\phi_3 = 2\mathrm{I}e^{-h\lambda}(\lambda_1 - \mu\lambda)/(\lambda_1 + \mu\lambda); \quad (40.2)$$

so that

$$H_x = \int_0^\infty \frac{4I\lambda_1}{\lambda_1+\mu\lambda} e^{-h\lambda} e^{y\lambda_1} d\lambda \cos x\lambda, \quad . \quad . \quad (41.1)$$

$$H_y = \int_0^\infty \frac{4I\lambda}{\lambda_1+\mu\lambda} e^{-h\lambda} e^{y\lambda_1} d\lambda \sin x\lambda. \quad . \quad . \quad (41.2)$$

For non-magnetic material $\mu=1$, so that in this case

$$H_x = \int_0^\infty \frac{4I\lambda_1}{\lambda_1+\lambda} e^{-h\lambda} e^{y\lambda_1} \cos x\lambda\, d\lambda, \quad . \quad . \quad (42.1)$$

$$H_y = \int_0^\infty \frac{4I\lambda}{\lambda_1+\lambda} e^{-h\lambda} e^{y\lambda_1} \sin x\lambda\, d\lambda, \quad . \quad . \quad (42.2)$$

while

$$\phi_3 = 2Ie^{-h\lambda}(\lambda_1-\lambda)/(\lambda_1+\lambda), \quad . \quad . \quad . \quad . \quad . \quad (43.1)$$

$$H_{1x} = 2I\int_0^\infty e^{-(h+y)\lambda}\left(\frac{\lambda_1-\lambda}{\lambda_1+\lambda}\right)\cos x\lambda\, d\lambda, \quad . \quad (43.2)$$

$$H_{1y} = -2I\int_0^\infty e^{-(h+y)\lambda}\left(\frac{\lambda_1-\lambda}{\lambda_1+\lambda}\right)\sin x\lambda\, d\lambda, \quad (43.3)$$

and $k^2 = 4\pi\omega\sigma$.

These equations are identical with those deduced by Carson* by a direct method in connexion with earth currents.

The flat plate may also be considered as a particular case of the cylinder considered in the previous section. For this purpose the internal radius a of the cylinder is made infinite, while $b-a$ is finite and equal to $2t$. The displacement of the current from the centre, c, is also infinite, but $a-c$ is finite and equal to h. The equations of the present section may then be derived, making use of the definite integral expressions for the Bessel functions. In the particular case of the semi-infinite solid the connexion can be seen by comparing the methods of Pollaczek† and Carson. In the more general case the deduction is tedious and not of much importance, so that it will not be given here.

In dealing with the cylinder it was shown that if the outer boundary (the external surface) were taken to infinity then the eddy-current solution contained the return current. The same reasoning applies when the flat plate is made infinitely thick. Accordingly equations (40) to (43) are the solution for the case when the current returns through the semi-infinite solid.

* Carson, Bell Tech. Journal, v. p. 539 (1926).
† Pollaczek, *Elek. Nach.* iii. p. 9 (1926).

(d) *Eddy Currents and Magnetic Distortion separately.*

If the effect of eddy currents alone is required it is only necessary to put $\mu=1$ in equations (35) and put $k=4\pi\omega\sigma j$. If only magnetic distortion is to be investigated then the conductivity of the material is assumed zero, so that k is zero and $\lambda_1=\lambda$. The solutions for these two cases may then easily be written down.

(e) *Several Disturbing Currents.*

If there is more than one current parallel to the plate a solution may still be obtained by the same method. We now have, instead of equation (29),

$$H_x' = \sum_{m=1}^{m=p} 2I_p \int_0^\infty e^{-(h_p-y)\lambda} \sin(x-x_p)\lambda \, d\lambda, \quad . \quad (44)$$

with a similar expression for H_y'. Since the position of the y axis is arbitrary, that is, the origin from which x_p is measured, then, by a proper choice of this origin, equation (44) may be written

$$H_x' = \int_0^\infty \phi(\lambda_1 h_1, h_2, \text{etc.}, x_1, x_2, \text{etc.}) \cos x\lambda \, d\lambda, \quad (45)$$

with a similar expression for H_y'. The analysis then follows as before. The method adopted is equivalent to finding the vector sum of a number of vectors,

$$e^{-(h_p-y)\lambda} \times e^{-ix_p\lambda},$$

and then choosing the initial line from which the phase $x_p\lambda$ is measured, so as to coincide with the resultant vector. This then determines the position of the y axis, and, in effect, gives the position of the effective resultant current. The latter, however, has strictly no definite position on the y axis, since the function ϕ in (45) is not necessarily of the form

$$e^{-(h-y)\lambda}.$$

(f) *Return Current through the Plate.*

When the current returns through the plate the solution, if the plate is finite, can be obtained by making H_x' and H_y' zero when $y<-t$. This gives

$$\phi_1 = 4Ie^{-(h-t)\lambda} \Big/ \left(1+\frac{\mu\lambda}{\lambda_1}\right)(1-e^{-4\lambda_1 t}), \quad . \quad (46.1)$$

$$\phi_2 = -4Ie^{-(h-t)\lambda} \Big/ \left(1-\frac{\mu\lambda}{\lambda_1}\right)(1-e^{-4\lambda_1 t}). \quad (46.2)$$

IV. General Considerations.

(a) *Completeness of Solution.*

It is of interest briefly to note that the preceding solutions involve certain formal assumptions. Thus, in the case where a solution of the form $J_n \sin n\theta$ has been used n is usually an integer from considerations of symmetry and from the fact that the integral of the eddy-current density is zero over the cross-section except when there is a circulating or return current. The solutions may be generalized in the usual way by the use of generalized Bessel functions and integrals, but there is another method of some interest by means of successive approximation. Dwight has used this method for obtaining complete solutions for proximity effect from first principles, but Carter has also used it for completing a first solution for particular cases of eddy currents in cable sheaths, the first solution having been obtained, as mentioned before, by classical methods. The method may also be applied to the more general treatment of the present paper. The solution having been obtained for the given disturbing field H′, namely, H_1, H, and H_0, for the secondary fields in the different regions, as already shown, then a second solution may be found in the same manner by replacing H′ by H_1. The new secondary fields so determined, ${}_1H_1$, ${}_1H$, and ${}_1H_0$, are due to eddy currents of the second order, which may be deduced by equations similar to those already given. In this way a complete solution may be built up in which the magnetic fields in the various regions are

$$H' + H_1 + {}_1H_1 + {}_2H_1 + \ldots,$$

$$H + {}_1H + {}_2H + \ldots,$$

$$H' + H_0 + {}_1H_0 + {}_2H_0 + \ldots,$$

while the total eddy currents are

$$i + i_1 + i_2 + \ldots$$

The disturbing currents have been assumed sinusoidal. More generally they may be analysed into Fourier components, and the partial solutions for the components may, neglecting saturation and hysteresis, be added.

(b) *The Increase of Resistance.*

When eddy currents are induced the resistance in the main current is increased owing to the energy loss due to the eddy currents. This may be expressed as

$$\triangle R = \frac{1}{\bar{I}} \iint \frac{i^2}{\sigma} dS\, dt \quad . \quad . \quad . \quad . \quad . \quad (47)$$

$$= \frac{1}{\bar{I}} \iint \sigma E^2\, dS\, dt, \quad . \quad . \quad . \quad (47.1)$$

the double integration being due to the time element t, so that an R.M.S. value may be obtained. But it is also clear from general electromagnetic theory that

$$\triangle R = \left| \frac{1}{\bar{I}} \int \mu H_\theta\, dr \right| \text{in-phase component}, \quad . \quad (48)$$

since the integral expresses the total inductance, and its in-phase component is a resistive voltage drop. In some cases (48) gives a useful approximation. Thus, if the disturbing material is magnetic, the contribution to the flux from the field outside the material is negligible, so that the integral need only be taken between the boundary surfaces. But from (4)

$$H_\theta = \frac{1}{\mu\omega j} \frac{dE}{dr}; \quad . \quad . \quad . \quad . \quad . \quad . \quad (4.1)$$

$$\therefore \quad \triangle R = \left| \frac{1}{\omega j \bar{I}} (E_1 - E_2) \right| \text{in-phase component}, \quad . \quad (49)$$

where E_1 and E_2 are the values of the longitudinal electric force E at the boundary surfaces. For simplicity the case of the cylinder has been taken, but the above applies, *mutatis mutandis*, to any other arrangement, Again, with an infinitely thick cylinder or semi-infinite solid the contribution of the "aerial" magnetic field is small and may easily be evaluated separately. Accordingly (49) applies here also, a feature of importance in connexion with earth currents. Under these circumstances E_2 is zero.

(c) *Effect on Inductance.*

The out-of-phase component of

$$\frac{1}{\bar{I}} \int \mu H_\theta\, dr$$

of equation (48) gives the effective self-inductance, the integration being extended either to an arbitrary surface or up

to the return current, according to the problem. If the return current flows in the same material as the eddy currents, then E_1/I of equation (49) gives the generalized impedance of the return path. Adding the portion due to the aerial field, the impedance of the main current path and return path may easily be deduced and expressed as $R + L\omega j$, where R and L are the effective resistance and inductance respectively. It is not necessary to give details of such a deduction, as examples are found in the work of Rudenberg, Pollaczek, Carson, etc. The value of E_1 is taken for the nearest portion of the surface of the solid. If the value of E_1 were taken for a portion of the surface at a distance from the orthogonal projection of the current on the surface, then, under these circumstances, E_1 I defines an effective mutual inductance *m*, which is partly complex, or

$$m = M + S\omega j.$$

By making a correction for the "aerial" field the complete mutual inductance *m* is obtained. Thus, if two currents flow parallel to the disturbing material, it is possible to arrive at coefficients R_1, L_1, R_2, L_2, and *m* for the resistances and inductances, assuming the currents return through the disturbing material. If these currents are equal and opposite then the voltage drop per cm. of the two-way circuit formed by the currents is

$$I\{(R_1 + R_2) + \omega j(L_1 + L_2 - 2m)\},$$

i. e.,

$$I\{(R_1 + R_2 + 2S\omega^2) + \omega j(L_1 + L_2 - 2M)\},$$

The total current in the material is zero, since the return currents cancel; therefore the above expression gives the effect of the disturbing material upon the impedance of a single-phase system. The problem may of course be solved more rigorously by the direct application of the analysis in preceding sections, but the above is a convenient approximation, particularly with a large mass of disturbing material. It may be noted that such a mass may be treated as a semi-infinite solid if $|kd| >$ about 10, where *d* is the thickness, without much loss of accuracy.

(d) *The Force on the Current.*

The magnetic distortion and eddy currents give rise to a secondary field in the medium surrounding the main current. This field has been denoted by H_1 in the preceding sections. The vector product $H_1 \times I$ gives the force on the current due

to the presence of the material. With the nomenclature used in Section II. the radial force on the current is $H_{1\theta}I$ and the tangential force $H_{1r}I$, while for Section III. the force on the current normal to the surface is $H_{1z}I$ and $H_{1y}I$ parallel to the surface. It is to be observed that a current at the centre of a cylinder experiences no force, and, if concentrated at a point away from the centre, is acted upon only by a radial force which is centripetal if eddy currents act alone or centrifugal if the material is magnetic and feebly conducting. In practice a ferro-magnetic material usually gives a centrifugal force, while other materials act in the opposite direction. In the case of the plate the force is normal to the plate and the current is attracted by magnetic distortion, but repelled by eddy currents, and in a practical case the direction of the force depends on the dimensions and properties of the material.

May 14th, 1930.

LXXVI. *Magnetism and Molecular Structure.*—Part II. *Influence of Position Isomerism on Diamagnetic Susceptibilities. By* Prof. S. S. Bhatnagar, *D.Sc.*(*Lond.*), *F.Inst. Phys., and* R. N. Mathur, *M.Sc.**

IN a previous paper † in this Journal the influence of position isomerism on diamagnetic susceptibilities of some liquids was investigated, and the following significant facts were observed :—

(1) The values of the molecular magnetic susceptibility x_M for aliphatic isomerides increase in the order primary–secondary–tertiary, and the difference between the values for tertiary and secondary is much less than that between the values for secondary and primary isomerides.

(2) In the case of aromatic isomerides the value of x_M for ortho- is maximum, and the values for meta- and paraisomerides, like their other physical properties, are near together.

(3) In every group the isomeride having a larger value of the molecular magnetic susceptibility has also a larger value of the molecular magnetic rotation.

* Communicated by the Authors.

† Phil. Mag., July 1930, p. 101 ; referred to as Part I. in this paper.

(4) In every group the isomeride of a higher boiling-point has a lower magnetic susceptibility.

(5) In the case of primary, secondary, and tertiary alcohols the member having a larger molecular volume has also a larger magnetic susceptibility. In the case of aromatic isomerides, however, the ortho having the smallest molecular volume has got the largest magnetic susceptibility.

(6) In every group the isomeride having a larger value of the depolarization factor "r" has a smaller value of the molecular magnetic susceptibility.

In the present investigation the results of experiments on some more groups of position isomerides have been described, and the conclusions arrived at in the previous paper have been confirmed and extended. In the case of benzene derivatives the influence of the size of the substituent groups on the difference between the diamagnetic susceptibilities of ortho- and para- (and ortho- and meta-) isomerides has also been studied. Further, the isomeric alcohols have been investigated at different temperatures in order to find whether the differences between the values of molecular magnetic susceptibilities for isomerides are due to the different degrees of their molecular association or to some other characteristic. A successful attempt to explain these results on the basis of the electronic significance of valency bonds has also been made in this investigation.

Experimental.

The apparatus used is similar to Bauer and Piccard's U-tube apparatus, with this difference, that the sides of both the reservoir and the tube are made double-walled; and readings for any temperature of the liquid under investigation are taken by circulating water from a thermostat electrically maintained at the desired temperature in the outer jackets around the tube and the reservoir. A complete description of the apparatus is given in Part I. The alcohols have been investigated only up to a temperature of 50° C. At higher temperatures the evaporation becomes so rapid that the meniscus becomes unsteady and satisfactory readings cannot be obtained.

In every case very great precautions were taken to obtain the substances as pure as possible. Physical constants like density, boiling-point, refractive index, and melting-point (where possible) were always determined carefully for the substances investigated and compared with the recognized values for the pure specimens. The values of the specific susceptibility x have been calculated by the usual formula

$$x = \frac{2\theta g}{H^2} + x_0 \frac{\rho_0}{\rho}.$$

For calculating the values of x at different temperatures in the case of alcohols the values of the density of air, ρ_0, at different temperatures were taken from Landolt and Börnstein's tables and the values of ρ, density of the liquid under investigation, at different temperatures were determined experimentally. These values have always been taken with respect to water at 4° C. The values of the specific susceptibility of air at different temperatures were calculated by assuming that it obeys Curie's law. Any error introduced due to this assumption will be very small, because the diamagnetic susceptibility of nitrogen is almost negligible as compared with that of oxygen, and the amount of other diamagnetic gases, of moderate susceptibility, in air is very small. Moreover, as we want only to compare the data for the isomerides, any error due to the above assumption will be common to every isomeride and will almost cancel out. The values of the displacement of the meniscus θ, in order to get rid of any effect due to evaporation, were taken both on applying and removing the field. The mean of the two readings, which differed, if at all, by a very small amount, was taken to be the real value of θ. Again, in the above equation x_0 is the specific susceptibility of the medium above the liquid and ρ_0 is its density. Ordinarily we take it to be air; but the space above the liquid, especially in the case of such volatile liquids as alcohols, and particularly at high temperatures, must be saturated with vapours of the liquid under investigation. Knowing the vapour density and applying the mixture law the susceptibility of the medium above the liquid can be easily calculated. This procedure, however, has not been adopted in the present investigation as the correction due to this factor is of little significance.

Experimental Results.

The experimental results are given in the following Tables. In every table the values of the specific susceptibility x are with respect to water ($x = -7{\cdot}25 \times 10^{-7}$).

TABLE I.

Propyl alcohol.		Isopropyl alcohol.	
Temperature °C.	$-x \times 10^7$.	Temperature °C.	$-x \times 10^7$.
25	7·93	25	8·18
30	7·93	30	8·18
35	7·94	35	8·14
40	7·95	40	8·15
45	7·91	45	8·16
50	7·92	50	8·17

TABLE II.

Normal butyl alcohol.		Tertiary butyl alcohol.	
Temperature °C.	$-x \times 10^7$.	Temperature °C.	$-x \times 10^7$.
25	8·25	25	8·38
30	8·25	30	8·39
35	8·25	35	8·40
40	8·26	40	8·40
45	8·22	45	8·36
50	8·24	50	8·38

TABLE III.

The values of x given below were all determined at 40° C. Only butyl and isobutyl bromide were investigated at 20° C.

Substance.	$-x \times 10^7$.
o-cresylmethyl ether	6·71
m-cresylmethyl ether	6·38
p-cresylmethyl ether	6·48
o-toluidine	7·06
m-toluidine	6·81
o-phenetidine	7·37
p-phenetidine	6·99
Butyric acid	6·30
Isobutyric acid	6·48
Butyl bromide	5·63
Isobutyl bromide	5·83

Discussion of Results.

In Part I. a similarity was traced between the magnetic and other properties of isomerides, and a few relations between them, given before in the introduction to this paper, were observed. In order to see whether these relations hold as well in the case of isomerides now experimented upon, the data have been collected together in the following table. The values of molecular magnetic rotations have been taken from Perkin's * papers. The values of the boiling-points are those carefully determined by us, and the values of the molecular volumes have been taken from Lossen's data †.

TABLE IV.

Substance.	Molecular magnetic susceptibility. $-x_M \times 10^6$.	Molecular magnetic rotation.	Molecular volume.	Boiling-point. °C.
o-cresylmethyl ether	81·94	15·19	146·1	171·2
m-cresylmethyl ether	77·91	14·65	147·5	176.7
p-cresylmethyl ether	79·13	14·71	147·7	176·1
o-toluidine	75·65	17·20	126·6	199·6
m-toluidine	72·97	16·21	128·1	202·3
o-phenetidine	101·1	—	—	230·0
p-phenetidine	95·86	—	—	254·0
Butyric acid	55·49	4·472	108·2	162·3
Isobutyric acid	57·08	4·489‡	108·9	153·5
Butyl bromide	77·14	7·908§	118·6	101·5
Isobutyl bromide	79·88	8·003	121·0	91·5

‡ In the case of butyric acid the value 4·472 is for 18·8° C. Hence the value 4·489 for isobutyric acid has also been calculated for 18·8° C. by taking the mean of the last six readings given by Perkin (Journ. Chem. Soc. xlv. p. 488 (1884)).

§ According to Perkin (Journ. Chem. Soc. xlv. pp. 562 & 574 (1884)) molecular magnetic rotation of normal bromides is given by $3·816 + n\,(1·023)$, where n is the number of carbon atoms in the molecule, and the value 7·908 for butyl bromide has been calculated by this relation.

It is clear from the above table that the relations given before hold for these isomerides as well. In Part I. ortho-, meta-, and para- varieties of cresol only were examined. The three isomeric cresylmethyl ethers have now been examined, and their magnetic susceptibilities again decrease

* Journ. Chem. Soc. xlv. p. 575 (1884) lxix. . 1236 (1896).

† *Ann. der Chemie*, ccliv. p. 42 (1889).

in the order ortho-, para-, meta-. Again, in Part I. the values of the depolarization factor "r" observed by Krishnan*, Ganesan†, etc., were also given in the table corresponding to Table IV. above, and it was shown that in every group the isomeride having a higher value of the depolarization factor "r" has got a smaller value of the molecular magnetic susceptibility. The values of "r" for any of the groups of isomerides now investigated could not be obtained, but if iso- and orthoisomerides have in general a higher value of "r" (*cf.* Ganesan, *loc. cit.*), then the above relation will again hold good. In

TABLE V.

Substance.	Formulæ showing substituent groups.	Molecular magnetic susceptibility. $-x_M \times 10^6$.	Difference.
o-cresol.	$C_6H_4\begin{cases}CH_3\\OH\end{cases}$	73·62‡	0·87
p-cresol.		72·75‡	
o-cresylmethyl ether.	$C_6H_4\begin{cases}CH_3\\O.CH_3\end{cases}$	81·94	2·81
p-cresylmethyl ether.		79·13	
o-phenetidine.	$C_6H_4\begin{cases}NH_2\\O.C_2H_5\end{cases}$	101·1	5·24
p-phenetidine.		95·86	
o-cresol.	$C_6H_4\begin{cases}CH_3\\OH\end{cases}$	73·62‡	1·30
m-cresol.		72·32‡	
o-toluidine.	$C_6H_4\begin{cases}CH_3\\NH_2\end{cases}$	75·65	2·68
m-toluidine.		72·97	
o-cresylmethyl ether.	$C_6H_4\begin{cases}CH_3\\O.CH_3\end{cases}$	81·94	4·03
m-cresylmethyl ether.		77·91	

‡ Values taken from Part I.

view of the recent work on optical and magnetic anisotropy it is proposed to discuss this point further in a future communication.

Again, if we examine the differences between the values of x_M for ortho- and para- (or ortho- and meta-) isomerides given in Table IV., we see that they are not the same in every group. In order to see any influence of the sizes of the groups substituting the hydrogen atoms in the benzene ring, the data have been collected together in Table V.

* Phil. Mag. [6] l. p. 697 (1925).
† Phil. Mag. [6] l. p. 1219 (1925).

It is clear from the above table that the difference between the magnetic susceptibilities of the ortho- and paraisomerides tends to increase as we go from cresols to phenetidines, and it is also evident that the size of the substituting groups increases in the same order. Hence the differences between the values of x_M for ortho- and paraisomerides increase with the size of the substituent groups. The above generalization also holds for the differences in the values of x_M between the ortho- and metaisomerides.

Further, we see from Table IV. that in every group the isomeride having a higher molecular magnetic rotation has also got a higher magnetic susceptibility, a conclusion previously arrived at by us in Part I. The significance of this is evident from the fact that the phenomenon of magnetic rotation and magnetic susceptibility must be closely allied. Apart from the similarity in their theoretical treatment there can be collected a number of observations to show that one phenomenon influences the other; for example, in the case of ferromagnetic elements the magnetic rotation is proportional to the intensity of magnetization, and not to the intensity of the magnetic field as is ordinarily the case. Secondly, when a substance passes from the liquid state into the crystalline state there is a big change in its magnetic rotation, but when it passes into the gelatinous state there is hardly any change *. The variation of magnetic susceptibility with change of state is analogous in character †. Thirdly, like magnetic susceptibility there are two types of magnetic rotation—the usual diamagnetic rotation and the paramagnetic rotation ‡. The latter arises from paramagnetic atoms, and, like paramagnetic susceptibility, varies inversely with the temperature. And finally, paramagnetic rotation does not vary with temperature in case the paramagnetic susceptibility is independent of it. Potassium dichromate furnishes such an example §. Thus the interrelationship between the two properties is fully borne out, and our observations furnish one more proof of the fact that there

* Chaudier, *Compt. Rend.* clvi. p. 1529 (1913).

† Oxley, Phil. Trans. Roy. Soc. ccxiv. p. 126 (1914).

‡ Ladenberg, *Zeits. f. Physik*, xxxiv. p. 898 (1925); Becquerel and de Haas, *Zeits. f. Physik*, lii. p. 678 (1929); Frenkal, *Zeits. f. Physik*, xxxvi. p. 215 (1926).

§ Ollivier, *Compt. Rend.* clxxxvi. p. 1001 (1928).

is a close relationship between the two properties, not only in the case of paramagnetics but also in the case of diamagnetic substances.

Again, the abnormal behaviour of liquids has very often been explained on the basis of their molecular association. In this paper, and Part I. as well, most of the liquids investigated by us, especially the alcohols and the acids, are known to be highly associated. It might therefore be suspected that the differences between the magnetic susceptibilities of position isomerides are also due to the different degrees of their molecular association. Weiss and Piccard * and Cabrera and Duperier † have found that the magnetic susceptibility of water increases slightly with temperature (by about 0·7 per cent. from 0°–100° C.), and this change is ascribed by the later workers to a decrease in the degree of molecular association of water with temperature. Hence the more associated a liquid is the lesser is its magnetic susceptibility. In the case of position isomerides also if the differences in their magnetic susceptibilities are due to the different degrees of their molecular association, the secondary should be less associated than the primary and the ortho- less than the para- or metaisomerides. A large number of methods have been used for determining the degree of molecular association in liquids. In general there is no theoretical basis for the formulæ used in these methods, and the results quite often do not agree in magnitude. For the present, however, we are concerned only with the comparative values of the degree of association for position isomerides, and although the different methods do not give the same result in magnitude, they might be taken to show to which of the isomerides is more associated than the other. In Table VI. we have given from MacLeod's ‡ collection of data the values for the degree of molecular association of isomerides by different investigators.

It is clear from the above table that, although the differences are small, ortho- and iso-compounds are more associated than the meta- and normal compounds respectively. Hence on the afore-mentioned view iso-compounds should be a little less diamagnetic than the normal ones and ortho-compounds a little less diamagnetic than

* *Compt. Rend.* clv. p. 1234 (1912).
† *J. de Physique et le Radium*, vi. pp. 121–138 (1925).
‡ Trans. Faraday Soc. xxi. p. 151 (1925–26).

the meta- ones. But we find that just the opposite is the case. A difference in the degrees of molecular association cannot therefore account for the differences between our values of x_M for the isomerides. In Table VI. we have, however, collected together the data by four investigators only. A large number of other methods and formulæ are available to calculate the degree of molecular association; and according to some of them * it is found on calculation that, unlike the results given in Table VI., the iso- and ortho-compounds are less associated than the normal and meta-compounds respectively. The differences, however, between the degrees of association for isomerides are found on calculation to be very small. Now in the case of

Table VI.

Substance.	MacLeod ‡.	Ramsay and Shields §.	Bingham ‖.	Batschinski ¶.
Propyl alcohol	3·05	2·25	—	5·03
Isopropyl alcohol	3·89	2·86	—	6·33
Butyl alcohol	3·53	1·94	—	4·79
Isobutyl alcohol	5·25	1·95	—	6·50
o-xylene	1·02	—	1·07	
m-xylene	0·92	—	1·00	

‡ *Loc. cit.*
§ Trans. Chem. Soc. lxiii. p. 1089 (1893).
‖ *Zeit. Phys. Chem.* lxvi. p. 1 (1909).
¶ *Zeit. Phys. Chem.* lxxv. p. 665 (1911); *ibid.* lxxxii. pp. 86, 90 (1913).

water, which is the most highly associated liquid, the degree of molecular association must be undergoing a considerable change † when it is heated from 0°–100° C., but the value of the magnetic susceptibility only changes by about 0·7 per cent. Hence in the case of isomerides it is difficult to believe that such small differences in the values of their degrees of association can produce such comparatively large differences in their values of magnetic susceptibilities.

* Longinescu, 'Chemical Reviews,' vi. pp. 387, 398, 410 (1929).

† According to MacLeod (Trans. Faraday Soc. xxi. p. 146 (1925–26)) the actual magnitude of this change is from 4·18 to 2·7, whereas on calculation by Longinescu's formulæ the difference in the degrees of association for isomerides investigated by us does not amount to even 1/20 of it.

Further, the degree of association, if at all, is very small in the vapour state. Hence the difference between the degrees of molecular association of two isomeric liquids will tend to decrease as the temperature rises up to their boiling-points, when it will be negligible. The difference between the values of x_M for isomeric alcohols should also therefore tend to decrease with rise of temperature, if it is due to the different degrees of molecular association. For the reasons given before the alcohols could not be investigated up to their boiling-points, but it is clear from the data given in Tables I. and II. that the difference between the values of x_M for isomeric alcohols is independent of temperature.

It is therefore clear from what has been given above that a difference in the degrees of molecular association cannot be responsible for the comparatively large differences between our values of x_M for the isomerides. If at all, it might be responsible for a very small fraction of these differences. An explanation has therefore to be sought for on the basis of the different molecular structures of isomerides. Diamagnetism is essentially a property of the nature and size of the electronic orbits. It is therefore necessary to examine carefully if any difference exists in the electronic orbits in the case of isomerides. During recent years several attempts have been made to explain magnetic data on the basis of the electronic significance of valency bonds (see Stoner, 'Magnetism and Atomic Structure,' chapter xiv.). We have also attempted below to give a similar qualitative explanation for the differences observed between the values of x_M for position isomerides.

Let us confine our attention to one particular case, say that of butyl and isobutyl bromide, for similar reasoning can be applied in every case. For convenience of reference the formulæ for the above isomerides are given below :

I. Butyl bromide.

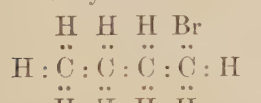

II. Isobutyl bromide.

In general there are two types of combinations between atoms, polar and non-polar. The combination of a carbon atom with a hydrogen atom or with a bromine

atom in the particular case under consideration is an example of the latter type. When Br and C combine there should therefore be two shared electrons, as Br requires one extra electron to complete the inert gas configuration. These shared electrons would move in orbits under the influence of two centres of force, the bromine and carbon nuclei, and the dimensions of these orbits will evidently depend upon the effective positive charges on the two nuclei. Now in formulæ I. and II. let us denote the carbon atoms with which the bromine atoms are linked by C_1 and C_2, and the corresponding bromine atoms by Br_1 and Br_2, and, without going into the spatial arrangement of the atoms with respect to one another, let us consider the linking or the sharing of the electron orbits by C_1 and C_2 with the other atoms. Leaving aside the bromine atom in both the cases, we see that both C_1 and C_2 have got six shared electronic orbits; but the three nuclei (two carbon and one hydrogen) with which C_2 is linked have got a greater positive charge than those (two hydrogen and one carbon) linked with C_1, and it is therefore clear that for combination with other atoms the effective positive charge of C_2 will be less than that of C_1. Further, if we consider Br_1 and Br_2, we see that Br_2 is surrounded by a greater number of positive nuclei than Br_1. It is a well-known fact that the presence of such positive nuclei around any nucleus decreases its effective positive charge. The effective positive charge on Br_2 therefore will also be less than that on Br_1. As noted before, the dimensions of the shared orbits increase with the decrease in the effective positive charges on the nuclei concerned. The dimensions of the shared orbits between C_2 and Br_2 will therefore be greater than the dimensions of the shared orbits between C_1 and Br_1, and therefore, according to Langevin's treatment of the subject, isobutyl bromide should be more diamagnetic than butyl bromide, as our observations reveal it to be. Further, in the above we have only considered the dimensions of the shared orbits. But X-ray evidence has shown that in the combination of atoms only the most firmly bound electrons of each atom continue to move in orbits, which differ little from those in the free state. Hence, in molecular formation, the outer electronic orbits of both Br_1 and Br_2 will increase in size because of the proximity of other positive nuclei. But for reasons given before

the increase in the dimensions of the electronic orbits of Br_2 will be greater, and for this reason as well the iso-compound should be more diamagnetic than the normal.

In the above treatment, however, we have not considered one factor. In formulæ I. and II., when Br goes from C_1 to C_2, one hydrogen atom, so to say, comes from C_2 to C_1. Its shared orbits will therefore decrease in size and there will be a decrease in diamagnetism due to it; but this decrease, on account of a much smaller number of the orbits affected as compared with those in the case of the bromine atom, will obviously be much less than the increase. The observations given before in Table V., that as the size of the substituent groups increases the difference in magnetic susceptibilities also increases, completely corroborate the above statement.

The magnetic behaviour of tertiary compounds can also be similarly explained. The corresponding carbon atom, say C_3, will have six shared electrons with the three carbon atoms around it. Hence the positive charges on the three nuclei with which it is associated will be still greater. Its effective positive charge will, therefore, be still less, and tertiary compounds will be still more diamagnetic, as we find them to be.

Let us now consider a group of isomerides in which the substituent, instead of a single atom like bromine atom in the present case, is a group of atoms like OH, as in the case of isomeric alcohols. In OH radicle, H atom will share its electron with oxygen atom. There will therefore be nine electrons in all around the oxygen nucleus, and in order to complete its inert gas configuration it will need one more electron; hence when OH combines with C there will be two shared electrons between them, and the position then becomes the same as that with the bromine atom.

The difference between the magnetic susceptibilities of ortho- and meta- or para-position isomerides can also be similarly explained. For convenience of reference let us denote the carbon atoms in the benzene ring by C_1, C_2.....C_6. Unlike the case of primary, secondary, and tertiary isomerides the carbon atoms in the benzene ring are all initially alike, and there is only one mono-substitution product; but when a hydrogen atom associated with any of the carbon atoms, say C_1, has been substituted, say, by a bromine atom, the remaining carbon atoms do

not remain all exactly alike. Being nearest, the decrease in the effective positive charges of C_2 and C_6 for combination with other atoms will be maximum. Moreover in the ortho-position the two substituent groups are nearest together. Their effective positive charges therefore will also be least in this position, and hence, according to what has been given before, ortho- should be more diamagnetic than meta- or paraisomerides. This actually is the case. The data at present available to distinguish between meta- and paraisomerides are very few, and hence discussion of this part of the problem has been reserved for a future communication.

A precise mathematical treatment of the above problem presents great difficulties; but the above qualitative treatment is sufficient to show that the magnetic properties of isomerides are in accordance with the accepted views on the arrangement of electronic orbits in molecular formation.

University Chemical Laboratories,
University of the Punjab,
Lahore, India.

LXXVII. *On the Production of Acoustic Waves by means of an Air-jet of a Velocity exceeding that of Sound.* By Jul. Hartmann, *Dr. techn., Professor of Technical Physics, Royal Technical College, Copenhagen* *.

[Plates VII.–XI.]

Fundamental Observations.

In a series of papers † it has been described how acoustic waves can be produced by means of an air-jet with a velocity exceeding that of sound. In the present paper

* Communicated by the Author.

† (1) "Om en ny Metode til Frembringelse af Lydsvingninger," *Kgl. Danske Vidensk. Selsk. math.-fys. Medd.* i. p. 13 (1919) (Danish paper). (2) "On a new Method for the Generation of Sound Waves," Phys. Rev. xx. p. 719 (1922). (3) "New Investigation on the Air-jet Generator for Acoustic Waves," *Kgl. Danske Vidensk. Selsk. math.-fys. Medd.* vii. p. 6 (1926). (4) "A new Acoustic Generator: the Air-jet Generator," Journal of Scientific Instruments, iv. no. 4 (Jan. 1927). (4) "Modus operandi of the Air-jet Pulsator," *Kgl. Danske Vidensk. Selsk. math.-fys. Medd.* x. p. 4 (1930).

it is proposed to give a review of the main facts disclosed by the various investigations with a view to conveying a general idea of the new means for production of sound waves.

The fundamental observations on which this production is based are illustrated in fig. 1 *a*. *b*. An air-jet, J, with a velocity exceeding that of sound is discharged from the nozzle N. It is known that the condition for the production of such a jet is that the excess pressure in the container is greater than 0·9 atm. provided the jet is

Fig. 1.

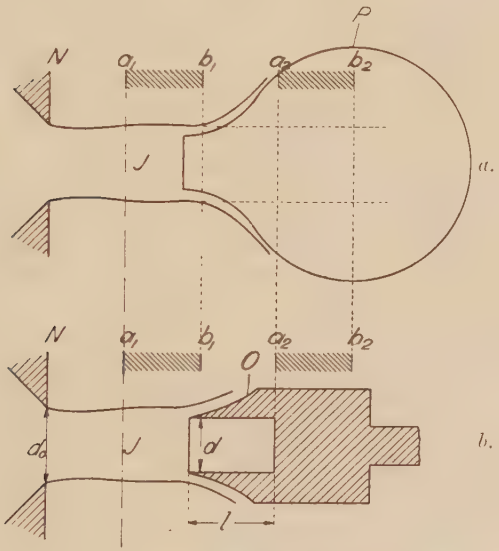

The air-jet pulsator and the air-jet oscillator.

emitted into the free atmosphere. If the excess pressure is not too high, say 2–4 atm. only, a series of equidistant intervals, $a_1 b_1$, $a_2 b_2$—*the intervals of instability*—are found in the jet exhibiting the following peculiar property:—If the mouth of a bottle P, *the pulsator*, is introduced, as shown in one of the intervals indicated, the bottle will take in air to a certain pressure, then discharge the air, then again charge to the same pressure as before, discharge, etc. Again, if the pulsator is replaced by a cylindrical *oscillator* (fig. 1, *b*), the latter will, with its aperture in one of the intervals of instability, and in such an interval only,

produce air vibrations approximately of the natural period of the oscillator. It was found in the very first investigations on the phenomena here considered that the intervals of instability are closely connected with what may be termed the *Pitot-curve* of the jet. This curve is determined by means of a simple Pitot apparatus

Fig. 2.

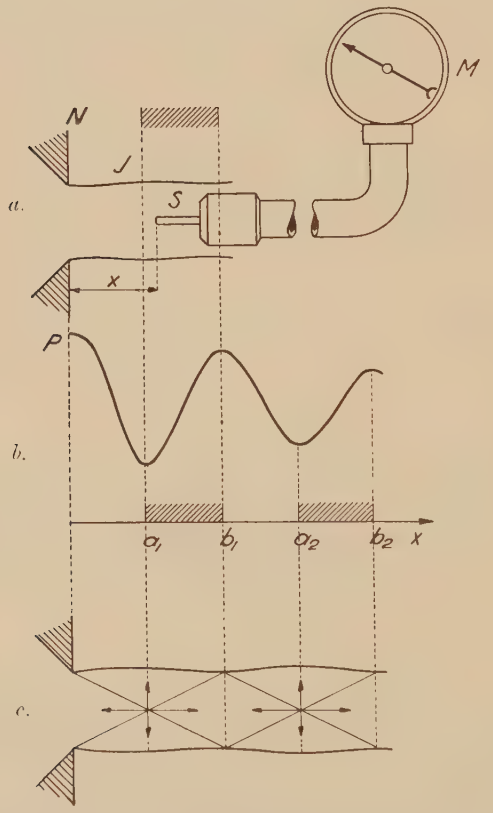

The positions of the intervals of instability relatively to the Pitot-curve and to the structure of the jet.

(fig. 2, *a*), the "sound" S of which is directed against the flow and moved by steps out along the axis of the jet. When the readings on the manometer M are plotted against the positions of the aperture of the sound a curve like that in fig. 2, *b*, is obtained. It is found that the intervals

of instability coincide with those parts of the jet where the Pitot pressure is rising, thus the parts $a_1 b_1$, $a_2 b_2$. . . . (fig. 2, *b*). It should be noted that a Pitot-curve of the periodic character (fig. 2, *a*) is characteristic of a jet with a velocity exceeding that of sound, while with a jet of a velocity smaller than that of sound the Pitot pressure is nearly constant. The periodicity in the former case is closely connected with the periodic structure of the jet known from photographs taken by the method of striæ. In fig. 3 (Pl. VII.) a series of such photographs is reproduced, and in fig. 2, *c* the positions of the jet-sections relatively to the Pitot-curve are indicated. The explanation of the structure is due to Prandtl*. In the middle of the sections the static pressure is a minimum, while the velocity is a maximum.

The Air-jet Oscillator.

We may now pass on to describe in more detail the properties of the two apparatus indicated above, commencing with *the air-jet oscillator*. The latter apparatus constitutes a means for the production of high-frequency waves of high intensity. In order to comprehend this we may note that the diameter d of the oscillator, fig. 1 *b*, must generally be chosen nearly of the same size as that, d_0, of the jet-orifice. Furthermore, that a depth l of the oscillator approximately equal to d is best suited for the production of vigorous vibrations. Finally, that these vibrations have, as indicated, nearly the natural frequency of the oscillator. This means that the length of the waves emitted may be determined approximately by

$$\lambda/4 = l + 0{\cdot}3\,d. \quad . \quad . \quad . \quad . \quad . \quad . \quad (1)$$

Now take a jet of, say, 1 mm.; then we may advantageously choose $l=1$ mm., $d=1$ mm., and so get $\lambda/4=1{\cdot}3$ mm., or $\lambda=5{\cdot}2$ mm., corresponding to a frequency $n=\frac{340000}{5{\cdot}2}$ $=65{,}000$ cycles per sec. With a jet of 0·5 mm. we may in the same way produce a frequency of 130,000 cycles per sec. If a hydrogen jet is used 3–4 times as high frequencies may be obtained, thus up to 300,000–500,000 cycles per sec.

* L. Prandtl, *Phys. Zeit.* p. 599 (1904); p. 23 (1907).

The high intensity indicated originates from the high density of the kinetic energy in the jet and from the comparatively high efficiency of the oscillator. The latter has been measured provisionally, and found to be something between 10 and 20 per cent. It means that the energy emitted in wave-shape amounts to 10–20 per cent. of the work used for the adiabatic compression of the air discharged in the jet. In figs. 4 *a* & 4 *b* two sets of curves are

Fig. 4 *a*.

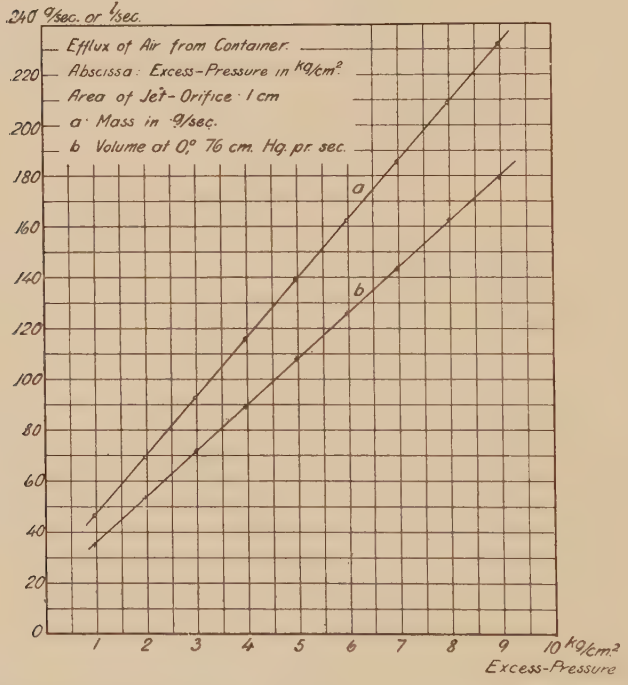

reproduced by means of which the compression work may be calculated and so an idea formed of the sound-wave power. Thus, with a jet-orifice of 1 mm., *i. e.*, an area of cross-section equal to 0·00786 cm.^{2} and an excess pressure of 3 kg./cm.^{2}, the efflux in gram. per sec. is found from fig. 4 *a* to be $93 \cdot 0{\cdot}00786 = 0{\cdot}731$ g./sec., and the adiabatic compression work per sec. is found from fig. 4 *b* to be $10{\cdot}3 \,.\, 0{\cdot}731 = 7{\cdot}52$ kgm./sec. or 73·7 watt. Hence the sound-wave power will at least amount to 7·4 watt, and is likely

to be double that value. With an orifice of $\frac{1}{2}$ mm. and an excess pressure of 3 kg./cm.^{2} the sound-wave power is four times smaller, *i. e.*, 2–4 watt. With heavier jets the sound-wave power is easily raised to several hundred watts or even to several kilowatts.

A most striking consequence of the high intensity of the waves, even with relatively light jets, may be found in

Fig. 4 *b*.

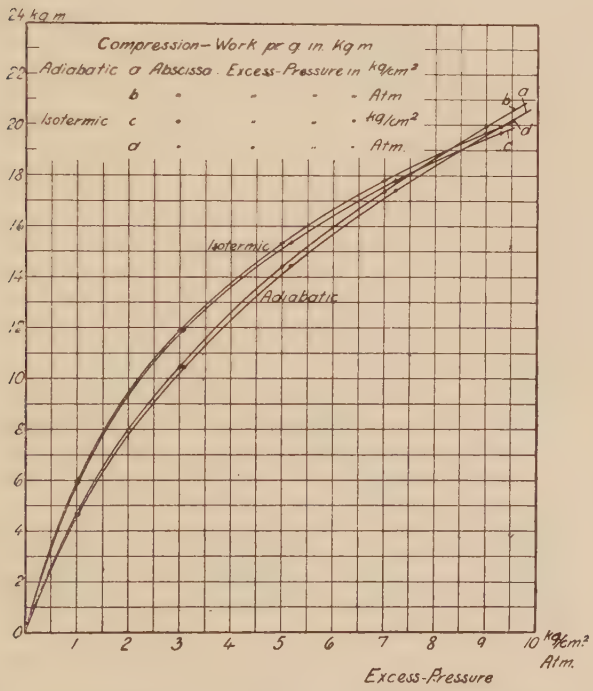

Curves for the determination of the work necessary for the production of the jet.

the fact that the rise of temperature caused by the absorption of the sound energy can be determined by the simplest means and used for the measurement of the sound-wave power. This effect was first demonstrated in connexion with an air-jet oscillator with a jet of 2 mm. and an excess pressure of 3–4 kg./cm.^{2}. The sound-wave power emitted was about 50 watt. A thermometer, the bulb of which was covered by cotton-wool, rose at

a distance of 0·32 metre from the oscillator to a steady temperature of about 3° C. above the surroundings.

Further evidence of the high intensity of the waves emitted from the air-jet oscillator is given in figs. 5 *a–c* (Pl. VIII.), representing photographs of a single train of waves and of interfering wave-trains. The pictures were obtained by the method of striæ. The distance between two circles is a whole wave-length. From this fact it may be concluded that the waves have a rather steep front. Figs. 6 *a–e* (Pl. IX.) show photographs of the vibrations of the air in or rather in front of the oscillator. These pictures, too, were obtained by the method of striæ. In the first column the aperture of the oscillator is outside the interval of instability, and consequently no vibrations take place and no waves are emitted. In front of the oscillator a sharp line is seen. It pictures the compression wave ("Verdichtungsstoss") which is always formed in front of any object stopping a flow with a velocity exceeding that of sound (or moving like a bullet through air with super-sound velocity). In the second column of fig. 6 (Pl. IX.) and in the first two pictures of the third column the oscillator is inside the first interval of instability. In front of the oscillator a rather wide band is now seen. It indicates a number of positions of the front wave during the vibration of the air in the oscillator, each photograph being taken with the jet illuminated by a great number of electric sparks, say 50. In the following pictures the vibrations first disappear, then reappear. Whenever waves were emitted which could be shown by means of a Kundt tube then the front wave described a band.

After this review of the properties of the high-frequency air-jet generator some results from a series of special investigations will be given. It is a characteristic feature with the generator that the intervals of instability are the more definite the smaller the excess pressure by which the jet is produced. With increasing excess pressure the intervals become wider and wider, and at last meet. The explanation of this fact may be derived from the pictures in fig. 3 (Pl. VII.), which show how the aspect of a jet of about 1 mm. varied when the excess pressure was raised by steps from about 3 to 6·5 atm. It will be seen that a white line perpendicular to the axis of the jet appears in the first jet-section in the last four pictures, being the

more pronounced the higher the excess pressure. This line represents a compression wave of the type indicated above. In such a wave the velocity of the flow is reduced from a value above to a value below the velocity of sound. Hence the wave is apt to break up the periodic structure of the jet, for, as stated above, this structure only occurs with jets of velocities exceeding that of sound. It is clearly seen from the pictures that the jet-sections beyond the first become less and less definite as the compression wave develops. The periodic structure does not entirely dissappear, for the compression wave does not yet cover the whole cross-section, but the structure becomes more or less irregular with the effect on the intervals of in-

Fig. 8.

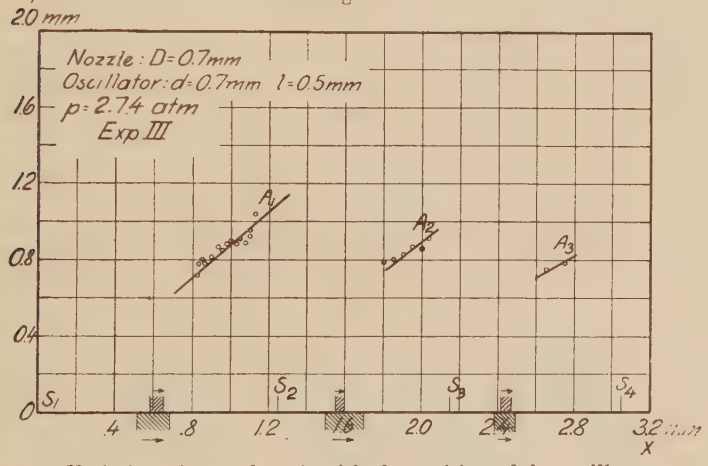

Variation of wave-length with the position of the oscillator.

stability stated above. In fig. 7 (Pl. VII.) a photograph is reproduced which illustrates the breaking-up of the jet-structure even better than fig. 3 (Pl. VII.). If a Pitot-curve is taken it, too, is found to lose its regular periodic character when the excess pressure is increased beyond a certain limit.

The photographs in fig. 6 (Pl. IX.) originate from an investigation on the variation of the wave-length with the position of the aperture of the oscillator within the intervals of instability. The wave-length is not solely determined by the dimensions of the oscillator, but depends to some extent on the position indicated. In figs. 8 & 9 the results

of two experiments are represented. (D = diameter of jet-orifice, d = diameter of oscillator, l = depth of oscillator, p = excess pressure, S_1, S_2, S_3. . . . = boundaries of the jet-sections.) The abscissa is the distance x from the nozzle to the front of the oscillator, the ordinate is one quarter of the wave-length λ, measured by means of a Kundt tube. It will be noted that $\lambda/4$ increases linearly with x or with the distance from the entrance to the jet-section. Approximately the increase of $\lambda/4$ is equal to the displacement of the oscillator. If it were exactly equal to the displacement this would mean that the "loop"

Fig. 9.

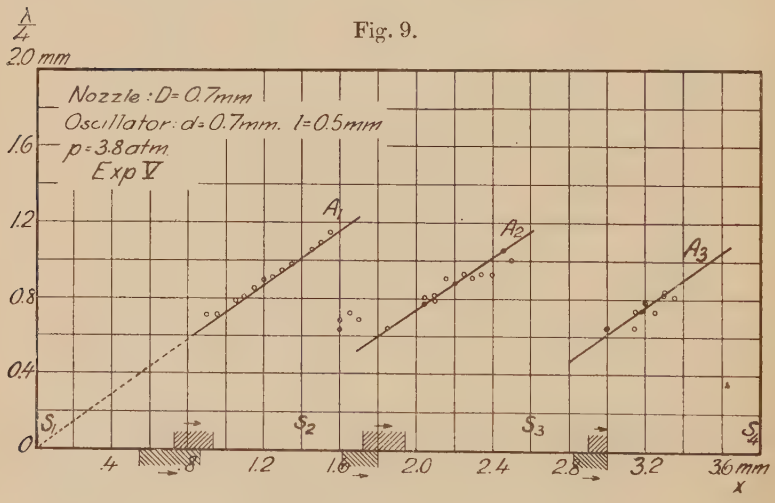

Variation of wave-length with the position of the oscillator.

of the vibrations maintained a fixed position in the jet when the oscillator was displaced. In order to see how fixed the position actually is lengths of $\lambda/4$ were marked off from the bottom of the oscillator in the direction toward the nozzle. The ends of these line-pieces are found to fall within certain intervals, the hatched areas above the axis of abscissæ. With the low excess pressure in fig. 8 the intervals are narrow, indicating that the rule of the fixed position of the loops is fairly correct. The higher, however, the excess pressure becomes the less exact is the rule, as appears from fig. 9 in comparison with fig. 8. The arrows above the intervals show in which

direction the loop moves when the oscillator is displaced in the direction of the flow of the jet.

Photographs of the type in fig. 6 (Pl. IX.) would seem suitable for a control of the conception suggested by the experiments indicated above. It would also seem that some information with regard to the intensity of the air vibrations might be derived from them. In fig. 10 the hatched area in front of the aperture of the oscillator (to the right) is to represent the band to which the compression wave in front of the oscillator is drawn out when the latter emits waves. With the notations used in the figure the amplitude of the air vibrations should be $\frac{x_0' - x_0}{2}$. Further, if the oscillations are considered as stationary waves reflected from the bottom of the oscillator, the quantity $l = x - \frac{x_0 + x_0'}{2} + l_0$ should be a quarter

Fig. 10.

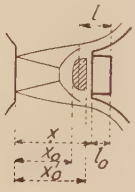

Measurement of the amplitude of the air vibrations.

of a wave-length measured at the temperature of the oscillator. Again, we should expect the middle point of the band to coincide with that of the loop, as found from the Kundt-tube measurement indicated above. The latter comparison is undertaken in figs. 8 & 9, where the hatched intervals below the axis of abscissæ indicate the regions inside which the middle points of the bands are found. They coincide fairly well with the intervals above the axis of abscissæ. In Table I. the comparison of l with the quarter-wave-length, as found by the Kundt-tube method, is performed, and the values of the "amplitude" $\frac{x_0' - x_0}{2}$ are quoted. The table originates from the same experiments as fig. 6 (Pl. IX.) and fig. 8. It is seen that l and $\lambda/4$ very nearly coincide, and that the amplitude reaches such high values as 0·28 mm. On the basis

of the table the variation of the amplitude inside the two first intervals of instability is pictured in fig. 11.

Some additional observations are finally given in Table II. Here a_0' denotes the abscissa of the first minimum of the Pitot-curve, while a_0 stands for the

TABLE 1.

Jet-orifice: $d_0=0{\cdot}7$ mm. Oscillator: $d=0{\cdot}7$ mm. $l_0=0{\cdot}5$ mm.
Excess pressure 2·74 atm. Plates no. 18–30.

Plate no.	$\lambda/4$, Kundt tube.	x_0.	x_0'.	$\frac{x_0+x_0'}{2}$.	x.	l.	$\frac{x_0'-x_0}{2}$.
	mm.	mm.	mm.	mm.	mm.	mm.	mm.
18	0·72	0·46	0·57	0·51	0·83	0·82	0·05
19	0·78	0·44	0·60	0·52	0·85	0·83	0·08
—	0·80	0·44	0·64	0·54	0·87	0·83	0·10
20	0·78	0·42	0·62	0·52	0·88	0·86	0·10
—	0·82	0·45	0·67	0·56	0·90	0·84	0·11
—	0·86	0·43	0·70	0·56	0·92	0·86	0·14
—	0·84	0·43	0·75	0·59	0·95	0·86	0·16
21	0·88	0·44	0·76	0·60	0·98	0·88	0·16
—	0·89	0·44	0·83	0·63	1·00	0·87	0·19
—	0·87	0·46	0·88	0·67	1·03	0·86	0·21
—	0·90	0·48	0·89	0·68	1·05	0·87	0·21
22	0·90	0·50	0·82	0·66	1·08	0·92	0·16
—	0·95	0·53	0·81	0·67	1·10	0·93	0·14
—	1·04	0·55	0·78	0·67	1·13	0·96	0·12
27	0·79	1·37	1·62	1·50	1·80	0·80	0·12
—	0·80	1·33	1·65	1·49	1·85	0·86	0·16
—	0·83	1·36	1·76	1·56	1·90	0·84	0·20
—	0·87	1·38	1·87	1·62	1·95	0·83	0·20
28	0·86	1·43	1·90	1·67	1·00	0·83	0·28
—	0·91	1·51	1·89	1·70	2·05	0·85	0·19
30	0·75	2·31	2·46	2·38	2·65	0·77	0·07
—	0·78	2·41	2·52	2·47	2·75	0·78	0·06

abscissa of the foremost boundary and a_m of the rear boundary of the interval of instability. According to what has been stated above a_0 is very nearly coincident with a_0'. It is seen that at the entrance to the interval of instability the quarter-wave-length $(\lambda/4)_0$, found by means of a Kundt tube, has almost exactly the theoretical value $l+0{\cdot}3\ d$, while the largest value $(\lambda/4)_m$ observed at the rear end of the interval of instability is on an average somewhat smaller than $(\lambda/4)_0+a_m-a_0$.

The Air-jet Pulsator.

The period of the pulsations with an air-jet pulsator is the longer the larger the volume of the pulsator and the narrower its aperture. With a pulsator of sufficiently small capacity frequencies of several hundred or thousand per sec. may be produced, thus an audible note. The latter has much the same character as that of a siren, and

Fig. 11.

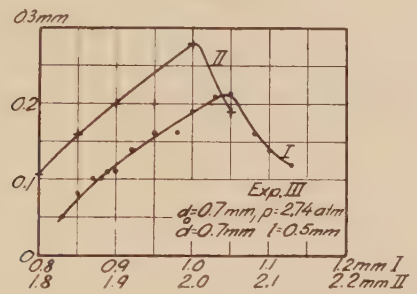

Variation of the amplitude inside the interval of instability.

TABLE II.

Wave-length, Dimensions, and Positions of Oscillator.

(1) d_0.	(2) d.	(3) l_0.	(4) p.	(5) a_3'.	(6) $(\lambda/4)_0$.	(7) $(\lambda/4)_m$.	(8) a_3.	(9) a_m.	(10) $(\lambda/4)_0 + a_m - a_0$.	(11) $l+0{\cdot}3d$.
mm.	mm.	mm.	mm.	mm.	mm.	mm.	mm.	mm.	mm.	mm.
0·7	0·7	0·5	2·74	0·8	0·7	1·0	0·80	1·1	1·00	0·7
0·7	0·7	0·5	3·79	0·8	0·7	1·1	0·95	1·6	1·35	0·7
0·7	1·0	0·5	3·80	0·8	0·6	1·2	0·85	1·6	1·35	0·8
0·7	1·0	0·5	5·65	1·1	0·6	1·3	0·85	2·0	1·75	0·8
4·6	5·0	5·0	6·00	7·3	6·5	11·0	7·00	15·0	14·50	6·5
4·6	5·0	10·0	6·00	7·3	11·5	18·0	7·00	17·0	22·50	11·5
4·6	5·0	25·0	6·00	7·3	30·0	39·0	8·00	20·0	42·00	26·5

may be used for signalling purposes. On the other hand, the pulsations may easily be made very slow, say of a frequency 1 in many minutes. Such slow pulsations are of course excellently suited for investigations on the *modus operandi of the pulsator*, and probably of the oscillator too, and have, in fact, been used for this purpose. Before these investigations were taken up the following conception with regard to the manner of working was formed.

In fig. 12 N_1 denotes the nozzle from which the air-jet J is discharged; N_2 is the nozzle of the pulsator; P_1 is the Pitot-curve of J. N_2 is thus placed in the first interval of instability. Now, what will happen when the jet J is started? Obviously the pulsator must fill with air, and probably to a pressure equal to the Pitot-pressure indicated by the ordinate to the point *c*. After that one might expect the flow of the jet to simply escape laterally. It is, however, easy to see that the state of the pulsator when charged to the said pressure cannot be a stable one; for any disturbance causing air to escape from the pulsator will undoubtedly set up a jet which at the outset will generally have a velocity higher

Fig. 12.

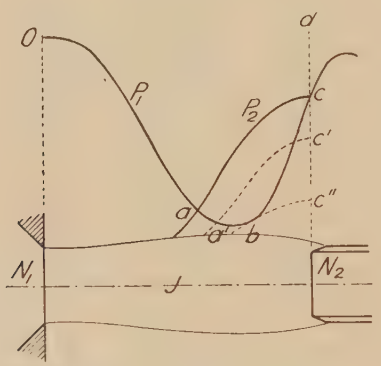

Conception of pulsation process.

than that of sound, thus a Pitot-curve P_2 of the same type as that of the main jet. As the curve P_2 will be above the curve P_1 out to the point *a*, the main jet will not be able to check the jet bursting forth from the pulsator within this distance from N_2. So it may be anticipated that the pulsator-jet will penetrate to *a*. As now the pulsator gradually empties, the Pitot-curve falls, as indicated in the figure, while at the same time the front of the pulsator-jet retreats. It was thought likely that the discharge would continue down to the pressure at which the Pitot-curve of the pulsator just touched the curve of the main jet. Then, at any rate, the state is again instable, as the curve-branch *bc* is at any point higher than *bc″*. So undoubtedly the main jet will burst forth to N_2 and recharge the pulsator.

In order to put the conception just indicated to the test the pulsation process was first studied by means of instantaneous photographs obtained by means of the method of striæ. Two samples are given in fig. 13 (Pl. X.) and fig. 14 (Pl. VIII.). During the better part of the process of filling the main jet is seen right up to the orifice of the pulsator nozzle. The aspect is nearly that shown in fig. 13, *f* (Pl. X.), where the main jet is coming from the right. When the pulsator is filled the discharge suddenly sets in with a characteristic click, and the picture changes to that of fig. 13, *a* (Pl. X.). A jet of the same character as the main jet is found to burst forth from the pulsator nozzle. Where this jet and the main jet meet a layer of some width is formed. Through this layer, the collision-layer, the air from the two jets escapes laterally. The layer is on either side limited by a sharp line. This is, as with the oscillator, the compression-wave which is formed in a flow of air moving with a velocity exceeding that of sound relatively to a body immersed in the flow or stopping the same. Here the collision-layer represents the body. During a considerable part of the discharge the collision-layer is seen on nearly the same spot, as appears from fig. 13, *a*—*d* (Pl. X.). Later on the layer is pressed back against the pulsator nozzles, and the radial flow of air from the layer is seen to bend gradually more and more towards the pulsator, indicating that the momentum of the flow from the pulsator decreases. Suddenly the resistance against the main jet gives way and the latter jet now penetrates to the pulsator, recharging the same. In fig. 14, *a*–*d* (Pl. VIII.), the process of pulsation is illustrated perhaps even still clearer than in fig. 13, *a*–*f* (Pl. X.).

It is seen that the photographs agree qualitatively with the anticipations stated above. These anticipations were also tested quantitatively. Before the results can be stated it is, however, necessary to review a special investigation of the Pitot-curve.

In fig. 15 (Pl. XI.) a series of instantaneous photographs is given of the sound of the Pitot apparatus during the determination of a Pitot-curve. It is seen that a compression wave of nearly the same character as that known from a bullet flying with super-sound velocity through air is formed in front of the sound. If a nozzle with a bore in a plane wall is used instead of the slender steel

sound seen in fig. 15 (Pl. XI.) a compression-wave is likewise formed in front of the nozzle, but the distance from the wave to the nozzle is now considerably greater than the corresponding distance with the sound. This fact is illustrated clearly in fig. 16, *a*, *b*, where W indicates the compression-wave in question. Now both apparatus (fig. 16, *a* and 16, *b*) can be used for the determination of a Pitot-curve, but if the readings on the manometer are plotted against the positions of the orifice, the curves obtained with the two apparatus will be displaced with regard to each other, and at the same time they will differ slightly in shape. If, however, the manometer

Fig. 16.

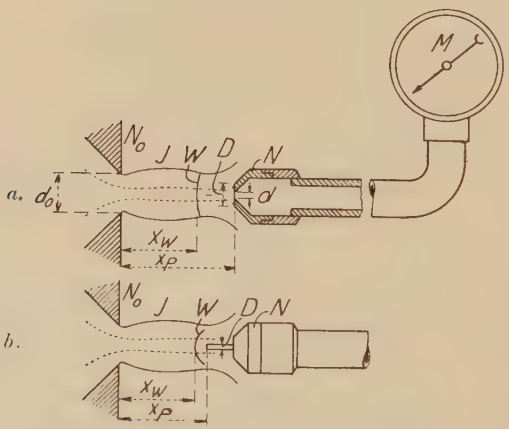

Pitot apparatus with bore and with sound.

readings are plotted against the positions of the compression-waves W, all types of Pitot apparatus give the same curve, *the normal Pitot-curve*. Experimental evidence hereof is seen in fig. 17, where the drawn curves are plotted against the positions of the various Pitot nozzles used, while the points to the left indicate the positions of the compression-waves. These points obviously determine one common curve, the normal Pitot-curve.

The test referred to above was now carried out in the following way:—The normal Pitot-curves were taken not only for the nozzles used for the production of the main jet, but also for the pulsator nozzles, and with the latter for a series of pressures prevailing in the pulsator during

the discharge. The curves were determined by means of a Pitot apparatus with a bore in a nozzle with a flat

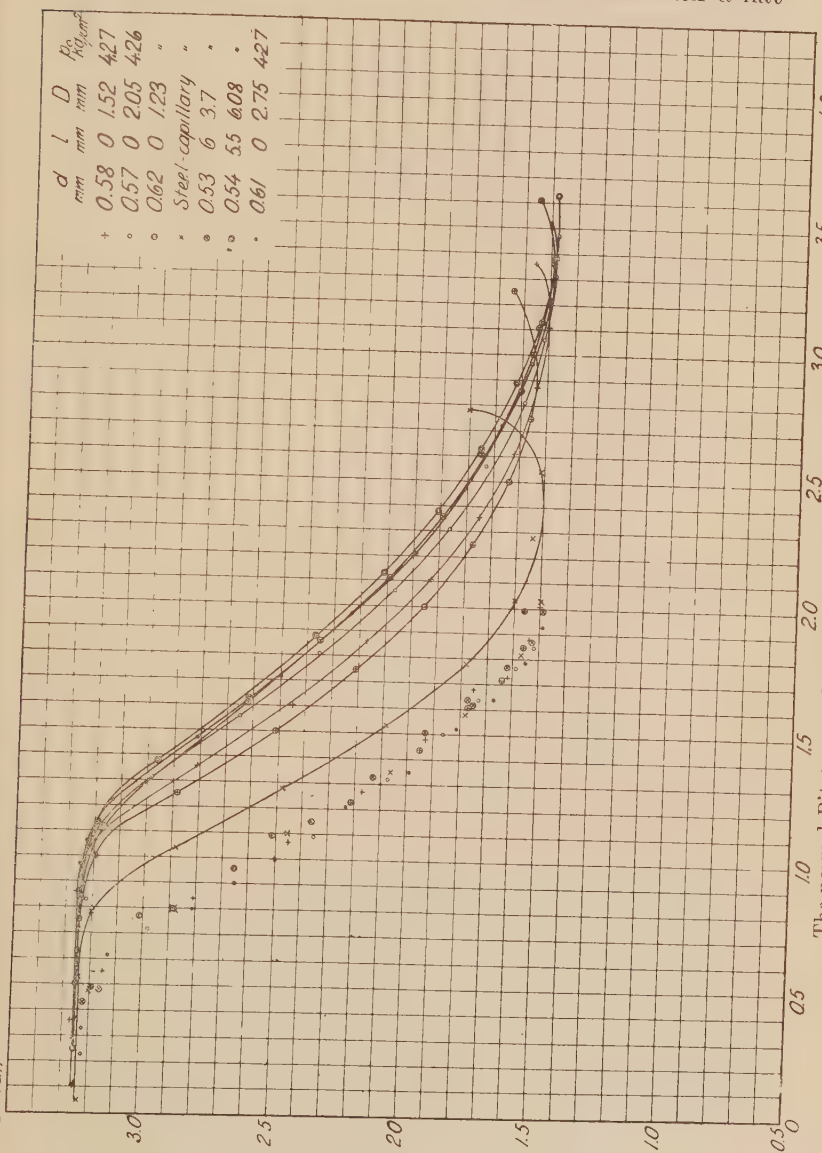

The normal Pitot-curve determined by various types of Pitot nozzles.

front (fig. 16, *a*). The diameter of the flat front was so large that the nozzle could be considered as consisting of

an infinite wall with a bore in it. From the photographs necessary for the determination of the normal Pitot-curve the distance from the compression-wave to the nozzle was found in every case, so that a curve, the wall-curve, indicating the position of the "infinite wall" stopping the jet, could be traced in connexion with every normal Pitot-curve. By means of this material the relations illustrated in fig. 18 were disclosed.

Here P_1 shows the normal Pitot-curve for the main jet emitted from the nozzle N_1. W_1 indicates the positions of the flat nozzle of the Pitot apparatus used in the determination of P_1—*i. e.*, the wall-curve. The horizontal

Fig. 18.

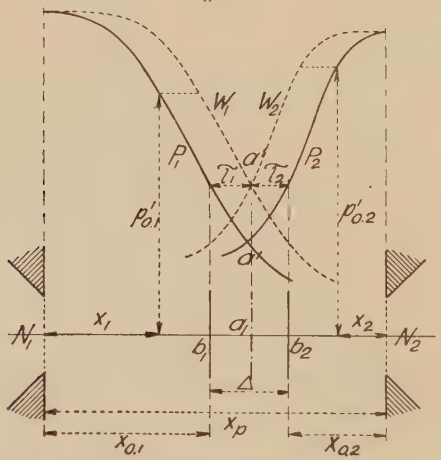

Collision between two jets with velocities exceeding that of sound.

distance between P_1 and W_1 is thus the distance from the Pitot nozzle to the compression-wave in front of it. P_2 is the normal Pitot-curve for the pulsator-jet at a certain moment of the discharge, and W_2 the corresponding wall-curve. The two wall-curves W_1 and W_2 intersect at the point a. A horizontal line is drawn through a. Under the points of intersection between this line and the two Pitot-curves P_1 and P_2, thus at b_1 and b_2, the two compression-waves limiting the layer of collision (comp. fig. 13 (Pl. X.) and fig. 14 (Pl. VIII.)) are found in the at the moment considered. The layer is thus at any moment of the period of discharge inclosed between two

points of the two jets corresponding to the same Pitot pressure, and the width of the collision-layer is just equal to the sum of the two wall-distances τ_1 and τ_2. This

TABLE III.

τ_1.	τ_2.	$\tau_1+\tau_2$.	Δ.
mm.	mm.	mm.	mm.
0·92	0·73	1·65	1·71
1·01	0·70	1·71	1·76
1·13	0·73	1·86	1·78
0·92	0·60	1·62	1·60
0·87	0·63	1·50	1·50
0·91	0·70	1·61	1·62
0·90	0·71	1·61	1·62
0·95	0·70	1·65	1·62
1·01	0·73	1·74	1·68
1·05	0·69	1·74	1·73
0·89	0·60	1·49	1·60

TABLE IV.

Excess pressure 4·15 atm.

P.	$x_{0\cdot1}$.	$x_{0\cdot2}$.	$p'_{0\cdot1}$.	$p'_{0\cdot2}$.
kg./cm.^{2}.	mm.	mm.	kg./cm.^{2}.	kg./cm.^{2}.
3·3	1·45	0·83	3·07	3·04
3·2	1·45	0·80	3·06	2·99
3·1	1·48	0·74	3·00	2·95
3·0	1·50	0·66	2·98	2·92
2·9	1·53	0·58	2·93	2·85
2·8	1·65	0·48	2·80	2·79
2·7	1·74	0·27	2·70	2·70

means that the collision takes place as if the two jets were stopped by a thin wall placed at a_1.

An experimental illustration of these statements is given in Tables IX. and X. In the former Δ denotes

the distance between the two compression-waves of the collision-layer for a number of positions of this layer during the discharge. It is seen that Δ, which is derived from a set of photographs like that in fig. 13 (Pl. X.), is equal to the sum of τ_1 and τ_2 (comp. fig. 18) found from the normal Pitot-curves in combination with the corresponding wall-curves. In Table IV. the positions $x_{0\cdot1}$ and $x_{0\cdot2}$ of the compression-waves limiting the collision-layer for a series of values of the pressure P in the pulsator during the discharge are recorded. The corresponding Pitot pressures $p'_{0\cdot1}$ and $p'_{0\cdot2}$, as found from the normal Pitot-curves, are compared, and it is seen that they practically coincide.

In the anticipations illustrated in fig. 12 it was thought likely that the discharge would come to an end when the pulsator pressure had dropped to a value corresponding to the Pitot-curve $b\ c''$ just touching P_1. Now it is found that the excess pressure in the pulsator generally falls to a value under that necessary for the production of a jet of a velocity exceeding that of sound. The Pitot-curve for the pulsator-jet is therefore, during the last phases of the discharge, a straight line parallel to the axis of abscissæ. Our anticipations therefore amount to the prediction of a pressure in the pulsator at the last moment of the discharge equal to the ordinate of the minimum point of the Pitot-curve of the main jet. This prediction was completely borne out by direct observation of the pressure indicated, and furthermore it was found that the last position of the compression-wave in the main jet was, at any rate, very nearly coincident with the abscissa of the minimum point of the Pitot-curve of the main jet.

Finally, it was thought likely that the pressure in the pulsator during the charging would rise to that of the Pitot-curve P_1. In order to put this hypothesis to the test instantaneous photographs were taken of the jet towards the end of the interval of filling. Two consecutive photographs are reproduced in fig. 19, *a*, *b* (Pl. X.). In front of the pulsator orifice (to the right) a compression-wave is formed. The distance between the latter and the orifice gradually increases. If the pulsator pressure at the last moment of the charging is plotted against the position of the compression-wave just before the discharge sets in, it is found, as shown in fig. 20 for various positions of the pulsator, that the point thus determined coincides

fairly well with the normal Pitot-curve of the main jet. This obviously means that the pulsator fills to the pressure which the jet is able to exert at the aperture of the pulsator nozzle. This was what was anticipated. Thus it is seen that the conception of the pulsation process illustrated in fig. 12 has proved to hold good in all essentials. Fig. 21 may hereafter serve to characterize the pulsation process with regard to the pressure variations in the pulsator. These variations take place between the two

Fig. 20.

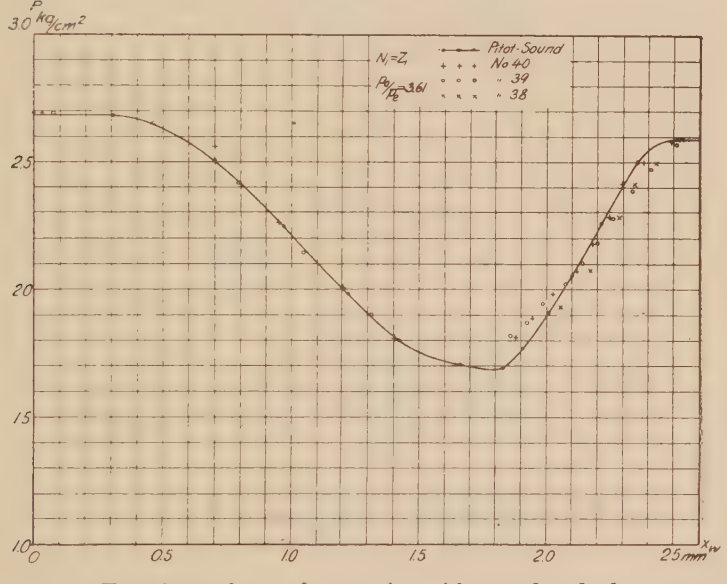

Experimental test of conception with regard to final pressure in pulsator.

limits given by the Pitot-curve (p_u) and a horizontal line (p_l) touching the Pitot-curve at its minimum point. Two reservations must, however, be taken. It is only with a pulsator nozzle furnished with a cylindrical bore (fig. 21, *b* and *c*) that the full Pitot pressure is reached during filling. With an obtuse conical bore (fig. 21, *a*) the pressure to which the pulsator fills is less definite and smaller than the Pitot pressure, as indicated by the dotted curve in fig. 21. The other reservation refers to the frontier of the interval of instability. If a pulsator with an obtuse

conical nozzle (fig. 21, *a*) is gradually removed from the orifice of the main jet pulsations set in as soon as the pulsator nozzle has reached the position $N_{2\cdot 0}$, at which the compression-wave formed in front of the nozzle is just below the minimum point *a* of the Pitot-curve P_1 of this main jet. Thus, with such a nozzle the interval of instability commences exactly at *a*. With cylindrical bores (fig. 21, *b*, *c*) the pulsations show some disinclination to set in with the nozzle in the foremost part of the interval of instability, the hatched part in fig. 21. The pulsations can, however, be started within this region by shielding the pulsator nozzle for a moment from the main jet.

Fig. 21.

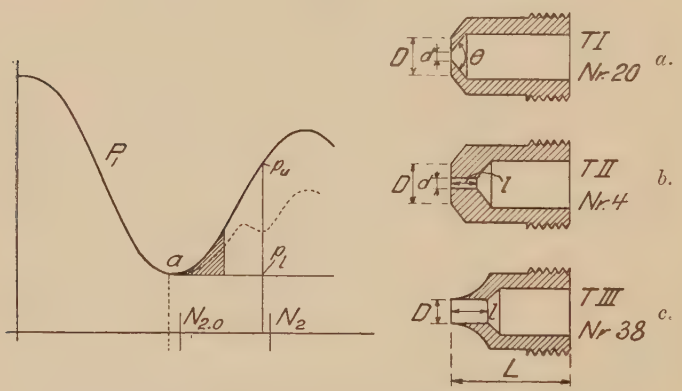

Diagram illustrating the pressure variations during the pulsation process.

The impact of the jet when let loose obviously causes the pulsations to set in.

Ultimate raison d'être *of the Air-jet Oscillator and of the Air-jet Pulsator.*

It has been shown how the pulsation phenomenon, and undoubtedly also the oscillation phenomenon, are a direct consequence of the periodic character of the Pitot-curve. Without rising branches on this latter curve no oscillations or pulsations can be expected. Hence the ultimate *raison d'être* of these phenomena is the same as that which accounts for the periodic Pitot-curve, namely, the compression wave ("Verdichtungsstoss") characteristic of

a flow with a velocity exceeding that of sound when this flow is obstructed by some hindrance. In fig. 22, *a*, *b*, two cases are contrasted. In fig. 22, *a*, a jet J with a velocity smaller than that of sound impinges on a wall, with the effect that the central stream-line tube of the jet is stopped. If a bore in the prolongation of the axis of the jet is connected to a manometer the pressure in the stopped flow of air, *i.e.*, the Pitot pressure, may be measured, and is found to be always very nearly the same as prevails in the container from which the jet is discharged. This fact shows that the main properties of the jet are in this case throughout derivable from the laws of a steady adiabatic and irrotational flow, but otherwise in the case

Fig. 22.

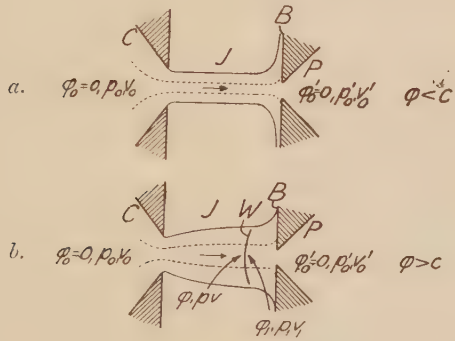

a. Stoppage of jet with a velocity smaller than that of sound.
b. Stoppage of jet with a velocity exceeding that of sound.

shown in fig. 22, *b*, where the jet has a velocity exceeding that of sound. Here, as already stated, a compression-wave is formed in front of the wall. The character of this wave, which occupies an extremely thin layer only, is rather obscure, but its effect is to reduce by some irreversible process the velocity of the jet to a value below the velocity of sound. At the same time the pressure is raised. The total effect is a reduction of the kinetic energy of the flow. Hence a manometer in connexion with a central bore in the stopping wall will indicate a pressure—the Pitot pressure—lower than the pressure p_0 in the container. The Pitot pressure, p_0', is solely determined by p_0 and the static pressure p just

in front of the compression-wave W. As p with a jet of a velocity exceeding that of sound varies periodically, as indicated above, it will be understood that the Pitot pressure will do the same. Such is the explanation of the Pitot-curve and thus of the pulsation and oscillation phenomena described above.

The investigations reviewed above were carried out by Miss B. Trolle in collaboration with the author. The financial means necessary for their completion were granted by the Trustees of the Carlsberg Foundation, Copenhagen.

Physical Laboratory II.
of the Royal Technical College,
Copenhagen.

LXXVIII. *The Magnetic Field of a Circular Cylindrical Coil.* *By* H. B. Dwight, *D.Sc.* (*McGill University, Montreal, Canada*), *Professor of Electrical Machinery, Massachusetts Institute of Technology**.

THE calculation of the value of the magnetic field at a given point near a circular coil or solenoid in a non-magnetic medium is a well-known problem. Considerable space is devoted to it in 'Absolute Measurements in Electricity and Magnetism,' by Andrew Gray, as is indicated by the references in this paper. The results of this problem are of use in laboratory measurements and in shielding problems. In electrical engineering the strength of the magnetic field in the neighbourhood of a current-limiting reactance coil is of interest in connexion with the effect on other apparatus and on structural steel members.

Two formulæ which have been published hitherto do not cover the region surrounding a cylindrical coil as completely as might be, and in this paper a number of formulæ are derived and presented which apply to certain parts of the field where they have rapid convergence. The relation to other formulæ which have been published is shown, so that an indication is given as to the best formula to use for a given case.

Two formulæ are given by Gray for the magnetic potential at a point due to a single circular turn of fine wire carrying a current of I amperes, where the dimensions are in cm. and

* Communicated by the Author.

are as indicated in fig. 1. The origin is on the axis of the circle, on the opposite side of the circle from the point P. The formulæ are *

$$\frac{\omega I}{10} = \frac{2\pi I}{10}\left[1+\cos\alpha-\sin^2\alpha\sum_{n=1}^{\infty}\frac{1}{n}P_n'(\cos\alpha)P_n(\mu)\left(\frac{r}{\rho}\right)^n\right], \quad (1)$$

and

$$\frac{\omega I}{10} = \frac{2\pi I}{10}\sin^2\alpha\sum_{n=1}^{\infty}\frac{1}{n+1}P_n'(\cos\alpha)P_n(\mu)\left(\frac{\rho}{r}\right)^{n+1}, \quad (2)$$

where

$$\mu = \frac{x}{r} = \frac{x}{\sqrt{x^2+y^2}},$$

and where P_n and P_n' denote zonal harmonics and their derivatives (see Appendices I. and II.). The letter n denotes integers. Formula (1) is to be used when $r<\rho$, and (2) when $r>\rho$.

Fig. 1.

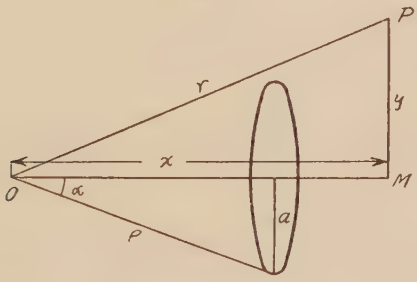

Circular filament.

If the circular filament have its centre at the origin of coordinates, as in fig. 2, the terms involving even values of n vanish. Equation (1) becomes

$$\frac{\omega I}{10} = \frac{2\pi I}{10}\left[1-\frac{r}{a}P_1(\mu)+\frac{1}{2}\frac{r^3}{a^3}P_3(\mu)-\frac{1.3}{2.4}\frac{r^5}{a^5}P_5(\mu)+\ldots\right]. \quad (3)$$

Equation (2) likewise becomes

$$\frac{\omega I}{10} = \frac{\pi I}{10}\left[\frac{a^2}{r^2}P_1(\mu)-\frac{3}{4}\frac{a^4}{r^4}P_3(\mu)+\frac{3.5}{4.6}\frac{a^6}{r^6}P_5(\mu)-\ldots\right], \quad (4)\ \dagger$$

where $r^2 = x^2+y^2$.

* 'Absolute Measurements in Electricity and Magnetism,' by Andrew Gray, ed. of 1893, ii. part i. p. 47, eq. (81) and (82).

† For eq. (4) see "Some Formulas for the Strength of the Magnetic Field of a Cylindrical Coil," by Robt. F. H. Chao, Journ. of Math. and Phys., Cambridge, Mass. vol. x. (1931), equation (2).

If the point P in fig. 1 is on the same side of the circle as the origin, equations (1) and (2) should be rederived from the beginning, as indicated in the footnote on page 245 of 'Absolute Measurements,' ed. of 1893, ii. part i. The equations then become

$$\frac{\omega I}{10} = \frac{2\pi I}{10}\left[1-\cos\alpha+\sin^2\alpha\sum_{n=1}^{\infty}\frac{1}{n}P_n'(\cos\alpha)P_n(\mu)\left(\frac{r}{\rho}\right)^n\right], \quad (5)^*$$

and

$$\frac{\omega I}{10} = \frac{2\pi I}{10}\left[2-\sin^2\alpha\sum_{n=1}^{\infty}\frac{1}{n+1}P_n'(\cos\alpha)P_n(\mu)\left(\frac{\rho}{r}\right)^{n+1}\right]. \quad (6)$$

With these equations the origin may be taken at the point M, and the equations become

Fig. 2.

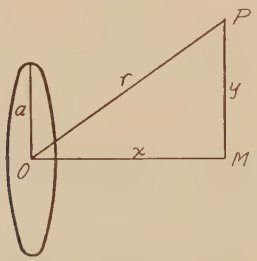

Circular filament with centre at origin.

$$\frac{\omega I}{10} = \frac{2\pi I}{10}\left[1-\cos\alpha-\sin^2\alpha\left\{\frac{1}{2.2}\frac{y^2}{\rho^2}P_2'(\cos\alpha)\right.\right.$$
$$\left.\left.-\frac{1.3}{2.4.4}\frac{y^4}{\rho^4}P_4'(\cos\alpha)+\frac{1.3.5}{2.4.6.6}\frac{y^6}{\rho^6}P_6'(\cos\alpha)-\ldots\right\}\right], \quad (7)$$

and

$$\frac{\omega I}{10} = \frac{2\pi I}{10}\left[2+\sin^2\alpha\left\{\frac{1}{2.3}\frac{\rho^3}{y^3}P_2'(\cos\alpha)-\frac{1.3}{2.4.5}\frac{\rho^5}{y^5}P_4'(\cos\alpha)\right.\right.$$
$$\left.\left.+\frac{1.3.5}{2.4.6.7}\frac{\rho^7}{y^7}P_6'(\cos\alpha)-\ldots\right\}\right]. \quad (8)$$

The distance from M to the centre of the circle may be called x, so that

$$\rho^2 = x^2+a^2.$$

* For eq. (5) see 'Absolute Measurements,' by A. Gray, ed. of 1893, ii. part i. p. 245, eq. (1), and ed. of 1921, p. 210, eq. (1).

Equation (4), which is a power series in $a/\sqrt{(x^2+y^2)}$ seems preferable in all cases to equation (8), which is a power series in $\sqrt{(x^2+a^2)}/y$.

By differentiating the expressions for $\omega I/10$ with respect to x and y, the axial and radial components of the magnetic field of a single circular turn are obtained. From (3), for points near the centre of the circle,

$$-\frac{I}{10}\frac{\partial\omega}{\partial x}=\frac{2\pi I}{10a}\left[1-\frac{3}{2}\frac{r^2}{a^2}P_2(\mu)+\frac{3.5}{2.4}\frac{r^4}{a^4}P_4(\mu)-\frac{3.5.7}{2.4.6}\frac{r^6}{a^6}P_6(\mu)+\ldots\right], \quad . \quad . \quad (9)$$

and

$$-\frac{I}{10}\frac{\partial\omega}{\partial y}=\frac{\pi I}{10}\frac{yr}{a^3}\left[P_2'(\mu)-\frac{3}{4}\frac{r^2}{a^2}P_4'(\mu)+\frac{3.5}{4.6}\frac{r^4}{a^4}P_6'(\mu)-\ldots\right]. \quad . \quad . \quad . \quad (10)$$

From (4), for points not near the centre of the circle,

$$-\frac{I}{10}\frac{\partial\omega}{\partial x}=\frac{2\pi I}{10r}\left[\frac{a^2}{r^2}P_2(\mu)-\frac{3}{2}\frac{a^4}{r^4}P_4(\mu)+\frac{3.5}{2.4}\frac{a^6}{r^6}P_6(\mu)-\ldots\right], \quad . \quad . \quad . \quad (11)$$

$$-\frac{I}{10}\frac{\partial\omega}{\partial y}=\frac{\pi I}{10}\frac{y}{r^2}\left[\frac{a^2}{r^2}P_2'(\mu)-\frac{3}{4}\frac{a^4}{r^4}P_4'(\mu)+\frac{3.5}{4.6}\frac{a^6}{r^6}P_6'(\mu)-\ldots\right]. \quad . \quad . \quad . \quad (12)$$

See equations (3) and (4) of the reference given with equation (4) of this paper.

For points whose distance from the centre of the circle is nearly equal to a, or for points close to the axis, expressions derived from (7) may be useful, as follows :—

$$-\frac{I}{10}\frac{\partial\omega}{\partial x}=\frac{2\pi Ia^2}{10\rho^3}\left[P_1'(\cos\alpha)-\frac{1}{2}\frac{y^2}{\rho^2}P_3'(\cos\alpha)+\frac{1.3}{2.4}\frac{y^4}{\rho^4}P_5'(\cos\alpha)-\frac{1.3.5}{2.4.6}\frac{y^6}{\rho^6}P_7'(\cos\alpha)+\ldots\right], \quad (13)$$

$$-\frac{I}{10}\frac{\partial\omega}{\partial y}=\frac{2\pi Ia^2y}{10\rho^4}\left[\frac{1}{2}P_2'(\cos\alpha)-\frac{1.3}{2.4}\frac{y^2}{\rho^2}P_4'(\cos\alpha)+\frac{1.3.5}{2.4.6}\frac{y^4}{\rho^4}P_6'(\cos\alpha)-\ldots\right]. \quad . \quad . \quad (14)^*$$

* Equations (13) and (14) are equivalent to equations (9) and (10), p. 212, 'Absolute Measurements,' ed. of 1921, changing 1680 x^4 to 1680 a^2x^4.

The strength of the magnetic field of a cylindrical coil can be found by integrating expressions (9) to (14) over the cross-section of the coil (see fig. 3). The cross-section is assumed to have uniform current density. Let F be the axial component of the field at the point P, and let R be the radial component, in lines per sq. cm.

From (9), when p and q are less than approximately a,

$$\mathrm{F}=\frac{2\pi \mathrm{NI}}{10b}\Big[\Big\{\frac{q}{a}\mathrm{P}_1(\mu_2)-\frac{p}{a}\mathrm{P}_1(\mu_1)\Big\}\Big(1+\frac{c^2}{12a^2}+\frac{c^4}{80a^4}+\ldots\Big)$$

$$-\frac{1}{2}\Big\{\frac{q^3}{a^3}\mathrm{P}_3(\mu_2)-\frac{p^3}{a^3}\mathrm{P}_3(\mu_1)\Big\}\Big(1+\frac{c^2}{2a^2}+\frac{3}{16}\frac{c^4}{a^4}+\ldots\Big)$$

$$+\frac{1.3}{2.4}\Big\{\frac{q^5}{a^5}\mathrm{P}_5(\mu_2)-\frac{p^5}{a^5}\mathrm{P}_5(\mu_1)\Big\}\Big(1+\frac{5}{4}\frac{c^2}{a^2}+\frac{7}{8}\frac{c^4}{a^4}+\ldots\Big)-\ldots\Big], \quad \ldots \quad (15)$$

Fig. 3.

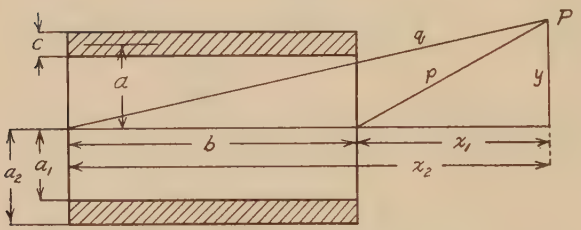

Cylindrical coil or solenoid.

where N = number of turns in the coil,

$$p^2=x_1^2+y^2,$$

$$q^2=x_2^2+y^2,$$

$$\mu_1=x_1/p,$$

$$\mu_2=x_2/q.$$

If, in fig. 3, the point P lie between the planes of the ends of the coil, x_1 and μ_1 are negative.

The last bracket in each term is

$$\Big\{\Big(1-\frac{c}{2a}\Big)^{-n}-\Big(1+\frac{c}{2a}\Big)^{-n}\Big\}\frac{a}{nc},$$

where n is 0 or an even number. In the case of $n=0$, the binomials are to be expanded and n cancelled out before n is

put $=0$, thus giving $\frac{a}{c}\log_e\frac{a_2}{a_1}$. These expressions may be used for extending (15) or they may be used directly in the case of thick solenoids.

From (10), when x_1, x_2, and y are less than approximately a,

$$\mathrm{R}=\frac{3\pi\mathrm{N}\mathrm{I}y}{20ab}\Big[\frac{1}{a^2}(x_2^2-x_1^2)\Big(1+\frac{c^2}{2a^2}+\frac{3}{16}\frac{c^4}{a^4}+\ldots\Big)$$
$$-\frac{5}{4a^4}\Big\{(x_2^4-x_1^4)-\frac{3y^2}{2}(x_2^2-x_1^2)\Big\}\Big(1+\frac{5}{4}\frac{c^2}{a^2}+\frac{7}{8}\frac{c^4}{a^4}+\ldots\Big)$$
$$+\frac{35}{24a^6}\Big\{(x_2^6-x_1^6)-\frac{15y^2}{4}(x_2^4-x_1^4)+\frac{15y^4}{8}(x_2^2-x_1^2)\Big\}$$
$$\times\Big(1+\frac{7}{3}\frac{c^2}{a^2}+\frac{21}{8}\frac{c^4}{a^4}+\ldots\Big)-\ldots\Big]. \quad . \quad . \quad . \quad (16)$$

The last brackets of the terms are similar to those of (15).

From (11), when p and q are greater than a,

$$\mathrm{F}=\frac{\pi\mathrm{N}\mathrm{I}}{10b}\Big[\Big\{\frac{a^2}{p^2}\mathrm{P}_1(\mu_1)-\frac{a^2}{q^2}\mathrm{P}_1(\mu_2)\Big\}\Big(1+\frac{c^2}{12a^2}\Big)$$
$$-\frac{3}{4}\Big\{\frac{a^4}{p^4}\mathrm{P}_3(\mu_1)-\frac{a^4}{q^4}\mathrm{P}_3(\mu_2)\Big\}\Big(1+\frac{c^2}{2a^2}+\frac{c^4}{80a^4}\Big)$$
$$+\frac{3.5}{4.6}\Big\{\frac{a^6}{p^6}\mathrm{P}_5(\mu_1)-\frac{a^6}{q^6}\mathrm{P}_5(\mu_2)\Big\}$$
$$\times\Big(1+\frac{5}{4}\frac{c^2}{a^2}+\frac{3}{16}\frac{c^4}{a^4}+\frac{c^6}{448a^6}\Big)-\ldots\Big]. \quad . \quad . \quad (17)^*$$

Tables for the zonal harmonics can be used†. For extending the formula note that the last bracket in each term is

$$\Big\{\Big(1+\frac{c}{2a}\Big)^n-\Big(1-\frac{c}{2a}\Big)^n\Big\}\frac{a}{nc},$$

where n is an odd number.

From (12), when p and q are greater than a,

$$\mathrm{R}=\frac{\pi\mathrm{N}\mathrm{I}y}{10ab}\Big[\Big\{\frac{a^3}{p^3}\mathrm{P}_1'(\mu_1)-\frac{a^3}{q^3}\mathrm{P}_1'(\mu_2)\Big\}\Big(1+\frac{c^2}{12a^2}\Big)$$
$$-\frac{1}{4}\Big\{\frac{a^5}{p^5}\mathrm{P}_3'(\mu_1)-\frac{a^5}{q^5}\mathrm{P}_3'(\mu_2)\Big\}\Big(1+\frac{c^2}{2a^2}+\frac{c^4}{80a^4}\Big)$$

* "The Force between Unequal Reactance Coils with Parallel Axes," by H. B. Dwight and R. W. Purssell, 'General Electric Review,' equation 4, p. 401 (July 1930).

† 'Fourier's Series and Spherical Harmonics,' by W. E. Byerly, first edition, p. 280 (Ginn and Co., Boston).

$$+\frac{1.3}{4.6}\left\{\frac{a^7}{p^7}\mathrm{P}_5'(\mu_1)-\frac{a^7}{q^7}\mathrm{P}_5'(\mu_2)\right\}$$
$$\times\left(1+\frac{5}{4}\frac{c^2}{a^2}+\frac{3}{16}\frac{c^4}{a^4}+\frac{c^6}{448a^6}\right)+\ldots\Big]. \quad . \quad . \quad (18)*$$

From (13), for points at a distance from the centre approximately equal to a, and for points close to the axis, for thin solenoids,

$$\mathrm{F}=\frac{2\pi\mathrm{NI}}{10b}\Big[\left(\frac{x_2}{v_2}-\frac{x_1}{v_1}\right)-\frac{a^2y^2}{2.2}\left\{\frac{1}{{v_1}^4}\mathrm{P}_2'\left(\frac{x_1}{v_1}\right)-\frac{1}{{v_2}^4}\mathrm{P}_2'\left(\frac{x_2}{v_2}\right)\right\}$$
$$+\frac{1.3a^2y^4}{2.4.4}\left\{\frac{1}{{v_1}^6}\mathrm{P}_4'\left(\frac{x_1}{v_1}\right)-\frac{1}{{v_2}^6}\mathrm{P}_4'\left(\frac{x_2}{v_2}\right)\right\}+\ldots$$
$$+\frac{c^2}{24}\left\{\frac{x_1}{{v_1}^5}({x_1}^2-2a^2)-\frac{x_2}{{v_2}^5}({x_2}^2-2a^2)\right\}$$
$$-\frac{c^2y^2}{32}\left\{\frac{x_1}{{v_1}^9}(2{x_1}^4-21{x_1}^2a^2+12a^4)\right.$$
$$\left.-\frac{x_2}{{v_2}^9}(2{x_2}^4-21{x_2}^2a^2+12a^4)\right\}\ldots\Big], \quad . \quad . \quad (19)$$

where

$${v_1}^2=a^2+{x_1}^2$$

and

$${v_2}^2=a^2+{x_2}^2.$$

The first part of (19) corresponds in form to (7), and may be extended in a similar manner. Equation (19) is equivalent to equation (31) of 'Absolute Measurements,' by A. Gray, ed. of 1921, interchanging the definitions of r_1 and r_2.

For thick solenoids, for a range similar to that of (19),

$$\mathrm{F}=\frac{\pi\mathrm{NI}}{10bc}\Big[2x_2\log_\epsilon\left(\frac{a_2+u_4}{a_1+u_3}\right)-2x_1\log_\epsilon\left(\frac{a_2+u_2}{a_1+u_1}\right)$$
$$+\left(\frac{y^2}{2x_2}-\frac{5}{8}\frac{y^4}{{x_2}^3}\right)\left(\frac{{a_2}^3}{{u_4}^3}-\frac{{a_1}^3}{{u_3}^3}\right)-\left(\frac{y^2}{2x_1}-\frac{5}{8}\frac{y^4}{{x_1}^3}\right)\left(\frac{{a_2}^3}{{u_2}^3}-\frac{{a_1}^3}{{u_1}^3}\right)$$
$$+\frac{33}{32}\frac{y^4}{{x_2}^3}\left(\frac{{a_2}^5}{{u_4}^5}-\frac{{a_1}^5}{{u_3}^5}\right)-\frac{33}{32}\frac{y^4}{{x_1}^3}\left(\frac{{a_2}^5}{{u_2}^5}-\frac{{a_1}^5}{{u_1}^5}\right)$$
$$-\frac{15}{32}\frac{y^4}{{x_2}^3}\left(\frac{{a_2}^7}{{u_4}^7}-\frac{{a_1}^7}{{u_3}^7}\right)+\frac{15}{32}\frac{y^4}{{x_1}^3}\left(\frac{{a_2}^7}{{u_2}^7}-\frac{{a_1}^7}{{u_1}^7}\right)$$
$$+\text{ terms in higher powers of } y\Big], \quad . \quad . \quad (20)$$

* "Some Formulas for the Strength of the Magnetic Field of a Cylindrical Coil," by Robert F. H. Chao, equation 5, 'Journal of Mathematics and Physics,' Cambridge, Mass. vol. x. (1931)

where

$$u_1^2 = a_1^2 + x_1^2,$$

$$u_2^2 = a_2^2 + x_1^2,$$

$$u_3^2 = a_1^2 + x_2^2,$$

and

$$u_4^2 = a_2^2 + x_2^2.$$

From (14), for a range similar to that of (19), for thin solenoids,

$$\begin{aligned} R = \frac{\pi N I}{10b}\Big[& a^2y\left\{\frac{1}{v_1^3}P_1'\left(\frac{x_1}{v_1}\right) - \frac{1}{v_2^3}P_1'\left(\frac{x_2}{v_2}\right)\right\} \\ & - \frac{a^2y^3}{4}\left\{\frac{1}{v_1^5}P_3'\left(\frac{x_1}{v_1}\right) - \frac{1}{v_2^5}P_3'\left(\frac{x_2}{v_2}\right)\right\} \\ & \qquad + \frac{1.3\,a^2y^5}{4.6}\left\{\frac{1}{v_1^7}P_5'\left(\frac{x_1}{v_1}\right) - \frac{1}{v_2^7}P_5'\left(\frac{x_2}{v_2}\right)\right\} \\ & - \ldots + \frac{c^2y}{24}\left\{\frac{1}{v_1^7}(2x_1^4 - 11x_1^2a^2 + 2a^4)\right. \\ & \qquad \left. - \frac{1}{v_2^7}(2x_2^4 - 11x_2^2a^2 + 2a^4)\right\} \\ & - \frac{c^2y^3}{64}\left\{\frac{1}{v_1^{11}}(8x_1^6 - 136x_1^4a^2 + 159x_1^2a^4 - 12a^6)\right. \\ & \left. - \frac{1}{v_2^{11}}(8x_2^6 - 136x_2^4a^2 + 159x_2^2a^4 - 12a^6)\right\} \ldots\Big]. \qquad (21) \end{aligned}$$

For thick solenoids,

$$\begin{aligned} R = \frac{\pi N I y}{10bc}\Big[& \log_e\frac{(a_1+u_1)(a_2+u_4)}{(a_1+u_3)(a_2+u_2)} + \frac{a_1}{u_3} - \frac{a_1}{u_1} - \frac{a_2}{u_4} + \frac{a_2}{u_2} \\ & - \left(\frac{y^2}{2x_2^2} - \frac{5}{8}\frac{y^4}{x_2^4}\right)\left(\frac{a_2^3}{u_4^3} - \frac{a_1^3}{u_3^3}\right) + \left(\frac{y^2}{2x_1^2} - \frac{5}{8}\frac{y^4}{x_1^4}\right)\left(\frac{a_2^3}{u_2^3} - \frac{a_1^3}{u_1^3}\right) \\ & + \left(\frac{3}{8}\frac{y^2}{x_2^2} - \frac{27}{16}\frac{y^4}{x_2^4}\right) - \left(\frac{a_2^5}{u_4^5} - \frac{a_1^5}{u_3^5}\right) \\ & \qquad - \left(\frac{3}{8}\frac{y^2}{x_1^2} - \frac{27}{16}\frac{y^4}{x_1^4}\right)\left(\frac{a_2^5}{u_2^5} - \frac{a_1^5}{u_1^5}\right) \\ & + \frac{105}{64}\frac{y^4}{x_2^4}\left(\frac{a_2^7}{u_4^7} - \frac{a_1^7}{u_3^7}\right) - \frac{105}{64}\frac{y^4}{x_1^4}\left(\frac{a_2^7}{u_2^7} - \frac{a_1^7}{u_1^7}\right) \\ & - \frac{35}{64}\frac{y^4}{x_2^4}\left(\frac{a_2^9}{u_4^9} - \frac{a_1^9}{u_3^9}\right) + \frac{35}{64}\frac{y^4}{x_1^4}\left(\frac{a_2^9}{u_2^9} - \frac{a_1^9}{u_1^9}\right) \\ & + \text{terms in higher powers of } y\Big]. \quad . \quad . \quad . \quad . \quad (22) \end{aligned}$$

Example.—Dimensions in cm.: $a = 100$, $b = 80$, $c = 20$, $x_1 = 200$, $x_2 = 280$, $y = 58$.

By equation (17), $$F = \frac{\pi NI}{10 \times 80}\left(0{\cdot}102 - 0{\cdot}021 + 0{\cdot}003\right)$$
$$= \frac{\pi NI}{10 \times 80} \times 0{\cdot}084 = 1{\cdot}05 \times 10^{-4}\pi NI.$$

By equation (19), $$F = \frac{2\pi NI}{10 \times 80}\left(0{\cdot}047 - 0{\cdot}006 + 0{\cdot}001\right)$$
$$= \frac{2\pi NI}{10 \times 80} \times 0{\cdot}042 = 1{\cdot}05 \times 10^{-4}\pi NI.$$

The collection of formulæ in this paper covers nearly all the field of a cylindrical coil except a region near the section of the coil. The accuracy of the result, in any case, should be determined by observing how rapidly the series used converges. The last term should in all cases be almost negligible. If this is not so the series should not be used for that particular case.

Appendix I.—Zonal Harmonic Functions.

$$P_0(\mu) = 1.$$

$$P_1(\mu) = \mu.$$

$$P_2(\mu) = \frac{1}{2}(3\mu^2 - 1).$$

$$P_3(\mu) = \frac{1}{2}(5\mu^3 - 3\mu).$$

$$P_4(\mu) = \frac{1}{2.4}(5.7\mu^4 - 2.3.5\mu^2 + 1.3).$$

$$P_5(\mu) = \frac{1}{2.4}(7.9\mu^5 - 2.5.7\mu^3 + 3.5\mu).$$

$$P_6(\mu) = \frac{1}{2.4.6}(7.9.11\mu^6 - 3.5.7.9\mu^4 + 3.3.5.7\mu^2 - 1.3.5).$$

$$P_7(\mu) = \frac{1}{2.4.6}(9.11.13\mu^7 - 3.7.9.11\mu^5 + 3.5.7.9\mu^3 - 3.5.7\mu).$$

. . . . . .

Note that the brackets contain binomial coefficients as well as other factors.

APPENDIX II.—First Derivatives. $P_n'(\mu) = \frac{d}{d\mu} P_n(\mu)$

$P_0'(\mu) = 0.$

$P_1'(\mu) = 1.$

$P_2'(\mu) = 3\mu.$

$P_3'(\mu) = \frac{1}{2}(3.5\mu^2 - 1.3).$

$P_4'(\mu) = \frac{1}{2}(5.7\mu^3 - 3.5\mu).$

$P_5'(\mu) = \frac{1}{2.4}(5.7.9\mu^4 - 2.3.5.7\mu^2 + 1.3.5).$

$P_6'(\mu) = \frac{1}{2.4}(7.9.11\mu^5 - 2.5.7.9\mu^3 + 3.5.7\mu).$

$P_7'(\mu) = \frac{1}{2.4.6}(7.9.11.13\mu^6 - 3.5.7.9.11\mu^4 + 3.3.5.7.9\mu^2 - 1.3.5.7).$

. . . . . .

LXXIX. *A Note on Twinkling.* *By* E. H. SYNGE*.

THE phenomenon of twinkling is generally explained by somewhat specious analogies. Simple refraction is assigned as a principal cause, and such cases as that of ripples on a pool, with the mottling of light on the surface below, are cited, the question being treated as one of geometrical optics. One need only observe that in the case of ripples the inequalities of the water will introduce changes in the direction of the wave-fronts of light amounting to degrees of arc, while under normal atmospheric conditions the directions of the wave-fronts from stars are, at most, changed by a very few seconds of arc. There is thus no true analogy at all. If the surface of a pool were as nearly a plane as is the wave-front from a star when it reaches the earth it would appear to the naked eye to be perfectly smooth, and there would be no mottling below.

A second cause is assigned which is still more open to objection. The question being still treated as one of geometrical optics, it is said that we have also to consider

* Communicated by the Author.

actual interfering pencils of light*. To realize the implications of this statement we may try to follow the course of any hypothetical wave-front through the atmosphere. It will be seen that such interference could not occur unless the wave-front had at some place become contorted and folded upon itself, and at this place the normal to the wave-front would take up directions making angles of all magnitudes with the direction of the star, which would appear, if viewed from the proper point, as displaced by 90° or more in the sky. This is, of course, a *reductio ad absurdum.*

What then is the explanation of twinkling? The fact is surely that twinkling is not a phenomenon of geometrical optics at all. It is essentially and entirely a phenomenon of diffraction. *The atmosphere plays the part of an ever-varying diffraction screen.* This is the true explanation of twinkling. And if we turn to Fresnel's method of finding the intensity at any point due to an advancing wave-front † it will be clear exactly how small disturbances in the atmosphere, which do not alter the directions of the wave-front by more than a few seconds of arc, may at the same time alter widely the intensity at various parts of the wave-front, and quite differently for different wave-lengths.

A concrete case may be considered. Let us take a plane wave-front in space, above the atmosphere, at, say, 100 kilometres from the earth, and calculate on Fresnel's methods the intensity resulting from this wave-front at a point on the earth. If there were no atmosphere the method, in its simplest expression, would introduce us to a system of concentric "half-period circles," a summation from which would give us our result. If, however, there is a disturbed atmosphere, and if we take this into account, the half-period curves, drawn on the hypothetical wave-front, will no longer be circles, and the summation, which is the small difference between two large quantities, will give quite a different result and one which will, of course, vary from moment to moment.

These considerations also suggest the explanation of a curious phenomenon, which is generally mentioned without explanation ‡. The spectra of stars near the horizon are crossed by interference bands which travel from blue to red when the star is rising and *vice versa* when it is setting. An application of Fresnel's method to such cases shows us that,

* C. A. Young, 'Manual of Astronomy,' p. 74 (1912).
† Preston, 'Theory of Light' fourth edition, pp. 65–70.
‡ C. A. Young, *loc. cit.*

even with a calm atmosphere, the half-period circles become a system of unsymmetrical curves whose shape depends upon the rapidly varying refraction, being most distorted near the horizon, and which should be calculable if the atmospheric refraction is known. It is only natural to expect that, with such a system, the resultant summation for the amplitude will give values which will change more than once in sign and take on zero values as we proceed upwards from the horizon. Further, if we consider light of two different wave-lengths the half-period curves drawn on a hypothetical wave-front beyond the atmosphere will be larger, and hence more distorted for the light of longer wave-length. Thus a given interference band, corresponding broadly to a given measure of distortion in the half-period curves, should tend to move from the blue to the red in the case of a star which is rising, for this measure of distortion is reached at a greater height from the horizon in the case of the red than of the blue. Needless to say this is only a rough outline of what one might expect if one were to undertake the very complicated and difficult task of calculating these curves and effecting the integrations and summations.

The consideration of the phenomenon of twinkling was suggested to the writer in connexion with the question of atmospheric disturbances as limiting the operation of interference methods in astronomy. It does not appear to him that the conclusions stated by him in recent papers * are materially affected, although the term "wave-front" must no doubt be used with a certain latitude.

He would like to take this opportunity of remarking that the design of apparatus suggested in the later of these papers is capable of further simplification. No difficulty will be found in dispensing with two of the mirrors, the siderostat mirrors, or the parts used of them, in this case not extending beyond the axis, one of them being below and the other above. The maintenance of path-equality would in this case be effected by tilting the achromatizing system, which, except when the base-line is comparatively short, should usually operate on one of the two beams only, and not, as he suggested elsewhere, upon both. It may be worth drawing attention to the possibilities of the apparatus for absolute measurements in the case of zenith stars, and to a possible very severe test of the earlier theory of relativity in connexion with aberration.

* "A Modification of Michelson's Beam Interferometer," Phil. Mag., August 1930; "Interference Methods and Stellar Parallax," Phil. Mag, November 1930.

It may also be permitted to the writer to correct a small error in another paper. In the design for a very large telescope * which he suggested the arrangement of the lenses K should be inversely and not directly similar to that of the reflectors P when the full resolution of the equivalent aperture is sought. This is due to the inversion of the images at I. . . . , and could be avoided by an auxiliary system of lenses which would correct the images and, incidentally, make a larger field available.

The simplest way to see how such resolution is obtained is to note that, if n^2 individual beams concur in phase at the centre of the combined image formed in the focal plane of S, the intensity at this point will be n^4 that at the centre of the image formed by any one of the beams singly. This indicates in a general way a reduction of the diameter of the combined image to $1/n$ that of a single image, and we have a mere problem of geometrical optics—to arrange the lenses K so that, with respect to any star not far from the axis, the n^2 corresponding plane wave-fronts proceeding from K should be coplanar.

From the fact that for any given wave-length and star, with a disturbed atmosphere, the diameter of the image will tend to vary inversely as the average resultant amplitude at its centre, it can easily be seen that for a very large equivalent aperture atmospheric conditions may occur in which a far higher degree of resolution will be obtained with long than short wave-lengths. For the n^2 beams of a long wave-length may have less than a quarter-phase difference between any two of them or parts of them at this point, while, at the same time, we may have to reckon with many full half-phase differences in the short waves.

It is possible that the superior detail in photographs of Mars with long wave-lengths may be partially due to this cause, and it is quite conceivable that under the best conditions at such a site as Mount Wilson the full theoretical resolution might be attained in the infra-red for the largest instrument of the kind which was mechanically feasible; while under the better conditions which one might expect at, say, latitude 10° or 15° such occasions might be common, and the full resolution attainable also, from time to time, in the short wave-lengths. The suggested instrument, designed for the full resolution, which one might perhaps call a *synthescope* (from the synthesized image) might thus prove more widely useful than the writer was at first inclined to think

* "A Design for a very large Telescope," Phil. Mag., August 1930.

likely. Since the component mirrors are all of manageable size, it might be practicable to construct it entirely of aluminium, the mirrors, made of aluminium, being silvered in a vacuum chamber. If a mirror-surface of silver were coated with a layer a few atoms thick of gold or platinum it would probably enjoy the latter's immunity from tarnishing, while affording the full reflecting power of silver—important considerations in the present case, owing to the numerous reflexions and the inconvenience of dismantling the instrument for resilvering.

LXXX. *The Starting Potentials of the Corona Discharge in Neon.* *By* F. M. Penning, *D.Sc., Natuurkundig Laboratorium der N. V. Philips' Gloeilampenfabrieken, Eindhoven, Holland* *.

1. *Introduction.*

THE corona discharge in helium and neon has been studied by L. G. H. Huxley[1]. He used a cylinder of 4·6 cm. and a wire of 0·165 or 0·2 cm. diameter, and found that for gas-pressures of 10 mm. and higher the starting potential for the positive discharge (wire positive) was lower than for the negative (wire negative). From this result he concluded that in this case the current could not be maintained by the liberation of electrons from the cathode. In a letter to the Editors[2] I suggested that this abnormal behaviour of the starting potentials should be ascribed to impurities in the neon used by Huxley. I had found that for pure neon the starting potential for the positive discharge was the higher, but that it could be made the lower by adding a small amount of argon. In his reply[3] to my letter Dr. Huxley suggested that, on the contrary, the neon used in my experiments should not have been pure. Under these circumstances it seems desirable to describe my experiments more fully, the more so as they have been repeated in the meantime with a better apparatus. The design of this apparatus was similar to that of Huxley; however, it had the advantage that the iron could be heated and degassed by high-frequency currents. Since the decrease of the starting potential of neon by small traces of impurities can be explained by the theory of ionization by metastable atoms, we will first give a short review of this theory.

* Communicated by the Author.

2. *Ionization by Metastable Atoms.*

Already, many years ago, Holst and Oosterhuis had concluded from non-published measurements that the starting potential of neon was decreased by addition of another gas, whose ionization potential was smaller than the excitation potential of neon (*e.g.*, 0·5—5 per cent. argon)[4]. In 1927 this phenomenon was studied more closely[1], and it was found that already very small quantities of admixtures produced this effect. For instance, in a tube with parallel plate electrodes at 1 cm. distance filled with 21 mm. neon the starting potential V_s was reduced from 410 v. to 330 v. by adding 0·0001 per cent. mercury vapour. The number of collisions of electrons with mercury atoms can be estimated in this case by means of a formula given by G. Hertz[5]. This number is far too small to produce such a considerable decrease of V_s. However, the mercury atoms can be ionized by metastable neon atoms. Especially for values of pd larger than those for which V_s is a minimum the electrons moving in the neon will not only *ionize* these neon atoms but also partly *excite* them. In this way metastable atoms are formed which have a rather long lifetime. The measurements of Dorgelo and Washington[6] show that in pure neon these metastable atoms can be destroyed in two ways—by collisions against the walls and by collisions in the gas. At high pressures, such as 20 mm., only the last way has to be considered. In pure neon[7] about 1 in 100,000 collisions with neon atoms will lead to destruction. Consequently the probability that a metastable atom collides with a mercury atom is already considerable with a mercury admixture of 1 : 1,000,000. Since the energy of a metastable neon atom expressed in volts is $V_{met.} = 16{\cdot}6$ v., it is sufficient for the ionization of a mercury atom (ionization potential $V_i = 10{\cdot}4$ v.). When we suppose that this process has a great probability the decrease of the starting potential can be satisfactorily explained.

Similar processes were already found by Franck and Cario in their work on "sensitized fluorescence." These experiments showed that metastable mercury atoms can *excite*[8] atoms of Tl and other metals. Formerly Franck had already drawn attention to the possibility of *ionization* by excited atoms[9].

The following control-experiments confirm the assumption that the decrease of the starting potential is due to ionization by metastable atoms :—

(*a*) For this process to occur we must have

$$V_i' < V_{met.}; \quad . \quad . \quad . \quad . \quad . \quad . \quad . \quad (1)$$

however, it cannot occur when

$$V_{met.} < V_i' < V_i \quad . \quad . \quad . \quad . \quad . \quad . \quad . \quad (2)$$

(the letters with accents relate to the admixture, those without accents to the main gas). In fact measurements with argon [10] proved that the decrease of V_s by small traces of admixtures only took place when condition (1) was satisfied.

(*b*) The effect was also studied in a series of measurements on the ionization by electrons in a homogeneous field, using Townsend's method. Following this method, photoelectrons were emitted from a plate, and the variation of the current for constant field-strength X with the variation of plate distance was measured [11]. It was proved that, *e.g.* with $\frac{X}{p} = 3{\cdot}8$ v./cm. × mm., no perceptible ionization did occur in pure neon. With 0·01 per cent. Ar, however, the electron current increased considerably with the electrode distance Although in this way the influence of the metastable atoms is not proved directly, it is nevertheless quite evident that the amount of ionization is increased markedly by a small quantity of an admixture.

(*c*) If the decrease of the starting potential must be ascribed to the presence of metastable atoms, it follows that the starting potential will again increase when their number is diminished. This diminution can be produced by adding a third gas or by irradiating with neon light. The first case was realized by adding H_2 or N_2 to a mixture of Ar and Hg. The molecules of the former gases destroy the metastable argon atoms [12], however, without being ionized themselves. Indeed, it was possible to increase the starting potential in this way [13]. For instance, with Ar–Hg at 20° C. ($pd = 24$ mm. × cm.) V_s was 220 v. ; 1 per cent. N_2 increased V_s to 520 v. On the other side the addition of 1 per cent. N_2 to pure Ar had only a slight effect on the starting potential.

(*d*) The number of metastable atoms can also be diminished by irradiation with light emitted by the same gas. Fig. 1 shows the processes to be considered for a Ne–Ar mixture. For the sake of simplicity only the two most important $1s$-levels ($1s_4$ and the metastable $1s_5$) are given, while the tenfold $2p$-level is represented by one line. Transitions giving rise

to radiation are represented by drawn lines, radiationless transitions by dotted lines. When the discharge-tube is not irradiated the metastable states can be destroyed in two ways : first by collision with a neon atom they can be brought into the $1s_4$-state [12], from which they return to the normal level with emission of the resonance line 736 Å [14]; secondly they can ionize an argon atom. When the discharge-tube is irradiated by intensive light from a neon column the metastable atoms can be raised by this light to the $2p$-states, and from there return, at least partly, *via* the $1s_4$-level into the normal state. The result of this irradiation therefore

Fig. 1.

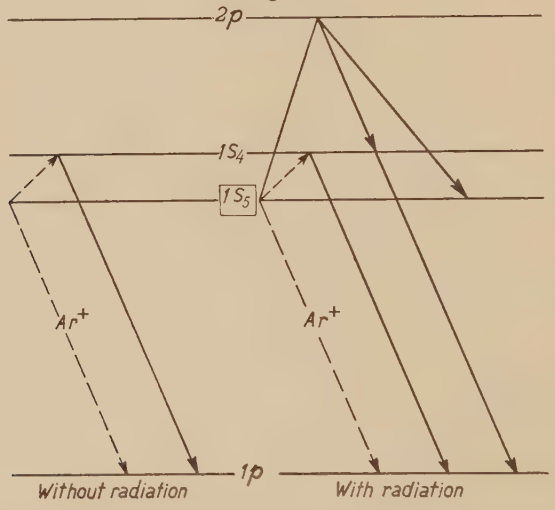

is that fewer argon atoms are ionized and that the starting potential increases. Indeed, this conclusion was confirmed experimentally [15]. The effect reaches high values with large light intensities ; not yet published measurements showed that under suitable conditions the starting potential of a Ne–Ar mixture could be increased by irradiation with neon light from 550 v. up to 900 v. It is difficult to see how this irradiation could cause such a large increase if the ionization were not due to metastable atoms.

These last experiments give a very sensitive means to control the purity of the neon. With the exception of helium almost all other gases have ionization potentials which are smaller than $V_{met.}$ for neon (16·6 v.), which explains why all admixtures examined up till now gave a

large decrease of V_s. Thus, with neon at not too high pressures (< 100 mm.), containing small traces of impurities (0.0001–0·1 per cent.)[16], an increase of V_s must result from irradiation with neon light; when in these circumstances no or hardly any increase occurs, we may conclude that the neon used is very pure. This method is of importance because it is very difficult to detect admixtures of, *e. g.*, 0·0001 per cent. by spectroscopic means. This method was applied in the experiments described hereafter.

3. *Description of Apparatus.*

The apparatus used is shown in fig. 2. One electrode consists of a Ni-wire E of 0·175 cm. diameter, mounted in the axis of three iron cylinders D, 0·1 cm. thick and 4·6 cm. wide. The current to the middle cylinder is measured, the other two cylinders serving as guard-rings. E is kept in place by a quartz tube A with three side-tubes. By means of tungsten wire the cylinders are fastened to the quartz tubes B, as shown in the figure. These quartz tubes are put around chromium iron rods C, which end at F in cylinders sealed to the glass of the tube. In addition each of the cylinders D is welded to one of the chromium iron rods. The leads of the cylinders are sealed into the glass at H and insulated by long quartz tubes G. The parts of the nickel wire E which project out of the cylinder are also screened off by glass or quartz.

A side tube I contains two parallel iron plates for the purification of the gas by means of a glow discharge. During this discharge a glass ring J is put around these electrodes to collect the sputtered metal. Fig. 2 shows the position of the ring during the measurement of the starting potential between the plates. In this way sparking between one of the plates and a conducting layer on the glass wall is prevented.

Further, the apparatus has ten side-tubes, provided with small glass bulbs, which can be shattered by a small iron ball. The upper tubes M (six in number) serve to seal the apparatus to the vacuum and filling system; after evacuation of the connecting tubes the glass bulb is shattered and the pressure can be lowered or the tube refilled. The lower tubes K (four in number) serve to admit small quantities of argon.

The apparatus was evacuated at 400° C.; after this the tubes K were filled with the desired quantity of argon, and shut off at L by a constriction of the tube. Then the

Fig. 2.

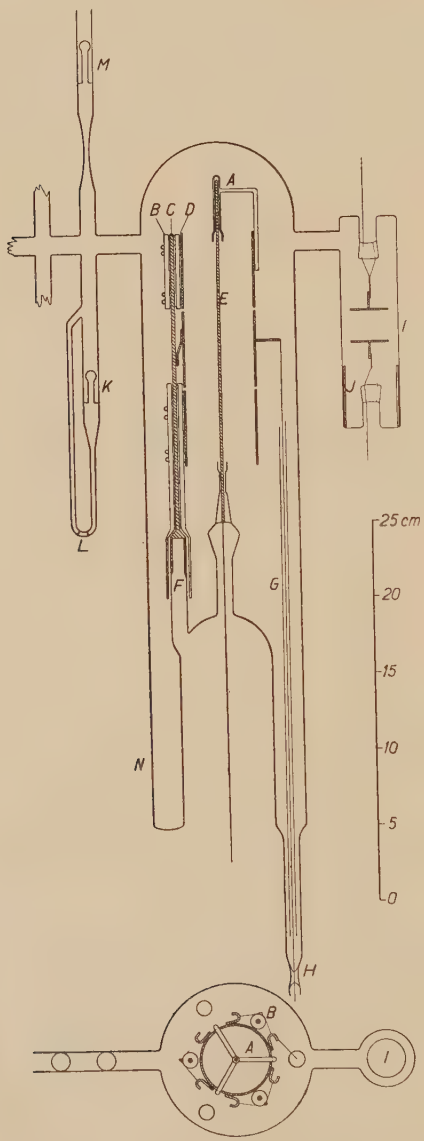

cylinders and the iron plates in I were heated for a long time by means of high frequency currents. The nickel wire E

was heated by a glow discharge in neon, after which the gas was removed.

Now the apparatus was filled with 40 mm. Ne, which had been carefully purified beforehand by means of silica in liquid air. To reduce the amount of gas set free by the melting of the glass the sealing place was heated before the filling until the glass softened.

From the measurements with neon, discussed in Sect. 2, it was concluded that very small traces of admixtures greatly influence the starting potential. Now it was found in earlier experiments that small traces of impurities could be removed by a glow discharge between iron plates in which the cathode is sputtered. These plates had beforehand been outgassed in vacuum by high frequency currents. In this way about the same value for the starting potential was obtained as with neon, purified either by circulation over charcoal in liquid air or by the sputtering of magnesium[17]. Consequently in order to free the neon from the last traces of impurity a glow discharge of 20–30 milliamps. was maintained during several days between the iron plates in I. In this way the starting potential reached a high constant final value. However, this final value not only depends on the purity of the gas, but also on the condition of the cathode surface. The difference between the results given here and those of my former publication[18] must probably be ascribed to the fact that the cylindrical electrodes were made of other material and also treated differently.

After the complete purification of the neon one of the tubes, M (fig. 2), was sealed to the vacuum system over a cooler in liquid air and a tap, the former being nearer to the tube. Then the bulb in M was shattered and the pressure could be lowered at will. For the measurements with an argon admixture the glass bulb in one of the side-tubes K was broken before sealing on the tube M. When the lowest pressure had been attained the whole tube was evacuated and the part I was raised to a temperature of 400° C., then the iron cylinders and plates were again outgassed by means of high frequency currents. After this the tube could be filled with new neon for the next series.

4. *Method of the Measurements.*

The electrical connexions are given schematically in fig 3. The middle cylinder D_2 is connected to a galvanometer of great sensitivity ($6 \cdot 10^{-11}$ amp. per mm. at 1 m.), which could be short-circuited, and to a μ-amp. meter with shunts (not given in the fig.). In this way currents from 10^{-11} to 10^{-3} amp.

could be measured. The potential difference between cathode and anode could be read within 1v. on an electrostatic voltmeter V (Hartmann and Braun). Cathode and anode were interchanged by commutating the storage battery.

Fig. 3.

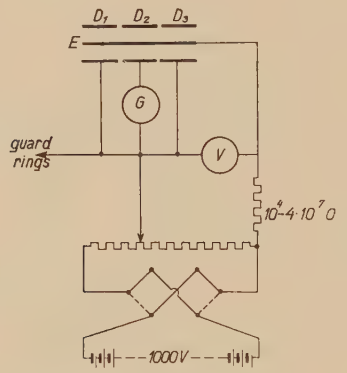

Fig. 4.

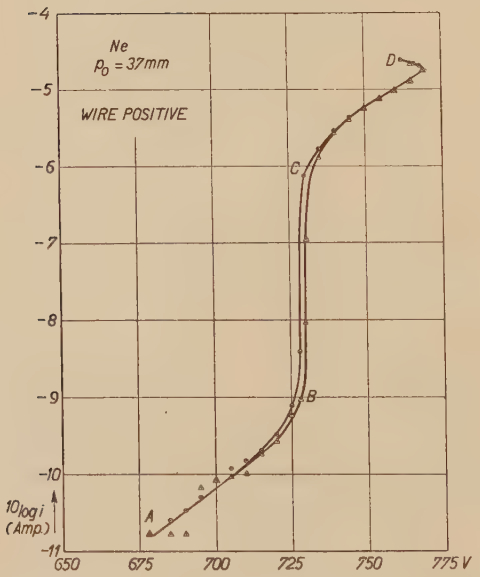

To avoid leakage currents the supports of the galvanometer and of the connecting wire were kept at the same potential as the galvanometer, and guard-rings were mounted at F (see fig. 2) and N on the glass wall.

Fig. 4 shows the increase of the current with the potential difference in pure neon (wire positive). The measurements were made with increasing current (circles) and with decreasing current (triangles). In the curve of fig. 3 three parts can be distinguished—AB, BC, and CD. In the part BC the current increases 1000-fold when the potential difference is increased by a few volts. The different theories show that the potential difference belonging to BC corresponds to the starting potential. In CD the potential difference first increases with increasing current and passes through a maximum. This is due to space charges, which alter the electric field distribution, first making it less favourable [19], and afterwards more favourable for ionization. Only a few points could be measured after passing the maximum in the potential difference, because the discharge became intermittent.

The part AB of the characteristic was not found with the wire negative ; *e. g.*, with the same gas pressure as in fig. 4 and with 530 v. the current was still $< 10^{-11}$ amp., while the maximum potential difference reached was 540 v.

The interpretation of the currents below 10^{-9} amp. requires a more detailed study. They cannot be due to leakage ; this follows not only from the position of the electrodes, but also from the exponential increase of the current. The following details may still be mentioned. A strong illumination of the cathode or an irradiation with a weak radioactive substance did not influence the intensity of the currents in AB. With pure neon at a pressure of 49 mm. BCD remained about the same in different runs, but AB varied considerably ; the potential range, in which the current increased from 10^{-11} up to 10^{-9} amp., varied between 40 and 140 v. ! Addition of argon decreased this interval ; in pure argon it was at maximum a few volts.

5. *Results.*

Six series of measurements were carried out with neon ; in each of them the starting potential was determined as a function of the pressure. The gas fillings were :

I. Pure neon.
II. Neon + 0·00015 per cent. Ar.
III. „ + 0·00030 „
IV. „ + 0·00088 „
V. „ + 0·0020 „
VI. Pure neon.

The results are given in figs. 5, 6, and 7. As abscissa is plotted p_0, the value which the pressure would have when the apparatus was brought to 0° C. This quantity has been

Fig. 5.

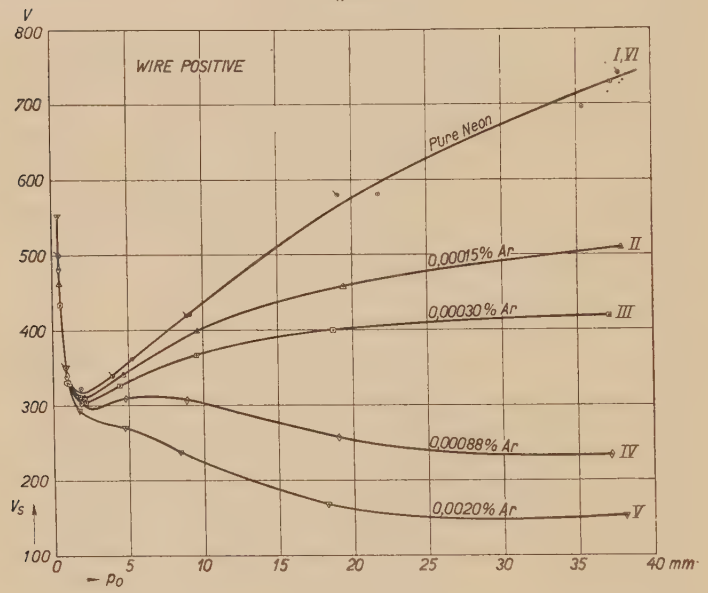

Fig. 6.

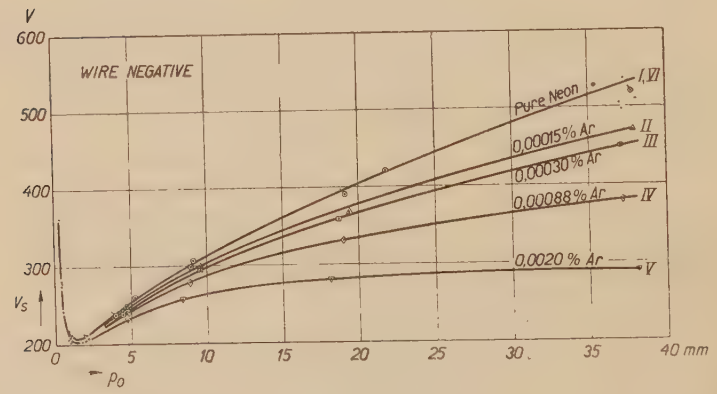

chosen because the electrical properties of a gas do not depend on the *pressure* but on the *density*; p_0 gives the density when that at 1 mm. pressure and 0° C. is taken as unity. V_S is the starting potential, defined as explained in Sect. 4.

The results of the Series I. and VI. are denoted by circles and dashed circles respectively. The values of V_S obtained for pure neon (p_0=37 mm.) in the Series II.–V., before opening the capillary containing the argon, are indicated by dots. The figures show that all measurements for pure neon coincide rather well, the greatest deviation from the average being 2 per cent. with the wire positive and 4 per cent. with the wire negative.

Some of the measurements for the parallel plates with and without irradiation have been plotted in fig. 7. A tube of about 1 cm. diameter wound into a helix and filled with

Fig. 7.

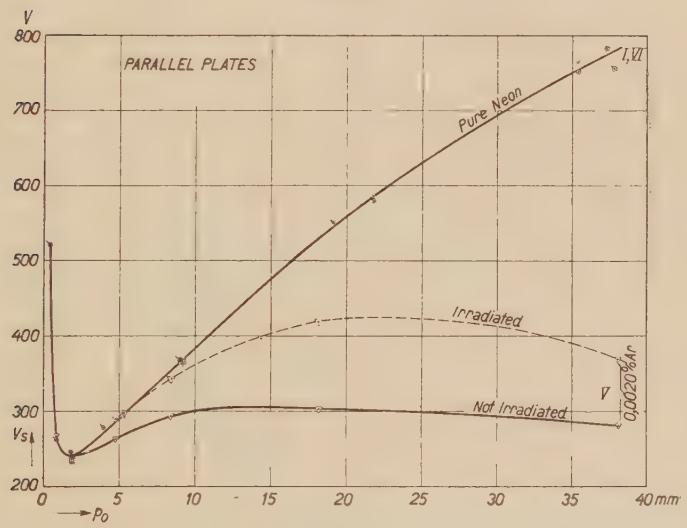

10 mm. Ne was put around the tube I. of fig. 2[20]. A current of 200 milliamps., giving a positive column, was led through the first tube in order to irradiate I. The tube was cooled by means of a strong air-current. With pure neon the increase of the starting potential at the highest pressure (p_0=37 mm.) was only 1 volt, with Series V., however, it reached a value of about 90 volts. This proves, as was shown in Sect. 2, that in the first case the neon was indeed very pure. With increasing p_0 the curve of Series V. shows a maximum after the first minimum. This is confirmed by other measurements, which will be published elsewhere; with still higher values of p_0 a second minimum of V_S is reached, after which the curve rises continuously. This

behaviour can also be explained by the theory of ionization by metastable atoms.

Finally, fig. 8 shows the variation of the starting potential for the different cases at a pressure $p_0 = 37$ mm. as a function of the added quantity of argon. This influence proves to be much greater with the positive than with the negative discharge.

Fig. 8.

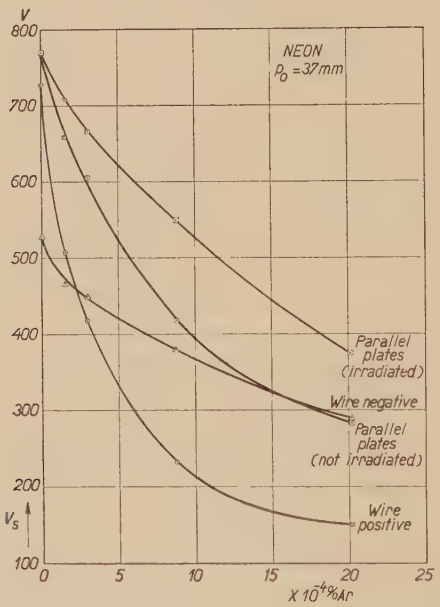

6. *Comparison of the Results with those of Huxley.*

In his answer to my letter (see Sect. 1) Huxley suggested that the neon used by me was purified *after* it had been put into the apparatus. This, however, was not the case; *the last small traces* of impurity only (perhaps 0·001 per cent.) were removed by a glow discharge between outgassed iron plates, former experiments proving that this method was very effective (see Sect. 3). The iron plates had been heated beforehand in vacuum to bright red; with the small currents (20–30 milliamps.) used no gas was set free from these electrodes. Huxley mentions that in his experiments the neon became impure when large currents passed between cylinder and wire; this, however, is easily understood, as these metal parts had not been glowed in vacuum.

With the exception of the mentioned admixture of helium the neon used by me was spectroscopically pure. Since, however, small traces of impurity already greatly influence the electrical properties, the starting potential is a much better criterion for the purity. This has also been pointed out by Townsend and MacCallum [21]. With neon the determination of the increase in starting potential by irradiation is still more effective. This method shows that in the above described experiments the neon was very pure (see Sect. 2).

Huxley remarks that a continuous background in the spectrum of neon is an indication for the presence of impurities. Several years ago the author found that a column with small current density gave in argon of high pressure a continuous spectrum ; this result was corroborated by Dorgelo and Washington [22]. Later this continuous spectrum was also found in neon. It was studied more closely in a tube of 10 cm. diameter and 12 cm. distance of the plane electrodes. With a current of some milliamps., this tube gave a column in which, besides the neon lines, a continuous spectrum occurred. By adding 0·0004 per cent. Ar this column, however, disappeared. Huxley stated that a continuous background of the spectrum could be made to disappear by means of a high frequency discharge ; our own experiment just mentioned shows that this fact cannot be taken as proving that the gas becomes purer.

Another argument of Huxley's is that his measurements could be very easily reproduced. This, however, does not prove that the gas was pure. Fig. 8 shows that the curve for wire positive has a minimum for a certain degree of impurity ; thus, near this minimum a small increase or decrease of the impurity does not influence the starting potential. The potential corresponding to this minimum (ca. 150 v.), proves to be about the same as the value found by Huxley at this neon pressure. A similar minimum was already found earlier [23] in Ne–Ar mixtures with parallel plates and $pd = 20$ mm. × cm. ; in that case the starting potential varied only 16 volts, when the Ar admixture changed from 0·04 to 1 per cent. At higher values of pd, such as used in the present experiments, the minimum is found for a smaller percentage of admixture. With He the same phenomenon occurs; the values of the starting potentials of Gill and Pidduck [24] are very well reproducible, although it is known at present that they relate to impure gas. More recent measurements of Townsend and MacCallum [25] and of Levi [26] have, indeed, shown that the values for pure He are much higher. Levi has pointed out that he values for pure

He are much more difficult to reproduce than those for impure gas.

The suggestion of Huxley that the neon used by me was impure is, apart from all the preceding arguments, very improbable. This may be seen from the following table, giving the starting potential with the wire positive and 40 mm. pressure. The neon used by Huxley is indicated by Ne(Hu), that used by the author by Ne(Pe):

Ne(Pe)	730 v.
Ne(Pe) + 0·00015 per cent. Ar.	510 v.
Ne(Pe) + 0·0020 per cent. Ar.	150 v.
Ne(Hu)	150 v.

If Ne(Hu) were pure neon we should have the remarkable case that first the starting potential of neon would rise to 730 v. by addition of impurity, then would decrease to 510 v. by further addition of $1\frac{1}{2}$ millionth of argon, and would reach again the value for "pure" neon at 0·0020 per cent. Ar.

It is possible that Huxley's results are due to the fact that his neon was contaminated by grease-vapour. It follows from his fig. 2 that there was a greased tap between his apparatus and the coolers in liquid air. In my experiments the usual procedure was followed: the cooler was connected immediately with the tube.

It may be remarked, further, that when my measurements are right the great difference in behaviour between Ne and other gases disappears. With nitrogen [27], for instance, the whole curve for the positive discharge lies above that for the negative; with hydrogen [28] this is the case for pressures >1 mm. For both gases Huxley's apparatus was used. According to my own measurements the relative position of the two curves is the same as in nitrogen and hydrogen not only for pure neon but also for pure helium and pure argon (see Sect. 8).

Finally, it may be remarked that my measurements agree with the general experience that the starting potential in slightly impure Ne or He increases with the purity of the gas [29].

7. *Discussion.*

(a) *Pure Neon.*

When the positive ions do not ionize in the gas, but liberate electrons from the cathode [30], the condition for sparking between parallel plates is according to Townsend [31],

$$1-\gamma(e^{\alpha S}-1)=0, \quad . \quad . \quad . \quad . \quad . \quad (1)$$

where S = the distance between the plates, γ = the number of electrons set free per positive ion from the cathode, α = the average number of ionizations per electron per cm. in the direction of the electric field. $\frac{\alpha}{p}$ is a function of $\frac{X}{p}$ (field strength : pressure). For cylindrical electrodes $\frac{X}{p}$ is not constant; according to Huxley [32] the expression $e^{\alpha S}$ in (1) must in this case be replaced by $e^{\int_0^S \alpha dx}$. In this way we get the following conditions :—

$$\text{(I.) wire positive } 1-\gamma_c\left(e^{\int_{r_1}^{r_2}\alpha dx}-1\right)=0, \quad . \quad (2)$$

$$\text{(II.) wire negative } 1-\gamma_w\left(e^{\int_{r_1}^{r_2}\alpha dx}-1\right)=0, \quad . \quad (3)$$

r_1 = radius wire, r_2 = radius cylinder, $\gamma_w = \gamma$ for the wire, $\gamma_c = \gamma$ for the cylinder.

Now, according to Huxley the starting potential with neon for $p > 10$ mm. is lower in case I. than in case II., also the corresponding values of a. Consequently, γ_c for case I. should be greater than γ_w for case II. Since it is very improbable that γ increases with decreasing field-strength, Huxley discards the hypothesis that in this case the positive ions liberate the electrons from the cathode.

According to my measurements the starting potential *in pure neon* is always higher for the positive than for the negative discharge, so that Huxley's objection does not hold for pure neon, and γ_c for case I. must be smaller than γ_w for case II. It seems natural to ascribe this to a difference in ion velocity, but this velocity is probably for both cases so small that it practically does not influence the value of γ. It was found [33] that an argon ion colliding with a neutral argon atom has a large probability to transfer its charge, the neutralized particle retaining practically the whole of the kinetic energy and giving only a very small fraction of it to the new ion. It is quite probable that the same phenomenon occurs in neon, and therefore the average ion velocity is very small for this high pressure. This, however, is no objection to the liberation of electrons. Various direct measurements in vacuum make it very probable that for neon ions with zero velocity the value of γ is still a few per cent. [34].

In the above formulæ (1), (2), and (3) this experimental value for γ can only be used when the liberated electrons

leave the metal with zero velocity. In reality this is not the case[35], and thus part of the liberated electrons will go back to the cathode[36]. Therefore γ, used in formulæ (1)–(3), must be defined as the number of electrons set free per positive ion, and not diffusing back to the cathode. The value of γ thus defined increases with $\frac{X}{p}$; so $\gamma_c < \gamma_w$. This explains why the curve for case II. with pure neon lies below that for case I.

(b) *Impure Neon.*

When we add argon to the neon the sparking potential in both directions will be lowered. This is due to the ionization by metastable atoms, considered in Sect. 2. The reason that the decrease is so much larger for the positive than for the negative discharge must still be studied more closely. There are, however, two reasons why for this case the formulæ (2) and (3) cannot be applied.

In the first place the ions moving towards the cathode in an Ar–Ne mixture are partly argon ions. When these argon ions collide with *great velocity* with neon atoms they lose considerably less energy than at collisions with argon atoms. For *small velocities* the collisions will probably approach the collisions between elastic spheres. So it is possible that the argon ions strike the cylinder in the positive discharge with a greater velocity than in the negative. In this way γ for Ne–Ar can exceed the value for pure neon[37].

In the second place we have implied in the formula that the ionization occurs in that place where the electron collides with the atom. In a neon argon mixture this is not necessarily true ; the electron forms a metastable atom, and the latter can move over a certain distance before ionizing an argon atom. By the diffusion of resonance radiation this distance can be considerably increased at high pressure. Langmuir and Found[38] have shown recently that in this way metastable atoms were formed at a pressure of some mm. at a distance of 20–30 cm. from the place where the atoms were excited. Consequently most of the electrons formed by metastable atoms in the positive discharge will on the average pass through a larger potential difference than if they were formed by direct collisions of the electrons. In this way the ionization increases and the starting potential for the positive discharge will decrease. For the negative discharge the reverse is true.

It is difficult to estimate quantitatively how much these effects influence the starting potential; at any rate the formulæ (2) and (3) cannot be applied without modification. It is clear, however, that both effects influence the difference in the starting potential for the positive and the negative discharge in the right way.

Fig. 9.

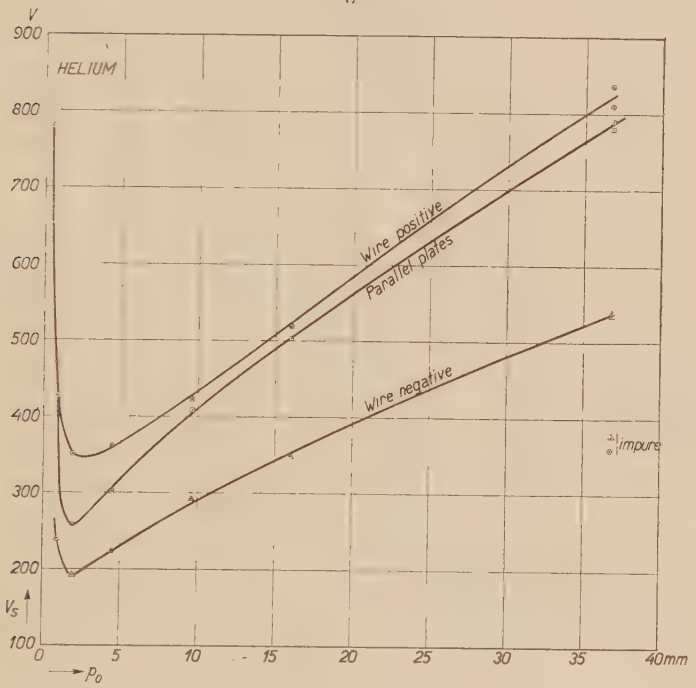

(c) *Striations.*

One of the arguments advanced by Holst and Oosterhuis in favour of their theory was the occurring of a striated discharge between parallel plates at very small current intensities. Immediately before the cathode lies an absolutely dark layer, followed by several light and dark layers. This proves that the electrons originate at the surface of the cathode, and not in the bulk of the gas. These layers also occur in the corona discharges studied here (wire positive) in pure neon as well as in the neon argon-mixtures; they are the most clear at a pressure of ca. 20 mm. This circumstance, too, is a strong argument for the assumption

that in all these cases the electrons are liberated from the cathode.

8. *Measurements with Helium and Argon.*

Preliminary measurements were also carried out for helium (see fig. 9) with the same apparatus. This helium contained some neon (less than 1 per cent.); V_i for neon being larger than $V_{met.}$ for helium the phenomenon described in Sect. 2 does not occur here, and therefore it is not likely that this neon admixture has much influence on the starting potential. Here, just as in pure neon, the curve for the positive discharge

Fig. 10.

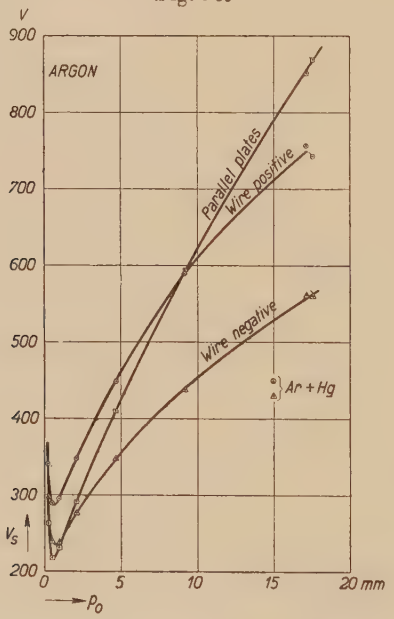

lies above that for the negative. In one series of measurements the helium was purposely made impure by heating the iron plates by means of high frequency currents. The values found for this impure helium were analogous to those of Huxley (see fig. 9); here again the starting potential for the positive discharge was below that for the negative.

Finally, similar results were also obtained for argon (fig. 10) With argon as the main gas most of the other gases do not satisfy the relation $V_i' < V_{met.}$, so that small quantities of these do not decrease the starting potential. For mercury vapour as impurity $V_i' < V_{met.}$, and, indeed, a drop of mercury

introduced into the tube decreased the starting potential, the decrease being again larger for the positive than for the negative discharge.

These measurements, too, confirm the considerations of Sect. 6.

9. *Summary.*

Experiments are described in which the starting potentials of a corona discharge between a wire and a cylinder are measured as a function of the pressure. The gases used were Ne, Ne with 0·00015 per cent., 0·00030 per cent., 0·00088 per cent., and 0·0020 per cent. Ar. The purity of the Ne was tested by measuring the starting potential between two parallel plates with and without irradiation from a neon column. With the pure gas, contrary to the results of Huxley, the starting potential of the discharge with the wire positive (positive discharge) was found to be higher than that with the wire negative (negative discharge). By addition of small amounts of argon both starting potentials are decreased. This is a result of the ionization of argon atoms by metastable neon atoms. The starting potential of the positive discharge is decreased much more than that of the negative ; with a sufficient amount of impurity the first became even lower than the second. A possible explanation of this effect is suggested. Finally, some preliminary measurements with pure and impure He and with pure and impure Ar are described. The results are similar to those with neon.

In conclusion, the author wishes to express his thanks to Mr. J. Moubis for his help as well in the construction of the tubes as in the measurements.

References.

(1) L. G. H. Huxley, Phil. Mag. v. p. 721 (1928).
(2) F. M. Penning, Phil. Mag. vii. p. 632 (1929).
(3) L. G. H. Huxley, Phil. Mag. viii. p. 128 (1929).
(4) British Patent, 181, 691.
(5) G. Hertz, *Zs. f. Phys.* xxxii. p. 298 (1925) ; F. M. Penning, *Zs. f. Phys.* xl. p. 4 (1926) ; M. J. Druyvesteyn, *Zs. f. Phys.* lii. p. 197 (1928).
(6) H. B. Dorgelo and T. P. K. Washington, Proc. Amsterdam, xxx. p. 33 (1927).
(7) The neon used by me contained some helium (about 1 per cent.). Owing to its high ionization potential, however, it has hardly any influence on the electric properties of neon. In this paper by "pure neon" is meant neon with no other admixtures than helium.
(8) J. Franck und P. Jordan, 'Anregung von Quantensprüngen durch Stösse,' p. 227 (1926).
(9) *Idem*, p. 191.

(10) F. M. Penning, *Zs. f. Phys.* xlvi. p. 335, table 2 (1928).
(11) F. M. Penning and M. C. Teves, 'Physica,' ix. p. 97 (1929). Similar but more extensive measurements were made at about the same time by Townsend and MacCallum for pure Ne (Phil. Mag. vi. p. 857 (1928)).
(12) H. B. Dorgelo and T. P. K. Washington, *l. c.*
(13) F. M. Penning, 'Physica,' x. p. 47 (1930).
(14) G. Hertz, *Zs. f. Phys.* xxxii. p. 933 (1925).
(15) F. M. Penning, Proc. Amsterdam, xxxii. p. 341 (1929); 'Physica,' viii. p. 137 (1928); *Zs. f. Phys.* lvii. p. 723 (1929).
(16) F. M. Penning, *Zs. f. Phys.* lvii. p. 723, figs. 5 and 7 (1929).
(17) F. M. Penning, *Zs. f. Phys.* xlvi. p. 335 (1928).
(18) F. M. Penning, Phil. Mag. vii. p. 632 (1929).
(19) Compare, *e. g.*, J. S. Townsend, Phil. Mag. (6) xxviii. p. 83 (1914).
(20) See fig. 2 of article, *Zs. f. Phys.* lvii. p. 723 (1929).
(21) J. S. Townsend and S. P. MacCallum, Phil. Mag. vi. p. 857 (1928); see pp. 875 & 878.
(22) H. B. Dorgelo and T. P. K. Washington, *l. c.*
(23) F. M. Penning, *Zs. f. Phys.* xlvi. p. 335 (1928); see figs. 5 & 6.
(24) E. W. B. Gill and F. P. Pidduck, Phil. Mag. (6) xxiii. p. 837 (1912).
(25) J. S. Townsend and S. P. MacCallum, *l. c.* sect. 16.
(26) F. Levi, *Ann. der Phys.* vi. p. 409 (1930).
(27) L. G. H. Huxley, Phil. Mag. x. p. 185 (1930).
(28) J. H. Bruce, Phil. Mag. x. p. 476 (1930).
(29) J. S. Townsend and S. P. MacCallum, *l. c.*; F. Levi *l. c.*; F. M. Penning, *l. c.*
(30) G. Holst and E. Oosterhuis, Phil. Mag. xlvi. p. 1117 (1923).
(31) J. S. Townsend, 'Electricity in Gases,' p. 331.
(32) L. G. H. Huxley, Phil. Mag. v. p. 721 (1928).
(33) H. Kallmann and B. Rosen, *Zs. f. Phys.* lxi. p. 61 (1930); F. M. Penning and C. F. Veenemans, *Zs. f. Phys.* lxii. p. 746 (1930).
(34) F. M. Penning, Proc. Amsterdam, xxxi. p. 14 (1928); xxxiii. p. 841 (1930); 'Physica,' viii. p. 13 (1928).
(35) M. L. E. Oliphant, Proc. Roy. Soc. A, cxxvii. p. 373 (1930); W. Uyterhoeven and M. C. Harrington, Phys. Rev. xxxvi. p. 709 (1930).
(36) W. Harries and G. Hertz, *Zs. f. Phys.* xlvi. p. 177 (1927).
(37) See for further particulars F. M. Penning and C. F. Veenemans, *l. c.* Compare also J. S. Thompson, Phys. Rev. xxxv. p. 1196 (1930).
(38) I. Langmuir and C. G. Found, Phys. Rev. xxxvi. p. 604 (1930) (letter to the editor).

LXXXI. *A Note on Heisenberg's Relation.* *By* H. L. Brose, *M.A., D.Phil., and* E. H. Saayman, *M.A., B.Sc., University College, Nottingham* *.

IN the papers that have so far appeared on quantum mechanics the various methods of treatment used seem to us not to have allowed the foundations of the subject to appear sufficiently clearly. For example, in the first

* Communicated by the Authors.

paper by Heisenberg (*Zeitschr. f. Phys.* xxxiii. p. 879, 1925) Bohr's frequency condition is assumed and the way in which quantum problems may be attacked from the point of view of matrix mechanics is discussed generally. In the slightly later paper by Born and Jordan (*ibid.* xxxiv. p. 858, 1925) the energy law and Bohr's frequency condition are deduced on the basis of Heisenberg's relation from the mechanical equations. The Heisenberg relations are simply *assumed*. Several text-books on the subject adopt the same course. In particular, in the case of the oscillator the classical equations of mechanics are assumed and the coordinates p and q are interpreted as matrices. When the ordinary rule for the multiplication of matrices is then applied it is found that pq is no longer equal to qp (see, for example, Sommerfeld, 'Wave Mechanics,' p. 31, Engl. edn.). It is at this stage that the convention called Heisenberg's Commutation Law (an unfortunately chosen term, as actually the law expresses the extent to which the algebraic commutative law is disobeyed, or to use Born and Jordan's expression, the "Mass der Nichtvertauschbarkeit") is introduced in the form

$$pq - qp = \frac{h}{2\pi j}\delta$$

(Sommerfeld, *loc. cit.* p. 32, eqn. (5)). On the application of this product rule to the equations it is then found that the limits of the matrices have yet to be fixed. This question is, of course, not affected by Heisenberg's rule. So far as we have been able to judge from the available material the way in which the normalization is subsequently effected is rather unnecessarily forced. Our present treatment is intended to show that a general solution of the equations of motion for the oscillator can be derived directly by postulating only Bohr's frequency condition and by assuming the definition of matrix multiplication. The solution includes Heisenberg's solution as a special case, and is obtained without using his rule. It is easy to see that by substituting different values for α in (viii.) we get different matrices. Equation (viii.) is to be regarded as the general solution of the problem. The value $\alpha = \frac{1}{2}$ gives Heisenberg's solution as a special case.

It is to be observed that some writers assume the Heisenberg relation and then deduce Bohr's frequency condition. There seem to us to be some advantages in following the reverse process, that is, to assume the Bohr condition as empirically given and to obtain the normalization and

solution naturally by means of the matrix calculus. It is hoped to extend this method to the rotator. It has been pointed out to us that if it can be generalized it cannot be more complicated for any arbitrary H-operator.

Let p, q have the usual meanings and p_{ik}, q_{ik} be the corresponding quantities relating to a "transition" from ith to the kth state.

We start with Bohr's "frequency relation"

$$w_{ik} = \frac{2\pi}{h}(E_i - E_k), \quad \ldots\ldots \quad \text{(i.)}$$

where $w_{ik} = 2\pi\nu_{ik}$ and E_i, E_k the energy characteristics of the ith and kth states. Although these characteristics may not actually be equal to the energies in the various states, the equation (i.) nevertheless holds good for their differences.

By (i.) the radiation during a transition is monochromatic. We *assume* that the frequency of this radiation is also the frequency of the oscillator and write

$$q_{ik} = a_{ik}\epsilon^{jw_{ik}t}, \quad \ldots\ldots \quad \text{(ii.)}$$

where $j = \sqrt{-1}$ and a_{ik} is a complex quantity which embraces the amplitude of the vibration as well as the phase. We write

$$\left.\begin{aligned} a_{ik} &= |\, a_{ik} \,| \, \epsilon^{j\beta_{ik}}, \\ q_{ik} &= |\, q_{ik} \,| \, \epsilon^{j(\beta_{ik} + w_{ik}t)}. \end{aligned}\right\} \quad \ldots \quad \text{(iii.)}$$

By (i.) $w_{ki} = -w_{ik}$. We can make $\beta_{ki} = -\beta_{ik}$ if we postulate that $q_{ki} = q_{ik}^*$, the conjugate to q_{ik}, and it then *follows* that $a_{ki} = a_{ik}^*$. Thus our q's are represented by a Hermitean matrix, and likewise our p's, for, since $p = m\dot{q}$, by definition

$$\begin{aligned} p_{ki} &= mjw_{ki}\, q_{ki} \\ &= -mjw_{ik}\, q_{ik}^* \\ &= m\,\dot{q}_{ik}^* \\ &= p_{ik}^*. \end{aligned}$$

If the matrix $A = \{a_{ik}\}$ and the matrix $B = \{b_{ik}\}$ be multiplied together, then, by definition,

$$AB = \{\sum_l a_{il}\, b_{lk}\},$$

and so

$$AB - BA = \{\sum_l (a_{il}\, b_{lk} - b_{il}\, a_{lk})\}. \quad \ldots \quad \text{(iv.)}$$

Now for the Harmonic Oscillator we have

$$\ddot{q} + w_0^2 q = 0,$$

so that by (ii.) we have

$$(w_0^2 - w_{ik}^2) q_{ik} = 0.$$

$$\therefore \quad w_{ik} = \pm w_0 \quad \text{when} \quad q_{ik} \neq 0.$$

From (i.)

$$w_{ik} = \frac{2\pi}{h}(E_i - E_k) = \pm w_0,$$

and so the E's form an Arithmetical Progression with common difference $\frac{hw_0}{2\pi}$. We may therefore write

$$E_i = (i + \alpha)\frac{hw_0}{2\pi}, \quad \text{where} \quad 0 < \alpha < 1, \quad . \quad \text{(v.)}$$

so that

$$w_{ik} = (i - k)w_0 = \pm w_0, \quad . \quad . \quad . \quad . \quad . \quad . \quad . \quad \text{(vi.)}$$

and

$$k = i \mp 1, \quad \text{when} \quad w_{ik} = \pm w_0. \quad . \quad . \quad . \quad \text{(vii.)}$$

Thus a our q's are zero with the exception of those adjacent to the principal diagonal of the matrix. It easily follows that the same result holds for the p-matrix.

The energy equation for the oscillator is

$$H = \frac{1}{2m}(p^2 + m^2 w_0^2 q^2).$$

Here H, p, q are now matrices.

By definition

$$p^2 = \{\sum_l p_{il} p_{lk}\}.$$

Now p_{il} and p_{lk} are always zero unless $l = i \pm 1$ and $l = k \pm 1$, so that the term in brackets is always zero unless $k = i$ or $i \pm 2$.

$$(p^2)_{i,\,i-2} = p_{i,\,i-1} p_{i-1,\,i-2},$$

$$(p^2)_{i,\,i} = p_{i,\,i-1} p_{i-1,\,i} + p_{i,\,i+1} p_{i+1,\,i},$$

$$(p^2)_{i,\,i+2} = p_{i,\,i+1} p_{i+1,\,i+2}.$$

Similar results hold for q^2.

$$\therefore \quad H_{i,\,i\mp 2} = \frac{1}{2m}(p_{i,\,i\mp 1} p_{i\mp 1,\,i\mp 2} + m^2 w_0^2 q_{i,\,i\mp 1} q_{i\mp 1,\,i\mp 2})$$

$$= \frac{mw_0^2}{2}(-q_{i,\,i\mp 1} q_{i\mp 1,\,i\mp 2} + q_{i,\,i\mp 1} q_{i\mp 1,\,i\mp 2}) = 0.$$

$$\begin{aligned} H_{i,i} &= \frac{1}{2m}\{p_{i,i-1}p_{i-1,i}+p_{i,i+1}p_{i+1,i} \\ &\quad + m^2w_0^2(q_{i,i-1}q_{i-1,i}+q_{i,i+1}q_{i+1,i})\} \\ &= mw_0^2(|q_{i,i-1}|^2+|q_{i,i+1}|^2). \end{aligned}$$

$\therefore$ H is a diagonal matrix.

Now $H_{i,i}$ is essentially positive and non-zero. If we agree to call $q_{0,0}$ the first element in our q-matrix, so that $q_{0,-1}$ and $q_{-1,0}$ are zero, then $H_{0,0}$ is the first element in our H-matrix.

Now

$$H_{n,n} = mw_0^2(|q_{n,n-1}|^2+|q_{n+1\ n}|^2);$$

$$\begin{aligned} |q_{n+1,n}|^2 &= \frac{H_{n,n}-H_{n-1,n-1}}{mw_0^2}+|q_{n-1,n-2}|^2 \\ &= \frac{h}{2\pi mw_0}+|q_{n-1,n-2}|^2, \end{aligned}$$

since the H's differ by $\frac{hw_0}{2\pi}$.

Let $n=2r$, then

$$|q_{2r+1,2r}|^2 = \frac{rh}{2\pi mw_0}+|q_{1,0}|^2,$$

and for

$$n=2r+1,\ |q_{2r+2,2r+1}|^2 = \frac{(r+1)h}{2\pi mw_0}.$$

$$\therefore\ |q_{2r+1,2r}|^2-|q_{2r+2,2r+1}|^2 = -\frac{h}{2\pi mw_0}+|q_{1\ 0}|^2,$$

and

$$\begin{aligned} |q_{2r+1,2r}|^2+|q_{2r+2,2r+1}|^2 &= \frac{(2r+1)h}{2\pi mw_0}+|q_{1,0}|^2 \\ &= \frac{H_{2r+1,2r+1}}{mw_0^2} \\ &= \frac{(2r+1+\alpha)h}{2\pi mw_0} \text{ by (v.).} \end{aligned}$$

$$\therefore \quad \left.\begin{aligned} |q_{1,0}|^2 &= \frac{\alpha h}{2\pi mw_0} \\ |q_{2r+1,2r}|^2 &= \frac{(r+\alpha)h}{2\pi mw_0} \\ |q_{2r+2,2r+1}|^2 &= \frac{(r+1)h}{2\pi mw_0} \end{aligned}\right\} \quad \ldots \quad \text{(viii.)}$$

If we now set $\alpha = \frac{1}{2}$ in (v.) and (viii.) we get

$$H_{n,n} = \left(n + \frac{1}{2}\right)\frac{hw_0}{2\pi}, \quad \ldots \quad \text{(ix.)}$$

and

$$q_{n+1,n}{}^2 = \frac{(n+1)h}{4\pi m w_0}. \quad \ldots \quad \text{(x.)}$$

We have therefore established the well-known results for the oscillator without appeal to Heisenberg's Commutation Rule. All these results follow quite naturally from the definition of matrix multiplication alone.

In (iv.) the matrix $AB - BA$ never vanishes unless

$$(\alpha) \quad a_{ik} = 0 \quad \text{for} \quad i \neq k,$$

and

$$(\beta) \quad a_{ii} = a_{kk}.$$

Thus the matrix vanishes only if A is a diagonal matrix in which the terms are all equal. Neither p nor q is such a matrix, and therefore, $pq - qp$ cannot be zero. By definition

$$pq - qp = \{\Sigma_i (p_{ii} q_{ik} - q_{ii} p_{ik})\}.$$

As before, the term in brackets vanishes always unless $k = i$ or $i \pm 2$.

$$(pq-qp)_{i,i\pm 2} = p_{i,i\pm 1} q_{i\pm 1,i\pm 2} - q_{i,i\pm 1} p_{i\pm 1,i\pm 2} = 0.$$

$$\begin{aligned}(pq-qp)_{i,i} &= p_{i,i-1} q_{i-1,i} - q_{i,i-1} p_{i-1,i} \\ &\quad + p_{i,i+1} q_{i+1,i} - q_{i,i+1} p_{i+1,i} \\ &= 2mjw_0 (q_{i,i-1}{}^2 - q_{i+1,i}{}^2) \\ &= -\frac{h}{4\pi m w_0} \cdot 2mjw_0 \quad \text{by (x.)} \\ &= \frac{h}{2\pi j}.\end{aligned}$$

$$\therefore \quad pq - qp = \frac{h}{2\pi j} \cdot \delta,$$

where δ is the unit matrix.

This is Heisenberg's Commutation Rule, according to which $pq - qp$ is a diagonal matrix whose terms are all equal to $\frac{h}{2\pi j}$. The rule has therefore been derived. But generally

$$(pq-qp)_{2r+1,2r+1} = \frac{(1-\alpha)h}{\pi j},$$

$$(pq-qp)_{2r,2r} = \frac{\alpha h}{\pi j}.$$

According to Heisenberg we ought to have

$$\frac{\alpha h}{\pi j} = \frac{(1-\alpha)h}{\pi j},$$

$$i.e., \quad \alpha = \tfrac{1}{2}.$$

Using the rule therefore amounts to setting $\alpha = \frac{1}{2}$, but it must be noted that (viii.) is the general solution when $\alpha \neq \frac{1}{2}$.

LXXXII. *A Note on Condensed Stars.* *By* Edmund C. Stoner, *Ph.D.*, *and* Frank Tyler, *B.Sc.**, *University of Leeds* †.

Introduction.

In stars of the white dwarf type the density is so great that most of the atoms must be completely ionized. The question arises as to whether there is any limit to the possible density of stars in which the "molecules" consist almost entirely of atomic nuclei and electrons. It follows from the Pauli exclusion principle, as embodied in the Fermi statistics, that an "electron gas," even at absolute zero, will have kinetic energy, the mean kinetic energy per electron increasing as the two-thirds power of the concentration. In a previous paper ‡ it was shown that if E_G is the gravitational energy of the idealized star, E_K the total electronic kinetic energy, n the number of electrons per unit volume, an equilibrium state will occur when

$$\frac{d}{dn}(E_G + E_K) = 0. \quad . \quad . \quad . \quad . \quad . \quad (1)$$

This leads to the conclusion that the limiting density would vary as the square of the mass of the star. In a second paper § a more detailed treatment was given in which the relativity change of mass of the electron with velocity was taken into account. The simple treatment was shown to be adequate for stars of small mass (less than half that of the sun), but for stars of greater mass the limiting density

* In receipt of a maintenance grant from the Department of Scientific and Industrial Research.

† Communicated by Prof. R. Whiddington, F.R.S.

‡ E. C. Stoner, Phil. Mag. vii. p. 63 (1929). (I.)

§ E. C. Stoner, Phil. Mag. ix. p. 944 (1930). (II.)

increased more rapidly. For stars of mass greater than 1·1 that of the sun gravitational kinetic equilibrium would not occur. A detailed discussion of the results was given with reference to the observational data on white dwarfs.

In both of these papers the star was idealized as a sphere of uniform density, though reference was made to the possible effect on the calculations of different assumptions as to the distribution of density. Attempts have been made to determine more precisely the kind of density distribution to be expected and to examine how far the previous results require modification. The problem has proved more intractable than was anticipated, and a completely satisfactory solution has not been reached. A short account is given here of the manner in which the problem has been approached and of the provisional conclusions. Some questions of cognate interest which have arisen in the course of the investigation are also briefly discussed. The note is to be regarded as a sequel or appendix to the two previous papers.

The Equilibrium Condition.

The equilibrium state has been found in I. and II. by the application of equation (1). When the non-relativistic treatment is adequate, however, the condition for equilibrium follows directly from the general theorem that for particles moving under the influence of inverse square law forces the potential energy is numerically equal to twice the kinetic energy*. For a condensed star the electrostatic energy may be neglected, and the equilibrium equation becomes simply

$$-\mathrm{E_G} = +2\mathrm{E_K}, \quad . \quad . \quad . \quad . \quad . \quad . \quad (2)$$

giving for the star of uniform density

$$\frac{3}{5}\mathrm{G}\frac{\mathrm{M}^2}{r} = 2\times\frac{3}{40}\left(\frac{3}{\pi}\right)^{2/3}\frac{h^2n^{2/3}}{m}\frac{\mathrm{M}}{2{\cdot}5m_{\mathrm{H}}},$$

or

$$n = 10^4\left(\frac{\pi}{3}\right)^5\frac{\mathrm{G}^3\mathrm{M}^2m_{\mathrm{H}}{}^4m^3}{h^6}, \quad . \quad . \quad . \quad . \quad (3)$$

as before.

With relativity mechanics equation (2) will no longer hold, except as an approximation for $\frac{v}{c}$ small†.

* See J. H. Jeans, 'Astronomy and Cosmogony,' p. 67.

† See A. Sommerfeld, 'Atombau und Spektrallinien,' p. 772.

It is of interest to note that, under the same restrictions, with E'_K as the kinetic energy per unit volume, the pressure is given by

$$P = \frac{2}{3}E'_K. \quad . \quad . \quad . \quad . \quad . \quad . \quad . \quad (4)$$

For any polytropic distribution of density the gravitational energy is given by*

$$E_G = -3\int P dv, \quad . \quad . \quad . \quad . \quad . \quad . \quad (5)$$

leading directly to equation (2).

Distribution of Density: Star as a Polytrope.

For a distribution of uniform electron density the total kinetic energy (see II., equation (2)) is

$$E_K = nV\bar{\epsilon} = nV\,\frac{3}{40}\left(\frac{3}{\pi}\right)^{2/3}\frac{h^2n^{2/3}}{m}. \quad . \quad . \quad (6)$$

If the star is not completely condensed it seems reasonable to take the expression

$$\frac{E_K}{V} = \frac{3}{40}\left(\frac{3}{\pi}\right)^{2/3}\frac{h^2}{m}n^{5/3}$$
$$= Cn^{5/3} \quad . \quad . \quad . \quad . \quad . \quad . \quad . \quad . \quad (7)$$

as giving the energy per unit volume, n being the concentration in the region considered. Since the pressure is proportional to E_K/V the distribution will then be polytropic, since

$$p = \kappa_1\rho^{5/3}. \quad . \quad . \quad . \quad . \quad . \quad . \quad . \quad (8)$$

This suggestion was made in II., where it was shown that this relation would hold for $\rho \ll 2{\cdot}4 \times 10^6$, while for $\rho \gg 2{\cdot}4 \times 10^6$ the relation would tend to

$$p = \kappa_2\rho^{4/3} \quad . \quad . \quad . \quad . \quad . \quad . \quad . \quad (9)$$

The density distribution in stars subject to

$$p = \kappa\rho^{\gamma} \quad . \quad . \quad . \quad . \quad . \quad . \quad . \quad (10)$$

has been worked out very completely by Emden†.

* See A. S. Eddington, 'The Internal Constitution of Stars,' p. 87.

† Emden, 'Gaskugeln' (Teubner, 1907). See Eddington, *l. c.* ch. iv. for a detailed account. For a somewhat simpler method of dealing with the polytropic equation, see F. Tyler, Proc. Leeds Phil. Soc. ii. p. 111 (1930).

For the gravitational energy of a polytropic star the general equation is

$$E_G = -\frac{3}{5-n'} G \frac{M^2}{r}, \quad . \quad . \quad . \quad . \quad . \quad (11)$$

where

$$n' = \frac{1}{\gamma - 1}.$$

For any given value of M the gravitational energy can therefore be readily obtained as a function of r.

For the $\gamma = 5/3$ polytrope the expression for the kinetic energy, on the above assumptions, becomes

$$E_K = \frac{3}{40}\left(\frac{3}{\pi}\right)^{2/3} \frac{h^2}{m} \int n^{5/3} dv. \quad . \quad . \quad . \quad . \quad (12)$$

Stars of Small Mass.—As long as the electron concentration is not too great the relation (8) will hold. The treatment given in II. shows that it can be applied as an approximation for stars of mass up to about half that of the sun ($M < \frac{1}{2}M_s$). Let ρ_0 be the central density. Emden's curves give (ρ/ρ_0) as a function of z for different values of γ, where z is proportional to R, the distance from the centre of the star. For the 5/3 polytrope ρ/ρ_0 becomes zero at $z = z_0 = 3{\cdot}657$, this corresponding to the radius r of the star. Let ρ be the mean density. For the 5/3 star the following relations hold :—

$$\frac{R}{r} = \frac{z}{z_0} = \frac{z}{3{\cdot}657}, \qquad \rho_0/\bar{\rho} = 6. \quad . \quad . \quad . \quad (13)$$

Taking the mean molecular weight as $2{\cdot}5m_H$, the integral in (12) can be written as

$$4\pi\left(\frac{1}{2{\cdot}5m_H}\right)^{5/3} \rho_0^{5/3} \int_0^r \left(\frac{\rho}{\rho_0}\right)^{5/3} R^2 dR.$$

Using the relations (13), and substituting M for $\frac{4}{3}\pi r^3\rho$, there results

$$E_K = \frac{3}{40}\left(\frac{3}{\pi}\right)^{2/3} \frac{h^2}{m} \frac{4\pi}{(2{\cdot}5m_H)^{5/3}} \frac{18M\rho_0^{2/3}}{4\pi(3{\cdot}657)^3} \int_0^{z_0} \left(\frac{\rho}{\rho_0}\right)^{5/3} z^2 dz. \quad (14)$$

The integral can be evaluated graphically with the aid of Emden's results. The value is 1·44. The final result may be written

$$E_K = C_1 M \rho_0^{2/3}, \quad . \quad . \quad . \quad . \quad . \quad . \quad (15)$$

where C_1 is a constant obtainable from the above equations involving h, m, m_H, and the value of the integral.

For the gravitational energy, using (11),

$$E_G = -\frac{6}{7} G \frac{M^2}{r}. \quad . \quad . \quad . \quad . \quad . \quad . \quad . \quad (16)$$

This can be written as

$$E_G = -\frac{6}{7} G \left(\frac{4\pi}{18}\right)^{1/3} M^{5/3} \rho_0^{1/3}$$

$$= -C_2 M^{5/3} \rho_0^{1/3}. \quad . \quad . \quad . \quad . \quad . \quad . \quad . \quad (17)$$

The equilibrium condition, (1) or (2), then gives

$$\rho_0 = \left(\frac{C_2}{2C_1}\right)^3 M^2. \quad . \quad . \quad . \quad . \quad . \quad . \quad (18)$$

Evaluation of the constants leads to the following results for the limiting central and mean densities :—

$$\left.\begin{aligned} \rho_0 &= 1{\cdot}279 \times 10^7 (M/M_s)^2, \\ \bar{\rho} &= 2{\cdot}132 \times 10^6 (M/M_s)^2. \end{aligned}\right\} \quad . \quad . \quad . \quad . \quad (19)$$

These are to be compared with the value for the limiting density for the star of uniform density (see II., equation (22) and note),

$$\rho = 3{\cdot}977 \times 10^6 (M/M_s)^2. \quad . \quad . \quad . \quad . \quad (20)$$

For a star of mass less than half of that of the sun, in which, on the assumptions made, the distribution of density is that of a 5/3 polytrope, the limiting central density is thus some four times as great, and the mean density about half as great, as that calculated for a sphere of uniform density. The results are shown graphically in the figure.

Stars of Greater Mass.—It was shown in II. that there was a critical value of n, which will be denoted by n_c, such that the relation (8) holds for $n \ll n_c$, and the relation (9) for $n \gg n_c$. The value of n_c is $5{\cdot}88 \times 10^{29}$, corresponding to $\rho_c = 2{\cdot}4 \times 10^6$. Assuming a polytropic density distribution, stars in the limiting state will certainly have central densities well above the critical value for $M > \frac{1}{2}M_s$ (this may be seen from the figure, where n_c is indicated, noting that log $\frac{1}{2}M_s = 33$). The determination of the density distribution in a star in which the exponent γ (in equation (10)) is variable, with the kind of variation indicated by equation 12 of II., presents a problem of an almost intractable type. An

attempt was made to obtain an approximate estimate of the equilibrium state for stars of mass somewhat greater than $\frac{1}{2}M_s$ by a graphical method. The density distribution was assumed to be that for a 5 3 polytrope. (This will be approximately true provided that the density is below the critical value for the greater part of the star.) For any

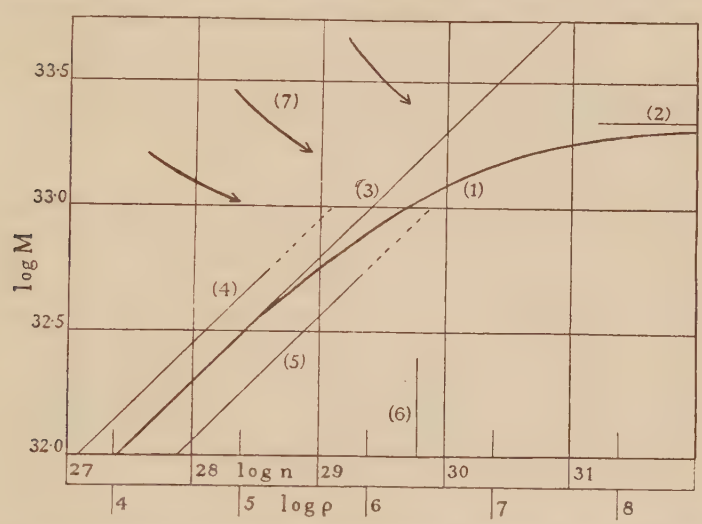

Variation of limiting electron concentration (n) and density (ρ) with mass (M) of a star.

$$\log \rho = \log n - 24 + \cdot 6180.$$

(1) Star as sphere of uniform density.

(2) Limiting mass for gravitational kinetic equilibrium.

$$M_0 = 2 \cdot 19 \times 10^{33}.$$

(3) Uniform density, neglecting relativity effect.

$$\log n = 2 \log M - 37 + \cdot 3798.$$

(4) Mean density and (5) central density for a polytropic distribution of density corresponding to $\gamma = 5/3$.

$$\log \bar{n} = 2 \log M - 37 + \cdot 1088.$$

$$\log n_0 = 2 \log M - 37 + \cdot 3798.$$

(6) Critical electron concentration.

$$n_c = 5 \cdot 88 \times 10^{29}.$$

(7) The arrows represent "directions" of evolution of stars.

given value of M, E_G could then be calculated as a function of r. E_K could be regarded as made up of two parts, one corresponding to the region in which the density varied from ρ_0 to ρ_c, and the other to the ρ_c to 0 region. The energy in the first part could be calculated from the expression

appropriate for high concentrations (see II., equation (12*a*)), and that in the second from the low concentration expression (12). E_K could then also be calculated as a function of r. Thus, for any given mass, E_K and E_G could be found for different values of r. By graphing the results the equilibrium value of r could readily be determined. The approximations involved in this method, however (particularly the assumption of a 5/3 density distribution and of a sudden transition at ρ_c), rendered the results of little value. In particular, it was not possible to extend the method in such a way as to draw any definite conclusion as to the way in which the value of the "limiting mass" was affected.

The general result of the treatment outlined in this section may be stated as follows:—If the star is incompletely condensed, so that elements of volume (large in themselves, but small in comparison with the volume of the star) may be treated as quasi-independent, the distribution of density in the star will be polytropic. For stars of mass less than half that of the sun the limiting mean density is about half that calculated for spheres of uniform density. For stars of somewhat greater mass the mean density will also be smaller, but no definite conclusion can be drawn as to the limiting mass.

For a completely condensed star, however, this method of treatment will not apply, as the elements of volume cannot be regarded as independent. This is discussed in the next section.

Distribution of Density and Equilibrium of completely Condensed Stars.

For a completely condensed star the kinetic energy of the electrons at absolute zero (the limiting state considered) will be determined by the total volume, V, of the star and the total number of electrons, N. Neglecting the relativity effect, the expression for the kinetic energy (the more general form of equation (6)) is

$$E_K = \frac{3}{40}\left(\frac{3}{\pi}\right)^{2/3}\frac{h^2}{m}\frac{N^{5/3}}{V^{2/3}}. \quad . \quad . \quad . \quad . \quad (21)$$

Thus the average kinetic energy per electron is proportional to $\bar{n}^{2/3}$, where $\bar{n}$ is the average concentration throughout the volume. The equation (21) may be written

$$E_K = \frac{3}{40}\left(\frac{3}{\pi}\right)^{2/3}\frac{h^2}{m}\frac{M}{2{\cdot}5m_H}\bar{n}^{2/3}$$
$$= \beta\bar{n}^{2/3}. \quad . \quad . \quad . \quad . \quad . \quad . \quad . \quad . \quad . \quad (22)$$

For the gravitational energy

$$E_G = \frac{3}{5-n'} G \frac{M^2}{r}$$

$$= \frac{3}{5-n'} G M^{5/3} \left(\frac{4}{3}\pi \times 2{\cdot}5 m_H\right)^{1/3} \bar{n}^{1/3}$$

$$= \frac{3}{5-n'} \cdot \frac{5}{3} \alpha \bar{n}^{1/3}. \quad . \quad . \quad . \quad . \quad . \quad . \quad . \quad . \quad . \quad (23)$$

In (22) and (23) α and β have the same significance as in I. For the equilibrium state

$$\bar{n} = \left(\frac{5}{5-n'}\right)^3 \left(\frac{\alpha}{2\beta}\right)^3. \quad . \quad . \quad . \quad . \quad . \quad (24)$$

$$= \left(\frac{5}{5-n'}\right)^3 n_u, \quad . \quad . \quad . \quad . \quad . \quad (24a)$$

where n_u is the concentration for a star of the same mass of uniform density.

Expressed in another way, the relation between the mass M and the mass M_u of a uniform density star (for which $n'=0$) for the same mean density is given by

$$\frac{M}{M_u} = \left(\frac{5-n'}{5}\right)^{3/2}. \quad . \quad . \quad . \quad . \quad . \quad . \quad (25)$$

If the density distribution is that of a 5/3 polytrope, for example, $n'=3/2$ and

$$M = (7/10)^{3/2} M_u$$

$$= {\cdot}586 M_u.$$

Distribution of Density.—The value of the effective n' is less (or of γ greater) the greater the concentration of mass towards the centre of the star (see Table IV. in II.). It becomes necessary to consider the distribution of density in a completely condensed star. The star is now regarded as a gigantic single molecule. The temperature is zero, but the kinetic energy of the electrons varies from zero up to a maximum. It seems reasonable to suppose that the distribution of electrons is such that the electrons of lowest energy are in the outer parts of the star and those of highest energy in the central parts. Under such conditions, even though there is no density gradient, there may be a pressure gradient, the pressure increasing towards the centre of the star; for at any given value of R the pressure will vary as the 2/3 power of the number of electrons external to the sphere of

radius R. In an equation of the type $p = \kappa\rho^{\gamma}$, therefore, the effective value of γ may become very large, so that the state will be approached in which the density is uniform throughout the star; the central concentration will certainly be less than for a 5/3 polytrope.

The indications are, therefore, that in a completely condensed star the equilibrium mass for the same mean density will be less than that for a star of uniform density—but only slightly less; the effective value of n' in equation (25) will approach zero. The argument given will apply to stars of any mass, so that it may be concluded that the equilibrium mass concentration curve will differ little from that shown in the figure (see p. 991) for stars of uniform density—the curve as a whole being somewhat lower and the "limiting mass" somewhat less.

Stars of Mass Greater than the "Limiting Mass."

The term "limiting mass" is used with reference to the particular type of equilibrium considered. For stars whose masses and mean densities correspond to points above the curve in the figure the decrease in gravitational energy on contraction is more than sufficient to maintain the star at absolute zero. On contraction the temperature of the star will increase. For stars of mass less than the limiting value, an equilibrium state will be reached. For stars of greater mass than this the factors considered in the present analysis impose no limit to the degree to which contraction, with increase of density, can proceed. Since contraction is accompanied by rise of temperature, however, radiation will occur, and the star will gradually lose mass. Thus, whatever the original mass of the star, the curve of the figure gives an approximate representation of the relation between mass and density of stars in their final "black dwarf" non-radiating state. The arrows in the figure are intended to give a rough indication of the "direction of evolution" of stars which this view suggests.

One further rather speculative point may be noted. When the electron concentrations become high, even though the temperature is zero, the maximum energy of the electrons also becomes high. Thus the maximum energies of the electrons for $n = 10^{30}$ and $n = 10^{33}$ are $2{\cdot}2 \times 10^{5}$ and $2{\cdot}2 \times 10^{7}$ volts respectively. With high concentrations of electrons with energies of this magnitude nuclear changes may be expected to become more frequent, and any accompanying radiation will result in loss of mass. Stars which reach a

quasi-equilibrium state corresponding to very high concentrations (greater than those in the figure) would therefore gradually lose mass, and reach a state corresponding approximately to a point on the part of the curve shown in the figure.

Summary.

As a sequel to two previous papers a number of points in connexion with condensed stars (of the white-dwarf type) are considered, the stars being idealized as composed of completely ionized atoms at absolute zero.

For stars of mass less than half that of the sun the equilibrium condition is given in a very simple form.

The distribution of density is considered. An incompletely condensed star of small mass (less than half that of the sun) may be treated as a polytrope, and precise calculations may be made. The mean density for such a star of given mass is about half that calculated for a star of uniform density.

For a completely condensed star the equilibrium mass for a given concentration will be less than that for a star of uniform density by an amount which is greater the greater the ratio of the central to the mean density. Reasons are given for concluding that the equilibrium mean density will differ little from that calculated for the uniform density star of the same mass.

For stars of mass greater than the equilibrium value for a given mean density contraction will result in increase of temperature, and so in loss of mass by radiation. Stars will tend to a final state approximately represented by a point on the equilibrium mass density curve, which is given in a figure.

Physics Department,
University of Leeds,
November 1930.

LXXXIII. *Theory of Dielectrics.*

To the Editors of the Philosophical Magazine.

Gentlemen,—

In a paper on the "Theory of Dielectrics," published in the 'Philosophical Magazine' for February 1931, Dr. G. Guében has deduced an expression for the conduction current in such materials of the form,

$$I_\infty = \frac{q\epsilon(u+v)Hl}{lx' + H(u+v)}.$$

Where

I = the final steady current,

ϵ = electronic charge,

u and v = ionic mobilities,

H = electric field,

l = thickness of dielectric,

and q and α' are constants in the law of recombination of ions,

$$\frac{dn}{dt} = q - \alpha' n.$$

In a series of papers on the conductivity of dielectrics (Phil. Mag. July 1916, Sept. 1917, and Oct. 1921) H. H. Poole has shown, however, that in general the conductivity of a dielectric when exposed to intense electric fields is given by the formula

$$\log K = A + BH,$$

where K is the conductivity and A and B constants. Subsequent work by H. Schiller and others has confirmed this result. It may easily be seen that these two expressions are incompatible, since from Dr. Guében's value of I we get

$$K = \frac{q\epsilon(u+v)l}{l\alpha' + H(u+v)},$$

and in this K will decrease with increase of H instead of increasing, as is shown by experiment.

A possible explanation of this discrepancy is that both metallic and electrolytic conduction may occur in a dielectric. This suggestion is supported by an experiment described by H. H. Poole in 'Nature,' July 7th, 1921, which seems to prove that at air temperature and large field strengths the conduction current in glass must be partly of a metallic nature, whereas, on the other hand, it is now well known from the work of Dr. R. C. Burt and others that sodium ions can be driven through glass at higher temperature by comparatively low field strengths. It seems conceivable that a more complete theory of the observed phenomena might be given by applying quantum mechanics to the problem.

Yours faithfully,

J. H. J. Poole.

Trinity College, Dublin.
Feb. 19th, 1931.

LXXXIV. *Radio Frequency Properties of Ionized Air.*

To the Editors of the Philosophical Magazine.

GENTLEMEN,—

THERE is one point in a recent paper by Appleton and Childs (Phil. Mag. vii. p. 969, 1930) on "Radio Frequency Properties of Ionized Air" to which we should like to call attention.

In their determination of a resonance capacity by the so-called Voltage Tuning method they completely ignore any effect which may be produced by the inductance of the leads to their test condenser. This would not affect their thesis if the air in the condenser were non-conducting, since all their results are obtained at the same frequency.

Lattey and Gatty (Phil. Mag. x. p. 985, 1929) have worked out fully the apparent capacity of a condenser with a conducting dielectric between its plates and whose leads possess inductance. The relation between the true capacity k and the apparent capacity K may be shown to be given by

$$k = \frac{1}{1+p^2\mathrm{K}l}\left\{\mathrm{K} + \frac{p^2l(\Delta\phi)^2}{p^4l^2(\Delta\phi)^2+(1+p^2\mathrm{K}l)^2}\right\},$$

where $\Delta\phi$ represents, in suitable units, the effect of conductivity due to ionization, l is the inductance between the point of attachment of the unknown capacity and the rest of the apparatus, and p is the periodicity. Though l will generally be small, yet terms involving $p^2l(\Delta\phi)^2$ may become quite appreciable when p and $\Delta\phi$ are large. In an apparatus of our own using condensers containing N/100 KCl solution with leads 10 cm. long and 5 cm. apart at a periodicity of $2{\cdot}5\times10^7$ the second term inside the bracket amounted to 5·2 per cent. of K*.

Appleton and Childs do not give enough detail to allow an estimate of this term for their apparatus, but as the correction must be added to the apparent value (K) it is highly probable that the supposed lowering of capacity when the air in the condenser is ionized may be only apparent.

In view of this we suggest that their observations are not conclusive evidence for a dielectric constant less than unity.

Yours faithfully,

Electrical Laboratory, Oxford.
February 24th, 1931.

R. T. LATTEY,
W. G. DAVIES.

* The numerical value of this term is not much altered by a change o frequency.

LXXXV. *Notices respecting New Books.*

Geometry of Four Dimensions. By A. R. Forsyth. (Cambridge University Press, 1930. 2 volumes, 75*s.* net.)

THIS impressive work is devoted to the intrinsic geometry of configurations postulated in abstract space. The treatment is analytical. In general the space to be discussed is supposed to be of four dimensions, but there are three sections dealing with configurations in multiple, space of an unspecific number of dimensions, and throughout there is a preference for processes which, though actually used for the most part for four-dimensional space, can in fact be extended for use in any multiple space. It is a pleasure to welcome the appearance of these tomes. It is not easy to over-estimate the extent to which the research geometer will be indebted to Professor Forsyth, who, in so magnificent a fashion, has put in accessible form this large body of knowledge.

Topology. By Solomon Lefschetz. (American Mathematical Society Colloquium Publications, vol. xii., 1930.)

The subject of Topology is of increasing importance nowadays, and it is of great value to students of the subject that this valuable new work by Professor Lefschetz has now appeared. The groundwork of the subject is, of course, covered by Veblen's Cambridge Colloquium Lectures 'Analysis Situs,' which, published in 1922, speedily became the standard work on the topic. The present work is concerned chiefly with new phases of the subject. Among the matters discussed are the theory of manifolds, their duality theorems, the intersections of chains on a manifold, product complexes, transformations of manifolds, and infinite complexes and their applications.

To the student of the subject this volume will be of the greatest importance. The reviewer has great pleasure in recommending it heartily.

Advanced Calculus: a Sequel to an Elementary Treatise on the Calculus. By the late George A. Gibson, University of Glasgow. (Macmillan & Co., 1931. 20*s.*)

This voume, on which Prof. Gibson was engaged at the time of his death in April 1930, has been seen through the press by Prof. MacRobert, who also gave much help in all the stages through which the book passed.

It is a very useful work and will be of great value to mathematical students reading for Final Honours. It contains an

exposition of Dedekind's theory of irrational numbers and the necessary theorems belonging to the theory of sets of points; existence theorems for implicit functions and the theory of Jacobians; some work on infinite series, complex functions of a real variable, Lagrange's expansion, infinite products, and Gamma functions. These subjects are followed by the integration of bounded functions, curvilinear integrals, multiple integrals, and surface integrals. The book closes with a chapter on the integration of series.

Numerical Mathematical Analysis. By J. B. Scarborough. (Published by the Johns Hopkins Press, U.S.A., and the Oxford University Press, 1930. 25*s.* net.)

This book, written by the Professor of Mathematics at the United States Naval Academy, is a useful compendium of all the usual methods used by computers. It treats Newton's formula of interpolation, central-difference formulæ, Lagrange's formula, and inverse interpolation and interpolation of a trigonometric type. The sections on numerical differentiation and integration follow: also sections on the solution of algebraic and transcendental equations. There is much useful information relating to the numerical solution of differential equations, to the normal law of error and the principle of least squares, and, finally, a discussion of harmonic analysis.

An Elementary Treatise on Actuarial Mathematics. By H. Freeman. (Cambridge University Press, 1931. 25*s.* net.)

This book was written by Mr. Freeman at the invitation of the Council of the Institute of Actuaries. It covers the actual knowledge of pure mathematics required for the examinations of the Institute. In cases where candidates for such examinations are not primarily mathematicians, it has often been difficult and laborious to cover the ground required, since it has previously been necessary to refer to a large number of text-books. Such a procedure, of course, had also the disadvantage of giving but a disconnected picture of the subject-matter. It is therefore a pleasure to welcome this book and to recommend it heartily to those for whom it is intended.

Radiations from Radioactive Substances. By Sir Ernest Rutherford, J. Chadwick, and C. D. Ellis. (Cambridge University Press, 1930. 25*s.*)

An extremely clear picture of the advances made in radioactivity in the last twenty years is given in 'Radiations from Radioactive Substances,' by Sir Ernest Rutherford, J. Chadwick, and C. D. Ellis

(Cambridge University Press). The first two chapters are devoted to an historical account of the establishment of the radioactive series, particular emphasis being placed on the importance of the α-particle in these early investigations. After describing the various methods which are used to detect single α-particles, the determination of the number of α-particles emitted per second by a gramme of radium is critically discussed. The low value $3{\cdot}4 \cdot 10^{10}$ α-particles per second obtained by Geiger and Werner in 1924 is discounted and the value $3{\cdot}7 \cdot 10^{10}$ adopted. From this point we are naturally led to the absorption of α-particles in matter. The range of an α-particle was first accurately defined by Henderson, who measured precisely the number of ions per mm. formed by the α-particles from RaC, and showed that the rapid decrease in ionizing power which occurs over the last half centimetre may be divided into two parts—a linear fall with a super-imposed Gaussian probability variation. By extrapolating the linear part, the distance from the source at which ionization would cease if there were no straggling is obtained and this is taken as the range.

The attempt to account for the shape of the ionization curve has shown that the process of absorption is complex. Measurements of the magnetic deflexion *in vacuo* of the α-particles from film sources shows that the velocity of emission from the nucleus is constant and that the different behaviour of the individual α-particles must be attributed to probability differences along the path in the gas.

The ionization along the path of the α-particles is due to the formation of δ-rays (100-volt electrons), and the capture of electrons by the helium nucleus to form a helium ion and in the last few millimetres of its path to form helium atoms. While there is an approximate agreement between the rate of expenditure of energy by the α-particle and the rate of formation of ions, the energy required to form an ion varies, markedly from gas to gas. Thus in helium (ionization potential 24·6 v.) 27·8 volts are expended in forming an ion, in nitrogen (ionization potential 17 v.) 35 volts are expended. Thus in air only half the original energy of the α-particle is accounted for. In a detailed and critical discussion of straggling the authors show that while this is approximately accounted for by the ordinary statistical variation, a quantitative agreement with the observed value for the modulus of the probability distribution is only obtained if it be assumed that the collisions mainly responsible for straggling are twice as numerous as those calculated on the classical theory.

Occasionally the α-particle passes near the nucleus and is deflected through large angles. An extended study of this type of scattering has shown that for the heavier elements the inverse square law is obeyed to distances as small as 2.10^{-2} cm., but that for light elements, such as magnesium and aluminium, when the distance of closest approach is less than 10^{-12} cm., deviations from this law occur. A discussion follows of Debye and Hard-

meier's theory of a polarizable nucleus, which is in excellent agreement with the experimental results for magnesium. In hydrogen and helium the deviations from the inverse square law are more pronounced and may be interpreted in terms of an unsymmetrical potential field surrounding the helium nucleus. Thus for central collisions between helium nuclei the law of force remains normal until the distance of closest approach is $3{\cdot}5 \cdot 10^{-13}$ cm., but for glancing collisions the critical distance is four times as great.

More rarely still the nucleus is broken up by the collision with the α-particle and ejects a proton.

Excepting carbon and oxygen, all light elements with an atomic number less than 19 (Potassium) suffer disintegration and the ejection of a proton; but, in general, the protons emitted by elements of odd atomic number are faster and more numerous than those from elements of even atomic number, a distinction which is also well known in the abundance of the elements in the earth's crust. In some disintegrations there is a gain in kinetic energy, but for the most part energy is absorbed from the α-particle by the new-born nucleus.

Blackett, using a Wilson chamber, observed that in the disintegration of a nitrogen atom the α-particle was incorporated in the new atom, which was presumably an isotope of oxygen with an atomic weight 17. Careful measurement of the angles of tracks before and after disintegration indicate that momentum is conserved in these inelastic collisions.

Although the first radiations observed by Becquerel were β-particles, our knowledge of β-particle disintegration is of recent growth. Measurement of the β- and γ-ray energies, especially by Meitner, show that after the α- or β-particle has been emitted from the nucleus the new element may emit penetrating γ-rays, which, for the most part, leave the atom and are the γ-radiation usually attributed to its parent. A small proportion, however, is absorbed photoelectrically by the extra-nuclear electrons, thus forming two new radiations, the characteristic X-rays of the newly formed element and sets of homogeneous β-rays all related in energy to that of the original nuclear γ-ray.

By comparing the total energy emitted as β-rays by the RaE atom with the maximum energy of the disintegration electrons, Ellis and Wooster have shown that these are not emitted from the nucleus with an energy characteristic of the element, but that the velocity of emission varies from atom to atom. This aspect of β-ray disintegration, which is common to all β-ray disintegrations which have been examined, is in sharp contrast to the homogeneity of the α-particles emitted on α-particle disintegration.

The absorption of γ-radiation is complex and difficult to measure. An admirable account of later work is given which has shown that the simple exponential absorption observed, especially by Russell, for the γ-rays of RaC was due to a combination of different types of scattering, and does not indicate the presence of

homogeneous γ-rays. Energy is removed from a parallel beam of X-rays in four ways:—the ejection of photoelectrons, unmodified scattering, Compton scattering, and the ejection of Compton electrons. For γ-rays the ejection of photoelectrons is negligible, while unmodified classical scattering is appreciable only at very small angles. Many attempts have been made to calculate the proportion of energy scattered by an electron from a beam of X-rays and the spacial distribution of the scattered X-rays, but the Dirac formula, as modified by Klein and Nishina, gives the best agreement with the meagre experimental results available. The differences between theory and experiment are not more than 5 per cent. and are not systematic, while systematic deviations as great as 40 per cent. are observed from the Dirac and Compton formulæ for scattering.

The photoelectric absorption of the nuclear γ-rays by the electron shells of the same atom, which gives rise to the β-ray spectra, has been attacked both theoretically and experimentally; while the results obtained are difficult to interpret, it is clear that in this type of absorption there must be a close coupling between the nucleus and the outer electrons. To take an extreme example, one of the γ-rays from RaC is absorbed so completely by the extra-nuclear electrons that it cannot be separately detected, and there is no reason to assume that it ever had a separate existence as a γ-ray.

The last two chapters deal with a variety of important radioactive topics which have not yet found their place in the general theoretical framework of modern physics, *e. g.*, the packing fraction, the abundance of the elements, the radioactivity of ordinary matter, and that of Rubidium and Potassium, together with an account of improvements which have been made in the technique of general radioactive measurements and the preparation of special sources.

The whole book (which has the format of 'Radioactive Substances and their Radiations') is copiously illustrated with plates and diagrams, and all those interested in atomic physics are indebted to the authors for having brought together a mass of information hitherto scattered through the scientific journals of the last twenty years.

Theory of Functionals. By Vito Volterra. Translation by Miss M. Long. (Messrs. Blackie & Son, Ltd., 50 Old Bailey, London, E.C. 4. Price 25*s.*)

Prof. Volterra's 'Theory of Functionals' is the second volume translated from the Italian, which appears in the series of mathematical books of Messrs. Blackie & Son, the 'Absolute Differential Calculus' of Prof. Levi-Civita having been published some months ago. Prof. Volterra's researches have extended over a period of

more than forty years, and in this volume the author has incorporated his own work and the notable contributions to the study of functional theory made by Hadamard, Fréchet, G. C. Evans, and others whose names appear in the extensive bibliographies at the end of the chapters. Prof. Evans's treatise on Functionals and their applications was published during the war, and was followed by Prof. P. Levy's on 'Functional Analysis.' 'Theory of Functionals,' based on lectures given at the University of Madrid five years ago, has been revised and extended by references to the numerous papers which have been published since that time. The additions to this English edition include the results of Prof. Evans and his pupils on integral and integro-differential equations. Of especial importance is the last chapter on the applications of the theory of functionals—applications arising from the calculus of variations, the oscillations of lakes, oceanic tides and hereditary phenomena, dynamics, elasticity, electromagnetism, and in such diverse fields as ballistics, statistics, and political economy. It is the author's earnest hope that the study of his book may lead others to follow new lines of research, and bring about a more complete and systematic presentation of this branch of mathematical analysis.

Quantum Mechanics. By E. V. Condon, Ph.D., and P. M. Morse, Ph.D. (International Series in Physics.) (Price 15*s.* net.)

Atoms, Molecules, and Quanta. By A. R. Ruark, Ph.D., and H. C. Vrey, Ph.D. (International Series in Physics.) (McGraw-Hill Publishing Co., Ltd., 6 and 8 Bouverie Street, London, E.C. 4. Price 35*s.* net.)

'Quantum Mechanics' contains the substance of the series of lectures given in the Columbia and Princeton Universities and gives an account of some of the advances in modern physics, atomic structure, and spectroscopic and electronic phenomena as interpreted by the wave mechanics of de Broglie and Schrödinger. The earlier chapters give examples of the application of the Schrödinger wave equation to various problems in atomic physics and then the more generalized theory due to Dirac, Jordan, and others, which contains the Schrödinger equation as a special case. Approximate methods of solving the wave equation are described and applied to the cases of the Stark effect in hydrogen, the simple Zeeman effect, and the problem of the helium atom. After an introductory section on the calculus of operators and its relation to the transformation theory consideration is given to collision phenomena, the interaction of radiation and matter, and the various phenomena connected therewith, the theory of the ejection of α-particles from the nuclei of radio-active substances, the scattering of electrons by atoms and of α-particles by atomic nuclei. As this work is intended primarily for physicists, no apology was

needed for the introduction of the remarks on elementary function theory.

'Atoms, Molecules, and Quanta' covers a vast field of modern research. The authors have presented an up-to-date account of the quantum theory and the related experimental researches. The first fourteen chapters deal with the earlier quantum theory and the progress made in the study of atomic and molecular structure. Among the topics discussed are optical and X-ray spectra, the theory of atomic and molecular spectra, including Kratzer's theory of the diatomic molecule and its application to the hydrogen halides, and the recent advance in the study of critical potentials. In the remaining chapters the authors describe the fundamental ideas of quantum mechanics and give an account of the wave properties of matter as shown in the recent experiments on the diffraction and reflexion of electrons; the Schrödinger theory and its application to the hydrogenic atom, the structure of the hydrogen molecule and other problems; the Heisenberg theory and the treatment of the harmonic oscillator, and in connexion with matrix perturbation, the anharmonic case, and, finally, the theory of the hydrogen and helium atoms and the equivalence of the wave and matrix mechanics; a section is devoted to the study of the relative intensities in line and band spectra. A table of physical constants and a list of theorems in electrodynamics are given in two appendices; quantum integrals, orthogonal functions, curvilinear coordinates, and Bechert's interesting and useful method of determining quantized energy values form the subjects of the remaining sections.

Text-book on Spherical Astronomy. By W. M. Smart, M.A., D.Sc. [Pp. xi+414, with 146 figures.] (Cambridge: At the University Press, 1931. Price 21*s.* net.)

Though following inevitably more or less conventional lines, some discussion has been given in this book of such matters as heliographic coordinates, the use of photography in astronomical measurement, and the determination of proper-motions, which are of considerable practical interest and are not amongst the subjects normally dealt with in text-books. A chapter is also devoted to the determination of position at sea, a subject on which the author is particularly competent to write. Methods of determining the orbits of binary stars, both visual and spectroscopic, are not usually included under spherical astronomy, but the author has given a brief outline of a few of the principal methods.

The book is based on lectures which the author has given in the University of Cambridge. The mathematical knowledge assumed is not extensive, and the formulæ of spherical astronomy which are used are developed in the first chapter. The book can be commended as a concise but comprehensive introduction to the subject.

In matters involving the use of data contained in the 'Nautical Almanac,' the current almanac, which differs in many important points from those of previous years, has been used. The student will thereby become familiarized with the new arrangement. The diagrams are numerous and, in general, are excellent, but the chronograph which will give a trace such as is shown in fig. 43 has yet to be constructed.

Annuario del Observatorio Astrónomico de Madrid, 1931. [Pp. 476, with figures.] (Madrid: Instituto Geografico y Catastral, 1930.)

The portion of this annual which is devoted to ephemerides and tables follows the usual lines and contains a detailed explanation of the use of the tables. The special articles include articles on New Stars by V. F. Ascarza, on the Temperatures of the Stars by P. Carrasco, on the Definitive Orbit of Comet Wilk (1929 *d*) by R. Carrasco, and on Observations of the Surface Markings of Jupiter by E. G. Senespleda. A summary is also given of solar observations and of observations of minor planets secured at the Madrid Observatory.

The Physics of Solids and Fluids, with Recent Developments. By P. P. Ewald, Th. Pöschl, and L. Prändtl. Authorised translation by J. Dougall, M.A., D.Sc., F.R.S.E., and W. M. Deans, M.A., B.Sc. [Pp. xii+372, with 322 figures.] (London and Glasgow: Blackie & Son, Ltd., 1930. Price 17*s.* 6*d.* net.)

In this volume are contained translations of the following articles which appeared originally as part of the 11th edition of Müller-Pouillet's *Lehrbuch der Physik*:—Elasticity and Strength of Material; Friction of Solid Bodies, by Th. Pöschl, Professor of General Mechanics and Hydromechanics at the Technical College, Karlsruhe; The Mechanical Structure of Solids from the Atomic Standpoint, by P. P. Ewald, Professor of Theoretical Physics at the Technical College, Stuttgart; The Equilibrium of Liquids and Gases; The Flow of Liquids and Gases, by L. Prändtl, Professor of Applied Mechanics in the University of Göttingen and Director of the Aerodynamical Institute, Göttingen. In the English edition, some revisions have been made and additional notes supplied by the respective authors. The articles are of particular value for their accounts of recent work, and this translation will make them available to a much wider circle of readers.

The last and longest of the articles, On the Flow of Liquids and Gases, is perhaps the most important and occupies nearly one half of the whole volume. Professor Prändtl is a distinguished investigator in this subject and possesses the physical intuition which is necessary for discussing complicated subjects with a minimum of

mathematics. The article contains much valuable information on discontinuous motion and the formation of eddies and jets, with a very interesting discussion of the flow round an aerofoil. The variation of lift and drag with the angle of incidence is discussed and the conditions for stream-line flow and stalling flow are elucidated. Airscrews and propellers are also discussed at some length. The article is illustrated by some excellent photographs of eddy and discontinuous motion in gases and liquids.

Next in importance from the point of view of modern work is the article on The Mechanical Structure of Solids from the Atomic Standpoint. A footnote points out that the article was written in 1927–8 and that many new discoveries in this domain of physics have since been made, some part of which has been recorded by the addition of references. It is a matter for regret that opportunity was not taken to bring this article completely up-to-date. The lattice theory of crystals is used as the physical basis, and stress, cohesion, and rupture strength are considered from this point of view. The mechanical properties of metallic single crystals are considered in detail and the geometry of glide motion is developed. The phenomena of multiple glide are considered and theories of gliding are discussed. Theories of elastic after-working and hysteresis are briefly referred to.

The other articles are of a more stereotyped nature but all are good. The article on Elasticity and Strength of Materials is extremely well written and contains a large amount of information in small compass.

The volume is well printed and illustrated.

LXXXVI. *Proceedings of Learned Societies.*

GEOLOGICAL SOCIETY.

[Continued from p. 800.]

January 28th, 1931.—Prof. E. J. Garwood, M.A., Sc.D., F.R.S., President, in the Chair.

THE following communication was read:—

'The South-West Highland Sequence.' By John Frederick Norman Green, B.A., F.G.S.

In 1923, the following sequence was proposed by the Author for Islay:—

Dark chloritic slates.

Calcareous passage beds.

Grey limestone.

Black sandstone (lenticular).

Arkoses with banks of nordmarkite-conglomerate.

(Line of erosion.)

Dolomitic flags.

Siliceo-argillaceous flags.

White quartzite with rusty cross-bedded films

Slightly felspathic quartzite.

Pebbly quartzite.

This sequence runs through Jura, Scarba, and the Garvellachs the quartzites, however, thinning out.

It is considered that the present succession near Ballachulish can be parallelled in detail with Islay. On attempting to apply the result to the neighbouring areas of Glencoe, Onich and Cuil Bay, it appears that the following amendments to current views are involved :—

1. The Appin Phyllites and Cuil Bay Slates must be identical with the Leven Schists (siliceo-argillaceous flags).

2. The Appin Limestone must be identical with the 'cream-coloured edge of the Ballachulish Limestone' (dolomitic flags).

3. The dark part of the Ballachulish Limestone must be distributed into two horizons; one corresponding to the grey limestone of Islay, the other a black limestone which comes in above the dolomitic flags and below the line of erosion.

The evidence supporting these amendments is then given.

As a result, the Eilde Flags of Loch Linnhe fall into position, and the structure of the Ballachulish–Appin area can be explained without large-scale dislocations, as can also the neighbouring Benderloch area, if the Garbh Ard Quartzite is placed with the arkoses.

The sequence about Tayvallich and Crinan is, when the 'Crinan Quartzite' has been divided into arkoses, flags, true quartzite and conglomerate, comparable with the Islay sequence, allowance being made for a volcanic series near the line of erosion. The beds are followed up to the neighbourhood of Loch Awe, where the volcanic rocks replace part of the sequence, which is, however, complete in the neighbourhood of Kilchrenan. The Loch Avich slates and grits are correlated with the dark chloritic slates and higher beds in Islay.

Thus, the three areas, Islay–Jura, Ballachulish–Appin, and Tayvallich–Loch Awe, are complex synclines of correlated rocks. Between these synclines appear grey calcareous phyllites. Between the phyllites and the flags or discontinuous quartzite occur shallow-water beds, composed essentially of quartzitic conglomerate and

calcareous sandstone, accompanied usually, but not always, by black slate. These beds, which may be referred to as the 'Shore Series', run north-east through Islay and Jura as the 'Jura Slates'; thence through many islands, and on the mainland, as the 'Easdale Slates'. They can be picked up on the opposite side of the phyllites near Kilmelfort, whence they can be traced south-westward into the 'Ardnoe type' of the Crinan area. They recur in Knapdale, and, as 'Shira Limestone', can be followed for 40 miles north-eastward again; they appear on the opposite side of Loch Awe east of Kilchrenan, and pass through the Pass of Brander to the edge of the Cruachan Granite at Loch Etive. The granite-margin gradually rises in the sequence till it touches the dolomitic flags in Glen Ure, and then descends again to the Shore Series in the sections which have been called 'the Windows of Etive'.

In the opposite direction, through the Pass of Brander, the Shore Series is met with about Dalmally, where it is overlain by quartzite passing into white quartzite of the Islay type, above which come flags altered to the condition of Moine schists.

The conclusion is that the structure of the whole of the Dalradian rocks of this part of the South-West Highlands can be explained by the following sequence:—

	Chloritic grits.
	Chloritic slates.
	Grey limestone.
Basal Beds.	Black slates, above or below arkoses, with banks of nord markite-conglomerate. Either may be absent.
	(Line of erosion.)
	Black limestone.
	Dolomitic flags.
	Siliceo-argillaceous flags.
	White quartzite. } May thin out.
	Slightly felspathic quartzite. }
Shore Series.	Quartzitic conglomerate and calcitic sandstone, usually with black slate.
	Grey calcareous phyllites.

[The Editors do not hold themselves responsible for the views expressed by their correspondents.]

FIG. 3.

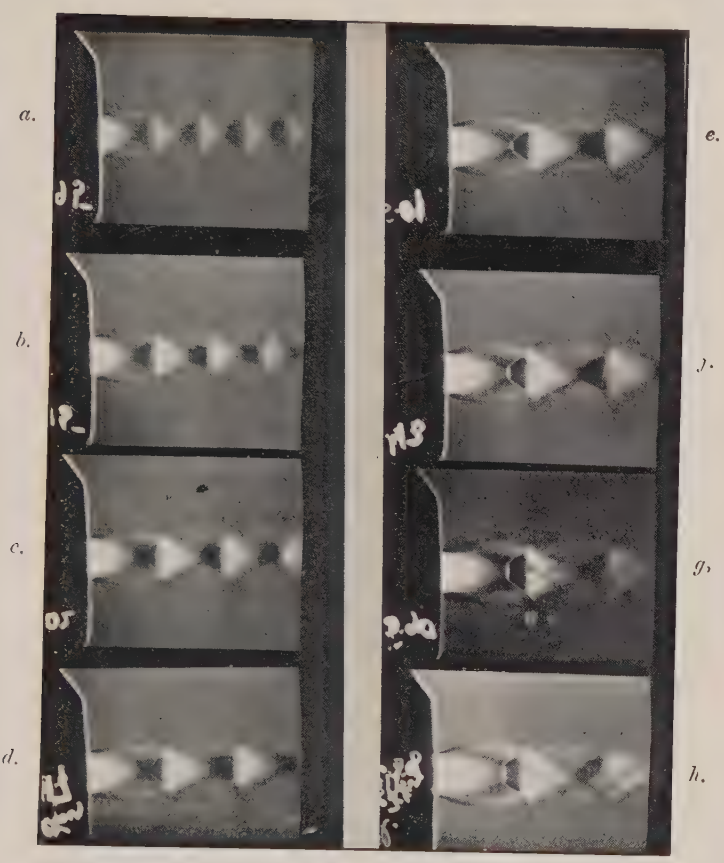

FIG. 7.

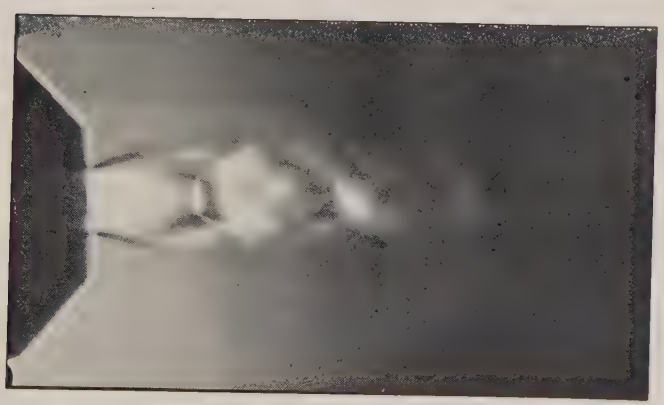

Fig. 3.—Photographs of the air-jet with a velocity exceeding that of sound.
Fig. 7.—The breaking-up of the regulur structure of the jet.

FIG. 5.

a.

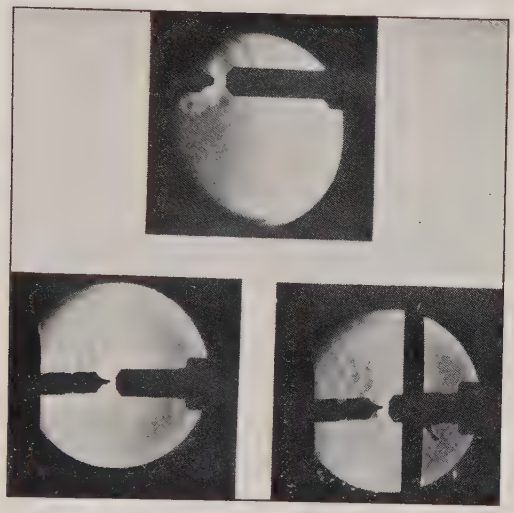

b. *c.*

Photographs of waves emitted from oscillators.

FIG. 14.

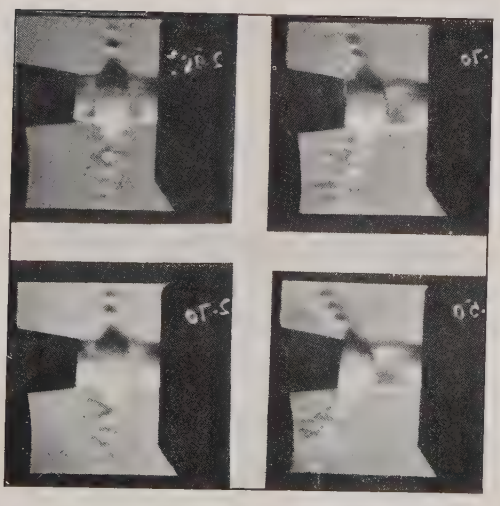

a. *c.*

b. *d.*

Photographs illustrating the discharge of the pulsator.

Photographs of air vibrations in an oscillator.

FIG. 13.

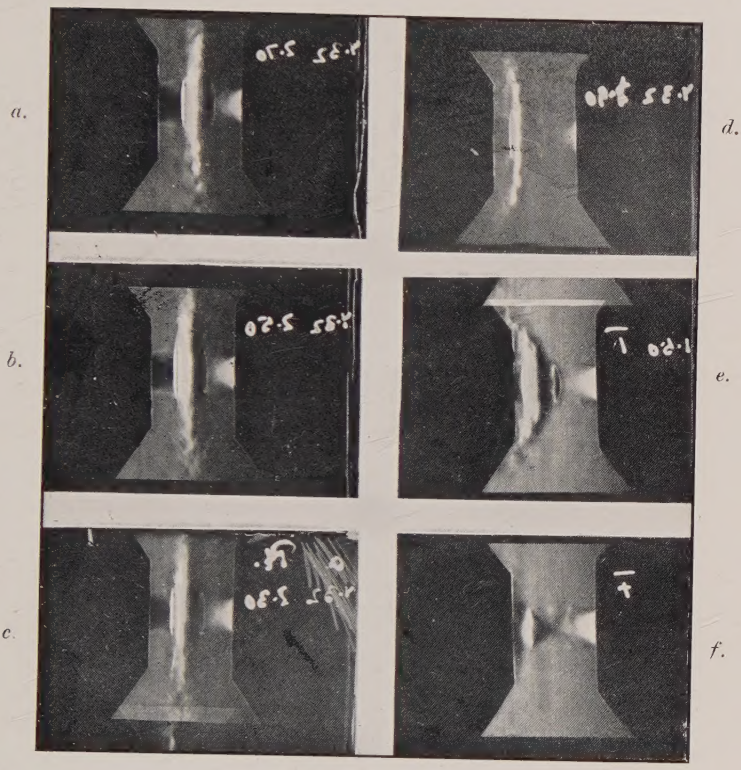

FIG. 19.

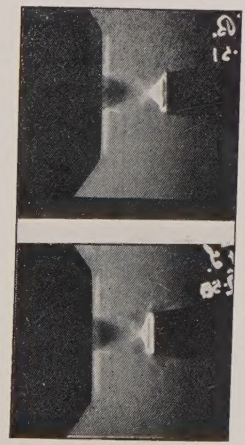

Fig. 13.—Photographs illustrating the discharge of the pulsator.
Fig. 19.—Development of a compression-wave in front of the pulsator nozzle towards the end of the period of charging.

Phil. Mag. Ser. 7, Vol. 11, Pl. XI

FIG. 15.

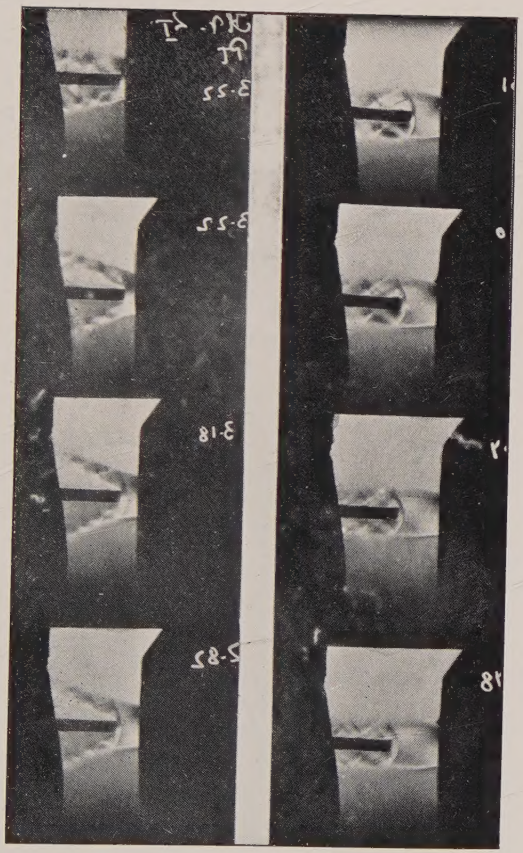

Photographs of compression-wave in front of Pitot sound.